Metal dynamics in the sediments of the Krka River estuary

Cukrov, Nuša

University of Zagreb

Faculty of Science
Department of Geology

Nuša Cukrov

METAL DYNAMICS IN THE SEDIMENTS OF THE KRKA RIVER ESTUARY

DOCTORAL THESIS

Zagreb, 2021

University of Zagreb

Faculty of Science
Department of Geology

Nuša Cukrov

METAL DYNAMICS IN THE SEDIMENTS OF THE KRKA RIVER ESTUARY

DOCTORAL THESIS

Supervisor:
Dr. Neven Cukrov

Zagreb, 2021

Sveučilište u Zagrebu

Prirodoslovno-matematički fakultet
Geološki odsjek

Nuša Cukrov

DINAMIKA METALA U SEDIMENTIMA ESTUARIJA RIJEKE KRKE

DOKTORSKI RAD

Mentor:
Dr. sc. Neven Cukrov

Zagreb, 2021.

This doctoral thesis was conducted at the Division for Marine and Environmental Research, Ruđer Bošković Institute in collaboration with the University of Toulon, under supervision of Dr. Neven Cukrov, in the frame of Doctoral study in Geology at Faculty of Science, University of Zagreb.

Acknowledgements

There are many who helped me along the way on this journey and to who I am sincerely grateful. First and foremost, I would like to express my respect and deepest gratitude to the late Dr. Cédric Garnier who encouraged me to choose this research topic and offered me unwavering support during the course of the research. His brilliant mind and enthusiasm for science were truly inspiring, his optimism, energy, and endurance contagious, and his continuous dedication to his PhD students admirable. Even though he has not seen me arrive at the end of this journey, I believe that without his guidance and persistent help this thesis would not have been achievable. I am also extremely grateful to my supervisor, Dr. Neven Cukrov, who went above and beyond to support and encourage me to reach my goals. Above all, I am grateful for his profound belief in my abilities and granting me independence which allowed me to grow as a researcher.

I would like to thank my thesis committee members Dr. Hana Fajković, Dr. Kristina Pikelj and Dr. Dario Omanović for their insightful comments and suggestions that helped to improve this work. I would especially like to express my deepest gratitude to Dr. Dario Omanović for his invaluable assistance and dedicated involvement in every step of this thesis.

I am very thankful to my colleagues from the Ruđer Bošković Institute for their wonderful collaboration, especially my colleagues from the Laboratory for physical chemistry of traces and Research Station Martinska for all the help they offered me during years and all the pleasant and inspiring conversations we had. I would like to acknowledge Dr. Ivana Tucaković for preforming the radiometric analysis and Dr. Maja Ivanić and Dr. Mavro Lučić for the assistance in performing granulometric analysis. I very much appreciate the effort of Saša Marcinek who numerous times handled faculty paperwork on my behalf.

I would like to express my sincere thanks to all the members of the PROTEE laboratory of the University of Toulon who extended me a great amount of assistance during laboratory work. I am also grateful to them for their friendship and the warmth they showed me during my time in France and for always making me feel so welcome. I am

especially indebted to Dr. Nicolas Layglon and his family who opened their home to me and who truly become my second family.

I am also grateful to the Dr. Darko Tibljaš and Zvonka Gverić for their help in mineralogical analyses.

I very much appreciate the contribution of the Public Institute Nature of Šibenik-Knin County. Their support in terms of providing boat and staff for the sampling greatly facilitated my fieldwork. Additionally, I am grateful to the French Government for the funding which enabled my research visits to University of Toulon.

Many thanks to my friend Nela, who was by my side from the Day 1 of my geology journey and has never let me down. Not only that she generously provided a place to stay for the many times I was in Zagreb due to the PhD obligations, but she also made those days enjoyable and fun. Thanks should also go to all my friends who provided happy distractions to rest my mind outside of research.

Last but not least, I would like to express my deep and sincere gratitude to my family for providing me with unconditional love and support throughout my life. To my big sister who is always looking after me and whose jokes about geeks only push me to be even better. To my parents who made me who I am today and taught me maybe the most important thing – to think with my own head. To my husband who was involved in process of making this thesis in many ways, from helping with sampling (and I mean the hard work of extracting sediment cores) to keeping me company during the long working nights and encouraging me to write for another half hour longer, I can thank in only one way - HŽV.

BASIC DOCUMENTATION CARD

University of Zagreb
Faculty of Science
Department of Geology

Doctoral Thesis

METAL DYNAMICS IN THE SEDIMENTS OF THE KRKA RIVER ESTUARY

Nuša Cukrov

Division for Marine and Environmental Research, Ruđer Bošković Institute, Zagreb

In the estuaries, sediments may represent both a sink and a secondary source of metals, due to the various biological and physico-chemical processes which control the metal dynamics in the sediment and the overlying water column. To evaluate the sediment contamination by metals and to identify the main metal input pathways, surface sediments were sampled at 40 locations in the Krka River estuary, an environment so far regarded as relatively unpolluted. To study the dynamics of metal behaviour in the estuarine environment and to quantify metal exchanges at the sediment water interface, sediment cores were retrieved from 7 locations within the estuary. To achieve research objectives, a comprehensive approach was used, which included geochemical characterization of dissolved (pore water) and solid fraction of the sediment and the overlying water column, determination of mineralogical and granulometric composition of the sediment, measurement of physico-chemical parameters of the sediment and water column and dating of one sediment core. Two distinct areas were distinguished; the upper unpolluted estuary and the lower estuary where sediment profiles reflected the history of anthropogenic metal input associated with the city of Šibenik. Three main point sources of contamination were identified: the former Electrode and Ferroalloy Factory, the Port of Šibenik and nautical marina/repair shipyard. The mobility of metals in the sediment was mainly controlled by the degradation of organic matter, either through primary redox reactions in the sediment, such as reductive dissolution of Fe and Mn oxyhydroxides by which metals are released to the pore water, either through secondary reactions which may remove metals from the pore water through formation of the authigenic phase or increase metals solubility by forming metal-DOM, metal-(poly)sulphide or metal-sulphide-DOM complexes. According to calculated benthic diffusive fluxes, sediment in the Krka River estuary is dominantly acting as a source of metals.

Keywords: contamination assessment, early diagenesis, Krka River estuary, metals, pore water, sediment

Thesis contains: 241 pages, 73 figures, 16 tables, 331 references, 26 appendices

Original in: English

Thesis deposited in: National and University Library of Zagreb, Ruđer Bošković Institute Library, Central Library of Geology at Faculty of Science

Supervisor: Neven Cukrov, Ph.D., Senior Research Associate, Ruđer Bošković Institute, Zagreb

Reviewers: Hana Fajković, Ph.D., Assistant Professor, Faculty of Science, Zagreb

Kristina Pikelj, Ph.D., Assistant Professor, Faculty of Science, Zagreb

Dario Omanović, Ph.D., Senior Scientist, Ruđer Bošković Institute, Zagreb

Thesis accepted: 11 January 2021

TEMELJNA DOKUMENTACIJSKA KARTICA

Sveučilište u Zagrebu
Prirodoslovno-matematički fakultet
Geološki odsjek

Doktorski rad

DINAMIKA METALA U SEDIMENTIMA ESTUARIJA RIJEKE KRKE

Nuša Cukrov

Zavod za istraživanje more i okoliša, Institut Ruđer Bošković, Zagreb

U estuarijima, sedimenti mogu biti krajnje odredište metala, ali i njihov sekundarni izvor zbog djelovanja različitih bioloških i fizikalno-kemijskih procesa koji kontroliraju dinamiku metala u sedimentu i na granici faza sediment-vodeni stupac. Kako bi se procijenilo onečišćenje sedimenta metalima i odredili glavni izvori onečišćenja, površinski sediment je uzorkovan na 40 lokacija duž estuarija rijeke Krke koji je smatran relativno čistim okolišem. Kako bi se istražila dinamika metala u estuarijskom okolišu te kvantificirala izmjena metala na granici faza sediment-vodeni stupac, jezgre sedimenta su uzorkovane na 7 lokacija u estuariju. Za postizanje ciljeva istraživanja, primijenjen je sveobuhvatni pristup koji je uključivao geokemijsku karakterizaciju krute frakcije sedimenta i dijela frakcije koje je prešao u otopinu (porna voda) te vodenog stupca, određivanje mineraloškog i granulometrijskog sastava sedimenta, mjerenje fizikalno-kemijskih parametara u sedimentu i vodenom stupcu, te datiranje jedne sedimentne jezgre. Na temelju rezultata, estuarij se može podijeliti na dva područja; gornji, nezagađeni tok i donji tok, gdje udio metala u sedimentnim jezgrama odražava povijest antropogenog utjecaja grada Šibenika na okoliš. Tri su glavna izvora onečišćenja: bivša tvornica elektroda i ferolegura (TEF), Luka Šibenik i nautička marina/remontno brodogradilište. Mobilnost metala u sedimentu uglavnom je kontrolirana procesima razgradnje organske tvari, bilo primarnim redoks reakcijama u sedimentu, poput reduktivnog otapanja Fe i Mn oksihidroksida u suboksičnoj zoni sedimenta pri čemu se metali oslobađaju u pornu vodu, bilo kroz sekundarne reakcije koje mogu ukloniti metale iz porne vode stvaranjem autigenih minerala ili povećati topivost metala stvaranjem kompleksa metal-DOM, metal-(poli)sulfid ili metal-sulfid-DOM u anoksičnom sedimentu. Prema izračunatim difuznim tokovima, sedimenti u estuariju rijeke Krke većinom predstavljaju izvor metala za pridneni sloj vodenog stupca.

Ključne riječi: procjena onečišćenja, rana dijageneza, estuarij rijeke Krke, metali, porna voda, sediment

Rad sadrži: 241 stranica, 73 slika, 16 tablica, 331 literaturnih navoda, 26 priloga

Jezik izvornika: engleski

Rad je pohranjen u: Nacionalnoj i sveučilišnoj knjižnici u Zagrebu, knjižnici Instituta Ruđer Bošković i Središnjoj geološkoj knjižnici Prirodoslovno-matematičkog fakulteta

Mentor: Dr. sc. Neven Cukrov, viši znanstveni suradnik, Institut Ruđer Bošković, Zagreb

Ocjenjivači: Doc. dr. sc. Hana Fajković, Prirodoslovno-matematički fakultet, Zagreb

Doc. dr. sc. Kristina Pikelj, Prirodoslovno-matematički fakultet, Zagreb

Dr. sc. Dario Omanović, znanstveni savjetnik, Institut Ruđer Bošković, Zagreb

Rad prihvaćen: 11. siječnja 2021.

TABLE OF CONTENTS

ABBREVIATIONS AND SYMBOLS

C_{org}	Organic carbon
DIC	Dissolved Inorganic Carbon
DOC	Dissolved Organic Carbon
DOM	Dissolved Organic Matter
EF	Enrichment Factor
Eh	Redox potential
EPA	United States Environmental Protection Agency
ERL	Effects-Range-Low
ERM	Effects-Range-Median
FEP	Fluorinated Ethylene Propylene
FSI	Freshwater – Seawater Interface
GPS	Global Positioning System
HDPE	High Density PolyEthylene
HR ICP-MS	High Resolution Inductively Coupled Plasma Mass Spectroscopy
IAEA	International Atomic Energy Agency
I_{geo}	Geoaccumulation index
ISO	International Organization for Standardization
K_d	Partition coefficient
LDPE	Low Density PolyEthylene
M	Metal
m-ERM-Q	Mean ERM Quotient
MQ	Milli-Q water
M_z	Mean grain size
OM	Organic matter
ORP	Oxidation-Reduction Potential
PAH	Polycyclic Aromatic Hydrocarbons
PC	Principal Component
PCA	Principal Component Analysis
PVC	PolyVinyl Chlorid
PZC	Point of Zero Charge

SHE	Standard Hydrogen Electrode
SMTZ	Sulphate-Methane Transition Zone
SQG	Sediment Quality Guidelines
SRP	Soluble Reactive Phosphate
SWI	Sediment – Water Interface
TBT	TriButylTin
TC	Total Carbon
TDL	Theoretical Dilution Line
TEF	Electrode and ferroalloy plant (hr. Tvornica Elektroda i Ferolegura)
UV	UltraViolet
VIS	VISible
XRD	X-Ray Diffraction

PROŠIRENI SAŽETAK

PROŠIRENI SAŽETAK

1. UVOD

Estuariji su, kao područja pogodna za naseljavanje i industrijski razvoj, diljem svijeta izloženi snažnom utjecaju čovjeka, što često za posljedicu ima onečišćenje ovih važnih, ali ranjivih ekosustava (Chapman i Wang 2001; Emili i sur. 2016; Kennish 2016;). Među najzastupljenijim onečišćivalima su metali i metaloidi (u daljnjem tekstu: metali), koji se u estuarijskim uvjetima veoma brzo adsorbiraju na suspendirane čestice i talože u sediment. Međutim, sediment ne može biti smatran samo krajnjim odredištem onečišćivala, već i potencijalnim sekundarnim izvorom iz kojeg se metali mogu otpustiti u vodeni stupac (Saulnier i Mucci 2000; Tankere-Muller i sur. 2007; Cukrov i sur. 2011; Duan i sur. 2015). Mobilnost metala u sedimentu ovisi o sastavu sedimenta (npr. organska tvar, Fe i Mn oksihidroksidi, sulfidi, minerali glina, karbonati,…), o fizikalno-kemijskim uvjetima u sedimentu i vodenom stupcu (npr. pH, Eh, organski i anorganski ligandi), o biogeokemijskim procesima (otapanje, precipitacija, sorpcija) koji se odvijaju u sedimentu za vrijeme rane dijageneze, kao i fizikalnim (difuzija, advekcija) i biološkim (bioirigacija, bioturbacija) transportnim mehanizmima. Kao pokretačka sila rane dijageneze često se navodi razgradnja organske tvari, tijekom koje dolazi do kemijskih transformacija sedimenta i porne vode. Promjene koje se odnose na dinamiku metala najznačajnije su u sedimentnim slojevima u kojima su Fe/Mn oksihidroksidi i sulfati krajnji akceptori elektrona. Naime, reduktivnim otapanjem Fe i Mn oksihidroksida, metali koji su na njih bili adsorbirani, otpuštaju se u pornu vodu. Otopljeni metali mogu difundirati prema granici faza sediment-voda i/ili dublje u sediment, te mogu biti ponovno adsorbirani na ili koprecipitirati s novooformljenim Fe i Mn mineralima (npr. karbonatima, sulfidima) ili precipitirati kao sulfidni minerali zajedno s otopljenim sulfidom, produktom redukcije sulfata, koja se odvija posredstvom bakterija. Ako je koncentracija nekog metala u pornoj vodi veća od koncentracije u pridnenoj vodi, gradijent koncentracije na granici faza sediment-voda uzrokovat će transport otopljenog metala iz sedimenta u vodeni stupac. Istraživanja su pokazala da je bentički difuzni prijenos metala iz sediment u vodeni stupac jednak ili čak premašuje riječni donos metala u mnogim obalnim područjima (Rivera-Duarte i Flegal 1997; Williams i sur. 1998; Warnken i sur. 2001; Santos-Echeandia i sur. 2009), što potvrđuje važan utjecaj sedimenta na kvalitetu vodnog okoliša. Razumijevanje učinaka različitih okolišnih uvjeta i biogeokemijskih procesa na pokretljivost, bioraspoloživost i toksičnost metala od presudne je važnosti za procjenu potencijalnog negativnog djelovanja zagađenog sedimenta na vodni okoliš. Pri rješavanju takvih okolišnih „zagonetki“, potrebno je primijeniti sveobuhvatni

pristup, u kojem će se analizirati i čvrsta i otopljena faza sedimenta te vodeni stupac iznad sedimenta.

2. PODRUČJE ISTRAŽIVANJA

Estuarij rijeke Krke je tipični krški uslojeni estuarij, s površinskim slatkovodnim/bočatim slojem koji teče prema moru, te pridnenim morskim slojem koji se kreće uzvodno. Recentna morfologija estuarija rezultat je geološke građe područja i klimatskih promjena koje su se dogodile nakon gornjeg pleistocena. Naime, rijeka Krka je tijekom glacijala usjekla kanjon u Sjevernodalmatinsku kršku zaravan, a porast razine mora tijekom holocenske transgresije doveo je do poplave doline i formiranja današnjeg estuarija. Dominantne naslage u slivu rijeke su gornjokredni i eocenski vapnenci, dok su klastične stijene manje zastupljene, a čine ih eocenske flišne naslage, te kvartarni lapori i gline (Prohić i Kniewald 1987; Prohić i Juračić 1989). Na sedimentaciju u estuariju rijeke Krke utječu dva glavna izvora materijala: (1) trošenje karbonatnih i nekarbonatnih stijena u drenažnom području i abrazija karbonatnih obala estuarija i (2) autigena biogena formacija karbonata (Juračić i Prohić 1991.). Nadalje, važna značajka estuarija je vrlo nizak unos terigenog materijala glavnim vodotokom rijekom Krkom. To je zbog činjenice da rijeka Krka protječe uglavnom kroz karbonatne naslage te ima sedrene barijere duž toka koje značajno smanjuju transport suspendiranog materijala. Glavni izvor terigenog materijala je pritok Guduča, koja se ulijeva u Prokljan. Sliv Guduče izgrađen je uglavnom od gornjoeocenski do oligocenskih flišnih naslaga, čijim se trošenjem stvara većina količina čestica, a duž svog toga nema sedrene barijere koje bi ih mogle zadržati (Prohić i Juračić 1989; Juračić i Prohić 1991; Cukrov i Barišić 2006). S obzirom na različite utjecaje rijeke Krke, pritoka Guduče te otvorenog mora na estuarij, postoje razlike u sedimentaciji između gornjeg i donjeg dijela estuarija. U gornjem dijelu, posebice u jezeru Prokljan, taloži se pretežno sitnozrnata mješavina marinskih karbonata i terigenog materijala, dok se u donjem dijelu estuarija, Šibenskom zaljevu, odvija marinska biogeno karbonatna sedimentacija (Juračić i Prohić 1991; Cukrov i Barišić 2006; Cukrov i sur. 2009).

S obzirom da je najveći dio slatkovodnog vodotoka rijeke Krke zaštićen kao nacionalni park, nema značajnijeg unosa onečišćivala u estuarij iz tog pravca, te se estuarij smatra relativno čistim. Međutim, prethodna istraživanja su pokazala da je antropogeni utjecaj grada Šibenika prouzrokovao povišenje udjela nekih metala u sedimentu donjeg dijela estuarija (Mikac i sur. 1989; Martinčić i sur. 1989, 1990; Kwokal i sur. 2002; Bogner i sur. 2004; Cukrov i sur. 2008).

Glavni onečišćivači su bili tvornica elektroda i feromangana (TEF), remontno brodogradilište, luka za pretovar rasutih tereta i neobrađene otpadne vode. Danas su neki od izvora onečišćenja eliminirani, TEF je zatvoren prije 25 godina, a otpadne vode se od 2007. godine obrađuju i ispuštaju van estuarija. Uklanjanje industrije iz estuarija dovelo je do razvoja nautičkog turizma, koji predstavlja ozbiljnu sezonsku prijetnju ekosustavu estuarija (Cindrić i sur. 2015).

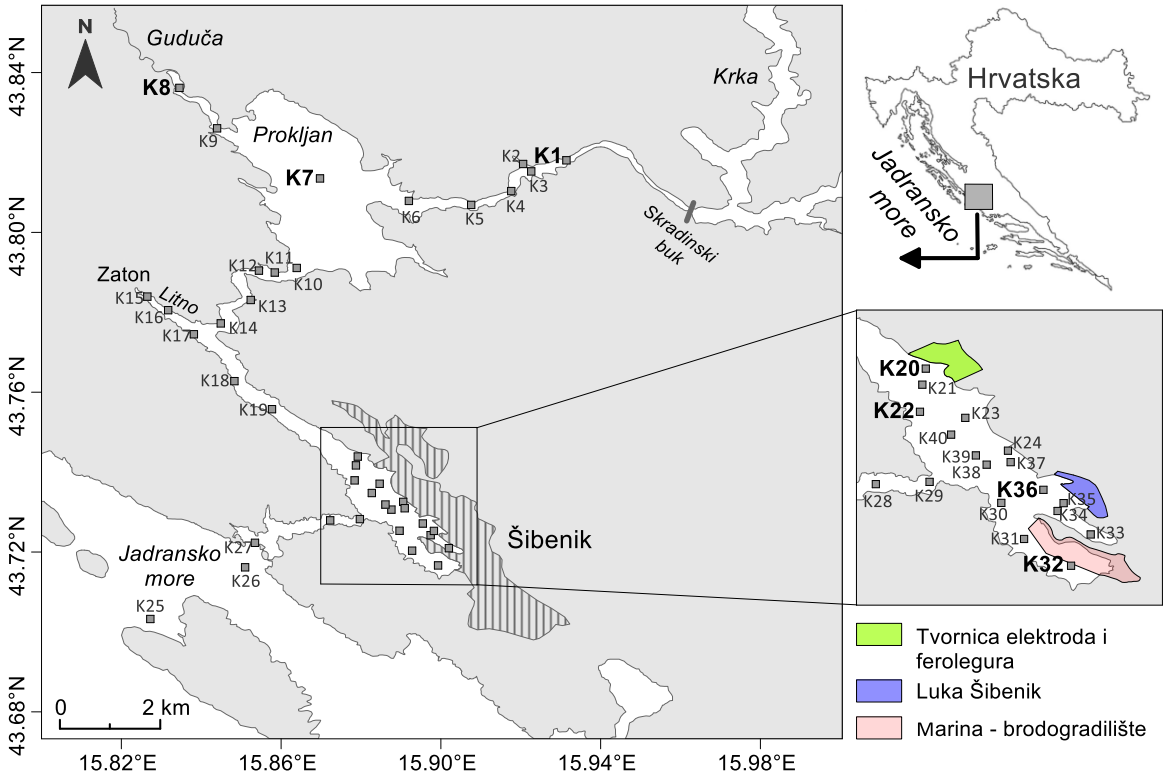

Slika 1. Karta estuarija rijeke Krke s označenim mjestima uzorkovanja i glavnim onečišćivačima. Tamno sivi kvadratni simboli označavaju mjesta uzorkovanja površinskog sedimenta, dok podebljani naziv mjesta uzorkovanja označavaju lokacije uzorkovanja jezgri.

3. METODE I TEHNIKE ISTRAŽIVANJA

Uzorkovanje površinskog sedimenta estuarija rijeke Krke provedeno je u ljeto 2016., kako bi se procijenilo stanje sedimenta s obzirom na udio metala i utvrdilo moguće onečišćenje. Uzorci su uzeti na 40 lokacija duž estuarija, uz pomoć gravitacijskog jezgrila (φ = 9 cm) (Slika 1). Vršnih 5 cm jezgre sačuvano je za analizu, zamrznuto (-18°C) odmah po dolasku u laboratorij, liofilizirano te prosijano na sito veličine otvora 2 mm. Dodatno su uzete jezgre sedimenta za određivanje vertikalne raspodjele te mobilnosti metala na 7 od 40 lokacija uzorkovanja površinskog sedimenta. Sve jezgre, osim K8, su uzorkovane tehnikom autonomnog ronjenja. Na svakoj lokaciji su uzete tri jezgre: (i) za rezanje, odnosno izdvajanje uzoraka sedimenta i

porne vode; (ii) za mjerenje pH i Eh, jezgra je uzeta pomoću jezgrila s izbušenim rupicama svakih centimetar; (iii) za prikupljanje uzorka pridnene vode na tri različite udaljenosti od površine sedimenta: 2, 5 i 15 cm. Uz to, na svakoj lokaciji je uzorkovan i vodeni stupac na 4 do 6 dubina, ovisno o dubini na pojedinoj lokaciji te poziciji halokline. Osnovni fizikalno-kemijski parametri vode su izmjereni uz pomoć multi parametarske sonde EXO2 (YSI).

Jezgre sedimenta transportirane su u laboratorij u roku od jednog sata od uzorkovanja. Sve radnje vezane za izvlačenje porne vode iz sedimenta obavljane su u struji dušika kako bi se spriječila oksidacija uzoraka. Jezgre su izrezane na odsječke od 1 ili 2 cm (ovisno o jezgri), te je svaki odsječak centrifugiran (4 000 rpm, 15 min, Centrifuge 5 804, eppendorf) kako bi se porna voda odvojila od ostatka sedimenta. Potom su uzorci porne vode filtrirani (0,2 μm filteri za šprice, Sartorius) te raspodijeljeni u odgovarajuće bočice, ovisno o vrsti analize. Kao i kod površinskog sedimenta, svi uzorci su zamrznuti, liofilizirani i prosijani na sito veličine pora 2 mm. Frakcija <2 mm je usitnjena u mlinu Planetary Ball Mill PM 100 (Retch).

Granulometrijski sastav sedimenta određen je metodom laserske difrakcije na instrumentu LS 13 320 (Beckman Coulter). Mineralni sastav sedimenta određen je metodom rendgenske difrakcije na prahu, korištenjem instrumenta s CuKα zračenjem Philips X'Pert Pro i sljedećim uvjetima snimanja: 40 kV, 40 mA, korak od 0.02°2θ s vremenom snimanja od 1 sekunde, raspon 4-63°2θ. Minerali su identificirani usporedbom s referentnim uzorcima, korištenjem programa Philips X'Pert HighScore software (Philips Analytical B.V., 2001).

Multi elementarna analiza uzoraka sedimenta provedena je korištenjem induktivno spregnutog masenog spektrometra visoke razlučivosti (HR ICP-MS, Element 2, Thermo). Prije analize, uzorci su razoreni na sljedeći način: 100 mg sedimenta izvagano je u teflonske epruvete od 15 ml u koje je potom dodano 10 ml zlatotopke (HNO_3: HCl 1: 3, Fisher Scientific® Trace Analysis). Epruvete su stavljene u UltraWAVE mikrovalni sustav s jednom reakcijskom komorom (Milestone Inc) pod kontroliranim uvjetima (snaga 1 500 W, tlak 100 bara, temperatura je prvo linearno povećana sa sobne temperature na 240°C u 20 minuta, a zatim održavana na 240°C sljedećih 20 min). Dobivena otopina razrijeđena je s 2% HNO_3 (suprapur) do koncentracije pogodne za mjerenje. Kao interni standard korišten je indij (In), a za kontrolu metode razaranja certificirani referentni materijali za morski i riječni sediment. Koncentracije žive u sedimentu određene su u netretiranim uzorcima (~10-100 mg) na instrumentu Advanced Mercury Analyzer AMA 254 (LECO Corporation). Za mjerenje dušika, te ukupnog i organskog ugljika u sedimentu korišten je uređaj Flash 2 000 Elemental Analyzer (Thermo Scientific). Koncentracije ukupnog ugljika i dušika su izmjerene u netretiranim uzorcima (~10-15 mg, ~5

mg za jezgru K20), dok je za određivanje sadržaja organskog ugljika alikvot uzorka sedimenta tretiran kloridnom kiselinom (6 M, Trace metal grade) kako bi se uklonio anorganski ugljik prije analize uzorka.

Analiza multi elementnog sastava vode (vodeni stupac, pridnena i porna voda) određena je na HR ICP-MS-u. Uzorci su razrijeđeni 10 puta s 2% HNO_3 (suprapur) kako bi se umanjio utjecaj matriks efekta povezanog s prisutnošću soli. Koncentracije kadmija u uzorcima vodenog stupca, uključujući pridnenu vodu, određene su metodom standardnog dodatka (diferencijalno pulsnom voltammetrijom anodnog otapanja) uz korištenje instrumenta Autolab (Methrom/EcoChemie) potenciostat/galvanostat u kombinaciji s troelektrodnim sustavom 663 VA Stand (Metrohm) i sustavom za automatsko doziranje. Za određivanje koncentracija otopljenog organskog (DOC) i anorganskog (DIC) ugljika korišten je uređaj TOC-V_{CSH} (Shimadzu). Ortofosfati, amonij, sulfati, otopljeni sulfidi i ortosilikati u uzorcima vode određeni su spektrofotometrijski na uređaju UV/VIS Lambda 45 (Perkin Elmer).

Karte prostorne raspodjele elemenata u površinskom sedimentu estuarija rijeke Krke izrađene su pomoću programa Surfer 15 (Golden Software) korištenjem metode inverzne udaljenosti za izračunavanje kontura. Pearsonov koeficijent korelacije odabranih parametara i analiza glavnih komponenti izračunati su pomoću softvera Origin 2019b (OriginLab).

4. REZULTATI I RASPRAVA

4.1. Prostorna raspodjela elemenata i procjena onečišćenja metalima u površinskom sedimentu estuarija rijeke Krke

Na temelju prostornih raspodjela odabranih elemenata u površinskom sedimentu estuarija rijeke Krke i provedene statističke analize, istaknuta su dva opća zapažanja: (1) elementi terigenog porijekla su najzastupljeniji na području ušća Guduče u Krku, uvali Zaton te na postaji K19 i (2) udio elementa pretežno antropogenog porijekla u sedimentu se veoma razlikuje između nezagađenog gornjeg dijela estuarija (Guduča, Prokljan, uzvodno od Prokljana do početka estuarija) i donjeg dijela estuarija koji je izložen antropogenim pritiscima grada Šibenika (Slika 2). Prostorna raspodjela terigenih elemenata u skladu je s prethodnim istraživanjima, kojima je utvrđeno da se donos terigenog materijala u estuarij odvija rijekom Gudučom te putem izvora Litno u Zatonu. Međutim, visoke koncentracije terigenih elemenata na postaji K19, koja se nalazi 1 km jugoistočno od Šibenskog mosta, nisu očekivane te njihovo porijeklo ostaje

nerazjašnjeno. Povišene koncentracije metala u sedimentu Šibenskog zaljeva većinom se mogu pripisati barem jednom od tri glavna izvora onečišćenja u promatranom području: TEF, Luka Šibenik i remontno brodogradilište/nautička marina. Na temelju izračuna pokazatelja kvalitete sedimenta (faktor obogaćenja i geoakumulacijski indeks), područje oko bivše tvornice je značajno onečišćeno sljedećim metalima: Mn, Pb, Bi, Hg, Zn, Cu i Ba. Područje luke specijalizirane za rasuti teret, prvenstveno za umjetna gnojiva i fosfate, je značajno opterećeno sljedećim metalima: Hg, Zn, Cd, Bi, U, Pb, Cu, Cr, As i Ag, a područje uvale Sveti Petar u kojoj se nalazi remontno brodogradilište i nautička marina sljedećim metalima: Hg, Bi, Pb, Cu, Zn i As. Prema ovim pokazateljima, među elementima mjerenim u sedimentima estuarija rijeke Krke, živa je najzastupljenije zagađivalo. Naime, na prostoru gotovo čitavog Šibenskog zaljeva utvrđeno je vrlo visoko ili ekstremno visoko obogaćenje živom, odnosno razina onečišćenja od vrlo zagađeno do ekstremno zagađeno. Usporedbom izmjerenih koncentracija u površinskom sedimentu estuarija rijeke Krke sa smjernicama kvalitete sedimenta (eng. Sediment Quality Guidelines – SQG) (Long i sur. 1995) procijenjen je potencijalni toksični utjecaj sedimenta na živi svijet koji obitava na dnu ili u sedimentu. Koncentracije Hg, Ni, Zn, Pb i Cd u sedimentu upućuju na vjerojatan negativan utjecaj na živi svijet, dok je za elemente As, Cu, Cr i Ag moguć negativan utjecaj. Međutim, koncentracije Ni, te dijelom As, su prirodnog porijekla što je vidljivo iz rezultata analiza dubljih slojeva analiziranih jezgri te iz izračunatih faktora obogaćenja. Prirodno porijeklo Ni je potvrđeno i analizom glavnih komponenti. Prirodno povišene koncentracije ovih elemenata u jadranskim sedimentima su zabilježene u prethodnim istraživanjima, te pripisane visokim koncentracijama u izvorišnim stijenama (Prohić i Juračić 1989; Cukrov i sur. 2014). Nikal stoga nije uključen u izračun kombiniranog utjecaja metala na toksičnost sedimenta (Long i sur. 2000), prema kojem je na 65% površine estuarija vjerojatnost toksičnosti sedimenta za živi svijet 21%, dok je u područjima koja okružju glavne izvore onečišćenja vjerojatnost 49%, odnosno 76%.

Istraživanjem površinskog sedimenta estuarija rijeke Krke utvrđeno je da je razina onečišćenja u Šibenskom zaljevu mnogo veća nego što se to dosada smatralo, te da koncentracije nekih elemenata, npr. Hg, Pb, Zn, Mn, Cd, Cu i As, dosežu vrijednosti koje su usporedive s nekim od izrazito zagađenih obalnih područja i estuarija Europe. Međutim, ovo zagađenje je uglavnom ograničeno na područje Šibenskog zaljeva. Iz karata raspodjela metala u površinskim sedimentima može se zaključiti da nema širenja onečišćenja izvan estuarija prema moru, što je najvjerojatnije posljedica nekoliko čimbenika: zatvorene morfologije estuarija, pridnenog sloja morske vode koji se kreće uzvodno sprječavajući transport metala u smjeru mora (Mikac i sur.

1989.) i brze adsorpcija metala na čestice i taloženja na morsko dno. Naime, proučavajući adsorpciju Hg, Zn i Pb na čvrste anorganske faze u vodama različitog saliniteta iz estuarija rijeke Krke, Bilinski i sur. (1991) pokazali su izvanrednu sposobnost samopročišćavanja estuarija. Iako karte raspodjele metala ukazuju na širenje metala uzvodno od izvora onečišćenja, vjerojatno zbog kretanja sloja morske vode, to ne utječe značajnije na udio metala u sedimentima gornjeg dijela estuarija.

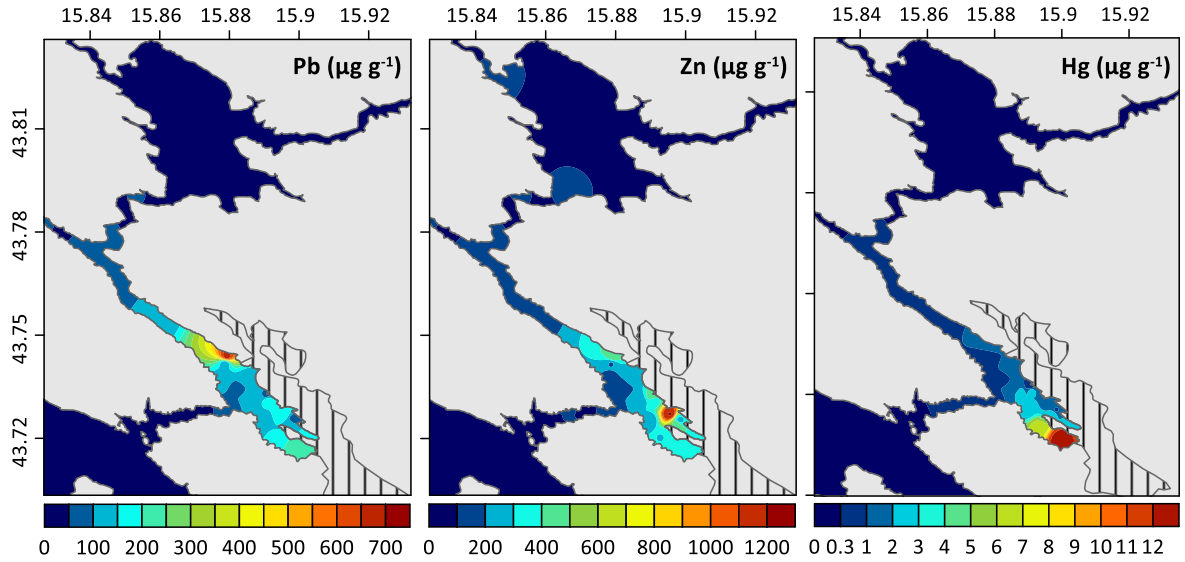

Slika 2. Prostorna raspodjela Pb, Zn i Hg u površinskom sedimentu estuarija rijeke Krke

4.2. Vertikalna raspodjela i dinamika metala u sedimentnim jezgrama estuarija rijeke Krke

Prostornom raspodjelom metala u površinskom sedimentu gornji dio estuarija rijeke Krke okarakteriziran je kao nezagađen. Takav zaključak potvrđen je i analizom sedimentnih jezgri uzorkovanih na početnom dijelu estuarija (K1), u Prokljanskom jezeru (K7) i rijeci Gudučoj (K8). Naime, vertikalna raspodjela metala u navedenim jezgrama uglavnom odražava prirodnu varijabilnost pozadinskih vrijednosti. Značajnije obogaćenje nekim metalom zabilježeno je samo u jezgri K1, gdje su na dva dubinska intervala koncentracije Pb izrazito porasle i mnogostruko premašile pozadinske koncentracije utvrđene u estuariju rijeke Krke, ali i drugim područjima na Jadranu Felja i sur. 2016; Dolenec i sur. 1998). Na temelju brzine sedimentacije od 2 mm/god u ovom dijelu estuarija (Cukrov i sur. 2007), utvrđeno je da prvi koncentracijski maksimum odgovara vremenskom razdoblju 1970-1980, što odgovara periodu 1960-1980 za koji su prijavljeni koncentracijski maksimumi Pb u sedimentima diljem sjeverne hemisfere (Cossa i sur. 2018).

Drugi i izraženiji koncentracijski maksimum najvjerojatnije može biti pripisan industrijalizaciji skradinskog područja krajem 19. stoljeća. Naime, 1887. godine s radom je započela tvornica kalcij karbida, ali proizvodnja prestaje već 1889. godine, kad je tvornica uništena u požaru (Raos 2018). Uočena je varijabilnost među jezgrama u gornjem dijelu estuarija, pa su tako koncentracije elementa koji se često smatraju zagađivalima, kao što su Ni, Cr, Co, Pb, Cu i As, veće u rijeci Gudučoj i Prokljanu nego na skradinskom području. Te razlike nisu posljedica antropogenog utjecaja, već razlike u donosu terigenog materijala rijekom Gudučom i rijekom Krkom. Niski faktori obogaćenja, popraćeni sa značajnom korelacijom s terigenim elementima, potvrđuju prirodno porijeklo navedenih elementa u sedimentu rijeke Guduče i Prokljanskog jezera.

Rezultati analiza jezgri sedimenta iz Šibenskog zaljeva (K20 – TEF, K22 – Istraživačka postaja Martinska, K32 – brodogradilište/marina, K36 – Luka Šibenik) odražavaju dugogodišnji negativni utjecaj grada Šibenika na estuarij. Iako su neki izvori onečišćenja uklonjeni (TEF) ili modernizirani kako bi se smanjilo onečišćenje (Luka Šibenik), nije uočeno značajno smanjenje udjela metala u recentnim sedimentima. Kemijskom analizom troske s područja bivše tvornice, potvrđen je utjecaj tvorničke prašine na povišene koncentracije metala (npr. Mn, Co, As) u okolnom sedimentu. Povišene koncentracije Zn, Hg, Cd, U, Pb i drugih metala na lučkom području mogu se pripisati fosfatnim rudama i umjetnim gnojivima. Na ove dvije lokacije sedimentne jezgre nisu bile dovoljno dugačke da se uzorkuje sediment istaložen prije početka rada onečišćivača. Međutim, u jezgri iz uvale Sv. Petra u kojoj se nalaze marina i remontno brodogradilište jasno je vidljiv početak rada brodogradilišta koji se očituje u naglom porastu udjela brojnih metala (npr. Hg, As, Zn i Cu) u sedimentu, što je potvrđeno i datiranjem jezgre pomoću radionuklida ^{210}Pb i ^{137}Cs.

Sveobuhvatnom analizom estuarijskog okoliša utvrđeno je da je dinamika metala u sedimentu pod dominantom utjecajem procesa razgradnje organske tvari, bilo da se radi o primarnim dijagenetskim redoks reakcijama u sedimentu ili o sekundarnim procesima, koji su izravno ili neizravno povezani s razgradnjom organske tvari. Vertikalni profili redoks senzitivnih metala, hranjivih tvari i produkata rane dijageneze ukazuju na klasičnu redoks stratifikaciju u sedimentu, ali su redoks zone milimetarskih i centimetarskih dimenzija, što upućuje na brzu potrošnju elektron akceptora. Suboksična zona, koja je karakterizirana reduktivnim otapanjem Fe i Mn oksihidroksida, detektirana je u prvim centimetrima ispod granice faza sediment-vodeni stupac. Preciznije, porast koncentracije otopljenog Mn zabilježen je u prva dva centimetra sedimenta na svim mjestima uzorkovanja u estuariju, dok su maksimumi koncentracija otopljenog Fe zabilježeni u istom ili sljedećem (2-4 cm) sloju. Iako je poznato da

Fe i Mn oksihidroksidi mogu adsorbirati veći broj metala, njihovom redukcijom u estuariju rijeke Krke dolazi samo do značajnijih otpuštanja As, odnosno Co u pornu vodu. Maksimumi koncentracija ostalih metala (npr. Pb, Zn, Cu, Ni) zabilježeni su u anoksičnom dijelu sedimentu, u slojevima u kojima je detektiran i sulfid. Ovakvo ponašanje nije uobičajeno, a ukazuje na značajan utjecaj sekundarnih dijagenetskih procesa na mobilnost metala u sedimentu, primjerice kompleksiranje metala s organskim i anorganskim ligandima što može povećati njihovu topivost unatoč prisutnosti sulfida u pornoj vodi. Remobilizacija metala u dubljem dijelu sedimenta može biti i posljedica otapanja manje reaktivnih Fe i Mn oksihidroksida.

Unatoč navedenim odstupanjima, zabilježeno je umjereno obogaćenje nekih elemenata (npr. U, Mo, Cd, Zn, Cu, Mn) u krutoj fazi sedimenta koje se podudara s prisustvom sulfida u pornoj vodi, te se može pretpostaviti da je uočeno obogaćenje rezultat autigenog formiranja minerala. Primjerice, obogaćenje Mo u jezgri K1 može se pripisati promjenama u specijaciji Mo koje se odvijaju u prisutnosti otopljenog sulfida. U oksičnim uvjetima Mo se nalazi u formi ne reaktivnog molibadata ($Mo^{VI}O_4^{2-}$), dok u anoksičnim uvjetima atomi kisika mogu biti zamijenjeni atomima sumpora, stvarajući kompleks $Mo^{VI}O_nS_4^{2-}$ koji se lako veže na Fe minerale i organsku tvar, te na taj način uklanja iz porne vode. Obogaćenje Cd, uočeno u jezgrama K1 i K7, može se pripisati precipitaciji netopivog CdS, do čije formacije dolazi već pri vrlo niskim koncentracijama otopljenog sulfida (Rosenthal i sur. 1995). Izrazito povećanje koncentracije Mn u sloju 4-6 cm jezgre K36 također je vjerojatnije posljedica dijagenetskih reakcija u sedimentu nego povećanog antropogenog unosa. Produkt redukcije Mn oksihidroksida, Mn^{2+}, difundira u dublje slojeve sedimenta gdje može precipitirati iz porne vode u formi čistih ili miješanih minerala karbonata, fosfata ili u manjoj mjeri sulfida (Burdige 1993; Ingri i sur. 2011; Gorny i sur. 2016; Dellwig i sur. 2018).

Za većinu razmatranih elemenata u estuariju rijeke Krke izračunat je negativan bentički difuzni tok, što sugerira da sediment u estuariju djeluje kao izvor metala za pridneni sloj morske vode. Najveći utjecaj difuznog prijenosa metala preko granice faza sediment-vodeni stupac uočen je u gornjem dijelu estuarija gdje su koncentracije Fe i Mn u prvih 15 cm vodenog stupca (gledajući od površine sedimenta) bile i do stotine (Fe) i tisuće (Mn) puta veće od onih zabilježenih u ostatku morskog sloja vodenog stupca. Iako primijećen, utjecaj difuznog toka nije bio toliko izražen u Šibenskom zaljevu. Razlog tome su niže stope zasićenja kisikom u pridnenom sloju gornjeg estuarija, kao posljedica dužeg vremena zadržavanja morske vode. U donjem dijelu estuarija pridnena voda je bogatija kisikom, što dovodi do brze oksidacije i taloženja difundiranih Mn^{2+} i Fe^{2+}.

5. ZAKLJUČCI

Prostorna raspodjela metala u površinskom sedimentu estuarija rijeke Krke istražena je kako bi se procijenilo onečišćenje sedimenta estuarija metalima te utvrdili glavni onečišćivači na području estuarija. Sedimentne jezgre su proučavane kako bi se procijenili povijesni trendovi unosa metala u estuarij i odredili glavni dijagenetski procesi koji kontroliraju mobilnost metala u sedimentu i na granici faza sediment-vodeni stupac. Rezultati se mogu sažeti:

- Prostorna rasprostranjenost terigenih elemenata u površinskom sedimentu estuarija rijeke Krke ukazuje na rijeku Guduču i izvor Litno (Zaton) kao glavne izvore terigenog materijala.
- Sediment gornjeg estuarija nije opterećen metalima, dok je u Šibenskom zaljevu opaženo značajno obogaćenje niza metala u sedimentu kao posljedica antropogenog onečišćenja iz tri glavna izvora: bivše tvornice elektroda i feromangana, Luke Šibenik i remontnog brodogradilišta/nautičke marine. Dobiveni rezultati pokazuju da je onečišćenje metala u donjem estuariju značajnije i raširenije nego što se prethodno smatralo, s koncentracijama nekih metala (npr. Hg, Pb, Zn, Mn, Cd, Cu, As) usporedivim s vrlo zagađenim obalnim područjima i estuarijima Europe. Prema kartama raspodjele metala, nema širenja onečišćenja izvan estuarija prema otvorenom moru, ali dio metala se transportira uzvodno od svog izvora zbog pridnenog kretanja morskog sloja estuarija u tom smjeru.
- Povijest unosa metala u estuarij je zabilježena u sedimentnim jezgrama. Primjerice, porast udjela metala u jezgri uzetoj na području marine/brodogradilišta podudara se s početkom rada brodogradilišta, što je utvrđeno datiranjem jezgre pomoću radionuklida ^{210}Pb i ^{137}Cs. Međutim, ponekad treba biti i oprezan s interpretacijom rezultata, zato što obogaćenje metala u sedimentu može biti i posljedica dijagenetskih reakcija, npr. formiranja sekundarnih Mn minerala, što je slučaj u sedimentu s područja luke Šibenik.
- Vertikalnom raspodjelom metala i drugih produkata rane dijageneze u pornoj vodi estuarija utvrđeno je da je dinamika metala u sedimentu dominantno pod utjecajem procesa razgradnje organske tvari, i to posebice reduktivnog otapanja Fe i Mn oksihidroksida i redukcije sulfata. Iako je opažena klasična dijegentska zonacija sedimenta, debljina zona je reducirana zbog vrlo tankog oksičnog sloja. Povećane koncentracije otopljenih metala u anoksičnoj zoni sedimenta ukazuju na međudjelovanje metala i otopljene organske tvari i/ili sulfida, te otapanje manje reaktivnih Fe i Mn oksihidroksida dublje u sedimentu. Za većinu mjerenih metala, bentički difuzni tok je negativan, što znači da sediment u estuariju predstavlja sekundarni izvor metala za vodeni stupac.

1. INTRODUCTION

1. INTRODUCTION

Estuaries, as transitional zones between marine and terrestrial environments, have been the focal point for a wide variety of human activities and have become sites of major port, industrial, urban, and recreational development (Ridgwaya and Shimmieldb 2002). Owing to the intense anthropogenic pressure, these complex and fragile environments are often subjected to consequent contamination (Kennish 2016). Among the contaminants present in the estuarine environment, trace metals and metalloids (referred to metals hereafter) are ones that pose the highest threat, owing to their toxicity, non-degradable and accumulative properties (Dou et al. 2013; Wang et al. 2014; Zhang et al. 2014). Although, metals are naturally present in the environment, their concentrations have been globally increased because of human activities, e.g. discharges of domestic and industrial effluents, mining and agricultural drainage. Once introduced in the aquatic environment, metals are rapidly and efficiently removed to the sediment via adsorption onto surfaces particles, precipitation, and incorporation into biogenic material (Valdés et al. 2005). However, sediment cannot be observed only as a sink, but also as a possible long-term source from which metals can be released to overlaying water through various biological and physico-chemical processes (Saulnier and Mucci 2000; Tankere-Muller et al. 2007; Cukrov et al. 2011; Duan et al. 2015).

The mobility of metals in the sediments depends greatly on the composition of the sediment (e.g. organic matter, iron and manganese hydroxides/oxides, carbonates, sulphides and clay minerals, etc.) (Ho et al. 2013) and on the physico-chemical conditions in both the sediment and water column (e.g. pH, Eh, salinity, concentration of organic and inorganic ligands) (Ho et al. 2013; Rigaud et al. 2013). Furthermore, the remobilization in sediments is strongly affected by processes occurring during the early diagenesis of sediment: biogeochemical reactions (sorption, precipitation, dissolution) and physical (diffusion, advection) or biological (bioirrigation, bioturbation) transport mechanisms (Santos-Echeandia et al. 2009; Rigaud et al. 2013; Dang et al. 2015; Kalnejais et al. 2015). The microbial degradation of organic matter (OM) below the sediment-water interface (SWI), being a driving force of early diagenesis, is known to strongly impact chemical transformations in the pore water and solid phase of sediments, especially when Fe and Mn oxides and oxyhydroxides (referred to oxyhydroxides hereafter) and sulphates are the terminal electron acceptors (Saulnier and Mucci 2000; Dang et al. 2015; Kalnejais et al. 2015; Duan et al. 2019). During these reactions, metals may be immobilized into the sediment or released to the pore water (Metzger et al. 2007a; Santos-Echeandia et al. 2009; Lesven et al. 2010; Campanha et al. 2012). Generally, when organic

matter is mineralized, the reductive dissolution of Fe and Mn oxyhydroxides occurs and is accompanied by remobilization of associated metals. Subsequently, the dissolved metals diffuse upward and downward along the sediment profile and can be readsorbed onto or coprecipitated with newly formed Fe and Mn minerals (e.g. carbonates, sulphides) (Gao et al. 2006; Rigaud et al. 2013; Dang et al. 2015; Duan et al. 2019) or form insoluble metal sulphide phases when sulphide is produced by sulphate reduction bacteria (Rosenthal et al. 1995; Morse and Luther 1999; Sundby 2006; Kalnejais et al. 2015). On the contrary, the oxidation of sulphides can release dissolved trace metals into pore water (Wang and Wang 2017). The relatively importance of these opposing reactions at the SWI is important for understanding trace metal cycling in the estuarine environment.

Moreover, sediment is a complex system in which metals can be present in both the particulate and the dissolved phase, i.e. in the pore water. The fate and toxicity of metals greatly depend on the partitioning between those two phases, where the fraction of the metal in the pore water is considered to be more bioavailable and toxic (Atkinson et al. 2007; Zhu et al. 2016; Huang et al. 2017). If the concentration of a metal in the pore water is higher than the concentration in the overlying water column, the concentration gradient at the SWI will cause the transport of the dissolved metal from the sediment to the overlying water (Lyons and Fitzgerald 1980; Ciceri et al. 1992; Sakellari et al. 2011; Campanha et al. 2012). The benthic diffusive fluxes of trace metals from sediments to the water column were found to be equal or even exceed riverine influxes in many coastal areas (Rivera-Duarte and Flegal 1997; Williams et al. 1998; Warnken et al. 2001; Santos-Echeandia et al. 2009), confirming the important influence of sediment on the quality of aquatic environment. The distribution schemes of metals in sediment can vary substantial both spatially and seasonally due to the variation of physical, chemical, and hydrological conditions (e.g., pH, temperatures, organic and terrigenous matter fluxes) (Kalnejais et al. 2015; Duan et al. 2019). The mechanisms for determining whether trace metals are permanently buried in sediments or remobilized to the water column under different environmental conditions have not been well established yet (Duan et al. 2019). Although a challenging task, understanding the effects of various environmental conditions on trace metal mobility, bioavailability and toxicity is of critical importance to assess the potential adverse effects of contaminated sediments to the surrounding environment. To achieve this goal, the analysis of the total metal concentrations in the solid fraction of the sediment is not enough. An integrated approach must be applied, where both solid and dissolved phase of the sediments will be analysed, as well as the overlying water.

1.1. Objectives and scope of the work

This study aims to better understand dynamics of metals in the sediment of the stratified karstic estuary, partly exposed to the human pressures. Emphasis will be placed to two main objectives: (i) to evaluate sediment contamination levels by metals and to detect main sources of contamination in the Krka River estuary and (ii) to study the metal dynamics in the sediment column and at the SWI and to assess their potential remobilization to the water column. To achieve the first goal, high resolution spatial distribution maps of metals in the surface sediments of the Krka River estuary will be made, which will enable determination of the extent of pollution by a given metal and detection of the main metal input pathways within the estuary. For the assessment of the state of sediment in the terms of the metal load different sediment quality indices and guidelines will be used, whereas statistical analysis tools will be used to distinguish between the influence of different pollution sources. A comprehensive approach, including the analysis of the dissolved and solid fraction of the sediment, as well as overlying water column should provide means to reach the second objective, i.e. to better understand the dynamics of metal behaviour in the estuarine environment and to quantify metal exchanges at the SWI. In addition to metal analysis in both sediment and water samples, other parameters that may facilitate interpretation of results will be determined, e.g. granulometric and mineralogical composition of sediment and diagenesis tracers (dissolved organic and inorganic carbon, NH_4^+, SO_4^{2-}, ΣHS^-, PO_4^{3-}; $Si(OH)_4$) in the water column.

Due to its unique characteristics, the Krka River and its estuary have been extensively studied over the last several decades, which resulted in numerous published papers on chemical and physical properties of the water column and in lesser extent on sediment characterization. The use of the pore water concentration in determining sediment contamination and in the evaluation of the contribution of sediment to the pollution of the overlying water column is a novelty in a Krka River estuary research. Knowledge of pore water concentrations is, moreover, important for the identification of the main biogeochemical reactions controlling the metal mobility in the sediment. Therefore, pore water analysis will not only give insight into these processes in the Krka River estuary but contribute to knowledge on metal mobility in these transitional environments in general.

2. LITERATURE OVERVIEW

2. LITERATURE OVERVIEW

Estuarine sediments may be derived from various sources such as atmospheric inputs, fluvial inputs, biological activity, and erosion of estuarine margins (Fig. 2.1.). Sources can vary considerably in the different regions of the estuary, with usually biological input being more important in the region of the higher salinity than in the upper estuary where terrigenous input dominate (Bianchi 2007). Owing to the geochemical processes governed by mixing of freshwater and seawater, estuaries are often sinks for land-derived material transported via rivers (Ridgway and Shimmield 2002; Fiket et al. 2017). Namely, suspended particles found in the estuarine water column are highly cohesive and readily flocculate, forming the following composite particles: agglomerates (organic and inorganic matter bound by weak surface tension forces); aggregates (inorganic particles bound by strong inter- and intramolecular forces); and floccules (non-living biogenic material bound by electrochemical forces), whose settling velocities are higher than those of the single small grain size particle. The flocculation processes are affected by salinity, particle size, clay composition, concentration of dissolved organic matter, etc. (Bianchi 2007).

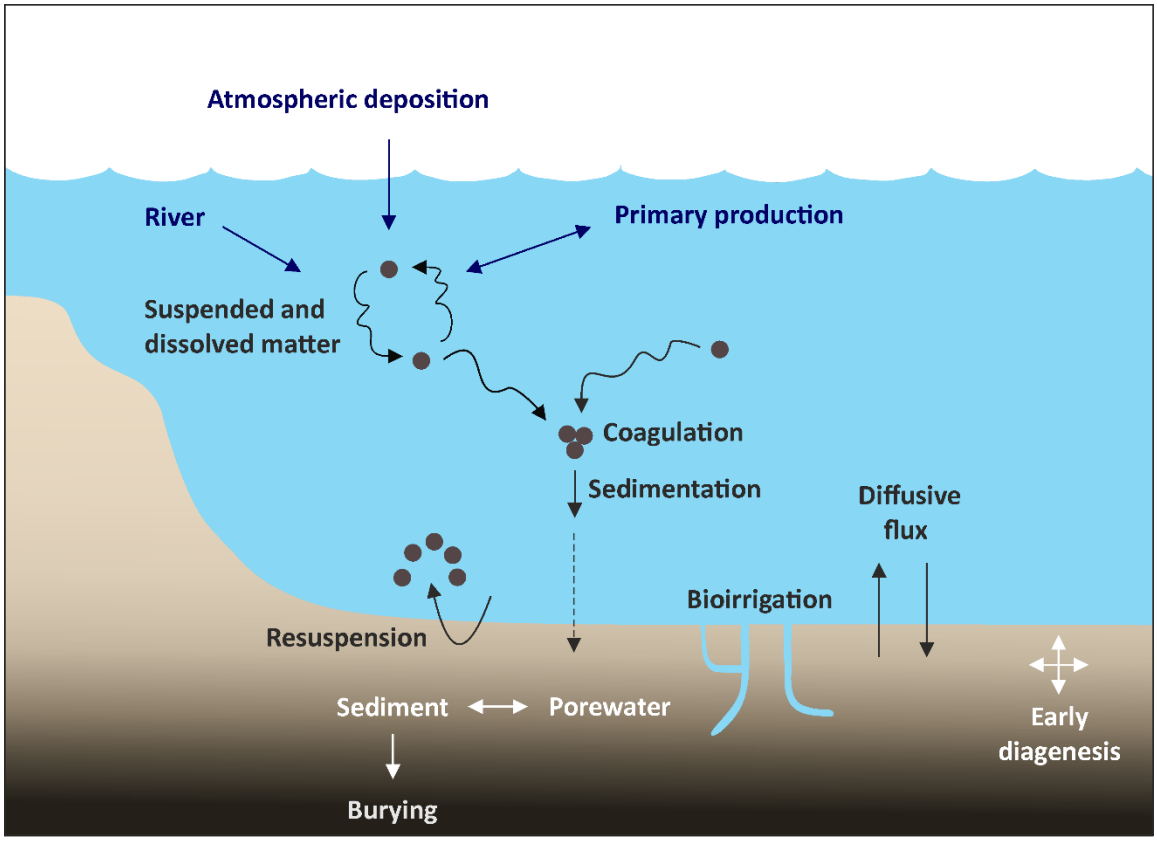

Figure 2.1. Biogeochemical and physical processes in the estuarine water column and at the sediment water interference (modified according to Santschi et al. 1990 and Dang 2014)

As a result of the diverse sources of material, the sediment matrix provides a variety of coexisting phases to which metals may be sorbed, such as organic matter, clay minerals, carbonates or sulphides. Their relative abundances are controlled by pH, redox conditions, and the depositional environment (Burton et al. 2006). Thus, there is a number of factors that influence the mobility of metals in the estuarine environment, including the geochemical and physical properties of sediment and pore water. Furthermore, different post-depositional behaviours mainly related to early diagenetic processes, including dissolution of metal-bearing phases and precipitation of authigenic phases through organic matter mineralization, affect the metal dynamic in these complex environments (Audry et al. 2010).

2.1. Sorption mechanism

The behaviour and fate of metals is to a large extent determined by their chemical form of occurrence. Generally, in the sediment metals may be present as water-soluble metals (free ions and/or complex with organic and inorganic ligands) or in association with solid fraction (adsorbed on clay surfaces or Fe and Mn oxyhydroxides, complexed with organic matter, bound within the crystalline lattice structure of primary minerals such as silicates) (Du Laing et al. 2008; Peng et al. 2008). As a result, the mobility of metals in sediment is affected by numerous processes, from which the most important is the partitioning of metals between the solid (particle) and the aqueous phase (pore water). The partitioning of metals in sediments will depend on many variables, such as pH, redox potential, nature and concentration of solid substrates, nature and concentration of ligands. However, pH is regarded as the most important control of metal partitioning (Tessier and Campbell 1987; Smith 1999).

The term sorption refers to the transition of metal ions from solution to a solid phase and is used when the exact mechanism of metal removal from solution is unknown (Smith 1999; Bradl 2004). This term covers three processes: (i) adsorption, by which substances accumulate at the contact of the dissolved and solid phases; (ii) surface precipitation, new phase growth on the particle surface and (iii) absorption, incorporation of metal ions into the particle structure (Sposito 1987; Honeyman and Santschi 1988; Bradl 2004).

Reactions occurring at the interface of solid surface with their surrounding aqueous medium originate from the fact that solids carry a surface charge in aquatic environments and thus attract counter-ions from solution to balance their charge (Warren and Haack 2001). According to Stumm and Morgan (1996) there are three principal origins of surface charge: (1) chemical

reactions at the surface of the particle; (2) crystalline imperfections, broken bonds, and isomorphous replacements within the crystal lattice and (3) sorption of a surface-active ion. When the charge is caused by lattice imperfections and/or nonstoichiometric isomorphous substitution of cations within the lattice, the charge is independent of the surrounding solution composition and is termed ″constant surface charge″. This type of charge is characteristic for clay minerals, where charge imbalance is resulting from the isomorphous substitution of Al^{3+} for Si^{4+} in the tetrahedral layers and/or substitution of Mg^{2+}, Fe^{2+}, etc. for Al^{3+} in the octahedral layers (McLean and Bledsoe 1992). The surface charge that develops as a result of the dissociation of the ionizable functional groups (e.g. -OH, -COOH, $-NH_2$) that can be found at the surfaces of the hydrous metal oxides, organic matter and edges of the clay minerals is dependent on the composition of the surrounding solution, thus it is generally known as ″variable surface charge″ (Smith 1999). In the presence of water these surface groups have ability of accepting or giving out protons, depending on their surroundings. These proton exchange reactions for surface functional groups may be expressed as:

$$S - OH \leftrightarrow S - S - O^- + H^+$$

$$S - OH + H^+ \Leftrightarrow S - OH_2^+$$

where S – OH is a surface binding site, and $S – OH_2^+$ and $S – O^-$ are proton-exchange surface complexes. Surfaces are thus negatively charged at high pH, subsequently they may act as a binding site for positively charged ions such as metals. At low pH, due to the association of the additional protons, surfaces become positively charged. Therefore, mineral solid surfaces behave like amphoteres (Bourg 1988; Warren and Haack 2001). The pH at which the overall surface charge is equal to zero is called the point of zero charge (PZC). For example, the reported PZC for goethite range from pH 6 to 7, whereas for birnessite range from pH 1.5 to 2.8 (Smith 1999).

The term adsorption generally refers to a specific form of sorption where sorbate accumulate at the interface between an aqueous solution and a solid adsorbent phase without the development of a three-dimensional molecular arrangement. There are two basic mechanism of adsorption: (1) non-specific, physical or outer-sphere adsorption and (2) specific, chemical, or inner-sphere adsorption. By the specific adsorption or surface complexation, metal is bound directly to functional groups on the mineral surface in the form of inner-sphere complex. Surface complex formation of cations by hydrous oxides involves the coordination of the metal ions with the

oxygen atoms and the release of protons from the surface, the reactions may be expressed as (Stumm 1992):

$$S - OH + M^{2+}(aq) \leftrightarrow S - OM^{+} + H^{+}$$

$$2S - OH + M^{2+}(aq) \leftrightarrow (S - O)_2M + 2H^{+}$$

This type of bonding takes place at the edges of clay minerals and metal oxides and oxyhydroxides. Specifically, adsorbed metal cations are considered to be relatively immobile and unaffected by high concentrations of the major cations due to large differences in their energies of adsorption (McLean and Bledsoe 1992). In contrast, non-specific adsorption or cation exchange is a form of an outer-sphere complexation in which the metal and surface species are attracted by electrostatic forces alone. The bond between the adsorbed ion and the particle surface is weak, and thus, metals are easily remobilized once when environmental conditions change (Warren and Haack 2001). The outer-sphere adsorption can be expressed by following reaction:

$$SOH + M^{2+}(aq) \leftrightarrow SOHM^{2+}(aq)$$

where SOH represents a surface hydroxyl site and M^{2+} represents a fully hydrated (waters omitted for clarity), divalent aqueous metal ion (Bradl 2004).

When the amount of the metal sorbed to surface increases, sorption can proceed from mononuclear adsorption to surface precipitation. Therefore, this type of sorption involves the growth of a new solid phase on the particle surface, which repeats itself in three dimensions and forms a 3D network (Apak 2002; Bradl 2004). There is often continuum between surface complexation (adsorption) and surface precipitation, where the contribution of surface precipitation to the overall sorption increases as the sorbate/sorbent ration increases (Sposito 1984). Apart from the relative quantities of metals and anions present, the pH has a substantial impact on the surface precipitation. The surface precipitation may be described by reaction (Farley et al. 1985; Bradl 2004):

$$S - O - MeOH_2^{+} + Me^{2+} + H_2O \leftrightarrow S - O - MeOH_2^{+} + Me(OH)_{2(s)} + 2H^{+}$$

Where Me^{2+} is a metal cation and S-O-$MeOH_2^{+}$ is a surface complex of metal Me and surface S, i.e., the adsorbed metal become a surface site itself. Depending on the environmental

conditions, metals can precipitate on the surface of the particles as oxides, hydroxides, carbonates, sulphides and phosphates.

The third principal mechanism of sorption involves the diffusion of an aqueous metal species into the solid phase and it is termed absorption. Like surface precipitation or coprecipitation, this type of sorption mechanism is three-dimensional in nature. An example of absorption is the diffusion of the metals that are specifically adsorbed onto secondary minerals such as clay minerals and metal oxides into the lattice structures of these minerals. These metals slowly become fixed into the pore spaces of mineral structure, thus the process is sometimes referred to as solid-state diffusion. Unlike adsorption, which is relatively reversible, in order to release absorbed metals to the environment, the total dissolution of the particles in which they are incorporated may be required (Apak 2002; Bradl 2004).

2. 2. Factors controlling the speciation and distribution of metals in sediment

2.2.1. pH

The pH, as a factor which dictates cation and anion partitioning between dissolved and solid fraction, is often considered to be the master variable controlling metal behaviour in aquatic environments (Warren and Haack 2001). Generally, high pH values promote adsorption of metals to the surface of both organic and inorganic particles. The exception to this trend may occur in competitive systems in which metals coexist in solution with some complexing substances, e.g. dissolved organic matter. Apart from these special cases, as pH increases in sediment, the adsorption of metal cations to particles increases as a result of the decreased competition with protons. This change in adsorption efficiency, where the proportion of metals bound to the particles increases from near zero to 100%, typically occurs over a very narrow pH range that is often referred to as the adsorption edge (Helios-Rybicka and Förstner 1986; Smith 1999; Benjamin and Lawler 2013). The position of this edge with respect to pH may vary for different metals on the same adsorbent, which generally reflects different affinities of the metals for surface sites or different sorption mechanism. For a given metal cation sorbing on different solid phases, the pH range of adsorption edge typically differs because of different surface charge properties and different surface sites (Reeder et al. 2006). In addition, the position of the adsorption edge depends on adsorbent concentration (Helios-Rybicka and Förstner 1986).

There is a variety of biogeochemical processes that influence pH values in sediment, increasing or decreasing free proton concentrations in pore water. The majority of these processes are linked to cycles of carbon, oxygen, nitrogen, phosphate, silicate, sulphur, iron and manganese and are associated with processes such as heterotrophic respiration, photosynthesis, precipitation, and dissolution of calcium carbonate. In addition, many of these reactions influencing the pH in sediment are redox sensitive or linked to reduction or reoxidation cycles. For example, the oxic mineralization and the oxic reoxidation of reduced substances (e.g. Fe^{2+}, Mn^{2+}) reduce pH in sediment, causing a decrease in pore water pH below the SWI. Generally, pH reaches its minimum at the oxic-anoxic transition zone. In the suboxic zone, pH often increases due to the influence of Mn and Fe oxyhydroxide reduction (Soetaert et al. 2007). However, due to the number of processes that have a profound effect on the pH in sediments, temporal and spatial changes in site specific conditions (e.g. permeability, grain size distribution) and disturbances of the biogeochemical zones in sediment due to the natural (e.g. bioturbation, storm event) or anthropogenic (e.g. dredging, trawling) impacts, there is a variability in pH profiles in sediment and it is often a challenging task to interpret observed pH profile (Silburn et al. 2017).

2.2.2. Redox potential

It is generally accepted that oxidation–reduction potential (redox potential), along the pH, is another very important factor controlling the mobility of metals in the sediment (Peng et al. 2009; Zhang et al. 2014). Redox potential is defined as a measure for the electron availability and its measurement allows the prediction of the stability and availability of various metals in sediment. It evolves from high to low when the redox status of the sediment changes from aerobic to anaerobic conditions (Du Laing et al. 2009). Based on the oxygen content, the redox zones in the sediment are divided vertically into: (i) the oxic (oxygen reduction), (ii) the suboxic (nitrate, manganese, and iron reduction) and (iii) the anoxic (sulphate reduction and methanogenesis). The differences between these zones are important in terms of the metal mobility and bioavailability and will be described in more detail in the Section 2.3.1.

In anaerobic sediments, the mobility of the divalent metals (e.g. Cd, Cu, Pb, Zn) is determined by their bound to sulphide minerals. With the increase of the redox potential in the sediment, an increase in the oxidation rate of sulphides and the degradation of the organic matter will

occur, thus promoting the release of adsorbed and complexed metals. The reaction can be expressed as:

$$MS_2 + \left(\frac{15}{4}\right)O_2 + \left(\frac{7}{2}\right)H_2O \rightarrow M(OH)_3 + 2SO_4^{2-} + 4H^+$$

The release of H^+ ions into pore water reduces the pH of the sediment, causing a secondary release of metals. A portion of the released metals will be readsorbed, especially onto the more labile binding fractions (Kelderman and Osman 2007; Peng et al. 2009). Consequently, seasonal variations of the redox potential in sediment may cause seasonal differences in release and fixation of the metals in the sediment (Peng et al. 2009).

Elements that are sensitive to changes in redox conditions are called redox-sensitive elements, such as Fe, Mn, As, Cr, Cd, Mo and U. They can undergo changes in oxidation state under common environmental conditions, often resulting in changes in solubility because of the formation of new compounds (Weiner 2008). Generally, metals are less soluble in their higher oxidation state, while solubility of the metalloids depends on both the oxidation state and the ionic form (Ross 1994). For example, under oxidative conditions, Fe and Mn will be present in the form of oxides and oxyhydroxides (Fe^{III}, Mn^{III}/Mn^{IV}), while in more reductive conditions they will be present in the dissolved form as Fe^{2+} and Mn^{2+}. These dissolved Fe^{2+} and Mn^{2+} may precipitate out of the sediment pore water as sulphide, carbonate or phosphate phases (Burdige 1993). Unlike Mn and Fe, Cr is highly mobile in its higher oxidation state Cr^{VI}, whereas Cr^{III} tends to precipitate and/or be adsorbed onto minerals and accumulate within sediments in reducing conditions (Gorny et al. 2016).

2.2.3. Salinity

Alongside pH and redox potential, in estuaries the salinity is another controlling factor for the partitioning of contaminants between sediments, overlying and pore water and all the three are the key-variables to control the bioavailability and the toxicity of metals bound to sediments (Chapman and Wang 2001; Riba et al. 2003).

Desorption of some metals from sediment may increase with increasing salinity due to complexation of metals (e.g. Cd) with seawater anions (Cl^- and SO_4^{2-}) forming soluble inorganic complexes and/or increasing competition for particle sorption sites with seawater

cations (Na^+, K^+, Ca^{2+}, Mg^{2+}) displacing both weakly and moderately sorbed metals such as Cr, Cu, Zn and Pb (Chapman and Wang 2001; Du Laing et al. 2009; Machado et al. 2016).

2.2.4. Oxyhydroxides

Iron and manganese oxyhydroxides play an important role in the biogeochemical cycle of many elements, including carbon, sulphur, phosphorus and some trace elements (Burdige 1993). They are considered as main sorbents of metal cations in sediment due to their charged, reactive hydroxyl surface sites and their high specific surface area (Dzombak and Morel 1987). The sorption is governed by the physicochemical properties of the oxyhydroxide minerals (chemical composition, structural morphology, specific surface area, mineral surface charge) and environmental conditions (pH, temperature, presence of competitive ions) (Warren and Haack 2001; Nia 2011; Heyden and Roychoudhury 2015). As already explained in Section 2.2.1., sorption is strongly pH-dependant, due to the pH-dependant surface charge. The surface is negatively charged when pH exceeds the PZC, and inversely, positively charged when pH is less than PZC (Dzombak and Morel 1987). The PZC values for Fe oxyhydroxide minerals are found in range 7 to 9 (Smith 1999; Violante et al. 2010), while Mn oxyhydroxides mostly have a very low PZC, usually in the range 1.5 to 4.6 (Tan et al. 2008).

Moreover, the mobility of metals is controlled by reduction and oxidation of the Fe and Mn oxyhydroxides. The association of some elements with oxyhydroxides is well know from the literature, e.g. Fe oxyhydroxides are commonly associated with As, Cu, Ni, Mn, and Zn, while Mn oxyhydroxides commonly contain Co, Fe, Ni, Pb, and Zn. By the precipitation of the Fe and Mn oxyhydroxides these elements may be removed from solution, while reductive dissolution of oxyhydroxides in anoxic environments results in release of these metals into pore water (Vesper 2012, Chen et al. 2013).

2.2.4.1. Fe oxyhydroxides

In sediment, under the oxic conditions, ferric iron is the thermodynamically favourable oxidation state and predominantly forms highly insoluble ferric oxide, hydroxide and oxide hydroxide mineral phases. These are often collectively referred to as oxyhydroxides and can be found as discreet crystals or as coatings on other mineral phases, most commonly clay minerals (Heyden and Roychoudhury 2015). Frequently, they precipitate as very small particles with

high associated surface area to volume ratios, what makes these minerals highly reactive (Warren and Haack 2001). Due to their high surface reactivity, their ubiquity and redox activity, Fe oxyhydroxides are known to have a strong control on the chemical properties of sediment, as well as on the metal behaviour and mobility (Heyden and Roychoudhury 2015). The most abundant Fe oxyhydroxides in sediments are hematite (α-Fe_2O_3), goethite (α-FeOOH) and ferrihydrite ($Fe_5HO_8 \cdot 4H_2O$), which is poorly ordered and will transform with time into a more stable member of the Fe oxyhydroxide group. Other Fe oxyhydroxides that can be found in sediment are lepidocrocite (γ-FeOOH), akageneite (β-FeOOH) and magnetite (Fe_3O_4) (Burdige 1993; Warren and Haack 2001; Heyden and Roychoudhury 2015).

2.2.4.2. Mn oxyhydroxides

When referring to Mn oxides or oxyhydroxides in sediment, the MnO_x formula is generally used, although there are other cations in the crystal lattice of these minerals. The above formula is non-stoichiometric because $x > 1$, and usually < 2. Manganese oxides and oxyhydroxides are generally thought to be amorphous or poorly crystalline forms and are often found as coatings on inorganic (e.g. clays) or biogenic (e.g. siliceous test) particles (Burdige 1993). It has been demonstrated that Mn oxyhydroxides are efficient scavengers of metals and are potentially more reactive than Fe oxyhydroxides (Warren and Haack 2001). Unlike Fe oxyhydroxides, whose oxidation may be linked to abiotic processes, the oxidation of Mn is thought to be a biologically controlled process (Sunda and Kieber 1994; Emerson 2000; Warren and Haack 2001). The most abundant Mn oxyhydroxides in the sediment are todorokite [$(Na,Ca,K)_2(Mn^{4+},Mn^{3+})_6O_{12}\cdot 3\text{-}4.5H_2O$)], birnessite $(Na,Ca,K)(Mg,Mn^{2+})Mn_6O_{14} \cdot 5H_2O$ and vernadite [$(Mn^{4+},Fe^{3+},Ca,Na)(O,OH)_2 \cdot n(H_2O)$] (Burns and Burns, 1981).

2.2.5. Organic matter

In aquatic environments there is a variety of solids other than minerals such as Fe and Mn oxyhydroxides that may be geochemically important substrates for metal transport, capture and fate. In particular, organic matter and bacteria are known to be effective scavengers of metals, thus having a strong impact on the metal behaviour in the sediment and representing a significant component of aquatic system (Warren and Haack 2001). There is a variety of organic matter sources in the aquatic environments, including autochthonous (e.g. organic matter

produced by primary production in the water column) and allochthonous (e.g. terrigenous organic matter transported from the land by wind, glaciers or rivers) (Rullkötter 2006). As a result, sedimentary organic matter is a heterogeneous and complex mixture of particles and molecules with a wide range of chemical and physical properties (Baldock et al. 2004; Pedrosa-Pàmies et al. 2015). The organic matter derived from primary production, i.e. phytoplankton debris, is composed predominantly of proteins (amino acids), carbohydrates (sugars), and lipids (Burdige 2007), whereas terrigenous organic matter is mainly composed of humic substances. This natural polymeric material, which arises from the chemical and biological degradation of plant and animal residues, is considered to be a major organic component of sediments (Whitby and Schnitzer 1978). The main compounds of the humic substances are the alkali-soluble humic (higher-molecular weight fraction) acid and the alkali- and acid-soluble fulvic acid (low-molecular weight fraction) (Whitby and Schnitzer 1978; Theng 1979). As both fulvic and humic acids originate from the degradation of the terrestrial organic matter, their types and concentrations in the aquatic environment will be highly dependent on the nature of the basin draining soils (Warren and Haack 2001). Important characteristics of all humic substances are their ability to form stable complexes with metal ions and hydrous oxides and to interact with clays and hydrophobic organic compounds (Whitby and Schnitzer 1978). The extent of interactions between the organic matter and mineral particles increases with decreasing particle size in accordance with an increased area of reactive mineral surfaces and the presence of multivalent cations in the cation exchange complex and various oxides and hydroxides (Baldock et al. 2004).

On contrary to the Fe and Mn oxyhydroxides that possess only one type of functional group (hydroxile), organic compounds are characterized by varying quantities of a number of different types of surface functional groups (e.g. carboxyl, phenolic, carbonyl). Due to the different functional groups that they possess, organic and bacterial surfaces can deprotonate at broad range of pH, from low (carboxyl pH ~3-5) to high (phenolic pH ~10). Therefore, the organic surfaces are always negatively charged in the pH ranges of the natural systems and demonstrate a high affinity for positively charged solid surface (Warren and Haack 2001). Although metals sorbed by organic matter are considered to be stable and more tightly bound than those to oxyhydroxides, over time they may be released back into solution as a result of the organic matter degradation (Warren and Haack 2001; Zhang et al. 2014). The process of organic matter mineralization (degradation) has a strong impact on biogeochemical dynamics in sediment, thus it will be described in more details in the following Section (2.3.1.).

2.3. Processes affecting the mobility and distribution of metals in sediment

2.3.1. The organic matter mineralization

Most of the biogeochemical processes occurring in the coastal and estuarine sediments during early diagenesis are directly or indirectly connected with the organic matter mineralization. This process controls the recycling of inorganic carbon, nutrients and electron-donor elements used by bacterial activity to oxidize the organic matter (O_2, N, Mn, Fe, S) (Arndt et al. 2013; Dang et al. 2015). Moreover, it affects the post-depositional mobilization of metals through the secondary processes, such as complexation of metals with dissolved organic and inorganic ligands, modification of surface properties of adsorptive particles, and formation and dissolution of metal precipitates (van den Berg et al. 2000).

In general, only a small fraction of the organic matter from the water column reaches the sediment surface and of which a small part is incorporated into the sediment, becoming the driving force for the early diagenesis processes (Schulz 2006). The settled organic matter provides food for the benthic communities, either at the sediment surface or upon burial into the sediment layers below (Jørgensen et al. 2019). The organisms decompose organic matter via multiple enzymatic reactions, involving different oxidants as well as a number of intermediate compounds. The terminal electron acceptors are utilised in sequential order O_2, NO_3^{2-}, Mn(IV), Fe(III) and SO_4^{2-}, and finally the organic matter itself [$(C^{IV}H_2O)_n$] (Arndt et al. 2013; Pennafirme et al. 2015). The order is based on the thermodynamics of the process and the free energy yield (Stumm and Morgan 1970; Froelich et al. 1979; Berner 1980; Vidal-Dura et al. 2018). The sequence of diagenetic reactions with the corresponding standard Gibbs free energies is given in the Table 2.1., while the schematic representation of the classical biogeochemical zonation with idealised pore water profiles of relevant dissolved species is shown in Fig. 2.2.

The aerobic respiration is the first step of organic matter degradation below the SWI, according to the reaction:

$$CH_2O + O_2 \rightarrow CO_2 + H_2O$$

In the coastal sediments, oxic zone is often limited to a thin uppermost layer, extending in only top few millimetres or centimetres of the surface sediment. The oxygen penetration depth is regulated by the balance between downward transport (molecular diffusion, advection induced

by bioturbation) of oxygen from above and by consumption processes of all benthic organisms and their metabolic products within the sediment (Cai and Sayles 1996; Kristensen 2000).

The oxidized zone that extends just below the upper oxic zone in sediments is frequently referred to the 'suboxic zone' (Froelich et al. 1979). In the suboxic zone processes of dentification and Mn/Fe oxyhydroxides occur. In the sediment, organic matter is a source of nitrogen. In simplified terms, organic nitrogen is converted to ammonium by hydrolysis, which in the presence of bacteria is oxidized to nitrites and then nitrates. In reducing conditions, which usually prevail in sediment, denitrifying bacteria reduce nitrates to gaseous nitrogen. The reduction of nitrate is accompanied by the oxidation of organic carbon according to the reaction:

$$5CH_2O + 4NO_3^- \rightarrow 2N_2 + 4HCO_3^- + CO_2 + 3H_2O$$

The process of denitrification is induced by the diffusive or advective transport of nitrate from lower part of the oxic zone where nitrification occurs or by the supply from overlying bottom water by means of bioturbation, bioirrigation, and diffusion (Seitzinger 1988; Hulth et al. 2005; Hensen et al. 2006). Moreover, other factors may influence denitrification, e.g. temperature, oxygen concentration and availability of organic matter. The process may be reduced at high sulphate reduction rates because low sulphide concentrations completely inhibit nitrification which in turn is necessary for denitrification (Seitzinger 1988).

In or below the zone of nitrogen reduction, Mn oxides and oxyhydroxides are reduced, resulting in accumulation of dissolved Mn^{2+} in the pore water. The reaction can be expressed as:

$$CH_2O + 3CO_2 + 2H_2O + 2MnO_2 \rightarrow 2Mn^{2+} + 4HCO_3^- + H_2O$$

The dissolved Mn^{2+} diffuse toward the SWI, where Mn^{2+} is reoxidized and precipitates as authigenic Mn oxyhydroxides which can subsequently be used in diagenetic processes (Schulz et al. 2006). As reaction with oxygen is not always complete, in some active sediments, Mn^{2+} can escape across the sediment unoxidized, across the SWI into the overlying water column (Thamdrup et al. 1994). Moreover, dissolved Mn^{2+} often extends deep into anoxic sediments, where its removal is mostly controlled by carbonate saturation and precipitation (Canfield and Thamdrup 2009).

Table 2.1. Sequence of organic matter degradation with the corresponding standard Gibbs free energies according to simplified (Jørgensen 2006) and more realistic (Schulz 2006) reaction expressions

	Diagenetic reactions with ΔG° (Schulz 2006)	Diagenetic reactions with ΔG° (Jørgensen 2006)
Oxic zone	**Respiration** **-3190 kJ mol^{-1}** $(CH_2O)_{106}(NH_3)_{16}(H_3PO_4) + 138\ O_2 \rightarrow 106\ CO_2 + 16\ HNO_3 + H_3PO_4 + 122\ H_2O$	**Respiration** **-479 kJ mol^{-1}** $(CH_2O) + O_2 \rightarrow CO_2 + H_2O$
Suboxic zone	**Manganese oxide/hydroxide reduction** **-3090 kJ mol^{-1}** $(CH_2O)_{106}(NH_3)_{16}(H_3PO_4) + 236\ MnO_2 + 472\ H^+ \rightarrow 106\ CO_2 + 236\ Mn_2^+ + 8\ N_2 + H_3PO_4 + 366\ H_2O$ **Denitrification** **-2750 kJ mol^{-1}** $(CH_2O)_{106}(NH_3)_{16}(H_3PO_4) + 84.8\ HNO_3 \rightarrow 106\ CO_2 + 42.4\ N_2 + H_3PO_4 + 148.4\ H_2O$ **Iron oxide/hydroxide reduction** **-1410 kJ mol^{-1}** $(CH_2O)_{106}(NH_3)_{16}(H_3PO_4) + 212\ Fe_2O_3 + 848\ H^+ \rightarrow 106\ CO_2 + 424\ Fe^{2+} + 16\ NH_3 + H_3PO_4 + 530\ H_2O$	**Denitrification** **-453 kJ mol^{-1}** $5(CH_2O) + 4\ NO_3^- \rightarrow 2\ N_2 + 4\ HCO_3^- + CO_2 + 3\ H_2$ **Mn oxide/hydroxide reduction** **-349 kJ mol^{-1}** $5(CH_2O) + 3\ CO_2 + H_2O + 2\ MnO_2 \rightarrow 2\ Mn^{2+} + 4\ HCO_3^-$ **Fe oxide/hydroxide reduction** **-114 kJ mol^{-1}** $(CH_2O) + 7\ CO_2 + 4\ Fe(OH)_3 \rightarrow 4\ Fe^{2+} + 8\ HCO_3^- + H_2O$
Anoxic zone	**Sulphate reduction** **-380 kJ mol^{-1}** $(CH_2O)_{106}(NH_3)_{16}(H_3PO_4) + 53\ SO_4^{2-} \rightarrow 106\ CO_2 + 53\ S^{2-} + 16\ NH_3 + H_3PO_4 + 106\ H_2O$	**Sulphate reduction** **-77 kJ mol^{-1}** $2(CH_2O) + SO_4^{2-} \rightarrow H_2S + 2\ HCO_3^-$
Methanogenesis zone	**Methanogenesis** **-350 kJ mol^{-1}** $(CH_2O)_{106}(NH_3)_{16}(H_3PO_4) \rightarrow 53\ CO_2 + 53\ CH_4 + 16\ NH_3 + H_3PO_4$	**Methanogenesis** **-136 kJ mol^{-1}** $4\ H_2 + HCO_3^- + H^+ \rightarrow CH_4 + 3\ H_2O$

After consumption of nitrate and Mn oxyhydroxides, oxidation continues by Fe oxyhydroxides reduction:

$$CH_2O + 7CO_2 + 4Fe(OH)_3 \rightarrow 4Fe^{2+} + 8HCO_3^- + 3H_2O$$

Analogue to Mn oxyhydroxide reduction, Fe oxyhydroxide reduction results in accumulation of dissolved Fe^{2+} in the pore water and its diffusion towards the SWI and deeper into the sediment. In most of the sediments, the upper boundary of the Fe^{2+} accumulation zone is controlled by reaction with Mn oxyhydroxide and nitrate, rather than oxygen. Hence, Fe^{2+} typically accumulates bellow the zones of nitrate and Mn oxyhydroxide reduction (Burdige 1993; Canfield and Thamdrup 2009). Into the deeper sediment, Fe^{2+} diffusion is limited by the coprecipitation with sulphide, carbonate and phosphate phases (Burdige 1993).

Bellow the suboxic zone, bacterial reduction of sulphate to hydrogen sulphide is the main pathway of organic matter mineralization and might account for up to 50% of organic matter mineralization in most continental shelf sediments. Reaction can be described by the following equitation:

$$2CH_2O + SO_4^{2-} \rightarrow HS^- + 2HCO_3^- + H^+$$

Due to its high concentration in seawater (~28 mM), sulphate diffuses meters down into sediment and supplies the sulphate reducing microorganisms with an electron acceptor for their respiration. Other sulphur species, such as elemental sulphur (S^0) and thiosulphate ($S_2O_3^{2-}$), can also serve as the electron acceptor (Bak and Pfenning 1987; Kramer and Cypionka 1989; Jørgensen 2019), but there are not of similar quantitative importance as sulphate (Jørgensen and Kasten 2006).

The upper boundary of the main sulphate reduction zone is defined by depletion of the energetically more favourable electron acceptors (oxygen, nitrate, Mn and Fe oxyhydroxides). These oxidants are rapidly depleted in the coastal sediments with high organic sedimentation, resulting in the start of the sulphate reduction zone already a few cm below the SWI. Nevertheless, sulphate reduction occurs even in the upper sediment layers, which are geochemically characterized by manganese and iron reduction. The sulphide produced in these partially oxidized zones is rapidly reoxidized.

Although a vast amount of sulphide is produced in coastal sediments through sulphate reduction, the sulphide may be undetectable if there is a high concentration of ‘reactive’ Fe in the sediment, causing an immediate reaction of sulphide with Fe and precipitation of Fe

sulphides. The precipitated authigenic minerals, e.g. pyrite (FeS_2), mackinawite (FeS1-x) and greigite (Fe_3S_4) are important sinks for iron and sulphur as well as for trace metals and play an important role in the global cycles of these elements. These reduced sulphur compounds may be buried in the sediment or transported up to the oxidized sediment layers by bioturbation, where they are subsequently reoxidized to sulphate.

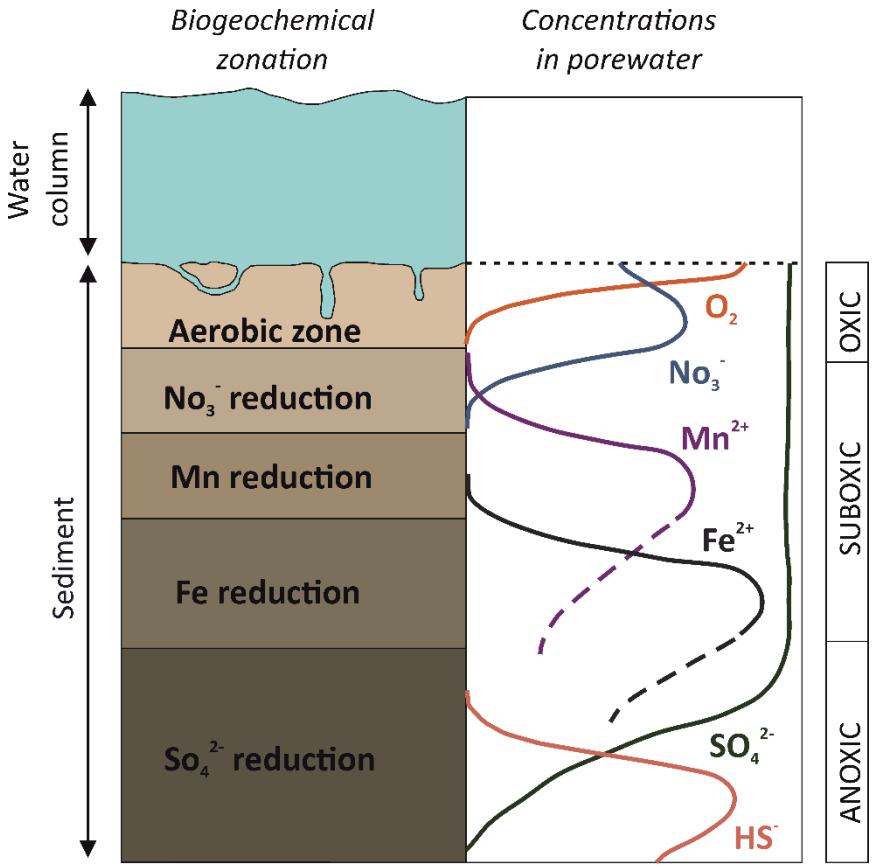

Figure 2.2. The schematic representation of the classical biogeochemical zonation in marine surface sediment with the idealised pore water profiles of oxidized compounds (electron acceptors)

The sulphur cycle in the sediment may also impact the cycle of barium via mineral barite ($BaSO_4$). In the sediments where sulphate reduction had led to the total depletion of pore water sulphate, barite becomes undersaturated and thus prone to dissolution. Dissolved barium diffuses upwards and reprecipitates as so-called authigenic or diagenetic barite, slightly above the sulphate penetration depth. The mobilization and precipitation of authigenic barite nevertheless may occur in the suboxic environments where sulphate reduction takes place, but pore water is not completely depleted in SO_4^{2-} (McManus et al. 1998; Griffith and Paytan 2012).

Although barite is often used as a geochemical tracer or archive for palaeoceanographic reconstructions, the formation of authigenic barite can obscure the primary record, consequently, lead to wrong interpretations (Jørgensen and Kasten 2006).

The last stage in the sedimentary degradation of the organic matter is methanogenesis, a process in which a group of strictly anaerobic archaea produce methane from a small number of different low-molecular-weight substances (e.g. acetate) and from the reduction of CO_2 by hydrogen:

$$CH_3COO^- + H^+ + \rightarrow CH_4 + CO_2$$

$$CO_2 + 4H_2 \rightarrow CH_4 + 2H_2O$$

In the marine sediments, this process occurs at higher depths, where all sulphate has been consumed (Rullkötter 2006).

Most of the methane produced through methanogenesis diffuses upwards until it reaches the lower sulphate zone where it is efficiently converted to carbon dioxide (CO_2) by anaerobic oxidation coupled to sulphate (SO_4^{2-}). Within this reaction zone, known as sulphate-methane transition zone (SMTZ), pore water methane and sulphate both are consumed to depletion (Jørgensen and Kasten 2006; Rullkötter 2006).

However, in the coastal and estuarine sediments, these organic matter degradation zones are not normally well delineated, and they can be overlapped because sediment profiles are often disturbed by mixing (bioturbation and/or resuspension) (Aller et al. 1994; Canfield and Thamdrup 2009; Vidal-Dura et al. 2018).

2.3.2. Resuspension of sediment

Sediment resuspension events in coastal and estuarine environments can occur due to natural processes, such waves, tides, and storms or be induced by human activities, such as dredging, trawling and shipping traffic. Regardless of whether resuspension is caused by natural or anthropogenic activities, it has the capacity to remobilise contaminated sediments and release contaminant from the sediment and pore water to the water column (Eggleton and Thomas 2004). In terms of the trace metals mobilization, resuspension of the anoxic sediment is more important than resuspension of oxic and suboxic sediments (Saulnier and Mucci 2000). Remobilization of metals depends on the magnitude and duration of the resuspension event, on

the characteristics of the sediments (e.g. grain size, organic carbon content), on the metal distribution, and on the physico-chemical conditions prevailing during the resuspension (pH, redox potential) (Cantwell et al. 2002; Ciffroy et al. 2019).

Furthermore, both the laboratory and in situ resuspension experiments demonstrated the influence of the several kinetics release (desorption/dissolution) and uptake (adsorption/(co)precipitation) processes from/to the suspended particles on the metal remobilization. Following the resuspension event, the amorphous FeS and MnS are rapidly oxidised (first few minutes), due to their relative solubility in oxic conditions, while pyrite (FeS_2) and covelline (CuS) are unlikely to be oxidised in the short term due to their slower oxidation kinetics (Caetano et al. 2003). Moreover, there are differences in desorption rates of metals adsorbed to sulphides, e.g. Hg, Pb and Cu are released more rapidly than Zn (Caille et al. 2003). The dissolved Fe and Mn, originating from the oxidation of sulphides, are rapidly reprecipitated and deposited as amorphous and poorly crystalline oxyhydroxides. These newly formed minerals play an important role as scavengers of metals, by incorporating the released metals by co-precipitation and/or adsorption (Saulnier and Mucci 2000; Cateano et al. 2003; Eggleton and Thomas 2004; Vidal-Dura et al. 2018). The resuspension studies have found that metals readsorbe at varying rates and extents, e.g. Zn, Cu and Pb are found to be readsorbed to particles rapidly upon oxidation, whereas Cd has been shown to stay in the solution much longer, possibly due to complexation with chlorides and other anions which can limit its sorption onto Fe and Mn oxyhydroxides (Caetano et al. 2003).

2.3.3. Bioturbation

One of the processes that has a strong impact on the behaviour and fate of metals in the sediment is bioturbation (Ciutat et al. 2007; Xie et al. 2019). It is defined as all transport processes carried out by organisms that directly or indirectly affect sediment matrices. These processes include both sediment particle reworking and burrow ventilation, i.e. transport of the overlying water and the pore water through burrows, also known as bioirrigation (Kristensen et al. 2012). Sediment ingestion (deposit feeding), defecating, construction of pits and burrows, and the ventilation of subsurface burrows with overlying water significantly alter rates of chemical reactions and sediment–water exchange, destroy signals of stratigraphic tracers, bury reactive organic matter, exhume buried chemical contaminants, and change sediment physical properties (Shull 2009). The extent of sediment modification by organisms is influenced by the

sediment properties, the benthic community structure, population density and type of biogenic activities (burrowing, feeding behaviour etc.), as well as the frequency of sediment reworking (Remaili et al. 2016).

By transporting newly deposited material and solutes to depths of tens of centimetres, bioturbation significantly alters sediment characteristics, such as oxygen concentration, pH, redox potential and porosity, thus influencing metal binding affinities between the solid and dissolved phases and provoking the mutual exchange of metals among the sediment, sediment pore water and the overlying water (Crusius et al. 2004; He et al. 2015; Amato et al. 2016; Remaili et al 2016; Hoang et al. 2018). For example, chemical oxidation of the dissolved reduced sulphur species and sulphide minerals may be mediated by Fe and Mn oxyhydroxides and/or oxygen-rich overlying water supplied into anoxic regions of sediment by bioturbation, resulting in release of metals into pore water (Gagnon et al. 1996; Amato et al. 2016; Remali et al. 2018). According to Schaller (2014) a strong impact of bioturbation on the metal remobilization is also dependant on the chemistry of the element itself.

Several studies have shown that the flux caused by the bioturbation, particularly by bioirrigation, was several times higher than the diffusion flux (Gill et al. 1999; Covelli et al. 2008; Hammerschmidt and Fitzgerald 2008; Benoit et al. 2009). However, such significant fluxes can only occur in areas densely populated by organisms (Schulz 2006).

2.3.4. Aging

An important aspect governing the partitioning of metals between pore water and solids is time. Generally, it is considered that metals are transformed or incorporated into more stable solid phases over time, which in turns lead to a decrease in metal mobility and bioavailability – a process referred to as aging (Ehlers and Luthy 2003; NRC 2003). The transformation processes that occur during sediment aging in the natural environment include, for example, the humification of natural organic matter, which lead to the formation of humic substances, i.e., the most reactive fraction of the organic matter (Nia 2011). Another process that diminishes availability of the metals over time is physical occlusion by deposition of new material. By this microscale burial, metals become sequestered within the solids and have minimal contact with surrounding aqueous solutions (NRC 2003). Moreover, aging can redistribute metals initially bonded to solid surface via electrostatic adsorption to form an inner-sphere complex or they may even become incorporated within the lattice structure of solids, subsequently decreasing

the availability of the metals. Indeed, most empirical studies demonstrated the redistribution of sorbed metals from the exchangeable and carbonate fractions to the refractory fractions (organic and residual phase) during prolonged aging of sediment (Burton et al. 2006; Zhong and Wang 2006; Zhong et al. 2012; Zhang et al. 2014). However, although scientists agree that aging reduces the bioavailability of metals, the time estimates are very different, varying from several days to several years, depending on the sediment, metal concentration and environmental conditions (Nia 2011). Furthermore, the influence of aging is most probably metal specific due to the diverse binding mechanism of different metals with particles (Zhong and Wang 2006; Zhong et al. 2012).

2.3.5. Diffusion at the sediment-water interface

The reactions that take place bellow the sediment-water interface, such us decomposition of the organic matter or dissolution of mineral phases of inorganic and biogenic origin, cause changes in concentrations of dissolved species in sediment pore water, thereby creating the concentration gradient between the two sides of the SWI and establishing conditions for the transport of chemical species by molecular diffusion across the SWI (Lerman 1978).

To determine the diffusion of ions or molecules in pore water, in the absence of bioirrigation, a modification of the Fick's first law is usually used:

$$F = -\Phi D_s \frac{\partial C}{\partial x}$$

where F is the flux of a solute with concentration C at depth x, Φ is the sediment porosity and D_s is the diffusion coefficient in the pore water volume of sediments. Modification of the standard Fick's diffusion formula includes the porosity value, due to the fact that in sediment diffusion can only take place within the pore water volume. Moreover, instead of the diffusion coefficient of the solute in the water, a diffusion coefficient in the pore water volume of sediments must be used, which may be calculated according to equitation:

$$D_s = \frac{D}{\theta^2}$$

where D is the diffusion coefficient of the solute of interest in water without the presence of the sediment matrix and θ is the tortuosity, a parameter that accounts for the tortuous and reduced diffusional fluxes through the pore space (Lerman 1978; Schulz 2006). Tortuosity can be

determined directly by measuring the electrical resistivity, or more commonly estimated from porosity (Boudreau 1996):

$$\theta = \sqrt{1} - \ln(\Phi^2).$$

Alternative way to calculate a diffusion coefficient in the pore water volume of sediments is to use empirical equations (Ullman and Sandstrom 1987):

$$D_{sed} = \Phi D \ (\Phi < 0.7)$$

$$D_{sed} = \Phi^2 D \ (\Phi > 0.7)$$

where D is the diffusion coefficient in water adjusted to in situ temperature using the Stokes–Einstein equation.

The sediment may act as a source of the dissolved species if solutes found within pore waters diffuse across the SWI (negative diffusive fluxes) (Kalnejais et al. 2010), as it is the case with the fluxes of dissolved reactants or products resulting from the early diagenesis (e.g. nutrients, carbon dioxide, iron, manganese), or it may represent a sink for the species whose consumption occurs below the SWI (positive diffusive flux), such as O_2 or sulphate (Dang 2014).

The transport of dissolved substances by diffusion at the SWI may be enhanced by bioirrigation in the upper 10 cm of the coastal and estuarine sediments (Boudreau 1984; Middelburg et al. 1996). The presence of well-irrigated worm burrows and other animal burrows in sediments modify the geometry of the pore water system in a way that solutes can diffuse through the burrow, i.e., it represents an additional boundary source or sink (Boudreau 1984). The neglection of possible solute transport by bioirrigation could lead to an underestimation of the fluxes, however, that kind of simplification will not compromise the general discussion of processes occurring in the sediment (Rigaud et al. 2013).

3. STUDY AREA

3. STUDY AREA

The Krka River estuary, located in the central part of the Eastern Adriatic coast, is a typical estuary of the Dinaric high karst region. Recent morphology of the Krka River and its estuary resulted from the geological setting of the area and climate changes after the Upper Pleistocene. During the glacial times, when the sea level was 120-125 m lower than today (Fairbanks 1989; Surić et al. 2005), the Krka River cut its canyon into the erosional plane. Rising of the sea level during the Holocene transgression led to flooding of the valley and formation of the recent estuary. In the postglacial period, due to the suitable climatic, geochemical, and biological condition, the tufa barriers were formed in the part of the valley above the recent sea level (Prohić and Juračić 1989). Nowadays, the estuary is stretching 22 km in length, from the last active tufa barrier – Skradinski buk, through Prokljan Lake to the St. Anthony Channel. The estuary bottom gradually deepens from the head of the estuary (2 m) to the St. Anthony Channel (42 m) (Prohić and Juračić 1989; Cukrov et al. 2008).

The catchment area of the Krka River is composed mainly of Upper Cretaceous and Eocene limestones, with a subordinate quantity of clastic rocks which consist primarily of Eocene flysch and flysch-like deposits, as well as Quaternary marls and clays (Prohić and Kniewald 1987; Prohić and Juračić 1989) (Fig. 3.1.). The geological setting and tectonic structures of the catchment area are described in more detail elsewhere (Prohić 1984; Juračić 1987).

The Krka River catchment area up to the last waterfall is 2 788 km^2 (Bonacci and Ljubenkov 2005; Bonacci et al. 2017). However, defining the catchment area in the karst is a very complex task due to the groundwater exchanges with adjacent aquifers through underground routes and to the fluctuations in the groundwater level, therefore, the catchment area of the Krka River presumably varies seasonally and annually (Bonacci et al. 2006). The measured flow over the last 50 years was found in the range 5 to 400 $m^3 s^{-1}$ with the mean annual flow between 40 and 60 $m^3 s^{-1}$ (Cindrić et al. 2015). Moreover, due to the sheltered geography and the low tidal range (0.2-0.5 m), the Krka River estuary is permanently vertically stratified (Buljan 1969). Along the vertical profile, there are three well-separated layers: (1) the upper fresh-brackish layer, (2) the freshwater-seawater interface (FSI) and (3) the bottom seawater layer (Cindrić et al. 2015). The fresh-brackish surface layer is moving seawards, whereas the bottom seawater layer is moving upwards.

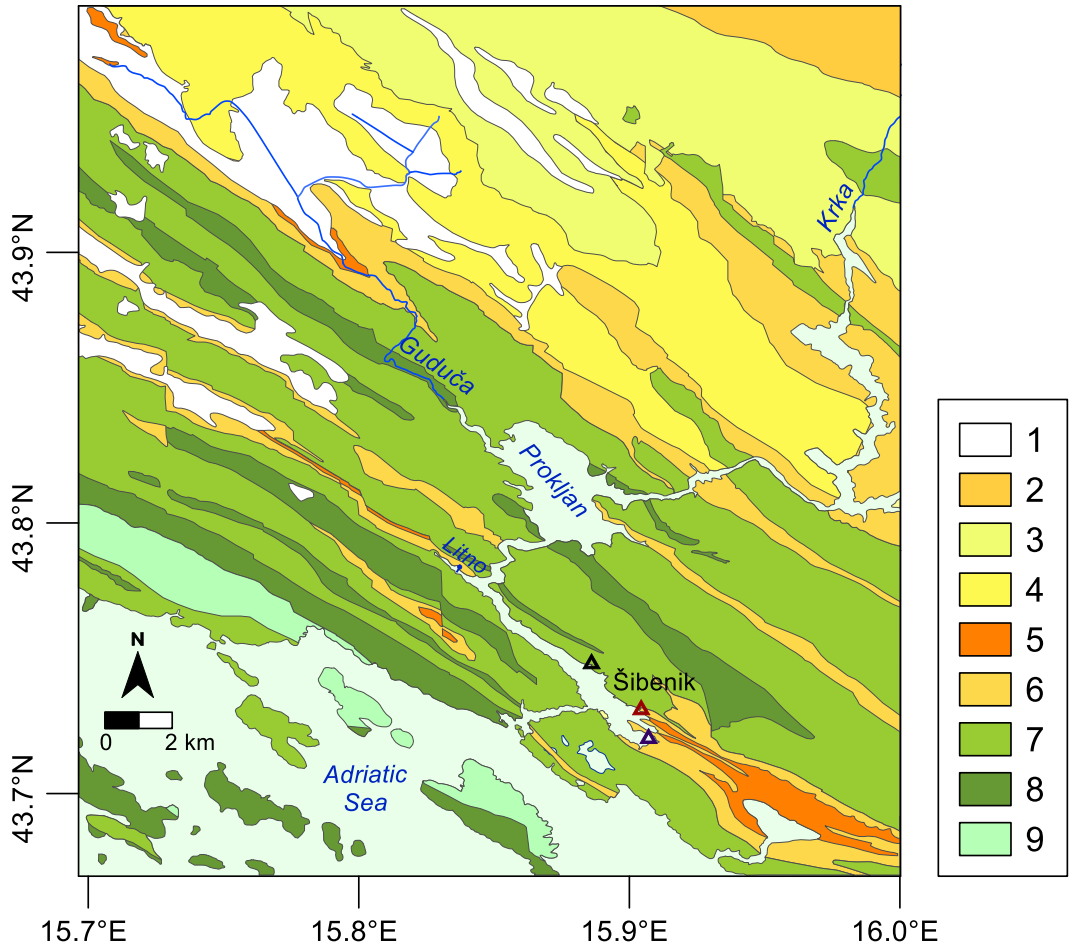

Figure 3.1. Geological map of the study area (modified after Mamužić 1971). Legend: 1 - Quaternary deposits, 2 – Upper Eocene and Lower Oligocene conglomerates and limestones, 3 - Upper Eocene conglomerates and limestones, 4 – Middle-Upper Eocene limestones, marls, and conglomerates, 5 – Middle Eocene Flysch, 6 – Lower-Middle Eocene foraminiferal limestones, 7 - Upper Cretaceous rudist-bearing limestones, 8 – Cretaceous limestone and dolomites, 9 – Cretaceous dolomites. Empty triangle symbols mark locations of the potential contamination sources; black – the Electrode and Ferroalloy Factory, red – the Port of Šibenik, violet – the nautical marina and repair shipyard.

3.1. Sedimentation in Krka River estuary

The sedimentation in the Krka River estuary is influenced by two major sources of material: (1) the weathering of carbonate and noncarbonate rocks in the drainage area and abrasion of carbonate shores within the estuary and (2) autigenous biogenic formation of the carbonate particles (Juračić and Prohić 1991). Furthermore, an important feature of the Krka River estuary is a very low input of terrigenous material via main watercourse Krka River. Generally,

suspended particulate matter (SPM) in Krka River estuary is lower than 5 mg L^{-1} (Cindrić et al. 2015). This is due to the fact that the Krka River drains mostly carbonate terrain and has tufa barriers along the stream which significantly reduce suspended material transport. The main source of terrigenous material is a small tributary, the Guduča River, which inflows in Prokljan Lake. Its catchment area is composed mainly of the Upper Eocene-Oligocene flysch and flysch-like deposits, which by weathering give most of the particulate material. Moreover, there are no tufa barriers along the stream, which could retain particulate material (Prohić and Juračić 1989; Juračić and Prohić 1991; Cukrov and Barišić 2006). However, from the granulometric and mineral distribution patterns (quartz, kaolinite, montmorillonite), it is evident that majority of the material brought by the Guduča River is being settled in Prokljan lake (Juračić and Prohić 1991). Juračić (1987) explains restriction of terrigenous sedimentation to Prokljan Lake through several reasons: (1) sheltered position combined with low energy of the environment and slow bottom currents due to the basin enlargement; (2) estuarine type of circulation with the bottom seawater layer moving landward and bringing back particles that sink from the surface fresh/brackish layer; (3) physico-chemically and biologically induced flocculation of fine grained matter in the surface layer of Prokljan Lake. Additional source of suspended material for the estuary is the source Litno located in the Zaton Bay. The catchment area of the Litno spring is composed of impermeable flysch deposits which form a barrier and direct all groundwater from its northeast to the spring (Fritz 1977, as cited in Prohić 1984).

According to previous studies (Juračić and Prohić 1991; Cukrov and Barišić 2006; Cukrov et al. 2009) there is difference in type and rate of sedimentation between the upper and the lower part of the estuary. In the upper part, especially in Prokljan Lake, sediment is a mixture of a marine carbonates and terrigenous material. The sedimentation rate in this area varies from 2 to 4-5 mm $year^{-1}$, depending on the distance from the mouth of Guduča River (Cukrov et al. 2007). In the lower part of the estuary, the Šibenik Bay, autigenous biogenic sedimentation prevails. It is characterized by coarse carbonate fraction of recent and subrecent biogenic origin, as indicated by presence of aragonite and Mg-calcite. The particles of abrasive origin (grains of limestone and dolomite) are present in lesser extent, while the amount of fine fraction of terrigenous origin is very low (Juračić and Prohić 1991). The sedimentation rate in the lower estuary is less than 1 mm $year^{-1}$, with exceptions found in the deepest parts of the estuary which act as a kind of a sediment trap and are located at the centre of the Šibenik Bay, where sedimentation rate is approximately 3 mm $year^{-1}$ (Cukrov et al. 2007), and in the Port of Šibenik area where sedimentation rate was estimated to be more than 4-5 mm $year^{-1}$ (Cukrov 2006).

Previously, other sedimentation rates were reported for the area, from negligible (Juračić 1987) to 5.2 mm $year^{-1}$ (Bogner 2001), but the authors concluded that obtained sedimentation rates are questionable because of the significant mixing of sediment by bioturbation. Furthermore, difference between the upper and lower estuary is evident from the sediment grain size. Namely, the mean grain size increases from Prokljan Lake (7 μm) toward the sea (410 μm). The coarsening of sediments seaward indicates either different source of sediment particles or non-depositional environment (Prohić and Juračić 1989).

3.2. Anthropogenic impact on Krka River estuary

The largest part of the Krka River freshwater watercourse is protected as a national park. Hence, there is no significant contamination entering the Krka River estuary from that direction and the estuary is considered comparatively unpolluted. However, several studies evidenced anthropogenic impact in terms of elevated trace metal concentrations in the lower part of the estuary, around the largest settlement in the area – city of Šibenik (Mikac et al. 1989; Martinčić et al. 1989, 1990; Kwokal et al. 2002; Bogner et al. 2004; Cukrov et al. 2008). The electrode and ferroalloy production (Cindrić et al. 2015), untreated wastewater discharge (Mikac et al. 1989, 1996), repair shipyard and a phosphate transhipment port (Mikac et al. 1989, 2006) were major sources of contamination for the estuary. Currently, some of the sources are eliminated: the Electrode and Ferroalloy Factory has been closed 25 years ago and since 2007 wastewaters have been treated and discharged outside of the estuary. However, removing industry from the estuary, led to development of the nautical tourism – a serious periodic (seasonal) anthropogenic threat to the estuary ecosystem (Cindrić et al. 2015).

3.2.1 The Electrode and Ferroalloy Factory

The industrial development of the city of Šibenik started in 1900 with a building of a carbide and cyanamide plant in a place called Crnica (a suburb of then Šibenik), at the location of the later Electrode and Ferroalloy Factory (TEF). The new production cycle starts just before the II World War by orienting the production on ferroalloys (ferromanganese, silicomanganese, ferrotungsten, and ferromolybdenum, etc.) (Internet Reference 1). The TEF factory was operating until the mid-nineties, and during the entire production period there was no strategy in metal pollution control implemented. Industrial fumes and dust were emitted directly into

the air while metallurgical slag was partially spread around or deposited in the vicinity of the smelter (Oreščanin et al. 2004). After the shutdown of production, the dismantling of the factory facilities was carried out. However, different types of waste resided on the site: 800 000 t of ferromanganese slag, tar, phenolic residues, carborundum, recycled separated granulate, waste graphite electrodes, etc. The soil at the location was contaminated with mineral hydrocarbons and polycyclic aromatic hydrocarbons – PAHs. Thus, remediation of the land was necessary, which was completed in few separate stages until 2013 (Fig. 3.2.).

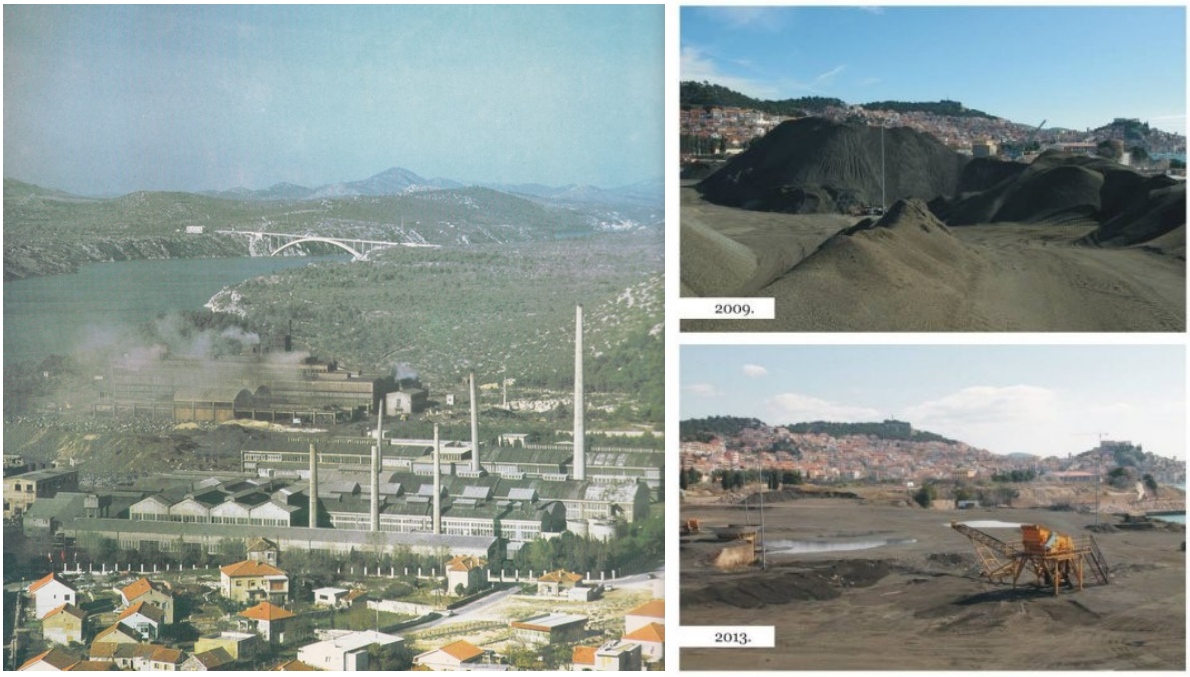

Figure 3.2. The former electrode and ferroalloy factory during the production (left), after the shutdown of production but before the land remediation (top right) and after the remediation was completed in 2013 (bottom right) (Internet Reference 2)

3.2.2 The Port of Šibenik

The Port of Šibenik is situated in the Krka River estuary and it is one of the best protected ports in Croatian Adriatic. The beginnings of the Port of Šibenik are closely linked to the exploration of the coal in hinterland, started in 1834. Around 60-70 thousand tonnes per year were exported through the port to Trieste, Syria, Turkey, and Egypt. During time and with construction of new railroads, the Šibenik Port developed more and more, and new operative coasts were built. From the middle 50s, with construction of 125 m of new coast and 67 000 m^2 of open space, the port became the port for bulk cargo. From 1982, when new terminal for bulk cargo has been

constructed, the Port of Šibenik has specialized for the transhipment of raw phosphates and artificial fertilizers. Nowadays port has the annual capacity of 2 million tons, and it is composed of three specialized terminals: terminal for transhipment of phosphates, terminal for bulk and general cargo and terminal for wood (Internet Reference 3) (Fig. 3.3.).

Figure 3.3. The view on the Port of Šibenik from the sea

3.2.3 Nautical marina and repair shipyard

Repair shipyard and nautical marina are situated in the St Peter's Cove, along the Mandalina peninsula. From 1905 this area was a central Austro-Hungarian naval base. Just after the World War II, the naval repair shipyard starts with its operation. With years, shipyard has been growing and in 1990 had more than 1 000 employees. In the middle 2000s the shipyard has been privatized and the shipyard's activities have been expanded to overhaul, servicing and maintenance of yachts and mega yachts and construction of commercial ships (Internet Reference 4). At the same time, part of the area was turned to the nautical marina. Today, marina has berthing capacity of 440, from 10 m up to 70 m with a maximum draft of 5.5 m (Internet Reference 5).

3.2.4 Wastewater

Just over a decade ago city of Šibenik did not have a uniform sewage system and its wastewater was discharged directly, without any prior treatment, into the lower part of the Krka River

estuary (The Šibenik Bay) from a 33 separate outflows along the waterfront. This included the industrial wastewater, as well. Discharging untreated wastewater into the semi-enclosed area such as Krka River estuary led to the environmental degradation in form of nutrient enrichment (Gržetić et al. 1991; Svensen et al. 2007) and water and sediment contamination by metals (Mikac et al. 1989, 2006, 2007; Cukrov et al. 2008). To solve this problem, a uniform system has been constructed consisting of the sewer running along the entire waterfront, water purification device, and a 5 km long undersea outfall which takes treated water out in the open sea (Nadilo 2003).

3.3. Trace elements in the sediment

The Krka River estuary has been, and still is, a subject of many studies. The researches have mainly focused on physical and chemical properties of the estuarine water column and especially the boundary FSI layer in which an enrichment of the organic matter and trace elements was found (Žutić and Legović 1987; Cauwet 1991; Elbaz-Poulichet et al. 1991; Legović et al. 1991; Svetličić et al. 1991; Bilinski et al. 1992, 2000; Vojvodić and Ćosović 1992; Sempéré and Cauwet 1995; Mikac and Kwokal 1997; Omanović et al. 2006; Louis et al. 2009; Plavšić et al. 2009; Cindrić et al. 2015, 2020; Pađan et al. 2019, 2020; Marcinek et al. 2020). Though, the water chemistry was a principal research subject, the studies were carried out on estuarine sediments as well (Hadžija et al. 1985; Prohić and Kniewald 1987; Mikac et al. 1989; Prohić and Juračić 1989; Martinčić et al. 1990; Šurija and Branica 1995; Kwokal et al. 2002; Cuculić et al. 2006; Cukrov et al. 2006, 2008).

The importance of conducting a complex investigation when assessing anthropogenic influence on the trace metal concentrations in sediments was demonstrated on the example of the Krka River estuary by Prohić and Juračić (1989). The authors combined analytical, geochemical and geological approach to identify different groups of trace elements in the estuarine sediment. The first group includes nickel (Ni) and zinc (Zn), found in ranges of 40-100 ppm and 20-50 ppm, respectively. Owning to their abundance in the flysch deposits and seawards decrease of their concentrations in the sediments, it has been concluded that increased concentrations of Ni and Zn found in the estuarine sediments are due to the natural enrichment in the source rocks. Lead (Pb) and copper (Cu), found in the ranges of 16-70 ppm and 2-65 ppm, were attributed to the second group, for which the anthropogenic sources were presumed. This conclusion was made due to the higher concentrations found in sediments than in source rocks and distal

sediments and by surface enrichment in the sediment core. The supposed anthropogenic source of Pb is the combustion of leaded gasoline, while antifouling paints and blue vitriol input from the vineyards in the drainage area are presumed to be sources of Cu. The third group is represented by redox-sensitive elements, manganese (Mn) and chromium (Cr). The first 5 cm of the estuarine sediments were found to be an oxidizing environment, causing precipitation and enrichment of Mn in the surface layer. Vice versa, in the oxidized layer Cr forms soluble CrO^{2-} and by transport to the deeper layers, it is reduced to Cr (III) and precipitates.

Furthermore, it is widely recognized that the distribution, mobility, and bioavailability of trace metallic and metalloid elements in the environment depends not only on their total concentration but also on the chemical form of the element and the association form in the solid phase to which they are bound. Sequential extraction analysis, although far from being perfect, has the ability to extract elemental species from particular solid phases in sediments and to provide noteworthy information about mobility of trace metals, bioavailability and ecotoxicity so as to assess contamination risk (Filgueiras et al. 2002). This approach was used by Prohić and Kniewald (1987) and Šurija and Branica (1995) to establish partitioning patterns of metals in the Krka River estuary sediments. In general, both studies found high levels of analysed metals (Mn, Cu, Pb, Zn, Ni, Co, Cr; Cu, Zn, Cd, Pb) in the carbonate fraction of the sediment. Therefore, it can be assumed that carbonate minerals are primary scavenging agents for most metals in the Krka River Estuary. Although this is normal for some elements due to similarity of their ionic radii to that of Ca, this cannot be said for example for Cr. The authors assumed that the surfaces of carbonate minerals were covered with organic matter or other particles that would enhance the adsorption properties of the minerals (Prohić and Kniewald 1987). The model adsorption experiments conducted in the Krka River water of various salinities, demonstrated that calcite mineral contributes to the remarkable self-purification ability with respect to Pb, Zn and Hg trace ions. For the Pb and Zn, a surface exchange with Ca ions was assumed, whereas for Hg an important role of natural organic ligands in promoting absorption on calcite was observed (Bilinski et al. 1991).

Mercury is undoubtedly one of the major contaminants present in the aquatic environments, due to its high toxicity, high mobility and accumulative behaviour in the environment and biota (Covelli et al. 2012; UNEP 2013; Song et al. 2018). Therefore, during the past 30 years a special emphasis was given to the studies of Hg in the Krka River estuary sediments. Kwokal et al. (2002) reported slightly elevated Hg concentrations (1.42 mg kg^{-1}) for the area around the city of Šibenik, while in other parts of the estuary Hg values were in the range 0.101–0.418 mg kg^{-1}.

Similar values were reported by Mikac et al. (1989) (0.256-1.49 mg kg^{-1}) and Martinčić et al. (1989) (0.17-0.41 mg kg^{-1}), although the authors used only clay/silt (< 75 μm) fraction to reduce grain size influence. The highest concentrations (3 mg kg^{-1}) were found in the Šibenik Port area (Mikac et al. 2006). The increased concentrations of Hg in the Šibenik Bay are attributed to the untreated municipal wastewater of the city of Šibenik, shipping activities which take place in this area and the transhipment terminal for the phosphate ores in the Port of Šibenik (Mikac et al. 1989, 2006).

4. MATERIALS AND METHODS

4. MATERIALS AND METHODS

4.1. Sampling protocols

To achieve the planned research objectives, different sampling campaigns were carried out in the Krka River estuary: (1) surface sediment sampling at 40 locations along the whole estuary transect, to evaluate the state of surface sediments in the Krka River estuary regarding the metal content and possible pollution; and (2) sediment core sampling at different parts of estuary, i.e., at 7 locations, to assess historical trends of metal input and to evaluate their mobility in the sediment column. The core sampling campaigns included the sampling of the water column as well. Sampling sites are presented in Fig. 4.1. and their GPS locations are given in the Table 4.1.

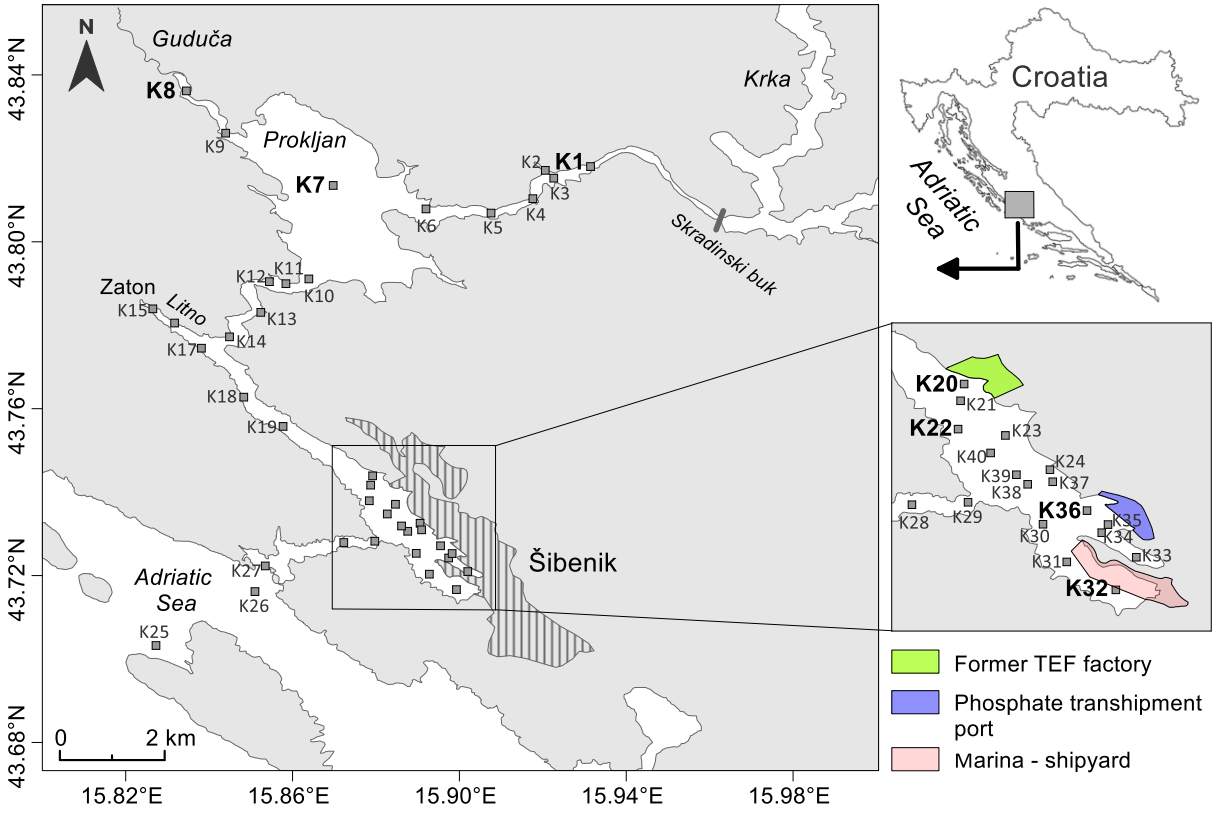

Figure 4.1. Map of the Krka River estuary with marked sampling locations and main sources of contamination. Dark grey squared symbols mark surface sediment sampling locations, while cores sampling locations are represented by bold labels on the left side of the symbol.

Table 4.1. Locations of surface sediments sampling in the Krka River estuary with the corresponding water depth measured by sounder

Site ID	Latitude	Longitude	Depth (m)
K1	43.81714	15.93189	7
K2	43.81476	15.92303	5
K3	43.81620	15.92207	6.3
K4	43.80903	15.91979	6.3
K5	43.80688	15.90759	12
K6	43.80788	15.89199	10.1
K7	43.81350	15.86974	15.8
K8	43.83617	15.83455	4
K9	43.82604	15.84397	10.2
K10	43.79110	15.86391	24.4
K11	43.78996	15.85841	17
K12	43.79044	15.85445	24.5
K13	43.78308	15.85239	16.5
K14	43.77722	15.84489	32
K15	43.78393	15.82651	9.5
K16	43.78053	15.83172	13.7
K17	43.77450	15.83816	24.9
K18	43.76277	15.84831	30
K19	43.75575	15.85772	34.4
K20	43.74390	15.87920	37
K21	43.74168	15.87873	38
K22	43.73793	15.87840	37.7
K23	43.73709	15.88467	39
K24	43.73255	15.89057	24.5
K25	43.70324	15.82726	19
K26	43.71617	15.85099	40
K27	43.72231	15.85346	42
K28	43.72792	15.87229	42
K29	43.72824	15.87972	42.5
K30	43.72533	15.88965	40
K31	43.72034	15.89280	25.5
K32	43.71664	15.89930	19
K33	43.72421	15.89743	21.5
K34	43.72096	15.90201	10
K35	43.72529	15.89826	16
K36	43.72714	15.89548	25
K37	43.73096	15.89094	32.7
K38	43.73062	15.88762	35.6
K39	43.73189	15.88613	38
K40	43.73477	15.88271	38

4.1.1. High-resolution surface sediment sampling

High-resolution surface sediment sampling was performed on August 31st and September 2nd, 2016. Sampling density was one to eight samples per two square kilometres, with the higher density in the Šibenik Bay, an area of the Krka River estuary presumably exposed to the highest anthropogenic pressure. A total of 40 surface sediment samples were collected along the estuary using a Uwitec gravity corer (PVC tube, φ = 9 cm, length = 60 cm) (Fig. 4.2.). GPS instrument Garmin GPSMap 76 CSx (Kansas City, MO, USA) (accuracy ± 5 m) was used to precisely determine each location. Only uppermost 5 cm were retrieved and used for analysis. Samples were placed in plastic containers, deep frozen (-18°C) immediately after the sampling, freeze dried as soon as it was possible and sieved under 2 mm.

Figure 4.2. Sediment sampling using Uwitec gravity corer

4.1.2. Sediment core and water column sampling

Seven sediment cores were taken in the Krka River estuary (K1 – the head of the estuary, K7 – Prokljan Lake, K8 – the Guduča River, K20 – the former Electrode and Ferroalloy Factory, K22 – the Research Station Martinska, K32 – the nautical marina/shipyard, K36 – the Port of Šibenik) to trace historical contamination by metals in the study area and to assess metal mobility in the sediment. The sampling sites were selected in such a way that different areas of sedimentation were present, as well as areas exposed to various anthropogenic threats. These sampling locations correspond to the surface sediment sampling sites which have the same notations. Cores were sampled by a diver using hand-driven Plexiglas corers, except the core

K8 which was sampled using gravity corer (Plexiglas tube, φ = 10 cm, length = 60 cm). Diver was taking special care to hold the cores vertically and not to disturb them. At each sampling location, three sediment cores were collected; one was used for slicing sediment, i.e. retrieving sediment and pore water samples, the second one was taken using the core with predrilled holes and was used to measure pH and Eh in the sediment with the resolution of 1 cm, the third one was used to collect supernatant water at different distances from the bottom – 2, 5 and 15 cm. Additionally, at each location water column was sampled at 4-6 depths along the vertical profile, depending on the water depth and position of the halocline. Horizontal water sampler was used for collecting the water samples, while 1 L pre-cleaned FEP (Fluorinated Ethylene Propylene) bottles were used for sample storage (Fig. 4.3.). The FEP bottle was first rinsed three times with the sample, then filled end stored in portable refrigerator. Upon arriving to the laboratory, samples were threated depending on the parameters that will be measured, following the same protocol as for pore water described in Section 4.2.2. Additionally, a fraction of water column samples was taken for the voltammetric determination of Cd concentration as described in Section 4.4.3. Moreover, vertical profiles of main physicochemical parameters (salinity, temperature, pH, and dissolved oxygen) were measured *in-situ*, using a multi-parameter probe (EXO2, YSI) (Fig. 4.4.). The details on sampling campaigns are given in the Table 4.2.

Table 4.2. Sediment core sampling details: Core ID, sampling location, water column depth (m), number of water column samples taken, core depth (cm) and sampling date. The depths were recorded by dive computer, except at the K8 sampling location where handheld depth sounder was used.

Sediment core ID	Location	Depth (m)	No. of water column samples	Core depth (cm)	Sampling date
K1	Head of the estuary	6.7	5	36	19 December 2017
K7	Prokljan Lake	16	6	36	24 July 2017
K8	Guduča River	7.3	6	26	4 December 2017
K20	TEF factory	33	4	22	2 February 2017
K22	Martinska	28	-	11	30 April 2014
K32	Marina/shipyard	16	-	25	1 May 2014
K36	Šibenik Port	23.7	6	18	15 July 2017

Figure 4.3. Filling 1 L FEP bottle with the sample taken with the horizontal water sampler

Figure 4.4. Multi-parameter probe EXO2 (YSI) (left), and the measurement of the water physico-chemical parameters by using the probe (right)

4.2. Sediment cores manipulation and sample preparation

4.2.1. Cleaning procedure

Particular attention was given to the prevention of the sample contamination, especially to the cleaning procedure of the plasticware used for the sampling and storage of both water and

sediment samples. All the tools used for the core slicing (e.g., spatula, funnel) and HDPE (High Density PolyEthylene) containers used for sediment samples were cleaned with 10% HCl (*analytical reagent grade*), rinsed several times with MQ water (Milli-Q water, 18.2 MΩ, Millipore), then left submerged for 24h in 10% HCl and finally rinsed thoroughly with MQ water. Syringes and bottles used for sampling and storage of fraction of water samples dedicated to the metal analysis were cleaned with 10% HNO_3 (*analytical reagent grade*), rinsed several times with MQ water and filled with MQ water until use. Glass tubes used for the dissolved organic carbon (DOC) and dissolved inorganic carbon (DIC) analysis were cleaned with 10% HCl, well rinsed with MQ water, dried in ambient temperature and calcinated for 4 hours at 450°C.

4.2.2. Core slicing

Sediment cores were transported to the laboratory within one hour from the sampling. In the laboratory, the excess supernatant water was drained out from the sediment core dedicated for retrieving the sediment and the pore water samples. Only about 10 cm of supernatant water was left in the core, to prevent oxidation of the uppermost layers of the sediment. Then, the sediment core was installed on the slicing table equipped with pyramidal glove box and a hydraulic jack, as shown in the Fig.4.5.

Figure 4.5. Positioning of the hydraulic jack below the sediment core previously installed on the slicing table (left) and working in pyramidal glove box (right)

Once when inert (N_2) atmosphere in the glove box was achieved, the rest of the supernatant water was removed, and the sediment core was sliced. The slicing resolution was 2 cm for the cores K1, K7, K8, K20 and K36, 1 cm for the core K22 due to the shortness of the core, and for the core K32 1 cm up to 15 cm of depth and 2 cm below that depth. Each subsample was placed in 150 mL HDPE container, where it was homogenised (Fig. 4.6.). In the next step, each subsample was dived to three 50 mL centrifugation tubes. Samples prepared in this way were immediately centrifugated (4 000 rpm, 15 min, Eppendorf Centrifuge 5 804) in order to separate pore water from the sediment.

Afterwards, centrifugated samples are again placed in the glove box where pore water was collected, filtered (syringe filters, nitrate, 0.2 μm, Sartorius) and stored in different tubes depending on the type of the planned analysis (Fig. 4.7.). Pore water sample fraction dedicated for the multi-elemental analysis was acidified with ultrapure concentrated HNO_3 (*suprapur*) to pH < 2. Samples for DOC and DIC analysis were stored in 24 mL glass tubes with Teflon/silicon septum and preserved with 20 μL of 1 M NaN_3. Pore water fractions for the analysis of the diagenesis tracers were stored in 2 mL microtubes. To preserve dissolved sulphide, 0.5 mL of the trap solution ($ZnCl_2$, gelatine, chloroform (Metzger et al. 2007b)) was placed in the microtube before adding the sample. Except sample for the determination of ammonium which was stored at -18°C, all the samples were kept at 4°C until analysis. A schematic view of the sediment core slicing, sediment and pore water samples preparation and subsequent analysis is shown in Fig. 4.8.

Figure 4.6. Slicing the sediment core under the inert atmosphere (left) and transferring the obtained slice into HDPE container through the funnel (right)

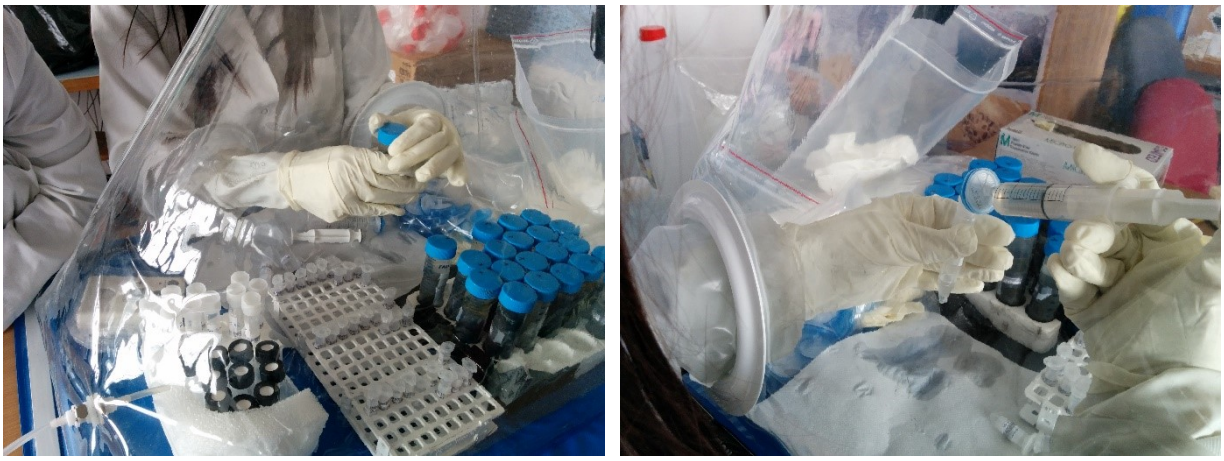

Figure 4.7. Collecting and filtration of the pore water from the centrifugated sediment samples

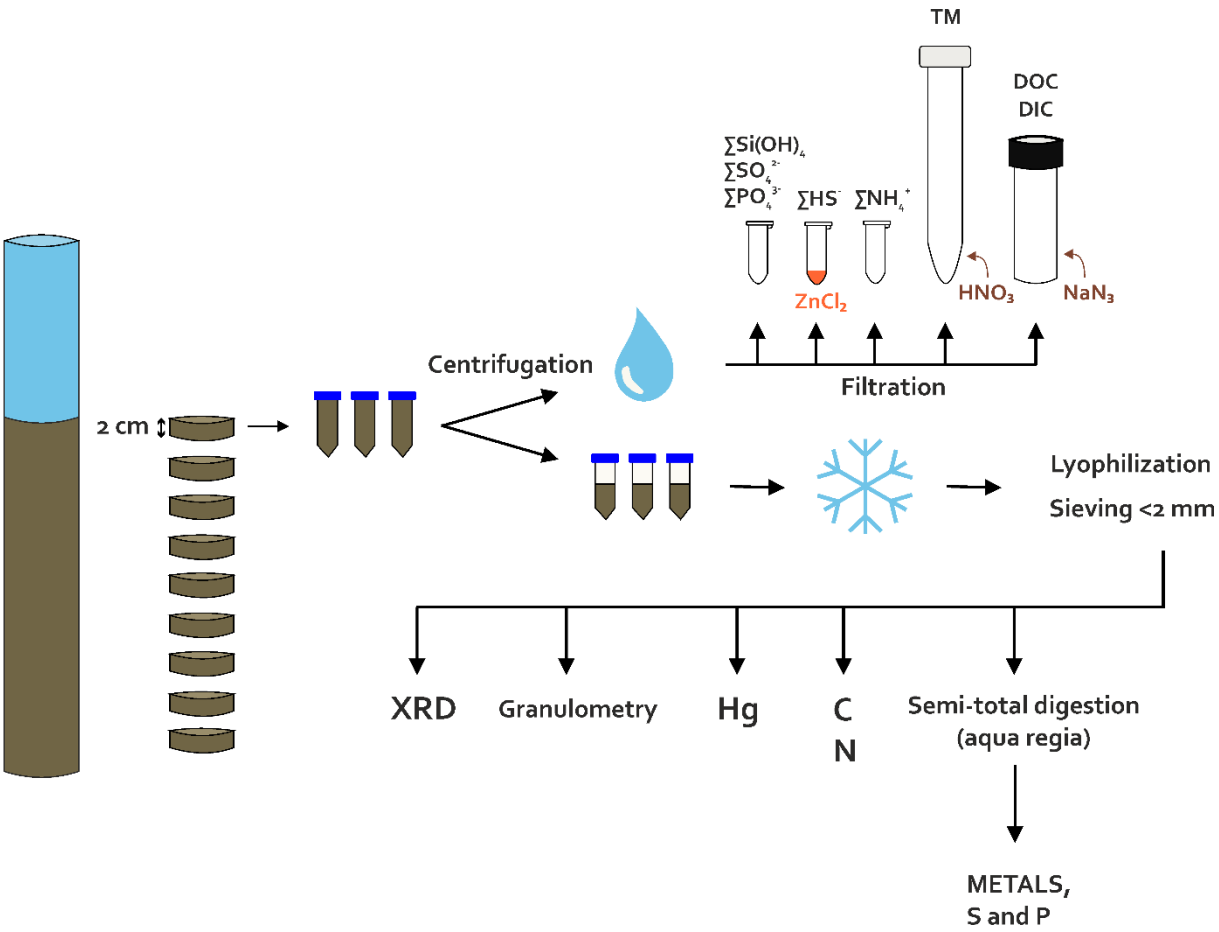

Figure 4.8. A schema of the sediment core handling procedures, from cutting the core to the pore water and sediment samples analysis

4.2.3. Supernatant water collection

Sediment core dedicated for retrieving the supernatant water was left to stabilize for one day in the laboratory before recovering samples at depths 2 cm, 5 cm and 15 cm from the SWI. A homemade device was used for collection, which consists of six syringes of 60 mL, connected two by two to Teflon tubes, resulting in a 120 mL of sample at each depth (Fig. 4.9.). In this way, it was possible to simultaneously sample at the three depths, which minimizes the possibility of homogenization of the bottom waters. The supernatant water samples were treated in the same way as the pore water samples.

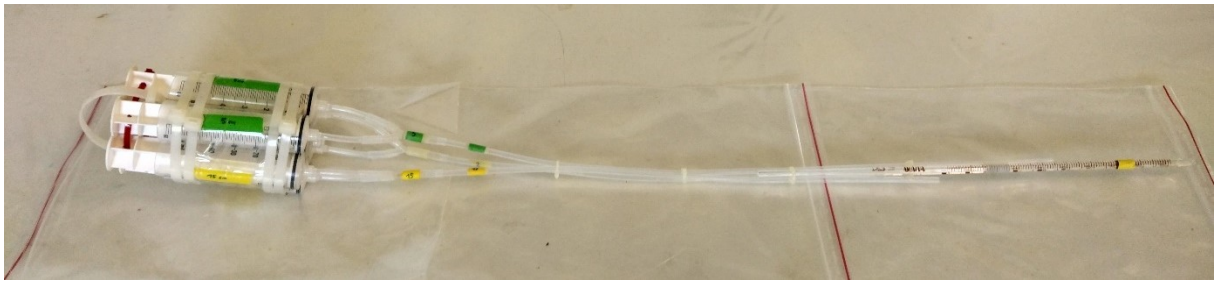

Figure 4.9. The homemade device for recovering supernatant water at three depths from the SWI (2 cm, 5 cm and 15 cm)

4.2.4. Measuring of pH and Eh in the sediment cores

For the measurement of the pH and Eh, sediment was collected in the core with predrilled holes each centimetre. The holes were covered with power tape from both inside and outside of the core before sampling. During measurement, only a small cut was made prior to inserting electrodes, which was re-taped after the value reading. The measurement was conducted by using combination of electrodes and an expandable ion analyzer EA 920 (Orion Research) (Fig.4.10.). For the pH a glass electrode Fisherbrand 1179-6348 was used, whereas for the Eh measurement Pt electrode was coupled to Ag/AgCl (saturated KCl) reference electrode. Obtained redox readings were converted to Eh values (voltage reading vs. the Standard Hydrogen Electrode (SHE)) by adding 199 mV to the reading, which is the difference between Ag/AgCl and SHE reference electrodes.

Figure 4.10. Measuring of the pH and Eh in the sediment pore water by using combination of electrodes and an expandable ion analyzer EA 920 (Orion Research)

4.3. Sediment analysis

In the framework of this thesis, a total of 140 sediment samples were collected within the Krka river estuary: 40 samples by sampling the surface sediment and 100 samples by recovering 7 sediment cores at different locations and slicing them. All samples were freeze dried and sieved through 2 mm sieve before subsequent analyses. Geochemical composition (C, N, S, P, Hg, Li, Be, Rb, Mo, Ag, Cd, Sn, Sb, Cs, Tl, Pb, Bi, U, Al, Ti, V, Cr, Mn, Fe, Ni, Co, Cu, Zn, Sr, Ba, As, Pt) was determined for all 140 sediment samples, except the organic carbon content which was measured only in the sediment cores samples. Granulometric and mineralogical composition was determined for the sediment cores samples, whereby the particle size was measured in all subsamples, while XRD analysis was done on one to four subsamples per core. The radiometric analysis was performed on all subsamples of the K32 sediment core.

4.3.1. Granulometric analysis

Granulometric composition of the sediment was determined using a laser diffraction particle-size analyser LS 13 320 (Beckman Coulter, USA) in the Laboratory for inorganic environmental geochemistry and chemodynamics of nanoparticles of the Division for Marine and Environmental Research, Ruđer Bošković Institute. The range of analysis is from 40 nm to 2 mm.

Freeze dried sediment samples were dispersed in deionized water and briefly treated in ultrasonic bath (3 min) prior to measurement. Each sample was measured in triplicates, and the average of the three was used to present the obtained results as a downcore stacked area plot. Sediments were classified according to the modified Wentworth (1922) grade scale with the clay–silt boundary at 2 μm and the Shepard's (1954) sediment classification scheme.

4.3.2. XRD analysis

The mineral composition of the sediments was determined by X-ray powder diffraction (XRD) on a Philips X'Pert Pro instrument using CuKα radiation at Department of Geology, Faculty of Science, University of Zagreb. The experimental conditions were following: 40 kV, 40 mA, step 0.02°2θ, step time 1 s and scanned range 4-63°2θ. Phases were determined by comparison with reference patterns using Philips X'Pert HighScore software (Philips Analytical B.V., 2001).

4.3.3. Multi-elemental analysis

A multi-elemental analysis of sediment samples was done by using High Resolution Inductively Coupled Plasma Mass Spectrometer (HR ICP-MS, Element 2, Thermo) in the Laboratory for physical chemistry of traces of the Division for Marine and Environmental Research, Ruđer Bošković Institute. Prior to analysis, samples were digested in the Laboratory of Processes of Transfers and Exchanges in the Environment (PROTEE) of the University of Toulon in the following manner: 100 mg of the sediment was weighted into 15 mL Teflon vials and 10 mL of aqua regia (HNO_3:HCl 1:3, Fisher Scientific®, *trace analysis grade*) was added. The vials were placed in the UltraWAVE Single Reaction Chamber Microwave Digestion System (Milestone Inc) under controlled conditions (power 1 500 W, pressure 100 bar, temperature was first linearly increased from room temperature to 240°C in 20 min and subsequently maintained at 240°C for the next 20 min). After digestion, samples were transferred into 30 mL LDPE (Low Density PolyEthylene) (Nalgene) bottles and diluted up to 25 mL with MQ water. Before analysis, samples were additionally diluted 10 times with 2% HNO_3 (*suprapur*). Indium (In) was used as an internal standard. To validate extraction method certified referent materials for marine (PACS-2, National Research Council of Canada) and river (LGC6187, LGC Group) sediments were used.

4.3.4. Mercury analysis

Mercury concentrations were determined in sediment samples (~10-100 mg) using an Advanced Mercury Analyzer AMA 254 (LECO Corporation) in the Laboratory of Processes of Transfers and Exchanges in the Environment (PROTEE) of the University of Toulon. The AMA 254 is based on thermal decomposition of the sample, followed by collection of the evolved mercury vapour on a gold amalgamator. Then, mercury is determined by a standard atomic absorption spectrophotometer at a specific wavelength (253.7 nm). To ensure accuracy and precision of the analysis replicated measurements of the certified reference materials (MESS-3, MESS-4 and PACS-3, National Research Council of Canada), blanks and duplicated samples were conducted.

4.3.5. Carbon and nitrogen analysis

A Flash 2 000 CHNS Analyzer (Thermo Scientific) was used for measurement of total carbon (TC), organic carbon (C_{org}) and nitrogen in the sediment samples. The analyses were done in the Laboratory of Processes of Transfers and Exchanges in the Environment (PROTEE) of the University of Toulon. Samples were weighed (~10-15 mg, ~5 mg for the K20 core) in a tin capsule and introduced into the combustion reactor via the Thermo Scientific™ MAS™ 200R autosampler together with a proper amount of oxygen. For analysis of nitrogen and total carbon content the samples were not additionally treated, while for the determination of the organic carbon content an aliquot of sediment sample was treated with hydrochloric acid (6 M, trace metal grade) to remove inorganic carbon prior to instrument analysis. The Soil NC Reference Material (Thermo Scientific) was used as a control sample.

4.3.6. Radiometric analysis

The radiometric analysis of ^{137}Cs, ^{210}Pb and ^{226}Ra activities was performed in the Laboratory for Radioecology of the Division for Marine and Environmental Research, Ruđer Bošković Institute.

Sediment samples were placed in a cylindrical measuring vessel of 125 cm^3 volume, hermetically closed and sealed. After the radiochemical equilibrium between ^{222}Rn and its daughter ^{214}Bi was established (approximately 4 weeks), the activities of radionuclides (^{226}Ra, ^{210}Pb and ^{137}Cs) were determined by the gamma-spectrometric method. The measurements

(counting) were performed using high resolution HPGe (High Purity Germanium) detector (BE5030P, CANBERRA) (Broad Energy, resolution (FWHM) at 1.33 MeV (^{60}Co) of 1.95 keV; relative efficiency of 48%). The spectra collection time was based upon the sample quantity, ranging from 80 000 to 200 000 seconds. For the processing of recorded spectra, the associated Genie 2 000 computer software (Canberra) was used. The activity of ^{226}Ra was determined by the activity of its daughter ^{214}Bi, calculated from the energy photo-peak of 609.4 keV. The activity of ^{210}Pb was determined from the energy photo peak of 46.5 keV, while activity of the anthropogenic radionuclide ^{137}Cs was calculated from the energy photo peak of 661.6 keV. The total budget of combined measurement uncertainty (k = 2) included the uncertainties of determining the net area of the photo peak, efficiency, and the speed of counting, including the uncertainty of the background rate. Calibration of the efficiency of the measurement setup was made mathematically using the LabSOCS tool by modelling the measuring vessel and individual sample and using detector characterization provided by the manufacturer. The detector system performance and calibration were regularly monitored via intercomparison measurements, while the precision and accuracy were checked by the simultaneous measurement of IAEA reference materials as well as using gamma mixed standards supplied by Ecker & Ziegler (Analytics USA).

The measured activities of radionuclides were used for the sediment age estimation. ^{210}Pb ($T_{1/2}$ = 22.2 years) is a member of the natural decay chain of ^{238}U, which has been widely used for very precise sediment dating on a 100-year time scale. In this study, for the age calculation the Constant Initial Concentration (CIC) model was applied (Robbins 1978). The value of supported ^{210}Pb in each sample was assumed to be in equilibrium with the in situ ^{226}Ra and excess ^{210}Pb was calculated by subtracting ^{226}Ra activity from total ^{210}Pb. The ^{210}Pb dating results were validated by using chronostratigraphic dates based on records of the anthropogenic radionuclide ^{137}Cs. ^{137}Cs ($T_{1/2}$ = 30.1 years) appears in environmental samples following the period of nuclear weapons testing beginning in the 1950s and peaking in 1963. After that time, activity of ^{137}Cs decreased until a precipitous rise in 1986 as the consequence of the contamination caused by the nuclear incident in Chernobyl. Therefore, the maximum values of ^{137}Cs activities were expected in the late 1980s and early 1990s, followed by a subsequent decline.

4.4. Pore water and water column sample analysis

4.4.1. Spectrophotometric methods

Orthophosphates, ammonium, sulphates, dissolved sulphides, and dissolved silica in the water samples were determined spectrophotometrically by UV/VIS spectrophotometer (Lambda 45, Perkin Elmer) in the Laboratory for physical chemistry of traces of the Division for Marine and Environmental Research, Ruđer Bošković Institute. The used methods are described below and explained in more detail in Dang (2014).

4.4.1.1. Soluble reactive phosphate

Concentrations of soluble reactive phosphate (SRP) in the water samples were measured by using method developed by Murphy and Riley (1958). In this method ammonium molybdate and potassium antimony tartrate react in an acid medium with orthophosphate to form a phosphomolybdic acid that is reduced to intensely coloured molybdenum blue by ascorbic acid. The potassium antimony tartrate is added as a catalyst for rapid colour development.

The mixed reagent used is a mixture of 10 mL of ammonium molybdate, 50 mL of sulfuric acid, 10 mL of antimony tartrate and 10 mL of ascorbic acid at 24.3 mM, 2.5 M, 4 mM and 0.6 M respectively. These solutions were pre prepared in individual flasks and the mixed reagent was done just before the analysis. Water samples were diluted by two to which 200 μL of the mixed reagent is added. The absorbance of the solution is measured at 885 nm after 5 minutes of reaction time. The protocol detection limit is 0.1 μM SRP, the calibration being linear up to 20 μM ($R^2 = 0.99$).

4.4.1.2. Sulphates

The sulphate concentrations were determined by the turbidimetric method, which is based on precipitation of sulphate ions as insoluble barium sulphates. As the main concern with this method is the stability of barium sulphate, a stabilizing agent Tween® 20 (Fisher) was used to keep precipitate in suspension. The turbidity of the suspension formed was measured at 650 nm. The reagent used was prepared by mixing 0.4 M $BaCl_2$ (Pro Analysis, Normapur) and Tween® 20 diluted by 4. The used calibration range was from 0.05 mM to 1 mM sulphates (R^2

= 0.99). For analyses, 40 µL of 1 M hydrochloric acid and 200 µL of reagent are mixed in 2 mL standard or 2 mL samples previously diluted by 50.

4.4.1.3. Ammonium

The ammonium concentrations in the water samples were measured using the Spectroquant® Kit 1.14752 (Merck). The method is analogous to EPA 350.1 and ISO 7150-1, which are based on the reaction between ammonia and chlorinating agent to form monochloramine. This in turn reacts with thymol to form a blue indophenol derivative that is determined photometrically. To the water samples diluted by 4, 160 µl of reagent NH_4-1 was added, subsequently a half of micro-spoon of reagent NH_4-2 was added and solution was vigorously until the reagent was completely dissolved. After 5 minutes, 3 drops of reagent NH_4-3 were added and left to stand additional 5 minutes before the measurement. The absorbance is recorded at 660 nm. The used calibration range was 0.05-5 mg L^{-1} $NH4^+$ (i.e., 3-300 µM $NH4^+$) (R^2 = 0.99).

4.4.1.4. Sulphides

The dissolved sulphides (ΣHS^-) in pore water and overlying water samples were analysed using Spectroquant® Kit 1.14779 (Merck). In this method, three reagents are added to sample. The addition of sulfamic acid (reagent S-1) minimizes the effect of nitrite ions likely to be present under suboxic/anoxic conditions. Sulphide reacts with dimethyl-p-phenylenediamine (reagent S-2) in the presence of ferric ions (reagent S-3) to form methylene blue, a dye which is measured at a wavelength of 665 nm after one minute of reaction time. This method is analogous to EPA 376.2 and ISO 10530. The used calibration range was 5 µM to 100 µM ΣHS^{-1} (R^2 = 0.99).

Due to the reactivity of dissolved sulphides, immediately after pore water extraction (or supernatant water sampling) 1 mL of sample was transferred to a tube containing 0.5 mL of trap solution made of zinc chloride and gelatine to precipitate ZnS (preventing sulphide oxidation and gas loss) (Metzger et al. 2007b). Samples were measured as soon as it was possible, that is immediately after slicing the core and extracting pore water.

4.4.1.5. Silicates

The silicate concentrations in the water samples were analysed using protocol from Aminot and Kérouel (2004). The method is based on the formation of the yellow silicomolybdic acid from silicates and molybdates. There are two isomers of the silicomolybdic acid: α and β, depending on the pH of the reaction mixture. The β is more suitable for spectrophotometric determination, therefore reagent ratios and pH are optimized to favour formation of the β isomer, which is then reduced by ascorbic acid to a stable, blue-coloured complex. To eliminate interferences related to arsenate and to phosphates, oxalic acid is added to the mixture to destroy complexes arsenio-molybdate and phosphor-molybdate (Truesdale and Smith 1975). Oxalic acid also degrades the silicomolybdate complex slowly. This is the reason why the reducing agent, ascorbic acid, is mixed with oxalic acid so that the latter act at the same time on the reaction mixture. The reagents were prepared as follows: 3 g of ammonium molybdate tetrahydrate was dissolved in the 30 mL of 1.5M sulfuric acid, oxalic acid solution was prepared by dissolving 1 g of oxalic acid in 10 mL of MQ water and ascorbic acid solution was prepared daily by dissolving 0.28 g of ascorbic acid in 10 mL of MQ water. The samples were diluted 5-fold with MQ water (except the samples from the K8 core which were diluted 10-fold) and then 100 µL of the molybdate reagent were added. After a reaction time of 10 min, 50 µL of oxalic and ascorbic acids were added. The absorbance was recorded 20 min later, at 810 nm. The calibration range used was 1-50 µM silicate ($R^2 = 0.99$).

4.4.2. Multi-elemental analysis

The multi-elemental (Li, Al, Fe, Mn, Ni, Co, Cu, Zn, Pb, U, Ba, Mo, V, As, Cr) analysis of water samples was done in the same manner as sediment samples, i.e., by the use of HR ICP-MS (Element 2, Thermo) in the Laboratory for physical chemistry of traces of the Division for Marine and Environmental Research, Ruđer Bošković Institute. Samples were diluted 10 times with 2% HNO_3 (*suprapur*) to minimize the matrix effect linked to presence of salt. Indium was used as an internal standard, and a certified reference material (CASS-5 - nearshore seawater reference material for trace metals, National Research Council of Canada) for validation of the analysis.

4.4.3. Voltammetric analysis of cadmium

Cadmium determination in the seawater by HR ICP-MS is an analytically challenge, due to the typically very low concentrations and salt matrix effect. Therefore, Cd concentrations in the water column samples were measured by differential pulse anodic stripping voltammetry (DPASV) in the Laboratory for physical chemistry of traces of the Division for Marine and Environmental Research, Ruđer Bošković Institute. Prior to analysis samples (both filtered and unfiltered) were acidified with ultrapure concentrated HNO_3 (*suprapur*) to a pH of < 2 and irradiated with UV light (150 W mercury lamp, Hanau, Germany) for at least 24 h in order to decompose natural organic matter (Omanović et al. 2006).

Autolab (EcoChemie) potentiostats (μAutolab 2 or PGSTAT128N) controlled by GPES 4.9 software in a three-electrode cell (663 VA Stand, Metrohm) were used for the measurement. Ag/AgCl/sat. NaCl electrode was used as the reference electrode, a Pt wire as the auxiliary and a static mercury drop as the working electrode. Used measurement parameters were adopted from Omanović et al. (2006). Concentrations were determined by means of standard addition method.

4.4.4. Carbon analysis

A total organic carbon analyser TOC-V_{CSH} (Shimadzu) equipped with ASI-5000A module was used to determine DOC and DIC concentrations in the water samples. The analyses were done in the Laboratory of Processes of Transfers and Exchanges in the Environment (PROTEE) of the University of Toulon. To determine the content of the total carbon the 680°C combustion catalytic oxidation method was used. This method achieves total combustion of samples by heating them to 680°C in an oxygen-rich environment inside TC combustion tubes filled with a platinum catalyst. The carbon dioxide generated in this way is detected using a non-dispersive infrared gas analyser. To quantify DOC in the water samples the non-purgeable organic carbon measurements were conducted. In this method samples are acidified with 2 M HCl and then degassed prior to being injected to furnace at 680°C. The inorganic carbon was calculated by subtracting organic carbon content from total carbon content.

Calibration was done with potassium hydrogen phthalate ($C_8H_5KO_4$) and hydrogen sodium carbonate/sodium carbonate ($NaHCO_3/Na_2CO_3$) standard solutions. The estimated detection

limit for this method is 0.1 $mg_C L^{-1}$. A satisfactory accuracy of analyses was validated using certified reference material ION-96.4 (Environment Canada).

4.5. Statistical analysis

Spatial distribution maps were generated for the sixteen elements (C, N, P, S, Al, Fe, Ni, Cr, Co, As, Cd, Cu, Pb, Mn, Zn, Hg), the seven element enrichment factors (Hg, Mn, Bi, Zn, Cd, Cu, Pb) and the mean ERM quotients by using the Surfer 15 software (Golden Software LLC, 2017). The spatial interpolation was based on the surface sediment data (0-5 cm, 40 sampling locations) and performed by using Inverse Distance to a Power algorithm.

Pearson's correlation coefficients and the principal component analysis (PCA) were calculated using the software Origin 2019b (OriginLab Corporation). The PCA based on the correlation matrix was applied to the two data sets. The first data set consisted of the analytical results of 32 elements measured in the 40 surface sediment samples. The second data set included 36 parameters (31 elements, C_{org}, granulometric fractions: < 2µm, < 63µm and > 63µm) for seven sediment cores (in total 100 sediment samples). Number of principal components to be retained were determined by the visual examination of a scree plot and by applying a Kaiser's rule, i.e., retaining only the principal components with eigenvalues that are greater than 1.

5. RESULTS

5. RESULTS

5.1. Spatial distribution of elements in the Krka River estuary

5.1.1. Spatial distribution of carbon, nitrogen, phosphorus and sulphur

Contour maps generated to illustrate spatial variability of total carbon, nitrogen, phosphorus and sulphur in the surface sediment (0-5) of the Krka River estuary are presented in Fig. 5.1. The observed concentration ranges were 6.46-12% for C, 0.072-0.340% for N, 0.023-4.28% for P, and 0.248-0.907% for S, respectively (Table 5.1.). The complete results are given in Appendix 1.

According to the spatial distribution of the total carbon concentration, highest C values were found at the mouth of the estuary, while lowest values were found in the Zaton Bay and at the mouth of the Guduča River. Conversely, highest N values were recorded in the sample from the Guduča River and lowest values were recorded in the samples from the mouth of the Krka River estuary.

Lowest concentrations of P (< 0.05%) were found in the upper estuary, from its head to Prokljan Lake, and at estuary mouth. Slightly higher values, in range 0.05-0.1%, were found in the Guduča River, Prokljan Lake and in the part of St Anthony's Channel. In the largest part of the Šibenik Bay, P concentrations were increased, with the maximum value exceeding 4% in the port area. Considering the Port of Šibenik is specialized for the transhipment of raw phosphates and artificial fertilizers, these high values could be directly attributed to the transhipment activities.

Highest total sulphur concentrations were recorded at the head of the estuary, in the Guduča River and at K17 sampling location, while lowest concentrations were found in St Joseph's Channel, St Anthony's Channel and Prokljan Lake. According to the spatial distribution, S concentrations in the port and marina/shipyard area were slightly elevated, indicating a possible S anthropogenic input.

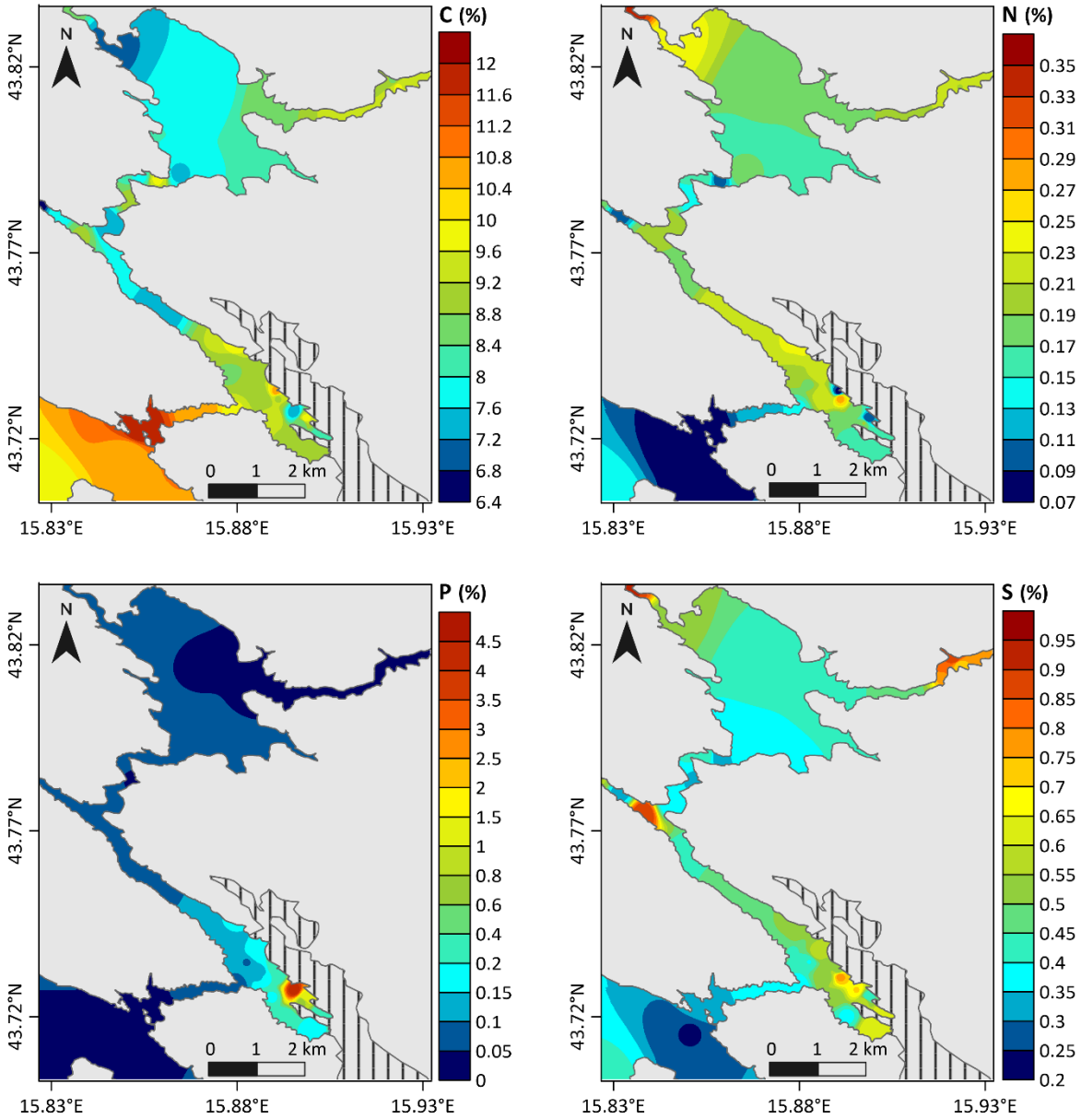

Figure 5.1. Distribution of C, N, P and S in surface sediment of the Krka estuary

5.1.2. Spatial distribution of metals

The spatial distributions of selected metals (Al, Fe, Ni, Co, Cr, Zn, Mn, Pb, As, Cu, Cd and Hg) in the surface sediment layer (0-5 cm) of the Krka River estuary are given as contour maps in Figs. 5.2. and 5.3. The obtained ranges and mean concentrations of all analysed metals are given in Table 5.1. The complete results are given in Appendix 1.

Aluminium and Fe, whose values ranged from 0.545 to 5.29% and from 0.647 to 1.94%, had a similar spatial distribution pattern. The highest values of these two elements were observed at

Guduča mouth, Zaton Bay, at sampling location K19 and at exit from the Joseph's Channel. The lowest values were found in the St Anthony's Channel, near the open sea, followed by low concentrations obtained in the broader Skradin area.

The spatial distributions of Ni, Cr and Co mostly corresponded to those of Al and Fe. Obtained values were in range 11.3-63.4 μg g^{-1}, 20.7-129 μg g^{-1} and 2.52-16.1 μg g^{-1}, respectively. However, the increased concentrations were found in the Šibenik Bay, in proximity to anthropogenic sources; the former Electrode and Ferroalloy Factory (Co, Ni) and the port (Cr).

Concentrations of As in the surface sediments of the Krka River estuary were found in range from 5.43 to 39.6 μg g^{-1}, with a mean value of 13.1 μg g^{-1}. The spatial distribution indicates larger input of As via Guduča River than the Krka River, yet the highest values were found in the samples from the shipyard/marina area, followed by those sampled in vicinity of the port and the ex-factory. Therefore, the main source of the As in the surface sediment of the Krka River estuary is presumably anthropogenic pollution.

Cd and Zn distributions followed a common trend in the surface layer of the Krka estuary sediments, with the highest concentrations (Cd_{max} = 11.2 μg g^{-1}; Zn_{max} = 1 200 μg g^{-1}) recorded in the port area. Regarding the fact that minimum observed concentrations were 0.11 μg g^{-1} and 37.6 μg g^{-1}, respectively, presumably the human impact has caused ~100-fold and ~30-fold increase in the port area.

Another two elements which have a common anthropogenic source, as indicated by the spatial distribution maps, were Pb and Mn. These two elements, with ranges 18.0-665 μg g^{-1} and 128-32 037 μg g^{-1}, showed elevated concentration across the Šibenik Bay, with distinct increase in the vicinity to the TEF factory.

Cu concentration in the surface sediment of the Krka River estuary ranged from 5.25 to 132 μg g^{-1}. Spatial distribution map revealed that elevated concentrations can be found in the entire lower part of the estuary, spreading from Zaton to Šibenik. Unlike other metals which are found in increased concentrations mainly in vicinity of just one anthropogenic source, Cu distribution suggests its connection to multiple anthropogenic sources: village Zaton and its marina, former TEF factory, the port, shipyard/marina area, small boats marina and Šibenik waterfront. The highest concentration was recorded in the sample taken at K24 location, at the Šibenik waterfront.

Total Hg concentrations in the surface sediments of the Krka River estuary ranged from 0.058 μg g^{-1} to 12.4 μg g^{-1}, with an average of 1.14 μg g^{-1}. From the Hg distribution map, it is evident that the upper estuary is quite pristine (< 0.3 μg g^{-1}), while the Hg distribution in the lower part of the estuary demonstrates a strong influence from the city of Šibenik, resulting in elevated concentrations in the Šibenik Bay area. The localized "hot-spot" of Hg contamination is the nautical marina/repair shipyard area, where the maximum Hg concentrations were reported.

Table 5.1. Basic statistical parameters (minimum (min), maximum (max), mean and standard deviation (SD)) for analysed elements in the surface sediment of the Krka River estuary. Values for C, N, P and S are given in %, and for other elements in μg g^{-1}.

Element	Min	Max	Mean	SD
C	6.46	12.0	8.91	1.10
N	0.072	0.340	0.180	0.055
P	0.023	4.28	0.250	0.683
S	0.248	0.907	0.512	0.161
Li	11.4	71.3	41.8	15.5
Be	0.423	2.31	1.44	0.493
Rb	7.07	90.2	50.8	20.8
Mo	0.701	7.03	1.84	1.10
Ag	0.091	1.77	0.470	0.354
Cd	0.112	11.2	0.909	1.78
Sn	0.733	19.8	6.47	4.22
Sb	0.264	1.64	0.633	0.329
Cs	0.701	7.18	4.30	1.70
Tl	0.129	0.834	0.527	0.180
Pb	18.0	665	93.9	107
Bi	0.145	5.04	1.39	1.33
U	1.67	25.0	3.51	3.64
Al	5 453	52 861	31 943	11 618
Ti	174	1 911	1 097	400
V	19.7	108	67.3	20.9
Cr	20.7	129	66.5	22.6
Mn	128	32 038	1 548	4 928
Fe	6 474	30 140	19 401	6 204
Co	2.52	16.1	7.09	2.71
Ni	11.3	63.4	40.9	14.1
Cu	5.25	133	44.0	32.2
Zn	37.6	1 201	203	204
Sr	237	1 989	977	514
Ba	33.1	477	144	85.6
As	5.43	39.6	13.1	6.39
Hg	0.056	12.4	1.14	0.007
Pt	0.008	0.039	0.025	0.007

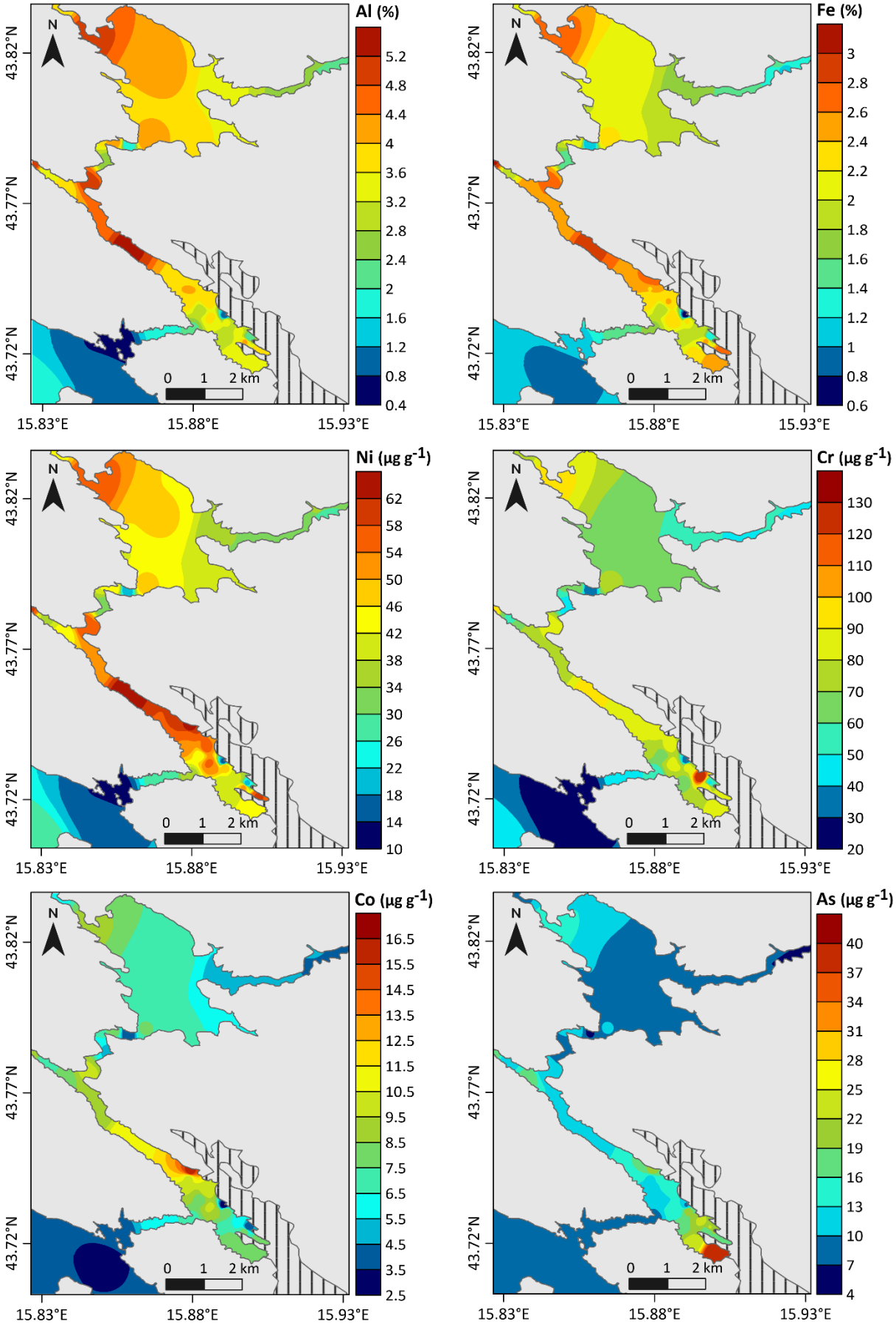

Figure 5.2. Distribution of Al, Fe, Ni, Cr, Co and As in surface sediment of the Krka estuary

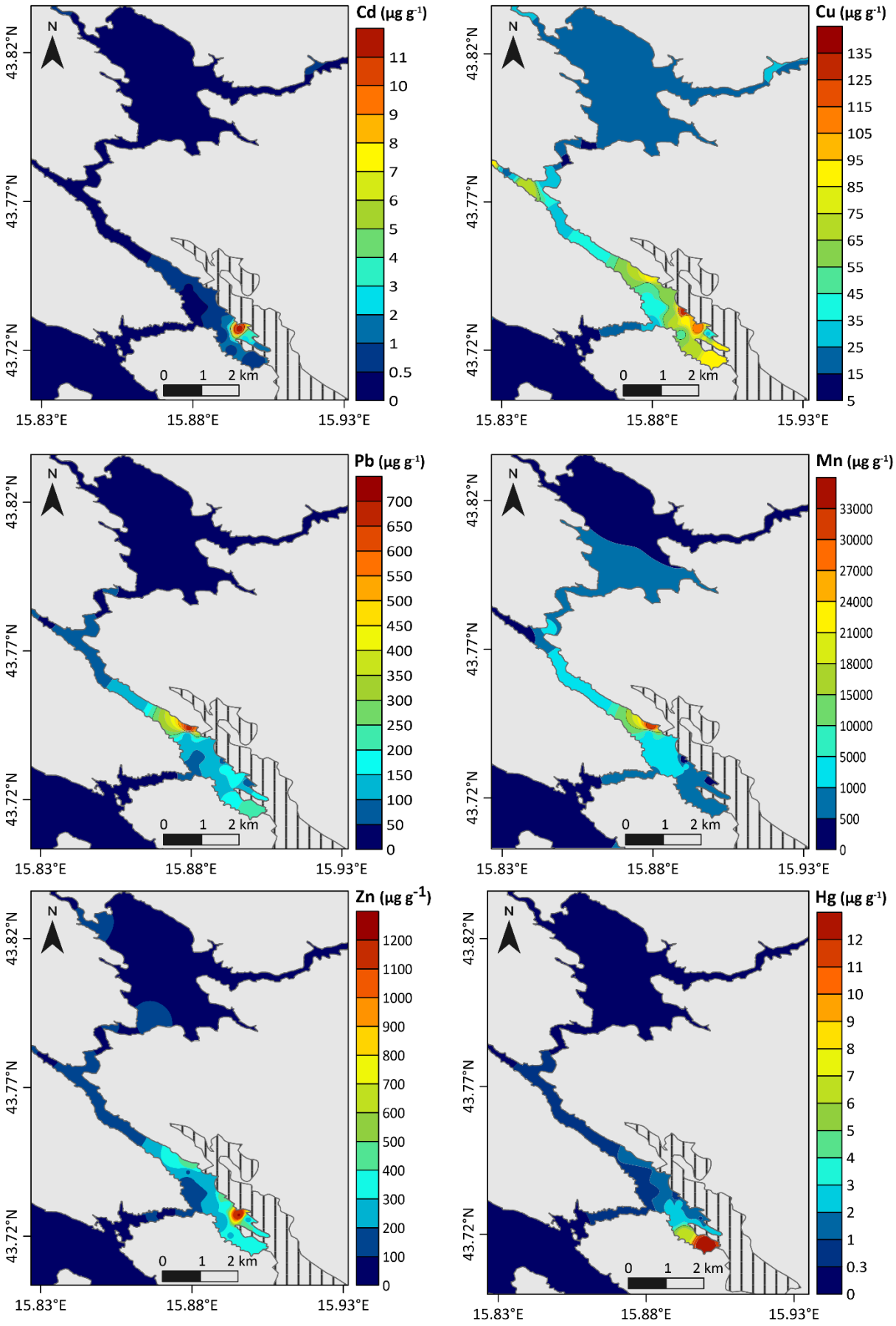

Figure 5.3. Distribution of Cd, Cu, Pb, Mn, Zn and Hg in surface sediment of the Krka estuary

5.2. Water column characterization

5.2.1. Water column physicochemical parameters

Vertical profiles of pH, oxidation-reduction potential (ORP), temperature, salinity and dissolved oxygen recorded *in-situ* in the water column by multi-parameter probe (EXO2, YSI) at sampling locations K1, K7, K8, K20 and K36 are shown in the Fig. 5.4. The temperature profiles reflect the different sampling seasons. In Prokljan Lake (K7) and in the port area (K36), sampling was done during summer season, and temperatures were in range 19.7-28°C and 22.2-25.1°C, respectively. At locations sampled during wintertime (K1 – the head of the estuary, K8 – the Guduča River and K20 – the TEF factory) temperatures were in range 7.9-17.9°C, with the distinct difference between upper and lower estuary. At site K20, temperature profile was quite uniform, with temperatures ~13°C and slightly lower temperatures recorded only in the top 0.5 m of the water column. Contrary, in the upper estuary (K1 and K8), a pronounced temperature vertical stratification was observed, with temperatures below 10°C in the surface layer and above 15°C in the seawater layer.

Furthermore, during winter period, a pronounced salinity stratification of the water column was observed in the upper estuary (K1 and K8), with a clear segmentation of the three separate layers and a sharp halocline. The vertical salinity profiles at other sampling locations also show stratification, but with a much smaller salinity range. At site K20, seawater layer was recorded at much lower depth (< 0.5 cm) than at all other sites.

In accordance with temperature and salinity profiles, dissolved oxygen concentration and saturation profiles at site K20 were rather homogenous, with the concentration range of 7.94-9.76 mg L^{-1} and saturation between 94% and 102%. At locations sampled during summer season (K7, K36), an oxygen maximum (up to 151%) was recorded at the lower edge of the halocline as a result of the high primary production by marine phytoplankton, as already reported by other authors (Legović et al. 1994; Cindrić et al. 2015). Namely, freshwater phytoplankton sinks to the halocline where it decomposes due to the high salinity, releasing the nutrients which favour blooms of marine phytoplankton. Legović et al. (1991b) observed hypoxia near the bottom in Prokljan Lake during autumn, resulting from sinking and decomposition of marine phytoplankton blooms. In this study, and as reported by Cindrić et al. (2015), hypoxia was not observed in Prokljan Lake during summertime, but there was a constant decrease of oxygen saturation from the observed maximum to the bottom (89%), which potentially may have led to hypoxia in autumn.

However, strong oxygen undersaturation (39-68%) was registered during winter period in the upper estuary. As seen from the profiles of other physicochemical parameters, the water column at the head of the estuary and in the Guduča River showed a distinct vertical stratification, with the temperatures in the bottom seawater layer as high as 17.9°C. The lack of water column mixing and the high bottom temperatures favour decomposition of the organic matter and consumption of oxygen, which may lead to hypoxia. Although hypoxia (<2 mg L^{-1}) was not reached, oxygen concentrations decreased substantially, up to 3 mg L^{-1}.

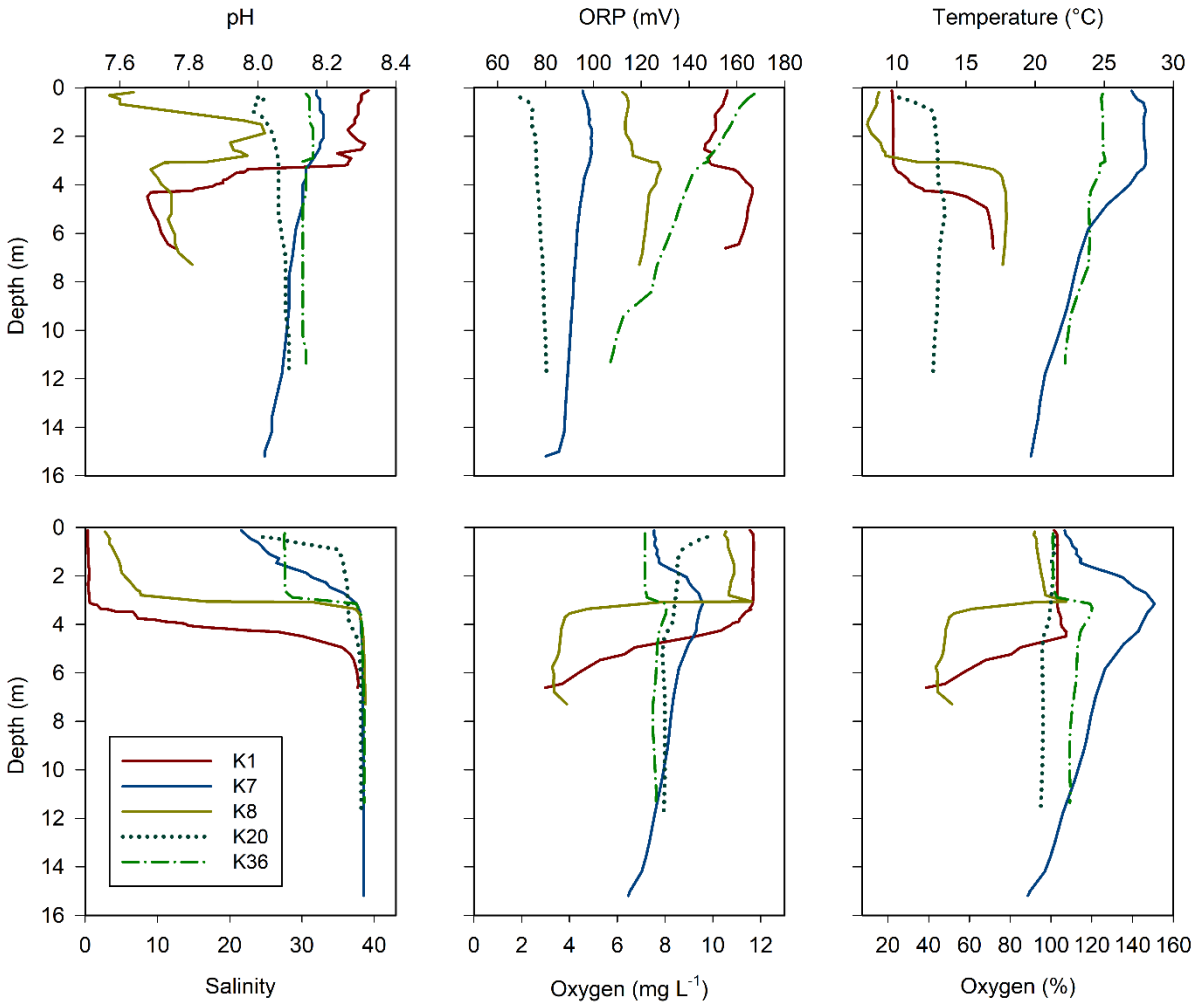

Figure 5.4. Vertical profiles of water column physicochemical parameters measured at sampling locations K1, K7, K8, K20 and K36.

The marked difference between the upper estuary (K1 and K8, sampled in the winter period) and the rest of the profiles was also shown by pH values in the water column. While in the Šibenik Bay (summer and winter period) and Prokljan Lake (summer), pH values were not changing considerably (8.0-8.2) along the depth, in the upper estuary (winter) pH was varying between 7.6 and 8.3, with a sudden drop observed bellow the FSI.

The oxidation-reduction potential measured in the estuary indicates oxidative conditions of the water column at all sampling locations.

5.2.2. Dissolved organic carbon (DOC) and dissolved inorganic carbon (DIC)

The dissolved organic carbon concentrations in the water column of the Krka River estuary were found in the range between 0.667 mgC L^{-1} and 1.75 mgC L^{-1} (Fig. 5.5.). Highest concentrations were found in the surface layer at K7 and K36 sampling locations, i.e., at locations sampled during the summer season. Lowest DOC values were recorded at the head of the estuary, where sampling was conducted during winter season.

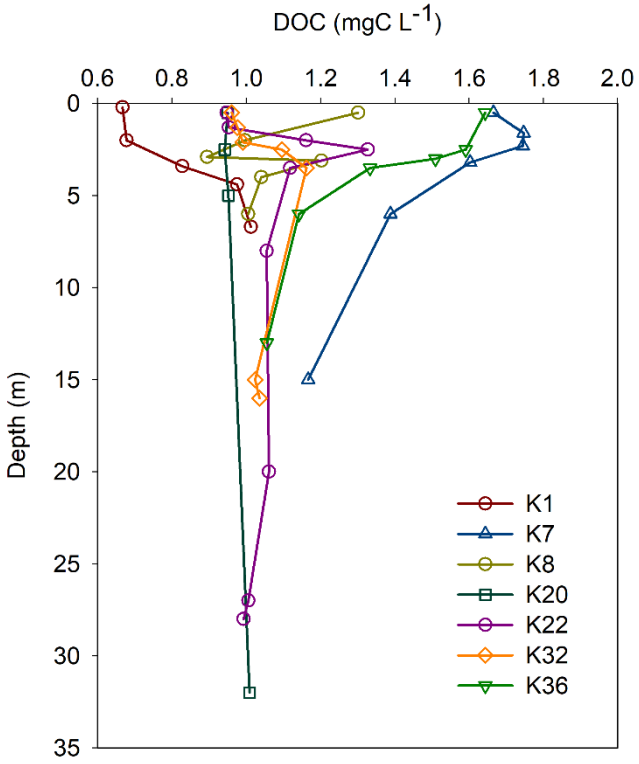

Figure 5.5. Vertical profiles of dissolved organic carbon (DOC) at sampling locations K1, K7, K8, K20, K22, K32 and K36

The dissolved inorganic carbon concentrations in the water column of the Krka River estuary were found in the range between 28.2 mgC L^{-1} and 61.1 mgC L^{-1} (Fig. 5.6.). Highest concentrations were observed at the upper estuary sites which were sampled in wintertime, i.e., K1 and K8. Values in range 45-50 mgC L^{-1} were found in the surface layer at locations K20, K22 and K32, i.e., in the sites of the Šibenik Bay which were sampled during winter and spring seasons. Lowest values recorded in the surface layer were at sites K7 and K36, sampled during

summer season. The DIC vertical distribution trend was similar at all sampling locations, with a rapid decline at the interface layer and uniform values in the sea layer.

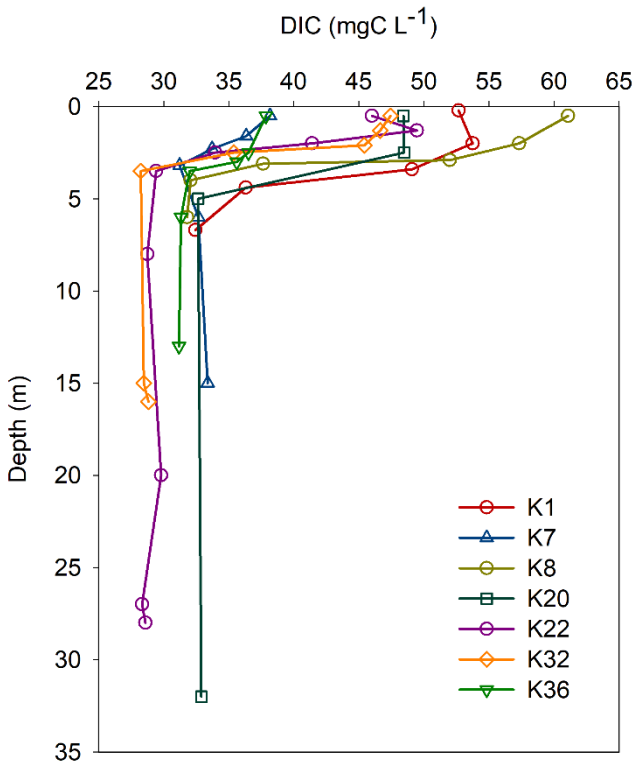

Figure 5.6. Vertical profiles of dissolved inorganic carbon (DIC) at sampling locations K1, K7, K8, K20, K22, K32 and K36

5.2.3. Trace elements distribution in the water column

Distributions of trace elements in the water column of the Krka River estuary sampled at five locations (K1, K7, K8, K20 and K36) are shown in Figs. 5.7.-5.11. The complete results are given in Appendices 2.-6.

According to the results of the measurements, it is not possible to give general conclusion on vertical and/or spatial distribution of trace elements in the estuary. However, some observations can be pointed out. Lithium, U, Mo and V had a similar distribution pattern, characterized by an increase of concentration in the seawater layer, at all sampling locations. The obtained ranges were 0.975-234 μg L^{-1}, 0.470-3.75 μg L^{-1}, 0.466-13.2 μg L^{-1} and 0.448-1.77 μg L^{-1}. The differences in concentrations between surface and seawater layer were more prominent at upper estuary sites K1 and K8 than in the rest of the estuary. For example, in Prokljan Lake (K7) and in the Šibenik Bay (K20 and K36) Mo and Li concentrations were 2-fold higher in the seawater

compared to surface layer, whereas at the head of the estuary (K1) the increment was up to 25-fold and 200-fold, respectively. Arsenic followed the same trend in the entire estuary, except at the former factory site (K20), where pronounced increase of As content was observed in the surface layer. That was also the maximum As concentration (3.02 μg L^{-1}) in the water column of the Krka estuary. The lowest As concentration was recorded in the surface layer at the head of the estuary (K1) (0.131 μg L^{-1}). The similar pattern was observed for Al distribution, but in this case, the exception was the port sampling site (K36). Aluminium concentrations were found in range 0.372-3.49 μg L^{-1}.

Contrary, concentrations of Cu, Cr and Co showed a decreasing trend with the depth at most of the sampling sites. However, the difference between concentrations in the surface and the bottom layer was not pronounced. Values were found in ranges 0.052-1.68 μg L^{-1}, 0.052-0.276 μg L^{-1} and <0.005-0.034 μg L^{-1}, respectively.

Furthermore, some elements had a marked concentration peaks at the FSI at most of the sampling sites, e.g., Fe, Mn and Pb. The obtained ranges for these three elements were 0.006-2.28 μg L^{-1}, 0.005-4.72 μg L^{-1} and <0.005-0.221 μg L^{-1}. The highest intra-site variability of concentration was that of Mn at the head of the estuary (K1), where high concentrations were found at the FSI and in the bottom layer (2.40 μg L^{-1} and 4.72 μg L^{-1}), whereas they were < 0.12 μg L^{-1} in surface layer and in one of the samples from the seawater. Apart from the increase of concentration at FSI, Pb had considerable increase in the bottommost samples in the Šibenik Bay (K20 and K36). In the upper estuary, Pb content near-bottom was below 0.02 μg L^{-1}, while in the lower estuary it was 0.2 μg L^{-1}. A notable increase of concentration at the bottom of the water column in the Šibenik Bay was observed also for Zn, but only at the port site (K36). At all other sites in estuary, Zn showed opposite trend, with the lowest concentrations (or close to minimum concentration) recorded at the bottommost layer of the water column. The obtained range was 0.357-5.71 μg L^{-1}.

Nickel water column concentrations were ranging from 0.077 μg L^{-1} and 0.472 μg L^{-1}, with different vertical distribution from site to site. At the head of the estuary (K1) and at the old factory site (K20), concentrations increased in the seawater layer. The peak at the FSI was observed at the port sampling location (K36) and in Prokljan Lake (K7), but the latter had a maximum concentration in the near-bottom sample. Contrary, in the Guduča River (K8) concentrations were 2-fold lower at FSI than in both surface and seawater layer.

Regarding spatial distribution, Ba showed lowest variation from site to site, with values ranging from 6.72 µg L^{-1} and 9.38 µg L^{-1}.

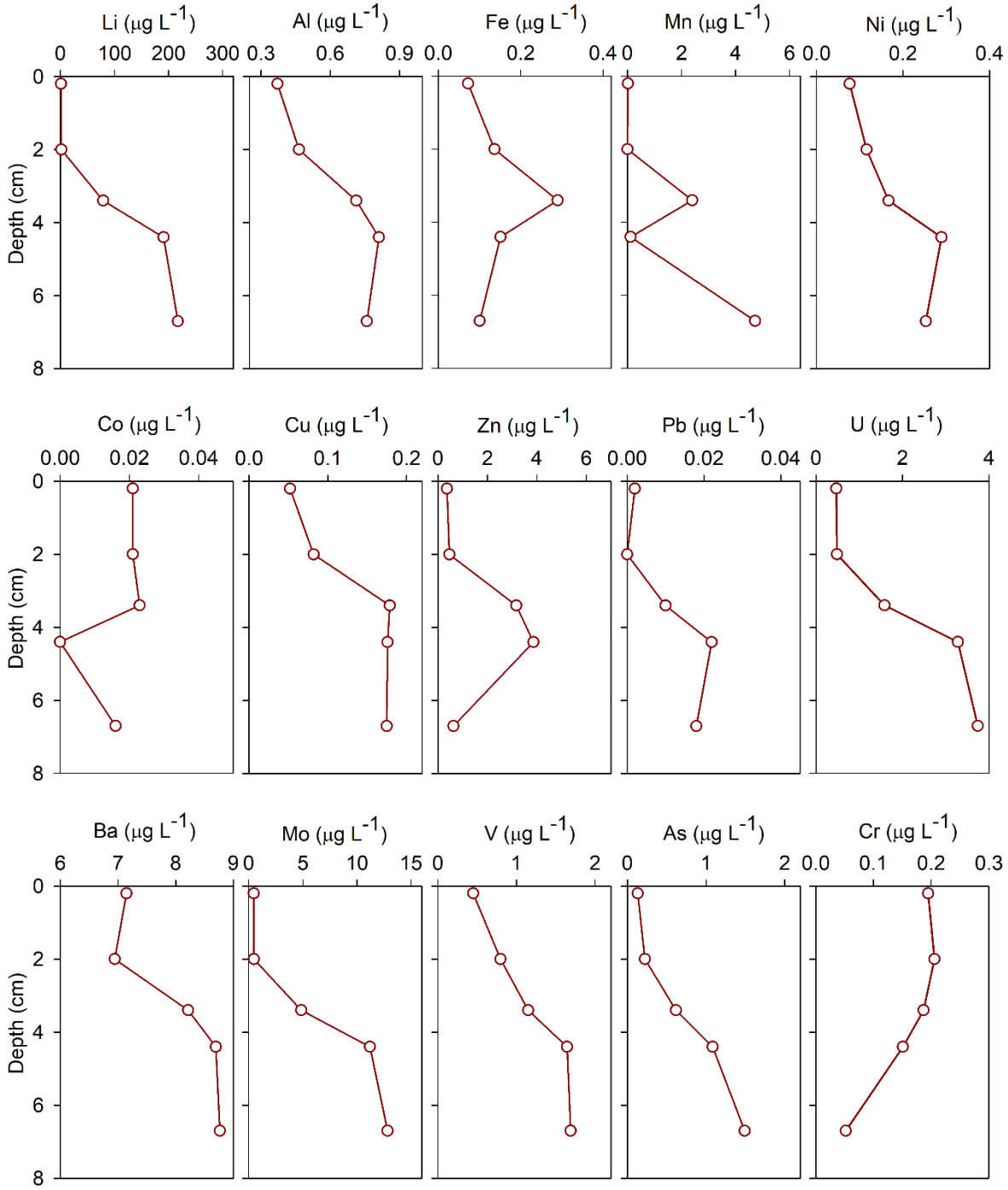

Figure 5.7. Vertical distribution of selected elements (Li, Al, Fe, Mn, Ni, Co, Cu, Zn, Pb, U, Ba, Mo, V, As, Cr) in the water column on sampling site K1

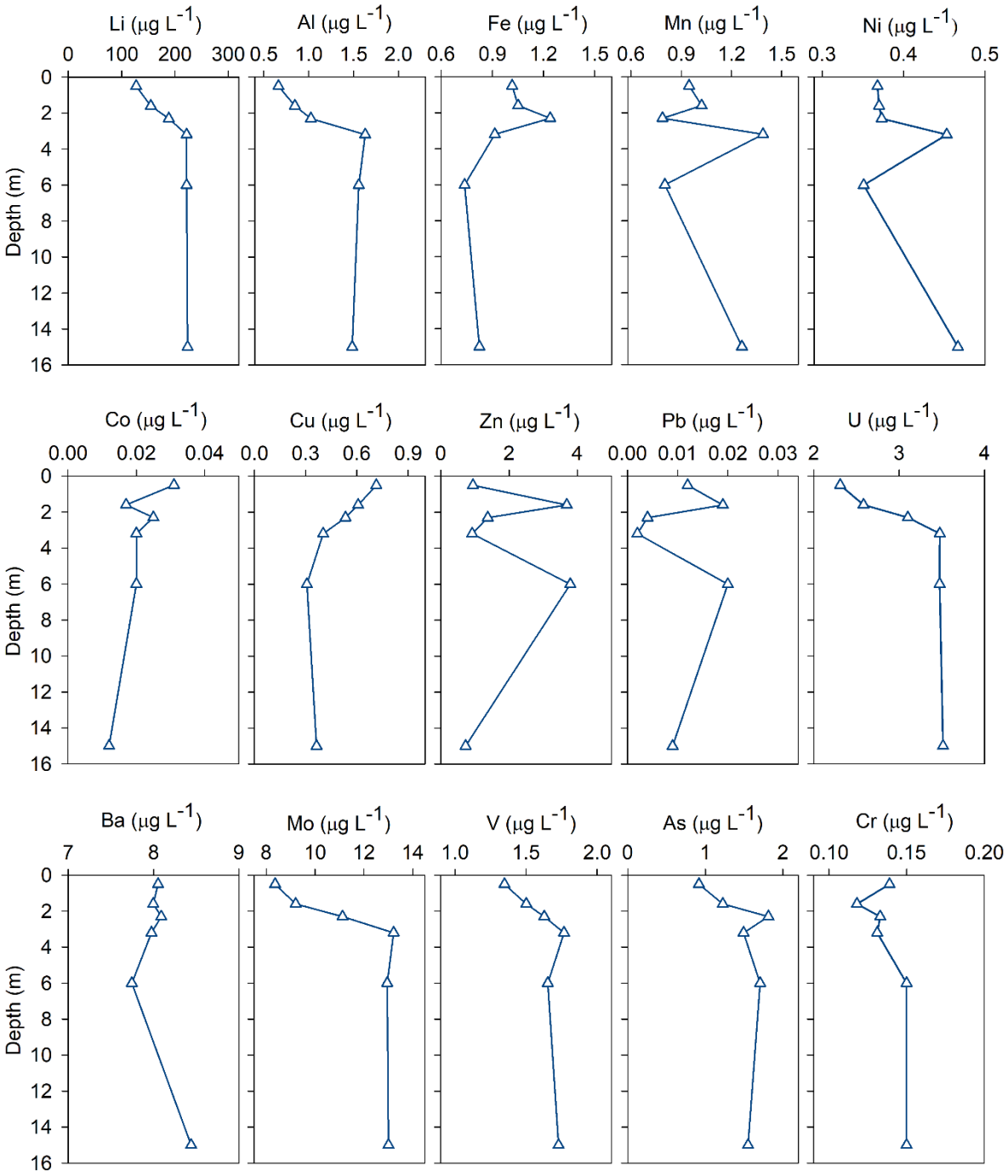

Figure 5.8. Vertical distribution of selected elements (Li, Al, Fe, Mn, Ni, Co, Cu, Zn, Pb, U, Ba, Mo, V, As, Cr) in the water column on sampling site K7

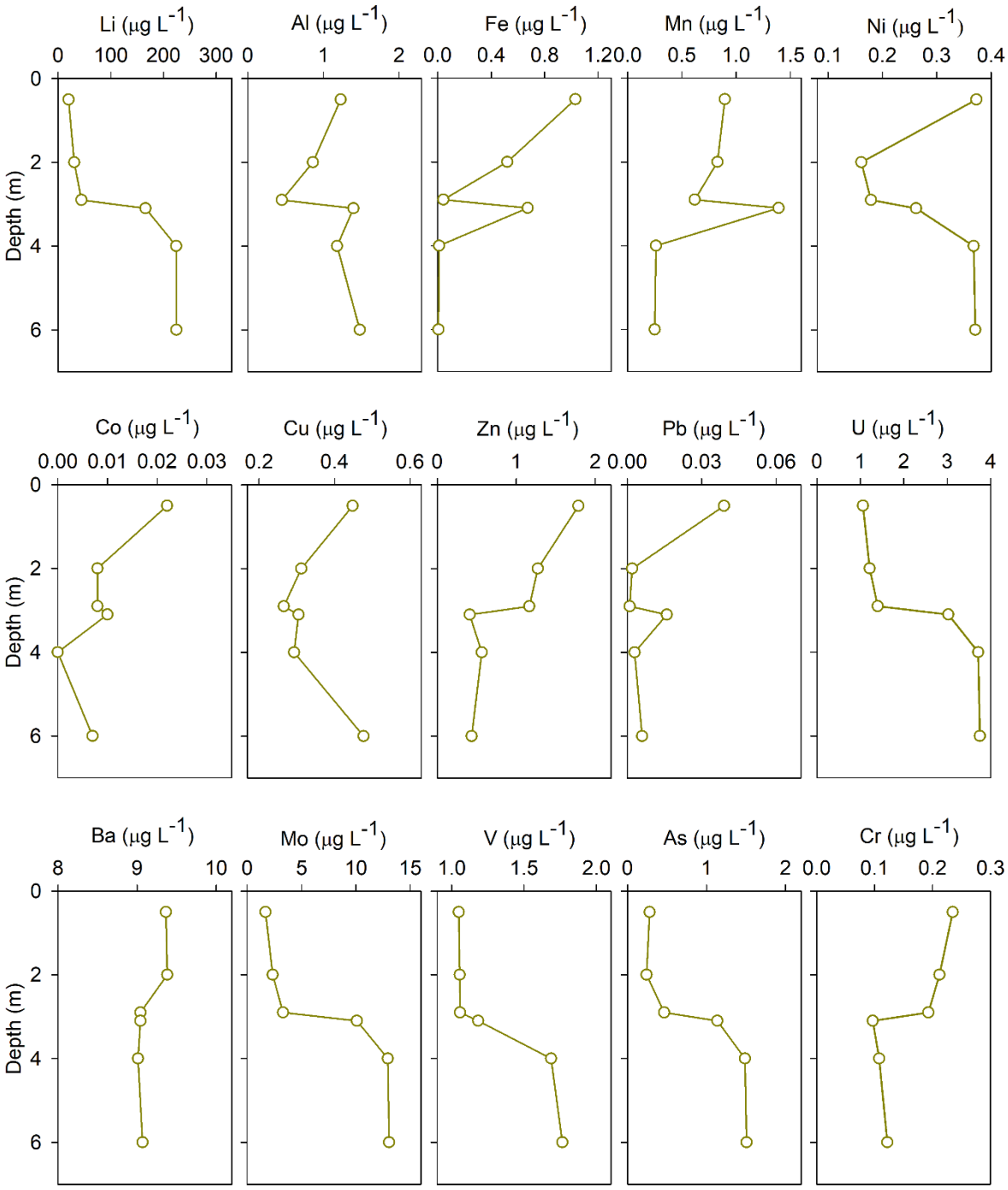

Figure 5.9. Vertical distribution of selected elements (Li, Al, Fe, Mn, Ni, Co, Cu, Zn, Pb, U, Ba, Mo, V, As, Cr) in the water column on sampling site K8

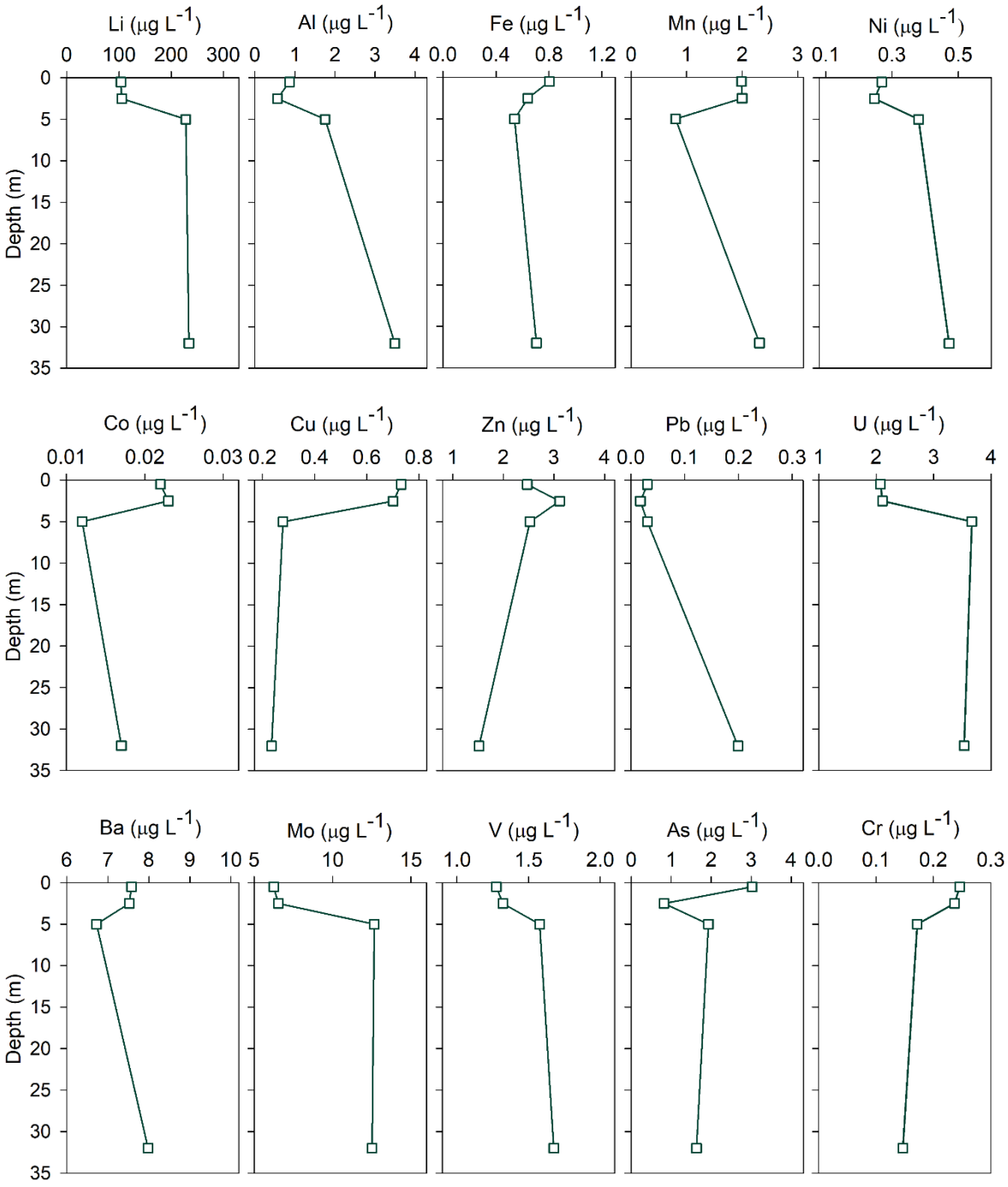

Figure 5.10. Vertical distribution of selected elements (Li, Al, Fe, Mn, Ni, Co, Cu, Zn, Pb, U, Ba, Mo, V, As, Cr) in the water column on sampling site K20

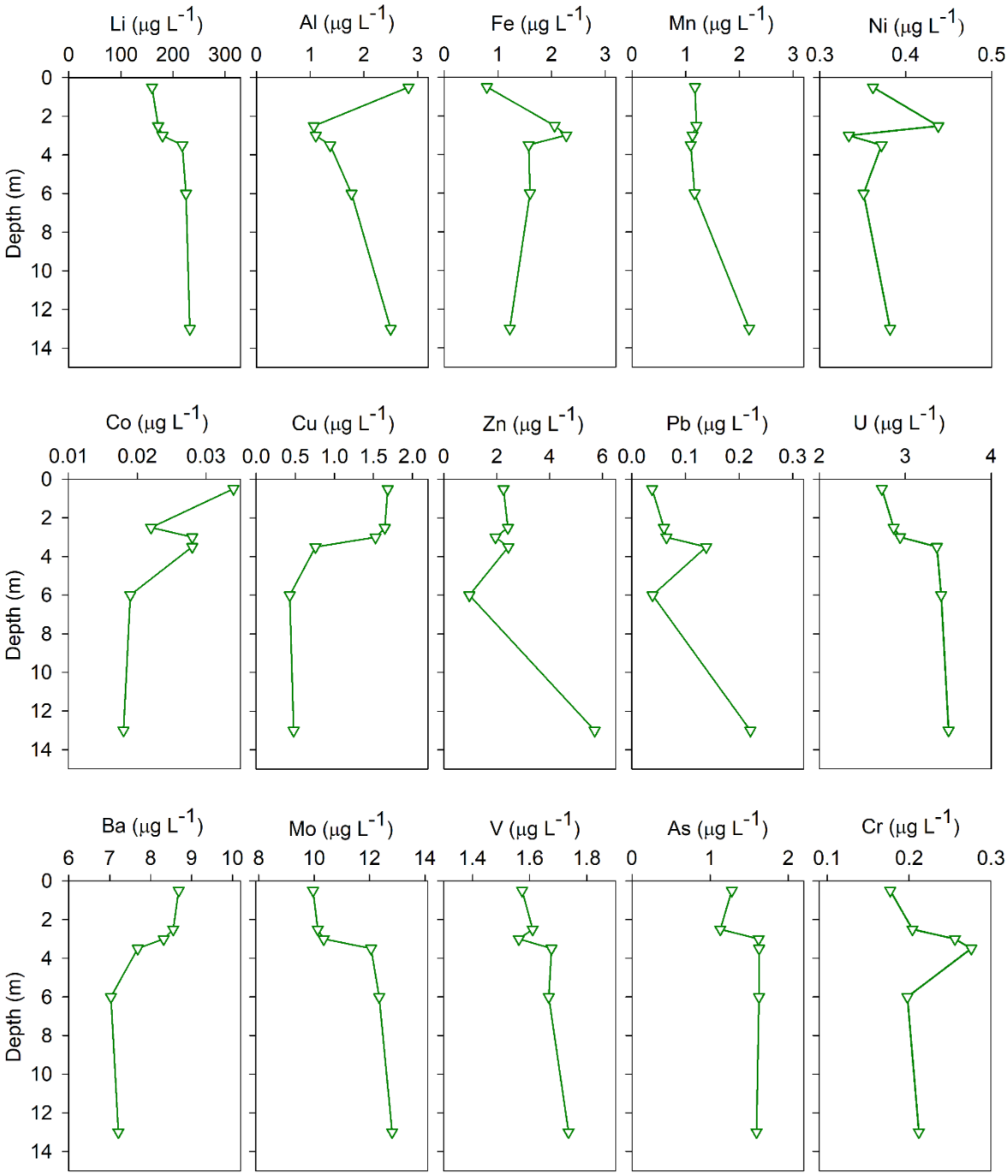

Figure 5.11. Vertical distribution of selected elements in the water column (Li, Al, Fe, Mn, Ni, Co, Cu, Zn, Pb, U, Ba, Mo, V, As, Cr) on sampling site K36

Cadmium in the water column samples was determined using anodic stripping voltammetry. The results are given in table 5.2.

The measured concentration ranges were 3.68-19.36 ng L^{-1} for dissolved and 4.03-21.18 ng L^{-1} for total Cd in the Krka River estuary water column. Generally, Cd vertical distribution showed downward increasing trend. Regarding spatial distribution, highest Cd content was found at K36 sampling location and lowest at K8 sampling location.

Table 5.2. Dissolved and total (in parentheses) Cd concentrations in the water column of the Krka River estuary. Cadmium is expressed in ng L^{-1} and depth in m.

K7		K8		K20		K36	
Depth	Cd	Depth	Cd	Depth	Cd	Depth	Cd
0.5	6.39 (6.64)	0.5	3.68 (4.03)	0.5	8.77 (9.44)	0.5	8.83 (10.9)
1.6	6.53 (6.92)	2	3.78 (4.24)	2.5	5.28 (9.11)	2.5	11.42 (12.58)
2.3	8.22 (9.37)	2.9	4.50 (5.32)	5	9.67 (11.24)	3	10.61 (11.67)
3.2	9.9 (9.92)	3.1	6.31 (7.02)	32	6.52 (8.66)	3.5	10.06 (11.48)
6	8.42 (17.1)	4	8.56 (9.08)			6	7.61 (8.47)
15	10.66 (10.97)	6	8.01 (8.52)			13	19.36 (21.18)

5.3. Sediment cores characterization

5.3.1. Granulometric composition of sediment cores

The particle size analysis was performed on each layer of the sampled cores, i.e., on a total of 100 sediment samples. According to the Shepard's (1954) ternary diagram, shown in Fig. 5.12., sediments from the upper estuary (cores K1 – the head of the estuary, K7 – Prokljan Lake and K8 – the Guduča River) were classified as clayey silt and silt, while sediment cores from the Šibenik Bay (K20 – the former Electrode and Ferroalloy Factory, K22 – the Research Station Martinska, K32 – the nautical marina/shipyard and K36 – the Port of Šibenik) were predominantly classified as sandy silt, with a several core subsamples falling into clayey silt (K22: 8-9 cm, 9-10 cm) and silty sand (K32: 15-17 cm, 17-19 cm; K36: 14-16 cm, 16-18 cm) class.

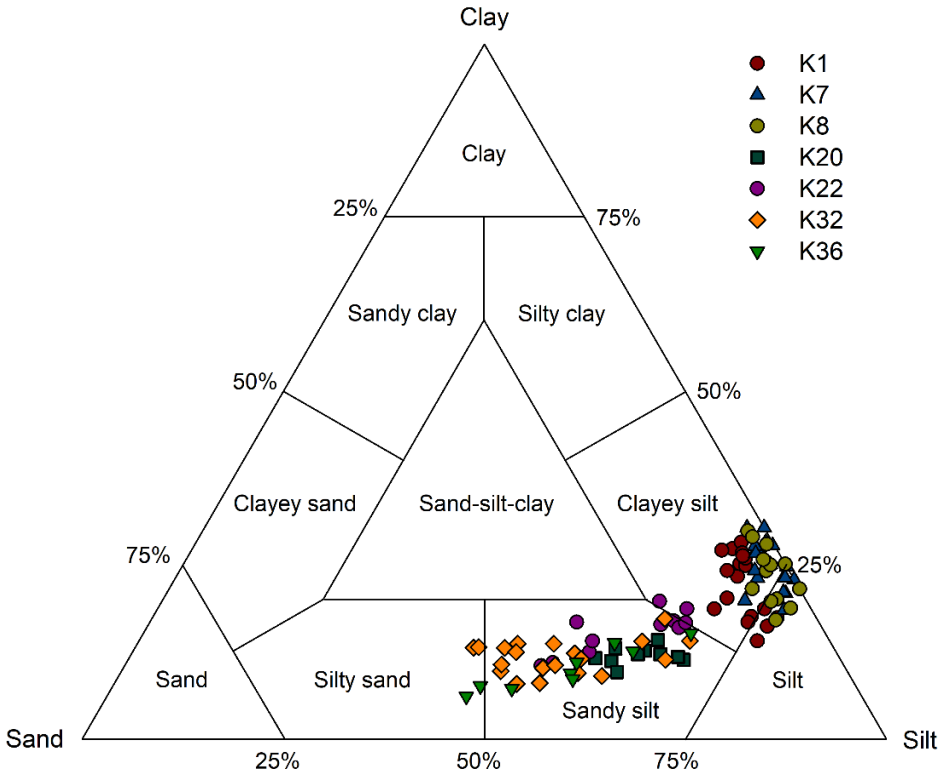

Figure 5.12. Ternary diagram for the classification of sediments (Shepard 1954) with cores subsamples from the Krka River estuary denoted based on the obtained ratios of sand, silt and clay

The difference in granulometric composition between upper and lower estuary is also evident from the down-core plots of different grain-size factions and mean grain size (Mz) shown in Fig.5.13. Cores from the head of the estuary (K1), Prokljan Lake (K7) and Guduča River (K8) were characterized by high proportion of the fine fraction, predominantly composed of silt. The sand proportions were low, even not represented in some subsamples. Skradin core had a higher sand proportion (3.9-12%) than Prokljan Lake core (0-7.6%) and Guduča River core (0-5.9%). The average grain size varied with depth from fine to coarse silt in the Guduča River (7.3-17 μm) and Prokljan Lake (6.3-20 μm), and from medium (13 μm) to coarse (29 μm) silt at head of the estuary.

In comparison to the upper estuary, cores from the lower estuary had a higher proportion of sand fraction, reaching 45% in the marina/shipyard area (K32) and 50% in the port area (K36). Therefore, mean grain sizes in the cores from the Šibenik Bay showed an increase compared to the upper estuary cores. Moreover, the lower estuary cores demonstrated much more down-core fluctuation of the mean grain size; from very coarse silt to very fine sand at the Martinska

(31-88 µm), the TEF factory location (33-67 µm) and the port area (34-108 µm) and from very coarse silt to fine sand in the marina/shipyard area (42-150 µm).

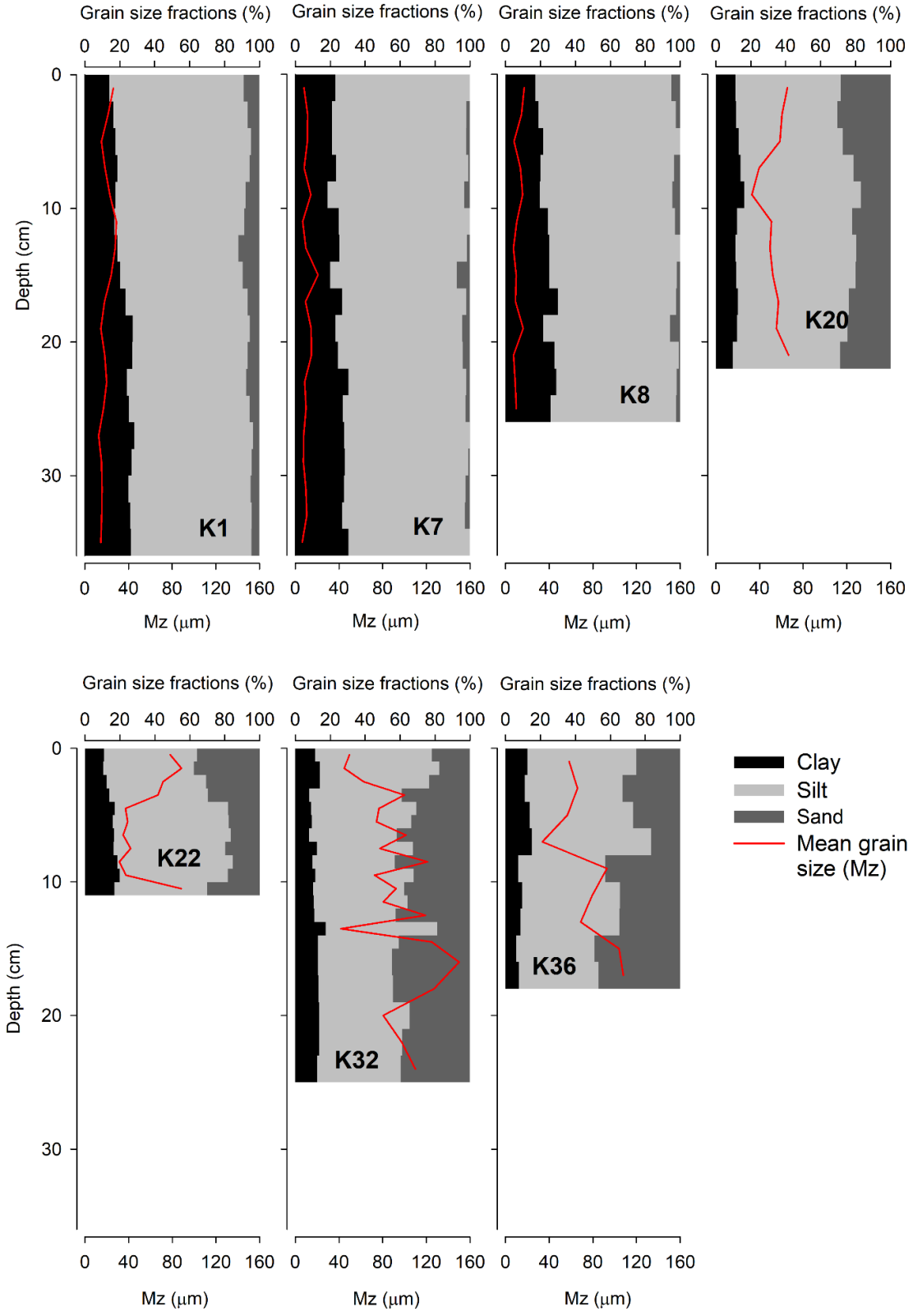

Figure 5.13. Down-core grain size distribution: clay (< 2 µm), silt (2-63 µm) and sand (63-2 000 µm)

Obtained results are in the agreement with the previously reported data on grain size distribution in the Krka River estuary which detected the coarsening of particles toward the sea (Prohić and Juračić; Juračić and Prohić 1991). More precisely, mean grain sizes obtained in those studies revealed gradual decrease from the Guduča River (15 μm) toward the lower part of Prokljan Lake (4.8 μm) and increase via Martinska (140 μm), toward the sea (410 μm). The authors explain preferentially deposition of the Guduča-borne small particles in Prokljan Lake due to the hydrographic conditions and salt-controlled flocculation. Moreover, the coarsening of sediments seaward indicates either a different source of sediment partices or a non-depositional environment. Similar results were presented by Bogner (2001), who analysed sediment at four locations in the Krka estuary: the Guduča River, Prokljan Lake, the Šibenik bridge and the Šibenik Bay.

5.3.2. Mineralogical composition of sediment cores

The mineralogical composition was determined for one to four subsamples per sediment core, in total 23 subsamples (K1: 0-2 cm, 12-14 cm, 22-24 cm, 34-36 cm; K7: 0-2 cm, 34-36 cm; K8: 0-2 cm, 12-14 cm, 18-20 cm, 24-26 cm; K20: 0-2 cm, 8-0 cm, 14-16 cm, 20-22 cm; K22: 0-1 cm; K32: 0-1 cm, 4-5 cm, 11-12 cm, 23-25 cm; K36: 0-2 cm, 4-6 cm, 10-12 cm, 16-18 cm). Obtained diffractograms are presented in Figs. 5.14.-5.20.

The results of XRD analysis revealed predominance of carbonates in all analysed subsamples. Four carbonate minerals were identified: calcite (Cal), aragonite (Arg), high-magnesium calcite (Mg-Cal) and dolomite (Dol). Amongst them, calcite was the dominant one and the only one detected in each subsample. Although aragonite was detected in all parts of the estuary, its abundance rose seaward. High-magnesium calcite and dolomite were detected only in the cores from the Šibenik Bay (K20 – the former Electrode and Ferroalloy Factory, K22 – the Research Station Martinska, K32 – the nautical marina/shipyard and K36 – the port). While high-magnesium calcite was observed in all the analysed layers of the cores from the lower estuary, dolomite was identified only in some of the layers; K22 (0-1 cm), K32 (11-12 cm, 23-25 cm), K36 (0-2 cm, 10-12 cm, 16-18 cm). The presence of Mg-calcite and aragonite in the lower estuary indicates to the carbonate biogenic sedimentation, as suggested by Juračić and Prohić (1991) and Bogner (2001). The presence of dolomite in the Šibenik Bay, moreover, indicate that part of the sediment could be of abrasive origin or that pre-Holocene sediments are present in the sediment (Juračić and Prohić, 1991).

The most abundant silicate mineral in the Krka River estuary is quartz (Qtz). Along with the calcite, it is an only mineral represented in all the analysed subsamples. The presence of feldspar was detected at some depth intervals of cores K1, K20, K22, K32 and K36. The clay (< 2 μm) fraction was not analysed separately, nevertheless, diffractograms of the bulk sediment samples indicate possible presence of the illite and/or muscovite in the sediment from the Guduča River (K8) and Prokljan Lake (K8).

Among other minerals, pyrite was detected in deeper layers of K1 and K7 sediment cores. It is possible that detection of pyrite in the sediments from the Šibenik Bay was limited due to the interference of the strongest peak of pyrite (2.70 Å) with (012) reflex of aragonite at the same position. In the sediment from the Šibenik Port (K36), minerals from the apatite group were identified in all the analysed layers.

Regarding the fact that sediments were not pre-washed with distilled water, in most diffractograms peaks corresponding to halite (Hl) can be observed. Moreover, in some samples the reflex at $2\theta = 44.58°$ was observed resulting probably from the aluminium sample holder.

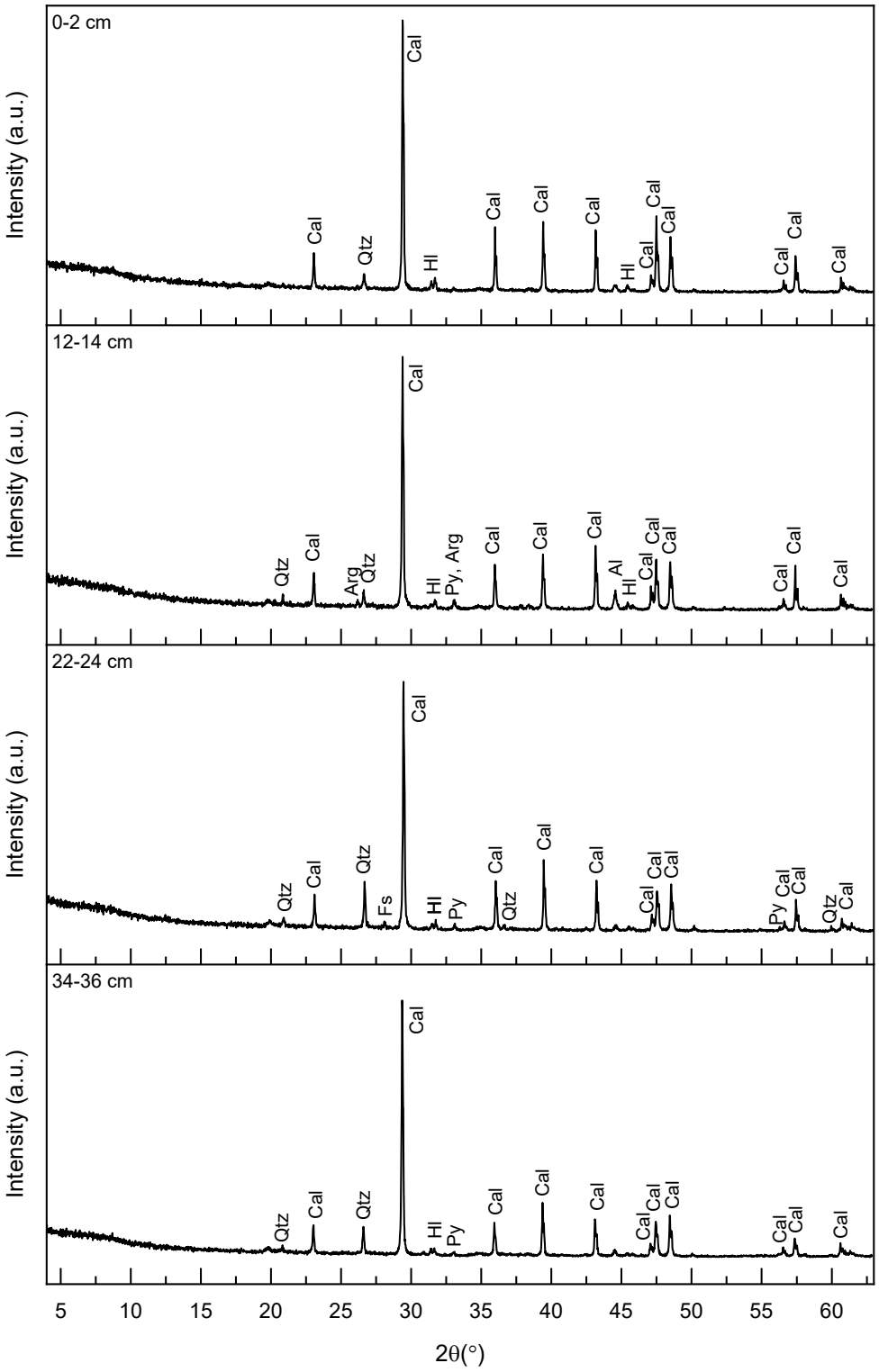

Figure 5.14. X-ray diffraction (XRD) patterns of selected bulk sediment subsamples of the K1 core. Mineral abbreviations: Arg-aragonite, Cal-calcite, Fs-feldspar, Hl-halite, Py-pyrite, Qtz-quartz.

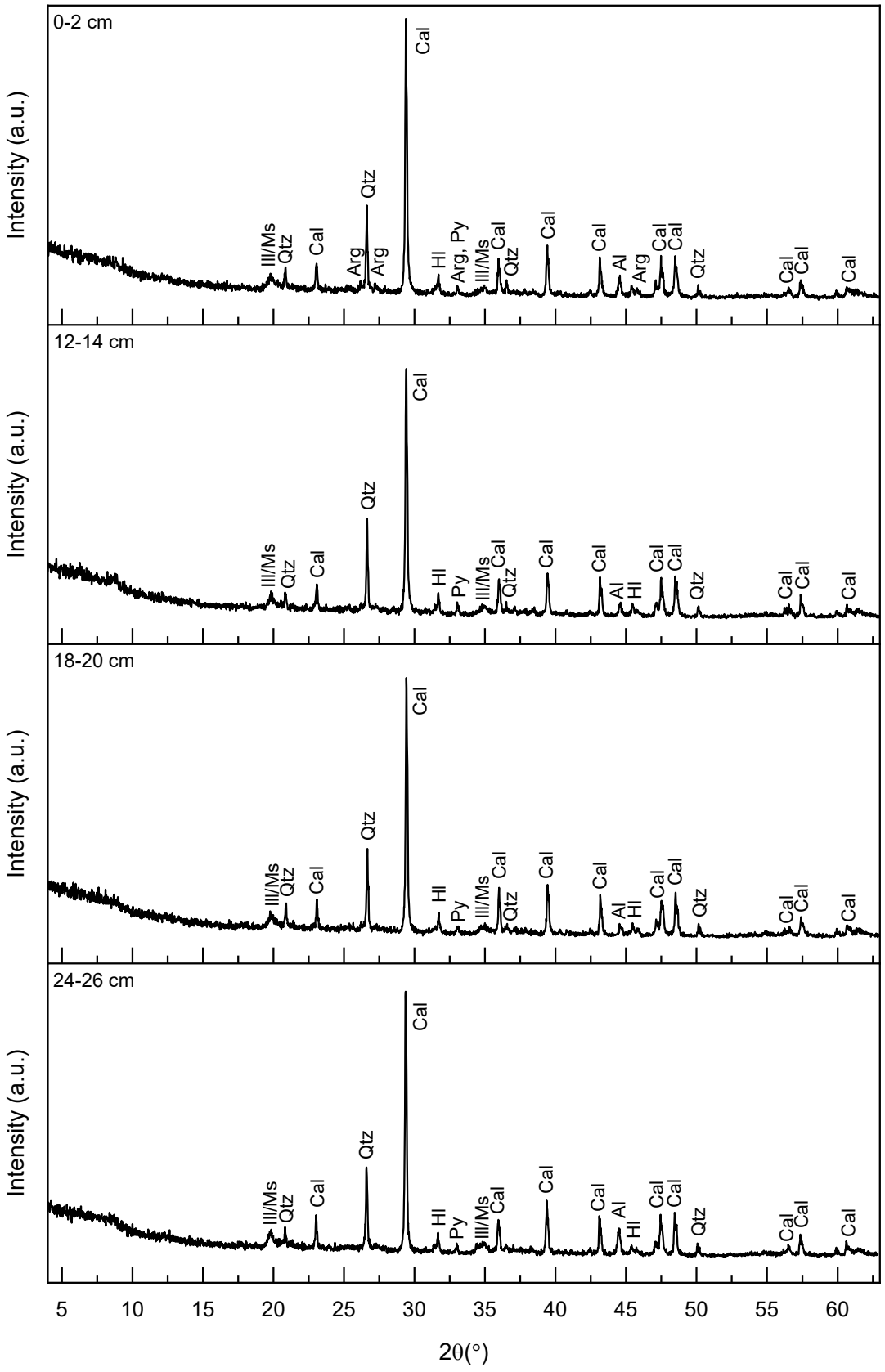

Figure 5.15. X-ray diffraction (XRD) patterns of selected bulk sediment subsamples of the K8 core. Mineral abbreviations: Arg-aragonite, Cal-calcite, Hl-halite, Ill/Ms-Illite/Muscovite, Py-pyrite, Qtz-quartz.

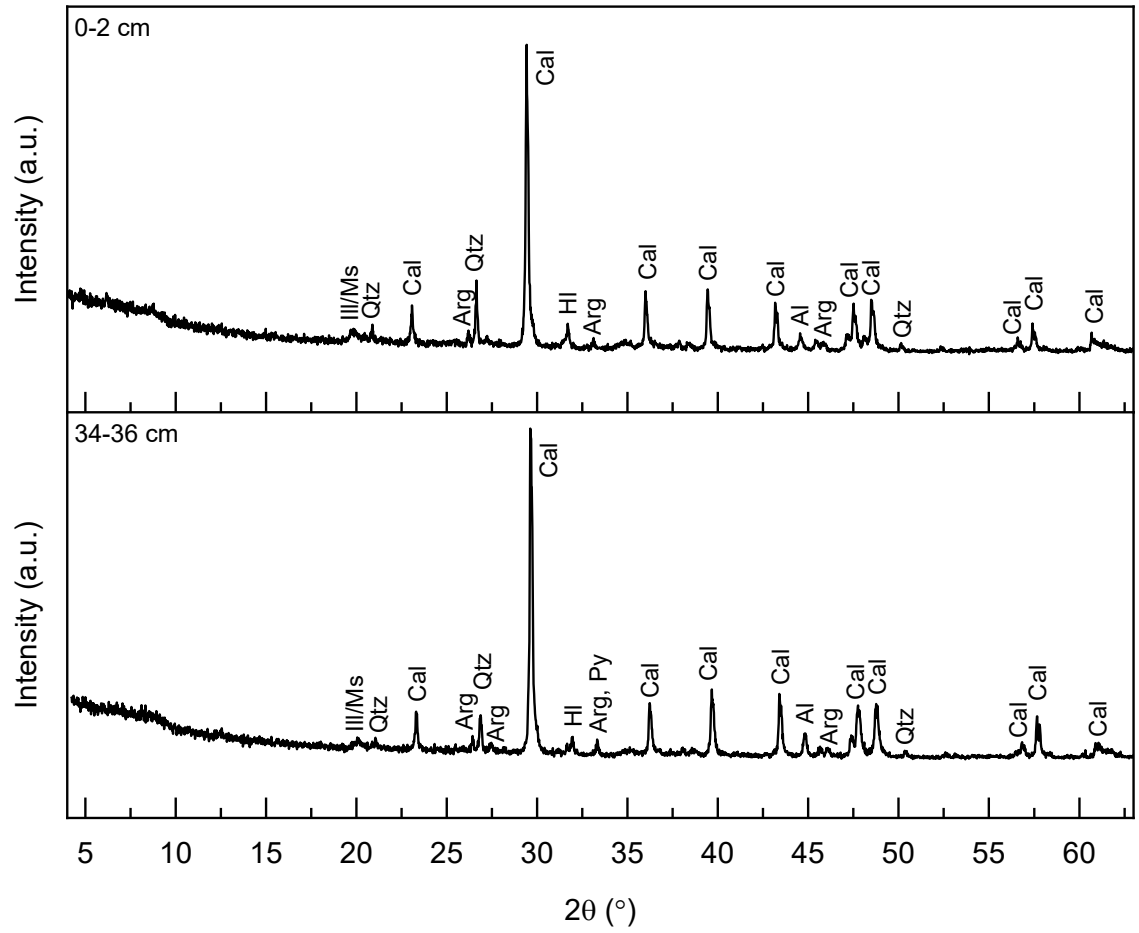

Figure 5.16. X-ray diffraction (XRD) patterns of selected bulk sediment subsamples of the K7 core. Mineral abbreviations: Arg-aragonite, Cal-calcite, Hl-halite, Ill/Ms-Illite/Muscovite, Py-pyrite, Qtz-quartz.

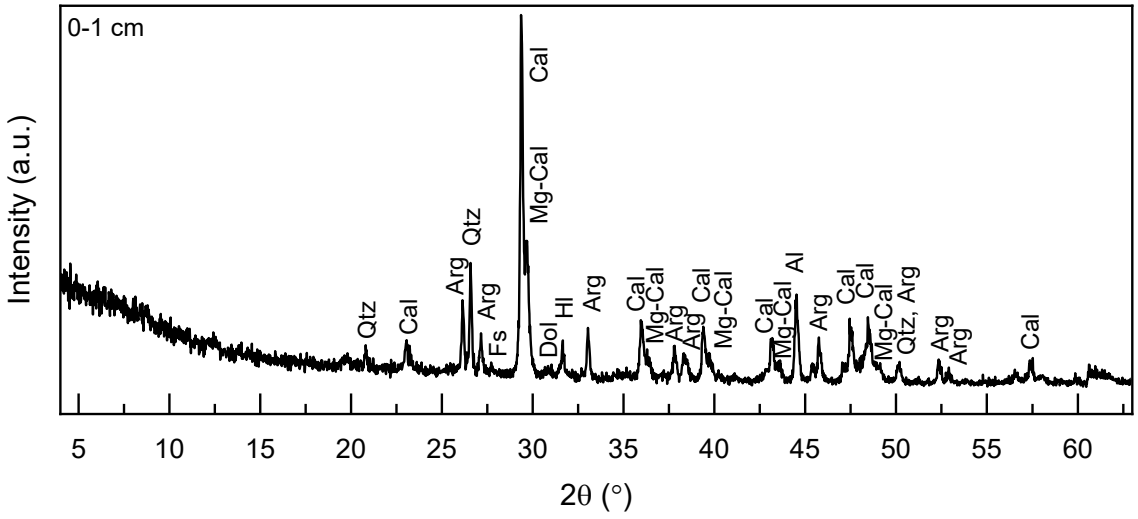

Figure 5.17. X-ray diffraction (XRD) patterns of selected bulk sediment subsample of the K22 core. Mineral abbreviations: Arg-aragonite, Cal-calcite, Dol-dolomite, Fs-feldspar, Hl-halite, Mg-Cal-high-magnesium calcite, Qtz-quartz.

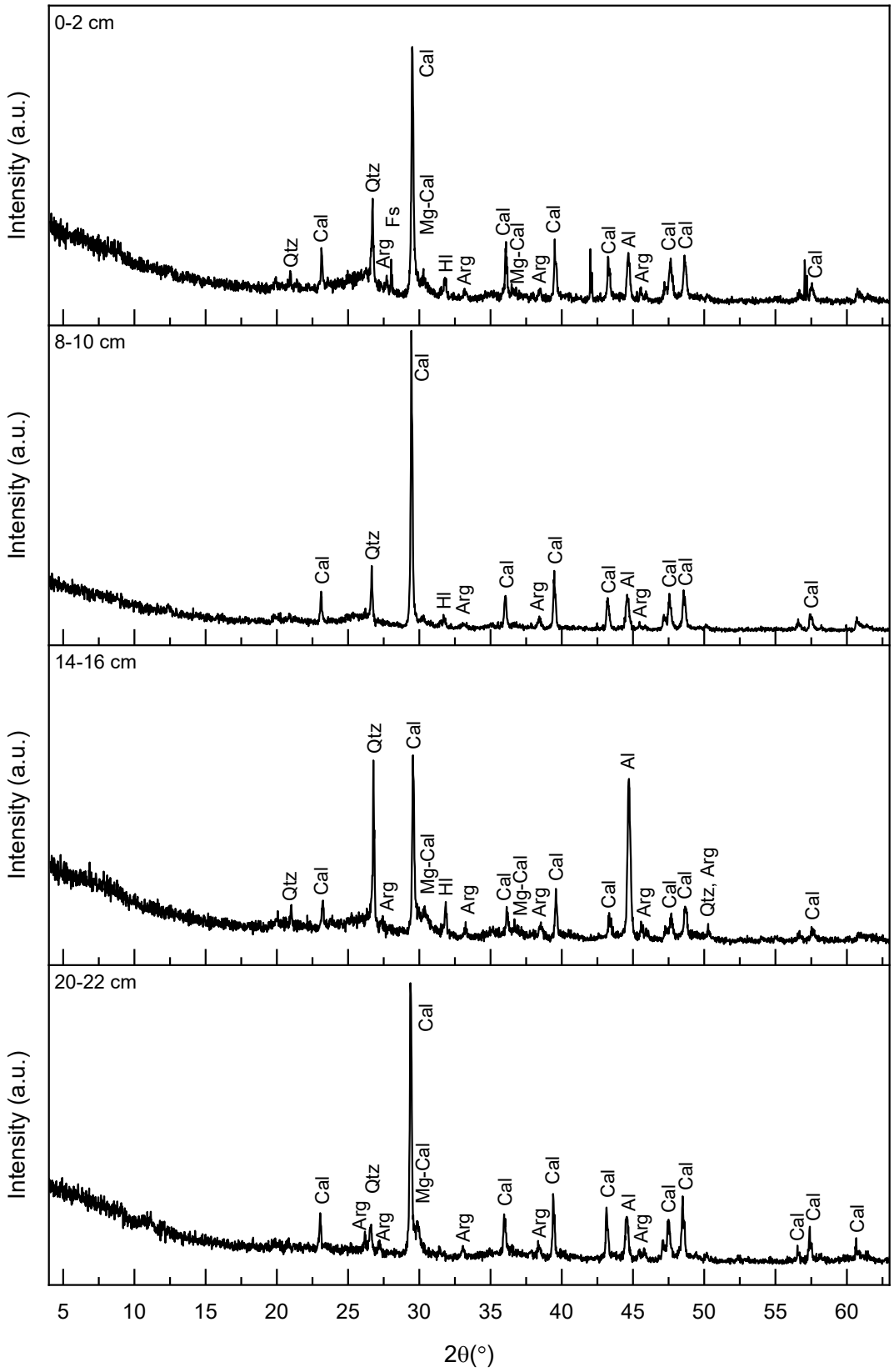

Figure 5.18. X-ray diffraction (XRD) patterns of selected bulk sediment subsamples of the K20 core. Mineral abbreviations: Arg-aragonite, Cal-calcite, Fs-feldspar, Hl-halite, Mg-cal-high-magnesian calcite, Qtz-quartz.

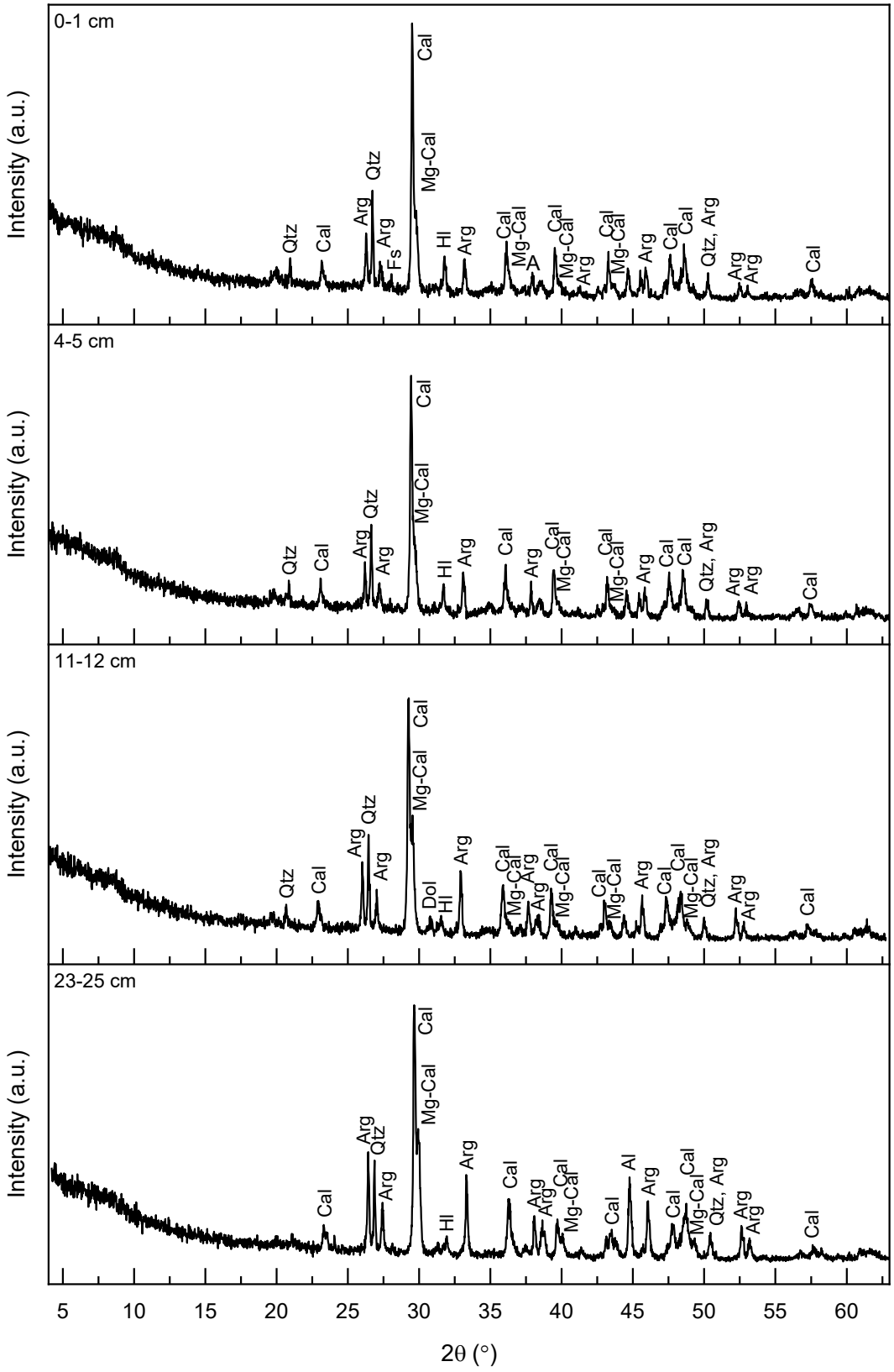

Figure 5.19. X-ray diffraction (XRD) patterns of selected bulk sediment subsamples of the K32 core. Mineral abbreviations: Arg-aragonite, Cal-calcite, Dol-dolomite, Fs-feldspar, Hl-halite, Mg-Cal-high-magnesian calcite, Qtz-quartz.

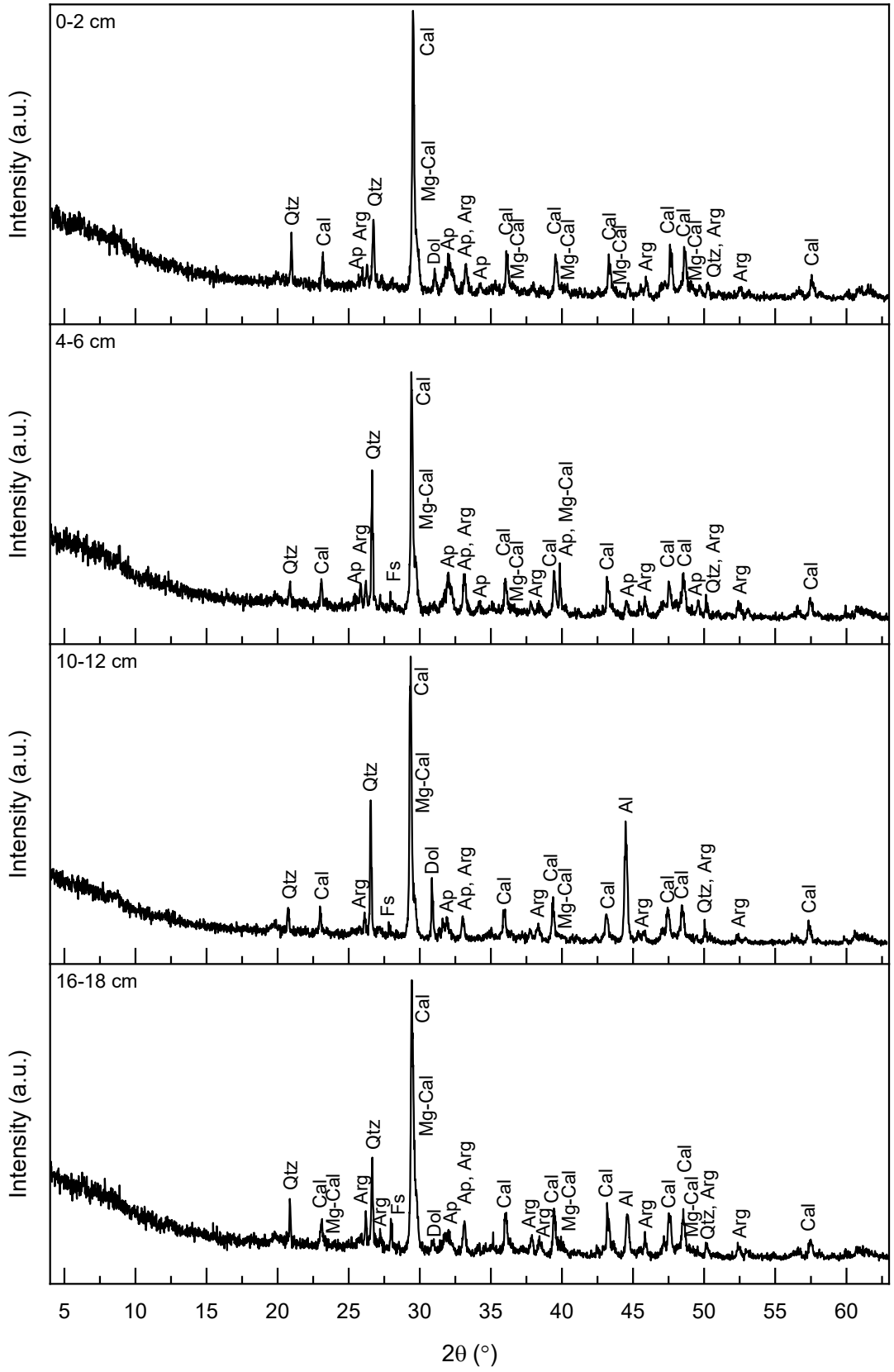

Figure 5.20. X-ray diffraction (XRD) patterns of selected bulk sediment subsamples of the K36 core. Mineral abbreviations: Ap-apatite, Arg-aragonite, Cal-calcite, Dol-dolomite, Fs-feldspar, Mg-Cal-high-magnesian calcite, Qtz-quartz.

5.3.3. Chemical composition of sediment cores

Concentrations of major, minor and trace elements, analysed on the 100 subsamples from seven sediments cores collected in the Krka River estuary (K1, K7, K8, K20, K22, K32, K36), are given in Figs. 5.21.-5.30. The complete results are given in Appendices 7.-13.

Concentrations of TC in sediment from study area were found in range 6.88% to 27.3%. Highest values were observed in the sediment core collected near the TEF factory (K20). At this location, TC content showed significant down-core variation, with the pronounced increase from the bottommost layer (12.5%) upwards, reaching the maximum value at 12-14 cm layer. Afterwards, it decreased in following layers and then rose up again to 22.4% in the uppermost layer. Generally, with the average value of 20.7%, TC concentrations from the K20 core by far surpass the values measured in sediment from other study sites. Concentrations of carbon in other sampling locations were rather invariable with the mean values of 12.7% (K1), 8.51% (K7), 7.39% (K8), 10.59% (K22), 10.48% (K32) and 10.72% (K36).

Same as for the TC, the highest C_{org} content was found in the K20 sediment core, with the values varying in range 2.39% to 21%. However, in this particular sediment core, there were problems with reproducibility during analysis, therefore results should be taken with caution. Apart from K20 core, highest values were found at the port study site (K36), where recorded values were in range between 1.56% and 3.49%. In the first 10 cm of K32 core, C_{org} concentrations varied from 0.485% to 1.36%, and then gradually decreased until the bottom of the core (0.153%). At Martinska site (K22), concentrations varied from 0.96% to 1.94%. Concentrations ranging from 0.269% to 1.13% and from 0.576% to 1.24% were found in sediment cores K1 and K7, respectively. In the Guduča River (K8), in the first 16 cm of sediment C_{org} values varied in range 0.244% to 0.562%, followed with marked increase up to 1.95% in deeper layers.

Nitrogen in the Krka River estuary was found in range between 0.062% to 0.386%. Generally, vertical N distribution in cores K1, K7, K8 and K32 had a decreasing trend, with the average values of 0.14%, 0.15%, 0.25% and 0.15%. Sediment cores K20 and K32 had an average concentration of 0.26% and 0.21%, with highest values found in the uppermost layer and in the layer 12-14 cm and 10-12 cm, respectively. Distribution of N in the first 9 cm of the sediment core K22 was rather constant with the mean value of 0.15%, below which it deceased to 0.11%.

Sulphur levels in the Krka River estuary were in the range 0.274% and 1.32%. Cores K7, K8, K22, K32 and K36 had a similar S distribution in which values gradually decrease from the

highest value towards the top and the bottom of the core. At the K20 study sites, S concentrations were in range 0.613% and 0.933%, with the highest value recorded in the uppermost layer of the sediment core. Concentration at the head of the estuary were in range 0.415% and 0.731%, with the maximum value observed at depth 8-10 cm.

Phosphorous contents in the sediment from the upper estuary (cores K1, K7 and K8) ranged between 0.026% and 0.064%. In the lower estuary, higher values were recorded (0.032-3.73%). By its high P concentrations, the K20 core distinguishes from the rest of the sampling location. After top 4 cm where values are in range of those obtained at other sites, a sudden increase of P levels occurred, with the highest value reaching 3.38% in the 8-10 cm layer. The K36 had a varied P distribution with values between 0.101% and 0.209%. At K22 and K32 sampling locations, P values were found in the ranges 0.061-0.129% and 0.032-0.164%, with observed decreasing trend along the depth.

Aluminium concentrations in the Krka River estuary were found in the range between 1.2% and 5.2%, with the mean value of 3%. In the sediment cores K1, K8 and K22, Al concentrations did not differ significantly along the core. However, a slight increase with the depth was observed in the K1 core, whereas opposite trend was observed in the K8 sediment core. In Prokljan Lake and at marina/shipyard location, Al content decreased gradually along the core, from 4.1% to 2.6% and from 3.5% to 1.3%, respectively. In the sediment cores K20 and K36, a highly variable Al distributions were observed.

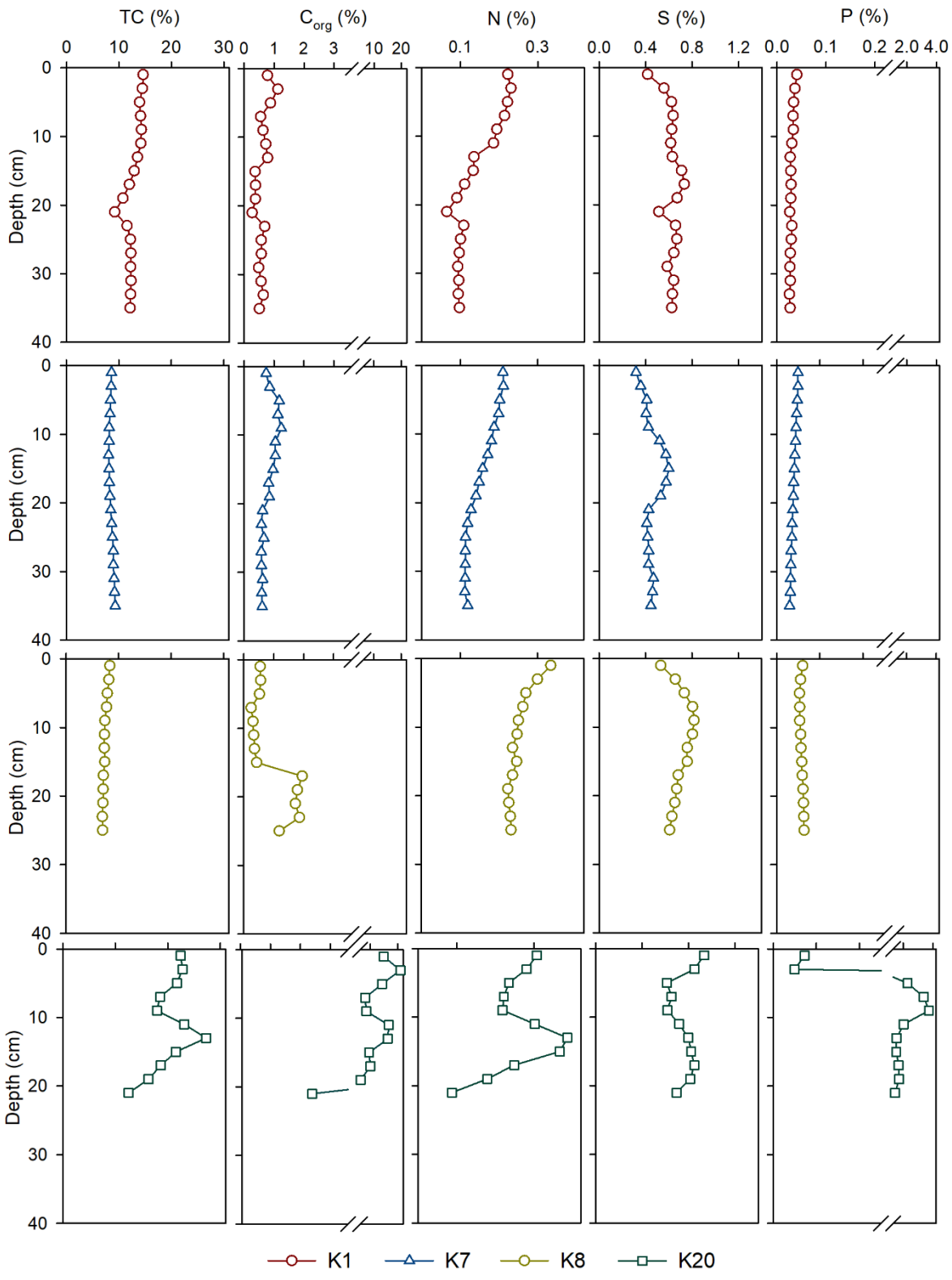

Figure 5.21. Vertical distribution of concentrations of total carbon (TC), organic carbon (C_{org}), nitrogen (N), sulphur (S) and phosphorus (P) in sediment cores K1, K7, K8 and K20.

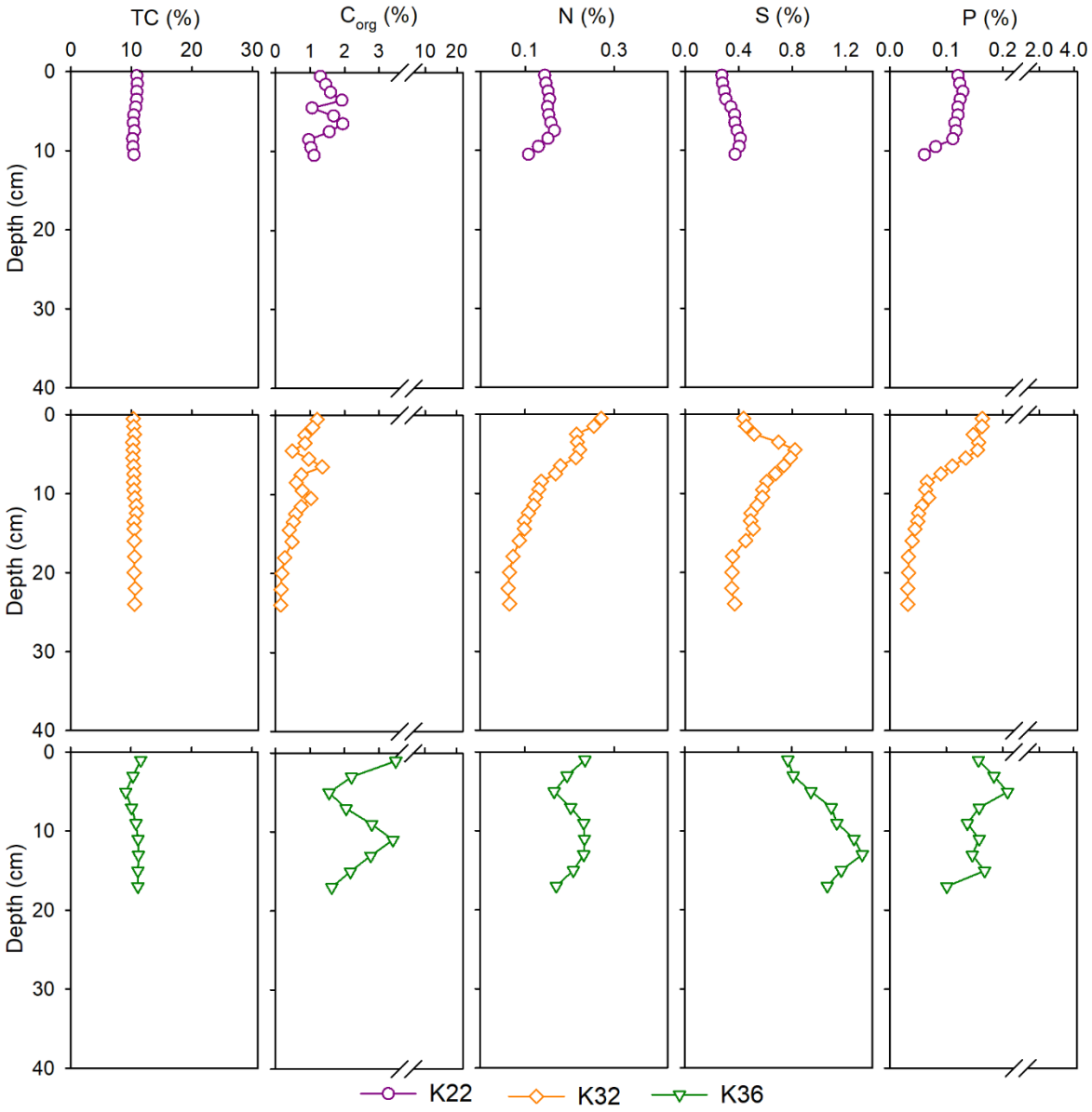

Figure 5.22. Vertical distribution of concentrations of total carbon (TC), organic carbon (C_{org}), nitrogen (N), sulphur (S) and phosphorus (P) in sediment cores K22, K32 and K36.

Iron in the sediment cores from the Krka River estuary showed a distribution trend very similar to that of Al. The obtained concentrations were in range 0.9% to 2.5%, with the mean value of 1.7%. Similar trend was also observed for Li, Ni and V, and for Co in the sediment cores from the upper estuary: K1, K7, K8. The divergence of Co from the Al trend in the Šibenik Bay indicate additional Co source in this area, most probably of anthropogenic origin. The highest Co content was found in the K20 sediment core, with distribution characterized by two distinct increases, a larger one at depth 6-8 cm, and a smaller one at depth 16-18 cm. The highest concentrations of Ni and V were also found in the K20 sediment core. The obtained ranges of

these two elements were 15.4-97.9 μg g^{-1} and 33.1-203 μg g^{-1}, respectively. Lithium content in the sediment cores of the estuary was found in range between 15.3 μg g^{-1} and 61.8 μg g^{-1}. Highest values were recorded in Prokljan Lake.

Manganese concentrations in the sediment cores from the Krka River estuary were found in the broad range between 127 μg g^{-1} and 21 389 μg g^{-1}. The extremely high values, varying from 7 058 μg g^{-1} to 21 389 μg g^{-1} along the core, were observed at the K20 sampling location. Maximum values were found at 14-18 cm of depth. As already seen in previous chapter, high Mn content at this site can be attributed to the former Fe-Mn factory. The influence of this anthropogenic source has been seen in other sampling sites in the Šibenik Bay, especially at site K22, which is closest to the K20 site and the factory, respectively. At this sampling location, Mn distribution was quite uniform in the first 9 cm of the core with the mean value of 1 627 μg g^{-1}, followed by sudden drop of Mn content in the last two layers of the core. Lowest Mn values in the Šibenik Bay were found in the K32 sediment core, were values gradually decreased from 695 μg g^{-1} in the uppermost layer to 150 μg g^{-1} recorded at the bottom of the core. In the upper estuary, mean Mn concentration was 253 μg g^{-1}.

Molybdenum content in the analysed cores was found in range between 0.575 μg g^{-1} and 12.5 μg g^{-1}, with an average value of 2.99 μg g^{-1}. There were similarities between distribution patterns in all cores, except K36. Molybdenum concentrations gradually increased with depth, until reaching the point of maximum value, after which they decreased to the bottom of the core. The maximum value was found at different depths, from the 4-5 cm in the K32 core to the 16-18 cm in the core K20.

Barium concentrations in the sediment cores were found in the range between 39.4 μg g^{-1} to 1 016 μg g^{-1}, with significant differences in Ba distribution between cores. The mean Ba values in analysed cores were as follows; 66.2 μg g^{-1} (K1), 82.9 μg g^{-1} (K7), 109.6 μg g^{-1} (K8), 623 μg g^{-1} (K20), 151 μg g^{-1} (K22), 255 μg g^{-1} (K32) and 319 μg g^{-1} (K36).

Broad range of Pb concentrations (15.3-550 μg g^{-1}) was observed in the core K1, with two sharp peaks at sediment depth of 8-10 cm and 20-22 cm, reaching the values of 340 μg g^{-1} and 550 μg g^{-1}, respectively. A different trend was observed at sampling locations K7 and K8. In the Prokljan Lake values gradually decreased with depth, from 37.5 μg g^{-1} to 14.6 μg g^{-1}, while in the Guduča River uniform values were found with the mean value of 25.2 μg g^{-1}. Slightly higher values, from 56.8 μg g^{-1} to 88.5 μg g^{-1}, were found in the K22 sediment core. In the rest of the Šibenik Bay, increased concentrations were found. Core K36 was characterized by mean Pb

concentration of 186 μg g^{-1} and absence of significant variation along the depth. At K20 sampling location, Pb ranged between 195 and 737 μg g^{-1}. In the first 10 cm of the sediment, values are rather uniform, followed by gradual increase with depth until reaching the maximum value in the layer 16-18 cm. In the K32 sediment core, highest values of 553 μg g^{-1} was found at the sediment depth of 4-5 cm, followed by gradual decrease until the last 8 cm of the core where values were as low as in the upper estuary.

Highest concentrations of U, Cd, Cr and Zn in the estuary were recorded in the sediment core from the port area. In this core, U and Cd showed a similar distribution pattern, with a maximum value recorded in the 6-8 layer. The mean Cd concentration in core K36 was 8.17 μg g^{-1}, which was more than 12 times more than mean Cd concentration from the rest of the estuary. The average U concentration in the core K36 was 14.4 μg g^{-1}, that is almost 5 times higher than mean value from other analysed sediment cores. Chromium in the core K36 had an average concentration of 524 μg g^{-1}, with a sharp increase in the uppermost 4 cm of the core. Elevated concentrations were also observed in the K20 sediment core, where mean Cr concentration was 156 μg g^{-1}. In the rest of the estuary, mean Cr concentration was 67.9 μg g^{-1}. Zinc concentrations showed distinct difference among upper and lower estuary. Low Zn concentrations, with the mean value of 66.6 μg g^{-1}, were found in the upper part of the estuary, whereas increased concentrations were recorded in the Šibenik Bay, with the mean of 530 μg g^{-1}. The low Zn values in the Šibenik Bay were found only in the bottom layers of the K32 core, at sediment depth of 17 cm and more.

Arsenic in the sediment cores from the Krka River estuary was found in the range between 4.64 μg g^{-1} and 101 μg g^{-1}. Lower values (<15 μg g^{-1}) were recorded in the cores K1, K7, K8 and K22, while in the cores K20, K32 and K36 increased concentrations were observed. Highest concentrations were found in the marina/shipyard area, as also seen from the spatial distribution of the surface sediment. At this site, As content ranged from 16.5 μg g^{-1} to 101 μg g^{-1}, with the maximum observed at depth 7-9 cm, followed by down-core gradual decrease. Similar to As, Cu concentrations were increased at K20, K32 and K36 sampling locations with the highest values recorded in the core from the marina/shipyard area. After the maximum value of 267 μg g^{-1} recorded at the depth 4-5 cm, values gradually decrease with depth, falling below 10 μg g^{-1} in the deepest layers of the core.

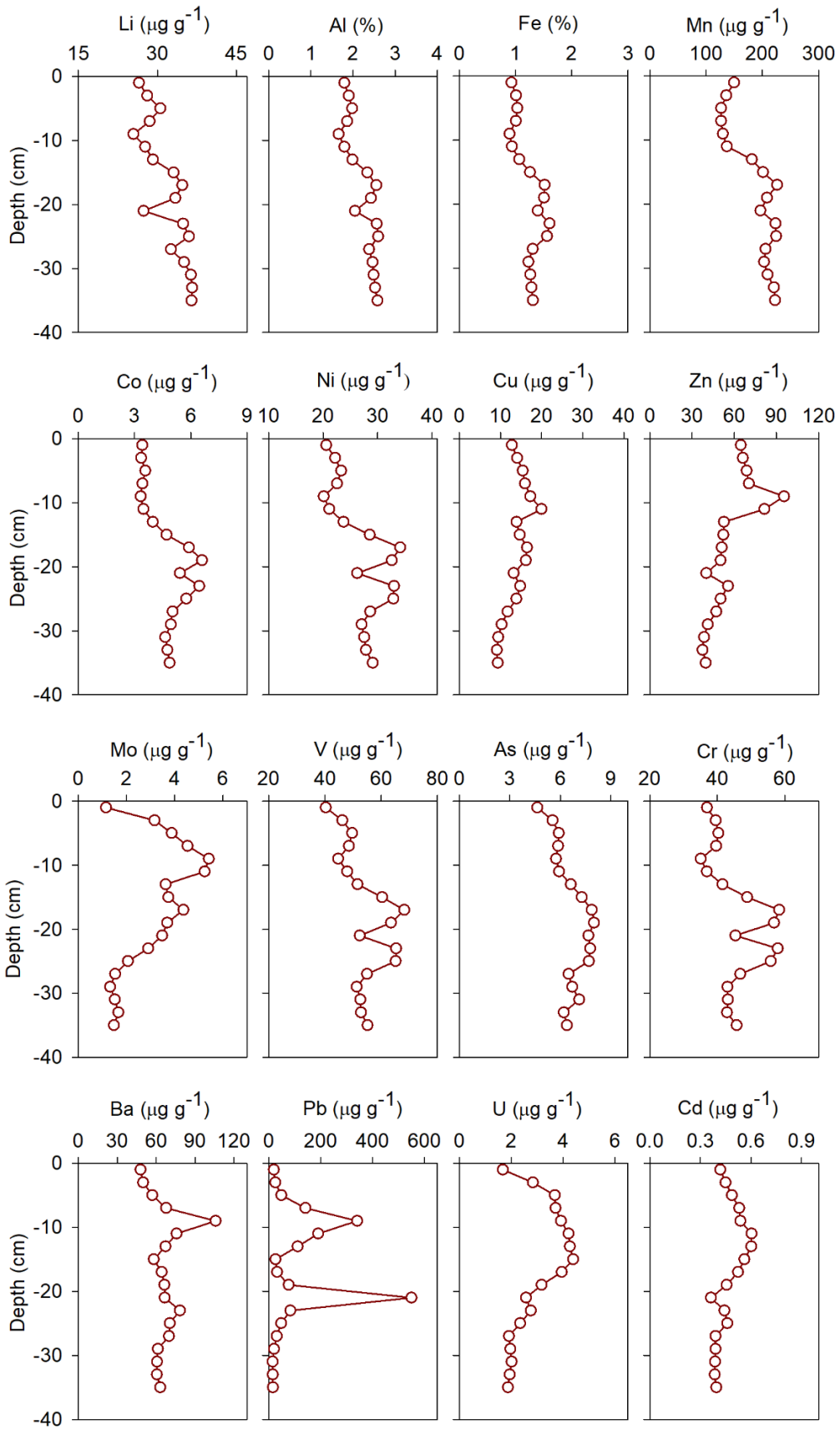

Figure 5.23. Vertical distribution of selected elements (Li, Al, Fe, Mn, Co, Ni, Cu, Zn, Mo, V, As, Cr, Ba, Pb, U, Cd) along K1 sediment core

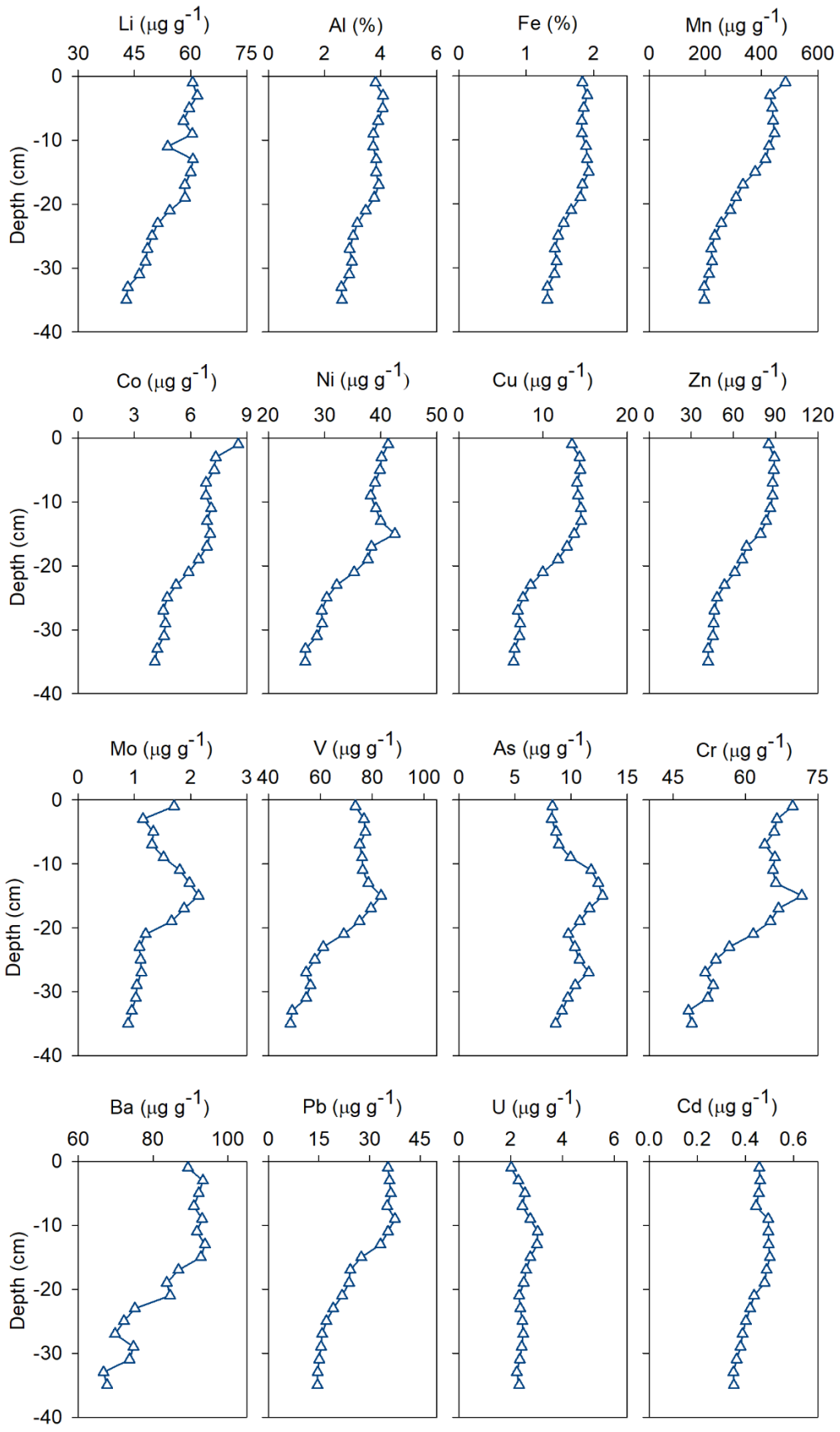

Figure 5.24. Vertical distribution of selected elements (Li, Al, Fe, Mn, Co, Ni, Cu, Zn, Mo, V, As, Cr, Ba, Pb, U, Cd) along K7 sediment core

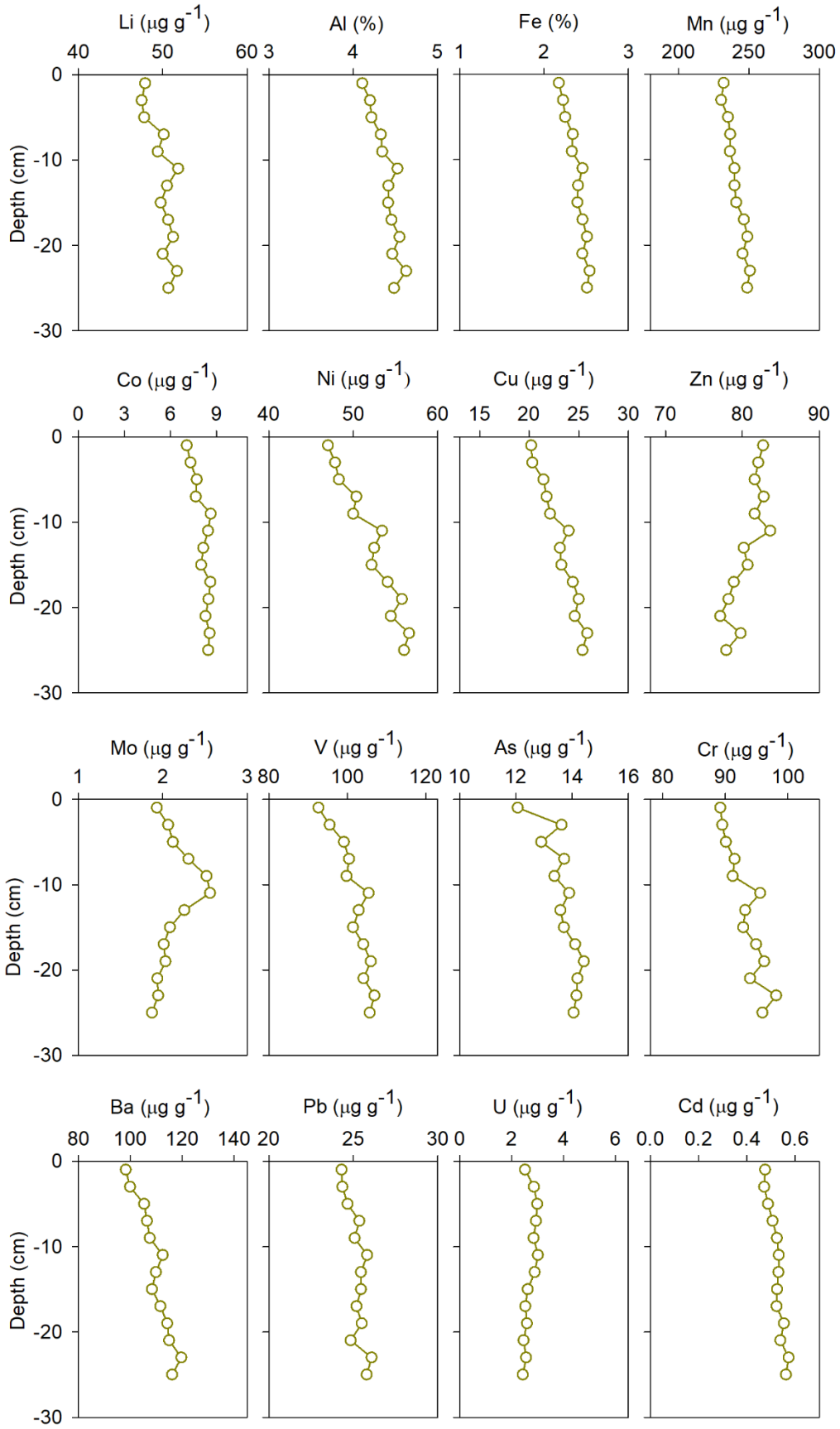

Figure 5.25. Vertical distribution of selected elements (Li, Al, Fe, Mn, Co, Ni, Cu, Zn, Mo, V, As, Cr, Ba, Pb, U, Cd) along K8 sediment core

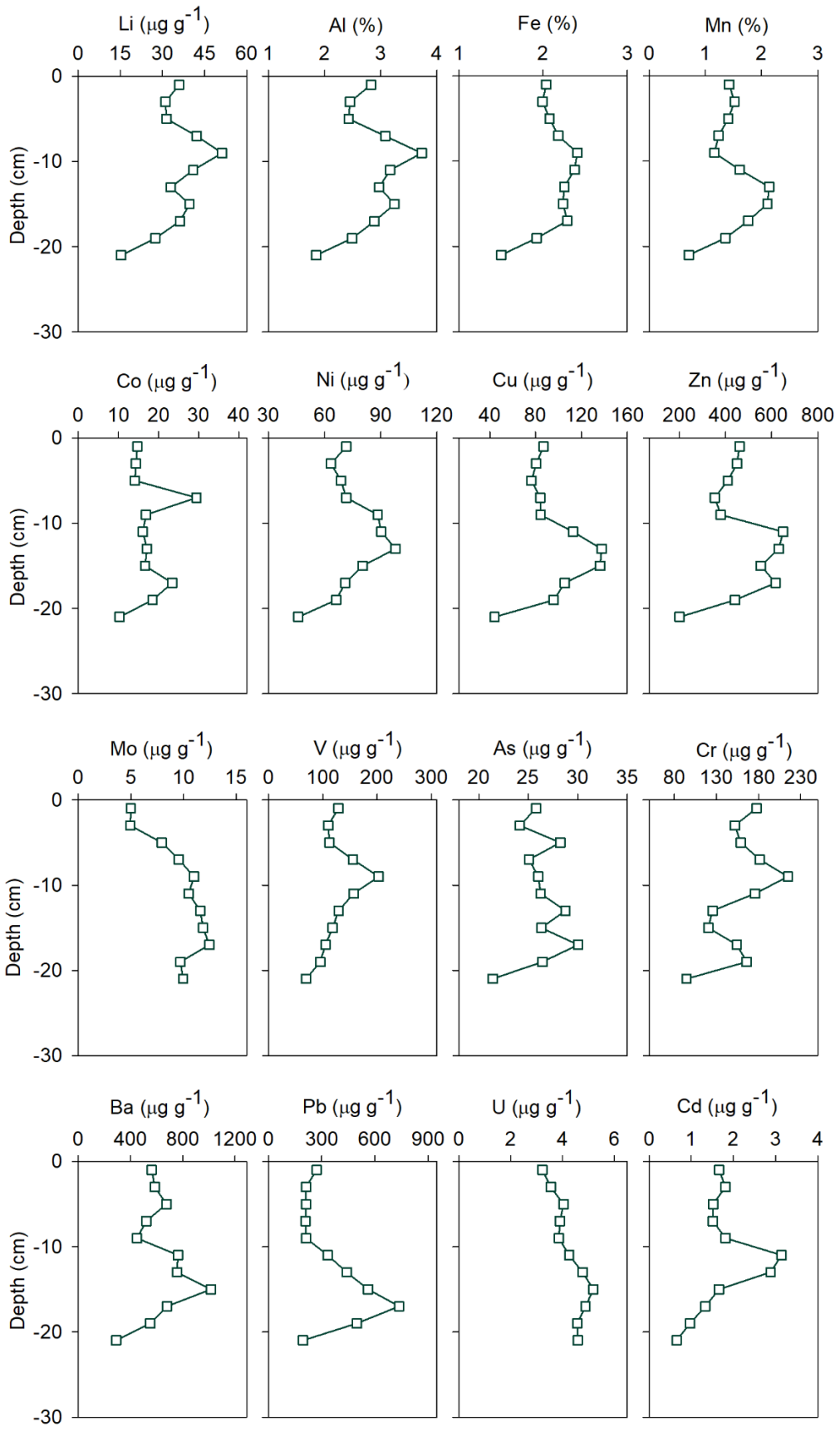

Figure 5.26. Vertical distribution of selected elements (Li, Al, Fe, Mn, Co, Ni, Cu, Zn, Mo, V, As, Cr, Ba, Pb, U, Cd) along K20 sediment core

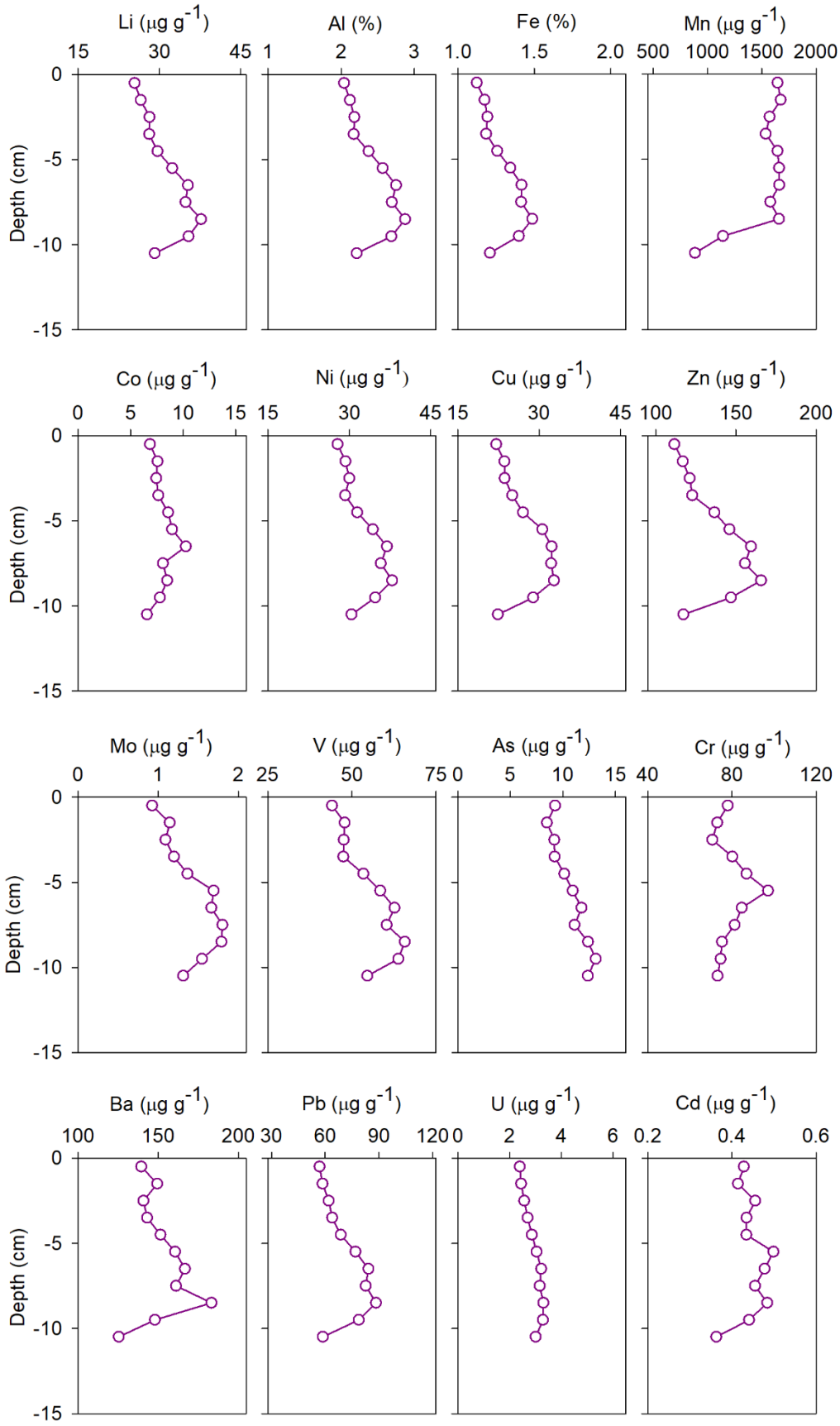

Figure 5.27. Vertical distribution of selected elements (Li, Al, Fe, Mn, Co, Ni, Cu, Zn, Mo, V, As, Cr, Ba, Pb, U, Cd) along K22 sediment core

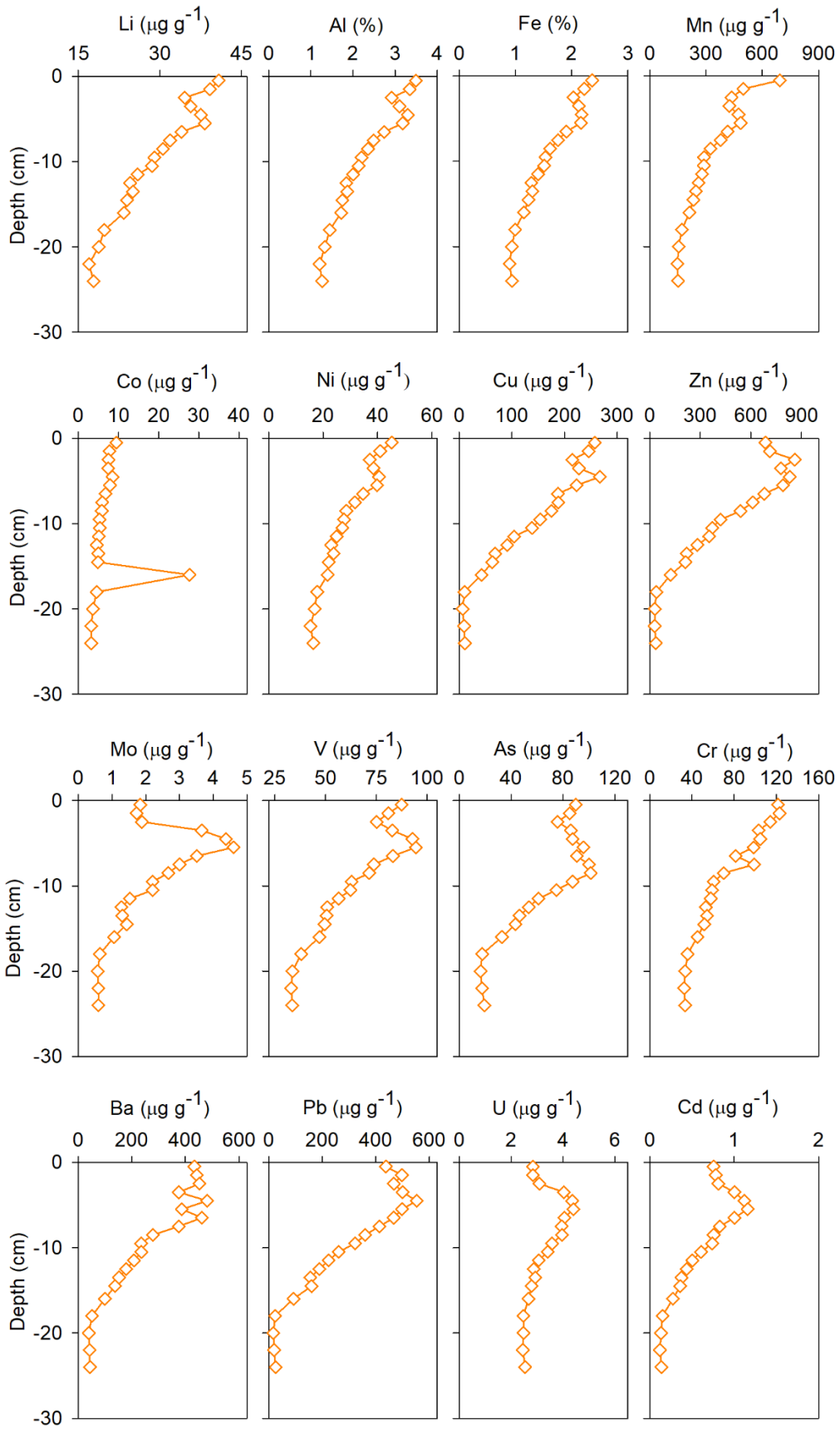

Figure 5.28. Vertical distribution of selected elements (Li, Al, Fe, Mn, Co, Ni, Cu, Zn, Mo, V, As, Cr, Ba, Pb, U, Cd) along K32 sediment core

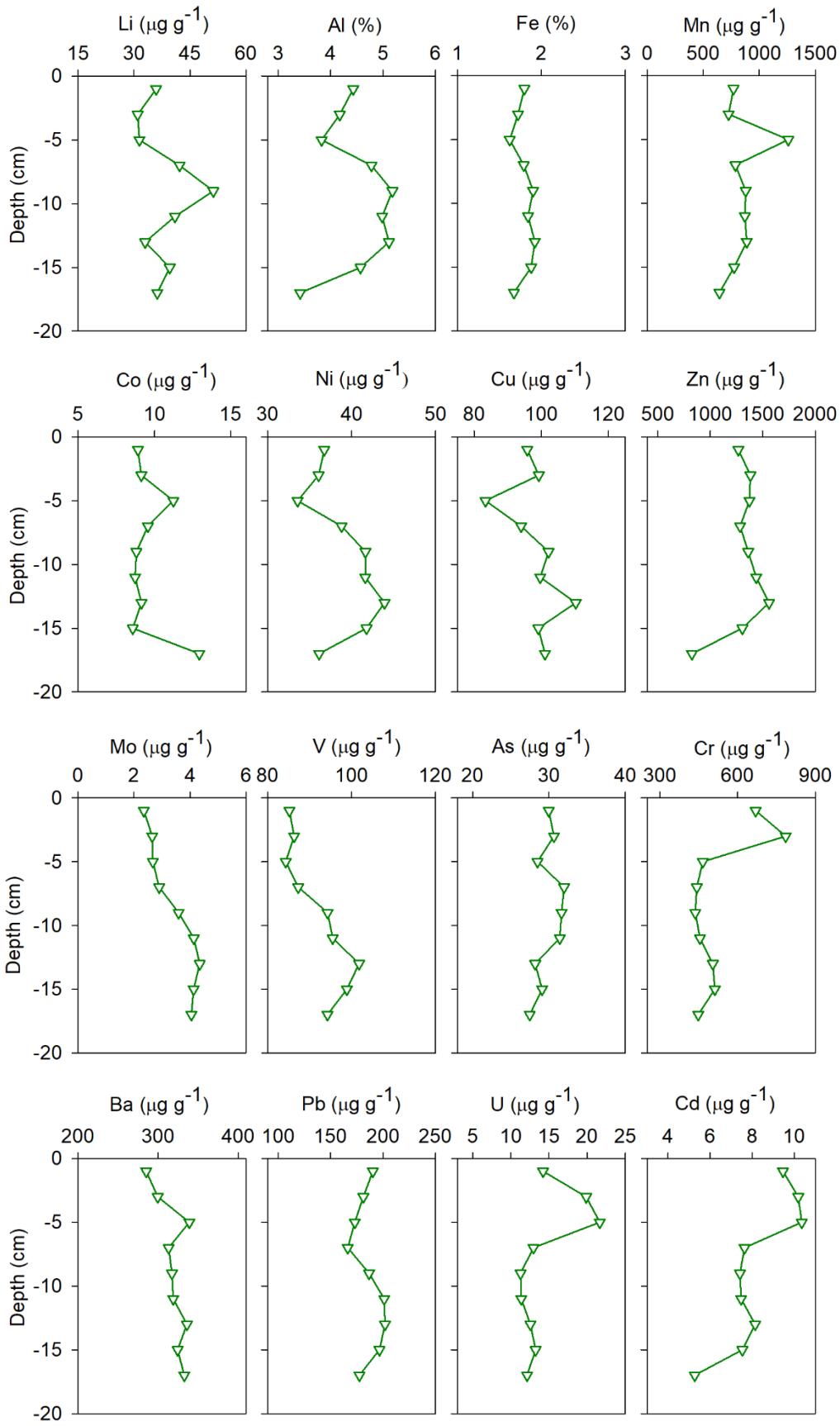

Figure 5.29. Vertical distribution of selected elements (Li, Al, Fe, Mn, Co, Ni, Cu, Zn, Mo, V, As, Cr, Ba, Pb, U, Cd) along K36 sediment core

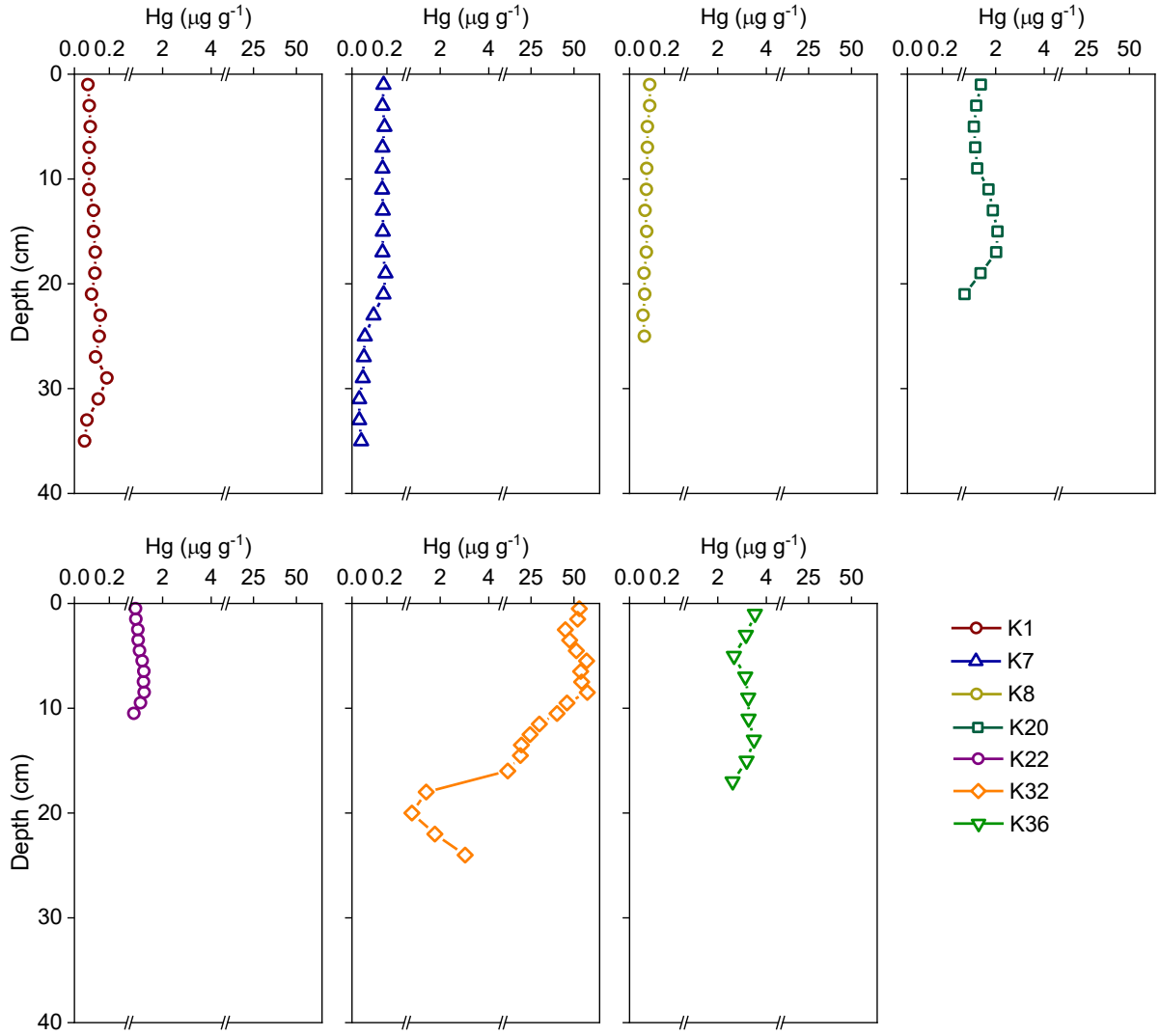

Figure 5.30. Vertical Hg distribution along the cores from the Krka River estuary (K1, K7, K8, K20, K22, K32, K36)

Mercury concentrations were found in the broad range from 0.042 to 57.4 µg g^{-1}, with significant differences observed between upper and lower part of the estuary. Low Hg values, ranging from 0.042 to 0.192 µg g^{-1}, were recorded in cores K1, K7 and K8. Core from the Guduča River had a most uniform distribution, while at the head of the estuary there where some variations with depth. In Prokljan Lake, values were invariable (0.176-0.192 µg g^{-1}) from the top of the core to the depth of 24 cm, where sudden decrease occurred. Thus, Hg concentrations in the last 12 cm of the core were rather low (0.042-0.068 µg g^{-1}).

In the cores from the Šibenik Bay Hg concentrations were found in the following ranges: 0.719-2.08 µg g^{-1} (K20), 0.819-1.24 µg g^{-1} (K22), 2.61-3.53 µg g^{-1} (K36). By far, highest concentrations were recorded in the K32 sediment core. In the top 10 cm, values were extremely

high, in range between 45 μg g^{-1} and 57.8 μg g^{-1}. In the following 10 cm, Hg concentrations were decreasing rapidly until reaching the value of 0.829 μg g^{-1}. In the bottommost part of the core, a rise in Hg content occurred, with recorded value of 3.03 μg g^{-1}.

5.3.4. Activities of radionuclides in core K32

Due to the lack of information on sedimentation rate in the marina/shipyard area and interesting vertical distributions of some toxic elements at this site, activities of radionuclides were determined in the core K32. Results of the radiometric analysis of ^{137}Cs, ^{210}Pb and ^{226}Ra activities are presented in Table 5.3. and calculated sediment age is shown in Fig. 5.31.

Table 5.3. Activities of radionuclides ^{137}Cs, ^{210}Pb and ^{226}Ra in core K32

Depth (cm)	^{137}Cs (Bq kg^{-1})	^{210}Pb (Bq kg^{-1})	^{226}Ra (Bq kg^{-1})
0-1	6.27 ± 2.11	149 ± 35	25.9 ± 6.2
1-2	6.39 ± 1.14	146 ± 30	22.7 ± 3.5
2-3	6.86 ± 1.57	124 ± 47	20.8 ± 4.2
3-4	5.74 ± 1.00	112 ± 24	21.2 ± 3.1
4-5	7.15 ± 1.30	110 ± 23	23.1 ± 3.6
5-6	7.21 ± 1.10	95 ± 20	20.9 ± 3.0
6-7	6.17 ± 1.06	83 ± 18	18.2 ± 2.6
7-8	6.32 ± 1.06	71 ± 16	16.8 ± 2.4
8-9	4.98 ± 0.68	53 ± 11	17.2 ± 2.3
9-10	4.59 ± 0.87	47 ± 11	16.7 ± 2.6
10-11	4.10 ± 0.73	42.5 ± 9.9	16.6 ± 2.4
11-12	3.26 ± 0.54	39.6 ± 8.7	15.4 ± 2.1
12-13	2.30 ± 0.59	34.4 ± 8.2	15.0 ± 2.1
13-14	1.78 ± 0.49	30.5 ± 7.7	14.0 ± 2.1
14-15	2.09 ± 0.60	29.5 ± 7.8	15.2 ± 2.2
15-17	1.46 ± 0.40	22.3 ± 6.0	14.0 ± 2.0
17-19	< 0.3	19.3 ± 5.2	13.0 ± 1.8
19-21	< 0.3	17.2 ± 5.6	12.3 ± 1.8
21-23	< 0.3	14.0 ± 4.2	11.6 ± 1.6
23-25	< 0.3	9.8 ± 4.2	12.1 ± 1.8

In the top 8 cm of core K32, activities of anthropogenic radionuclide ^{137}Cs were varying between 5.74 ± 1.00 Bq kg^{-1} and 7.21 ± 1.10. Afterwards, activities gradually decrease downcore and fall below detection limit at the depth of 17 cm.

The specific activities of natural radionuclides ^{210}Pb and ^{226}Ra were found in ranges from 9.8 ± 4.2 Bq kg^{-1} to 149 ± 35 Bq kg^{-1} and from 11.6 ± 1.6 Bq kg^{-1} to 25.9 Bq kg^{-1}, respectively, and showed a decreasing trend with increasing depth.

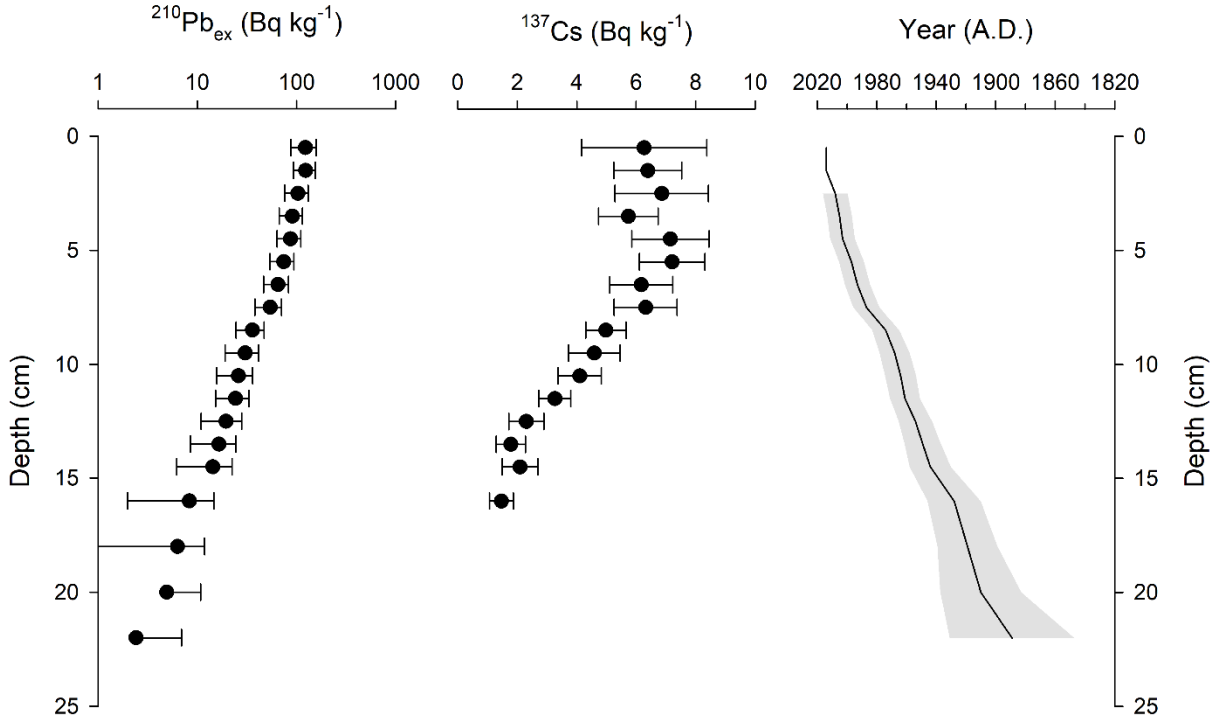

Figure 5.31. The activities of ^{210}Pb and ^{137}Cs and calculated sediment age for sediment core K32. The grey area around the line on the rightmost graph represents uncertainty in estimated ages.

5.4. Pore water characterization

5.4.1. Physicochemical parameters (pH and Eh)

Distributions of the pH and the redox potential (Eh) measured in the sediment pore water and in the overlaying water of the seven sediment cores collected in the Krka River estuary (K1, K7, K8, K20, K22, K32 and K36) are shown in Fig. 5.32.

The Eh values of the overlying water (5 cm) were quite high (303 mV to 502 mV) indicating oxidative conditions in the near-bottom waters. Below the SWI, Eh levels dropped abruptly and

continued to decrease with depth afterwards. Within the sediments in the Šibenik Bay (K20, K22, K32, K36), reducing condition prevailed, and the Eh values declined to 0 mV or below at depth 5-10 cm. In the upper estuary (K1, K7, K8), Eh decreased below 0 mV only in Prokljan Lake (K7).

The pH values in the overlying water were found in range between 7.5 and 8.0. The pH values in the sediment pore water were mostly lower than in the overlying water column, with a general decreasing trend along the depth at most of the sampling locations.

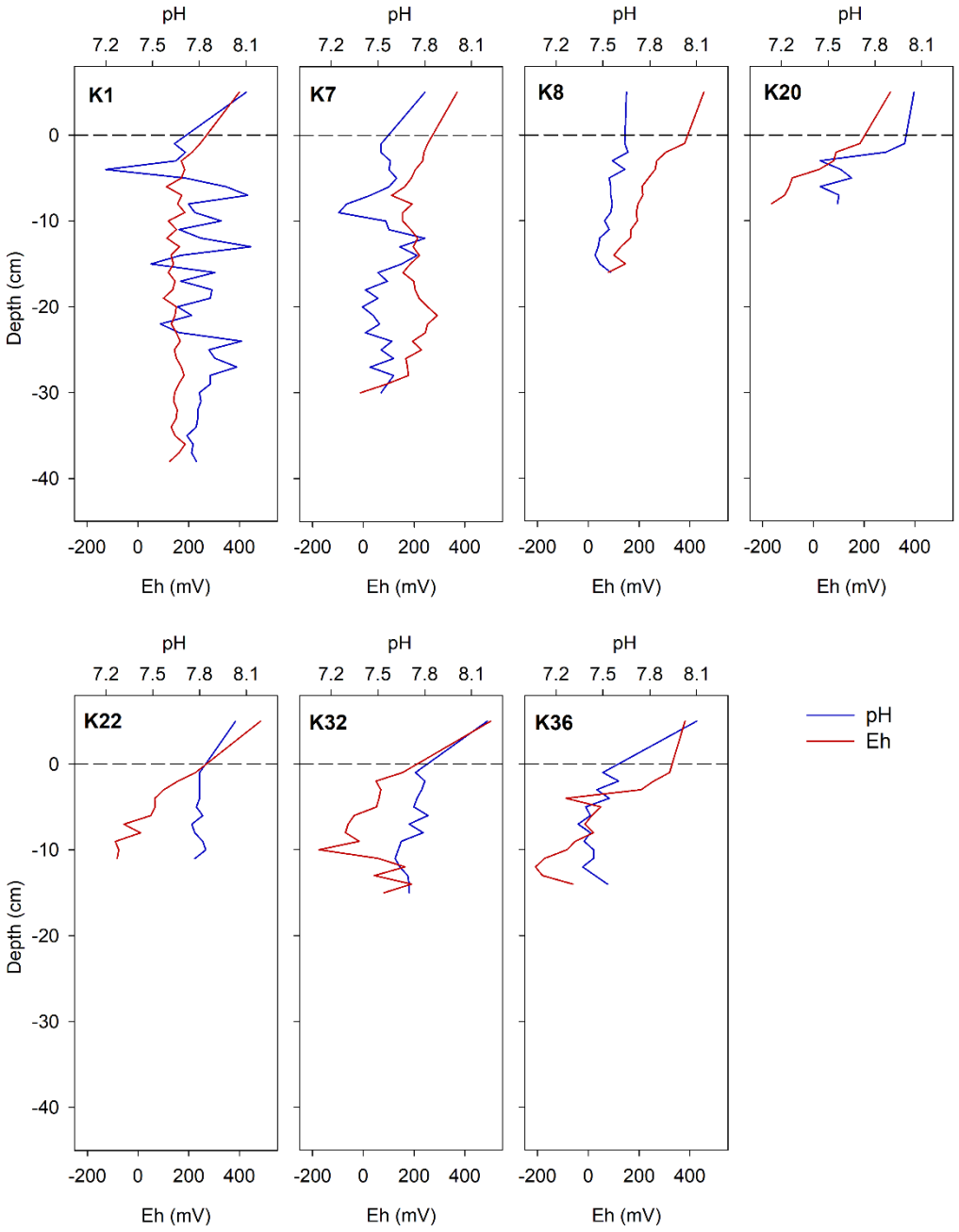

Figure 5.32. pH and Eh in the overlying water and pore water of the sediment cores from the Krka River estuary

5.4.2. Dissolved organic carbon (DOC) and dissolved inorganic carbon (DIC)

The DOC and DIC vertical distributions in the pore water and the bottom water are presented in Fig. 5.33. DOC levels in the supernatant waters ranged between 0.6 and 2.6 mgC L^{-1}, except for one sample at site K22 where value of 12.2 mgC L^{-1} was measured. Considering the spatial distribution of DOC in the supernatant water, a seaward increase was observed. The pore water DOC levels were significantly higher than those from the overlying water, with the obtained range between 2.6 mgC L^{-1} and 137 mgC L^{-1}. In Prokljan Lake (K7) and in the Guduča River (K8) the peak of pore water DOC content was observed just below the SWI, while in the Šibenik Bay (K20, K22, K32, K36) maximum was observed deeper in the sediment, at depths 5-10 cm. Sediment core from the port, with the maximum DOC value of 137 mgC L^{-1}, differed from the rest of the estuary where maximum DOC levels were found in range 10-30 mgC L^{-1}.

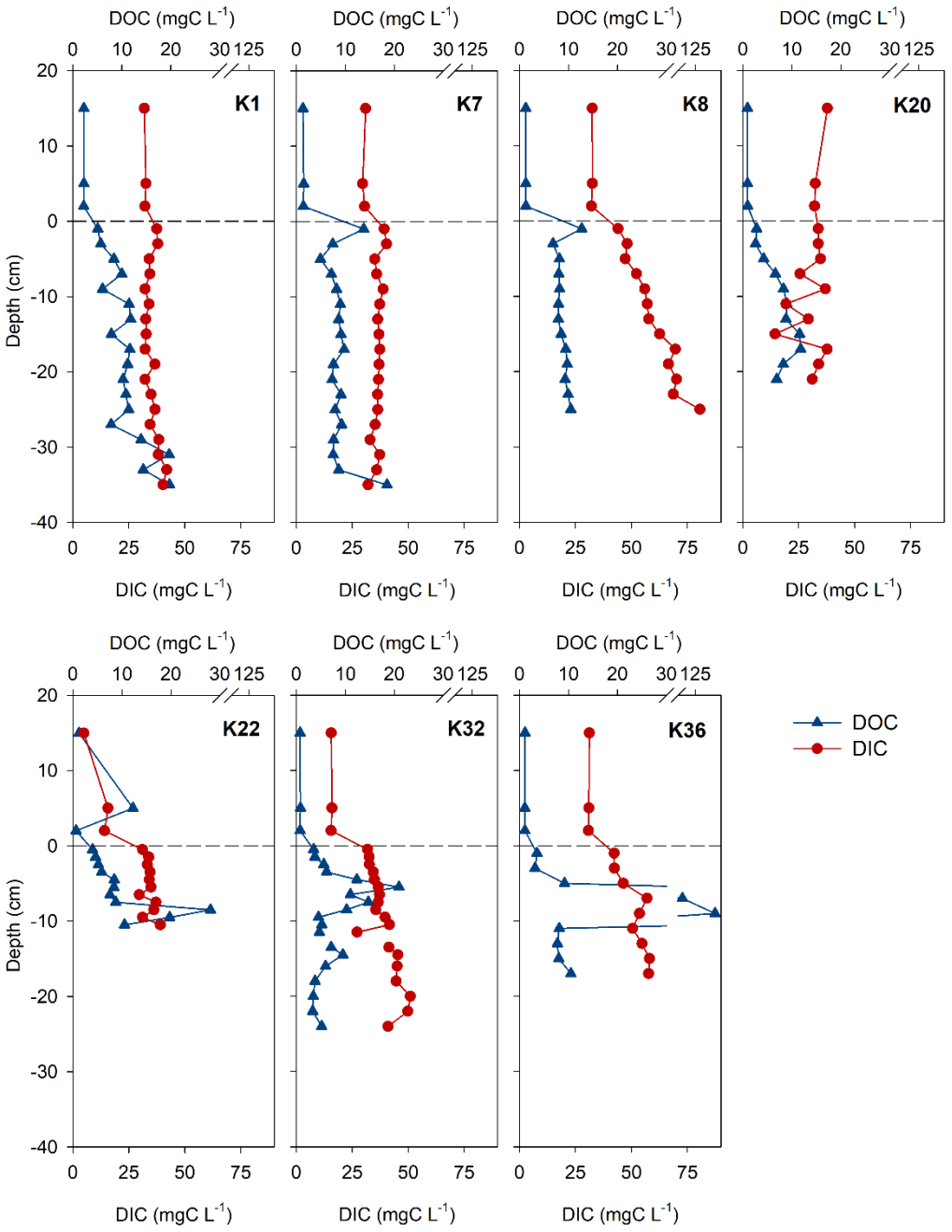

Figure 5.33. Dissolved organic carbon (DOC) and dissolved inorganic carbon (DIC) in the overlying water and pore water of the sediment cores from the Krka River estuary

5.4.3. Pore water nutrients, sulphate and sulphide distribution

The vertical variations of the supernatant and pore water concentrations of the orthophosphate, ammonia, silicate, sulphate and sulphide measured in cores from the Krka River estuary are presented in Figs. 5.34. and 5.35.

For all of the measured parameters, except sulphate, concentrations in the supernatant were lower than in pore water or even below detection limit. Sulphate in the pore water and overlying water was found in the range 5.88-46.9 mM, with no considerable variation between sites.

Recorded phosphate values in extracted pore water were ranging between 1.06 μM and 37.03 μM. Vertical distribution of phosphate followed the similar trend in the entire estuary, apart from the head of the estuary where trend was somewhat different. The phosphate increased downcore until reaching the maximum value at depths between 5 and 16 cm and decreased afterward. In Prokljan Lake, in layers subsequent to the observed maximum, phosphate was not detected. At the head of the estuary, phosphate concentrations gradually increased with depth, with maximum concentration registered in the core bottommost layer. The highest phosphate concentration was recorded at site K20.

Pore water silicate was ranging between 67.3 μM and 417 μM, with vertical distribution trend analogous to that of phosphate.

Concentrations of ammonia in the extracted pore water were found in the broad range from 8.19 μM to 1 262 μM. Except the concentration peak observed just below SWI in the Prokljan Lake (K7), vertical ammonium distributions at sites K1, K7, K20 and K22 were rather uniform with the values lower than 120 μM. In the Guduča River (K8), pore water ammonium gradually increased along the core, reaching the value of 354 μM. Highest ammonium content was recorded in the port area (K36), where concentrations increased significantly at depth between 6 and 10 cm.

Among measured parameters, sulphide distribution showed highest differences between sites. Namely, at two sites in Šibenik Bay which were sampled during spring season (K22 and K32), sulphide was not detected in the pore water nor in the overlying water. In the upper estuary (K1, K7, K8), sulphide was detected in 3-4 subsamples of each core, at depths between 2 and 16 cm. Obtained sulphide concentrations in the upper estuary were ranging between 2.43 μM and 25.3 μM. At the port and former factory sites (K36 and K20), sulphide was detected almost along the entire core, and even in one overlying water subsample at old factory site. Maximum sulphide concentrations recorded at these two sites were 55.0 μM and 111 μM, respectively.

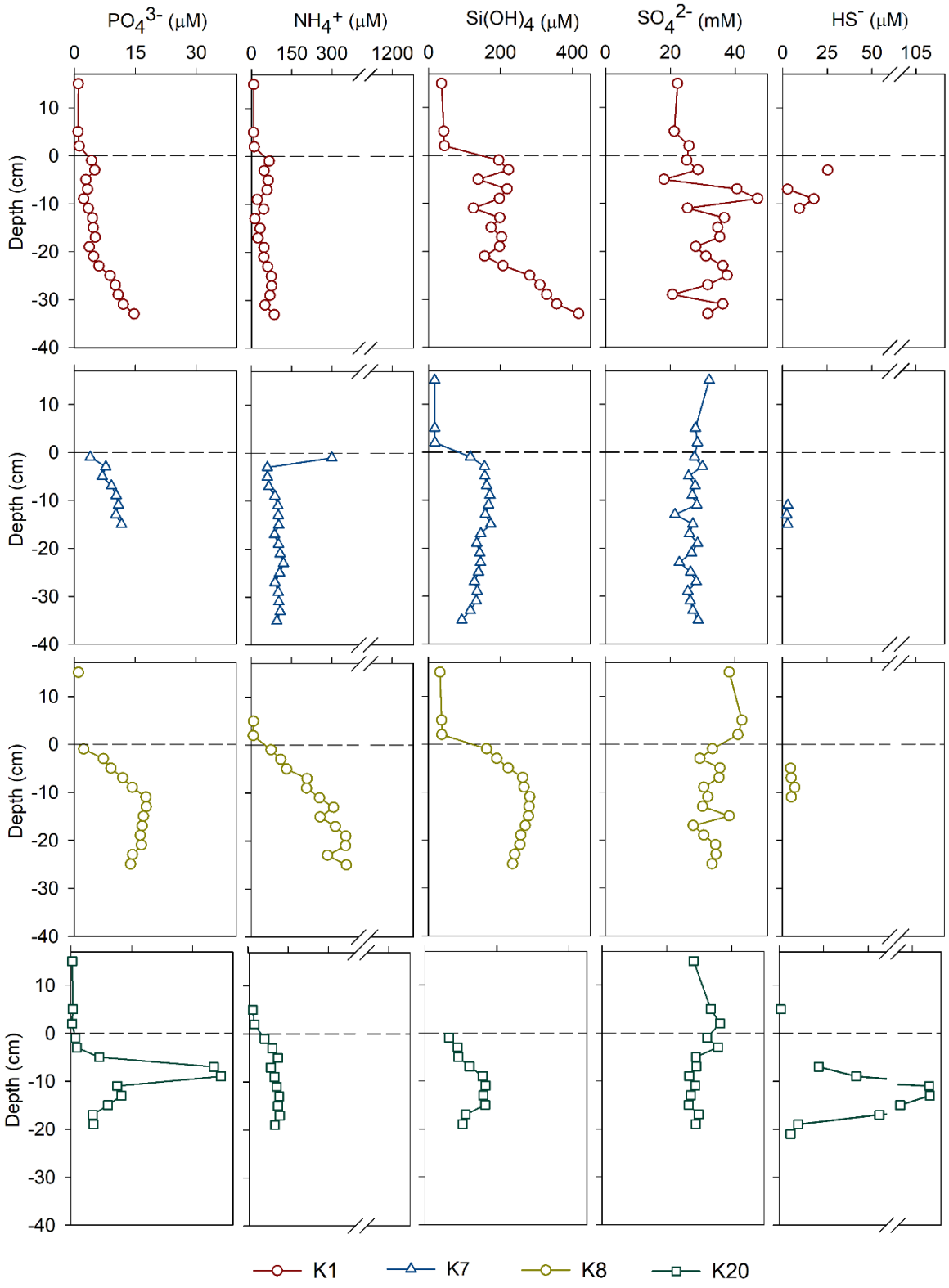

Figure 5.34. Dissolved orthophosphate, ammonia, silicate, sulphate and sulphide in the overlying water and pore water of the sediment cores (K1, K7, K8, K20) from the Krka River estuary

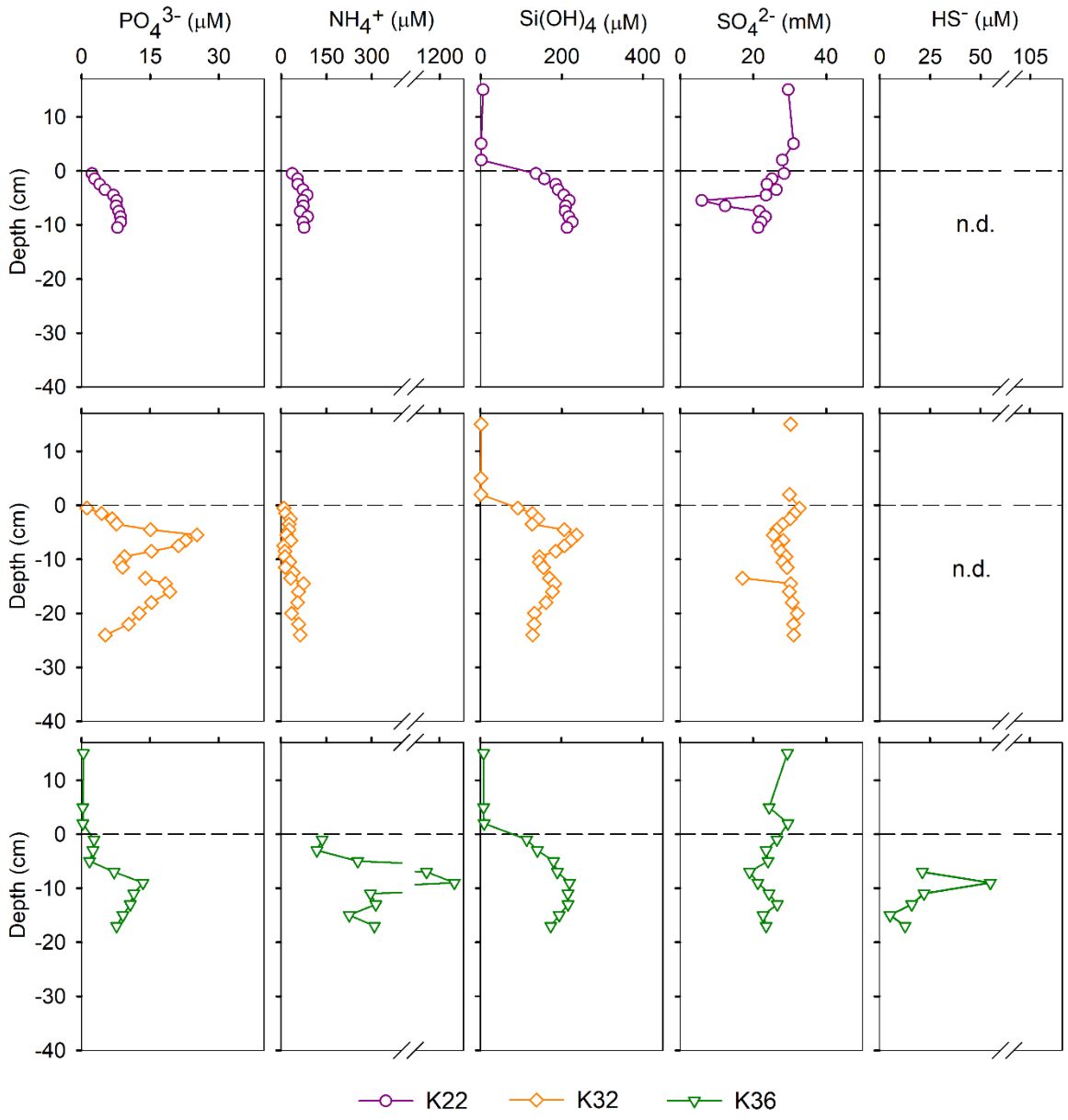

Figure 5.35. Dissolved orthophosphate, ammonia, silicate, sulphate and sulphide in the overlying water and pore water of the sediment cores (K22, K32, K36) from the Krka River estuary

5.4.4. Pore water trace element distribution

Vertical distributions of selected elements in the sediment pore water and the supernatant water (overlying water column) from the Krka River estuary are presented in Figs. 5.36.-5.40. The complete results are given in Appendices 2.-6.

For most of the elements (Li, Al, Ni, Pb, Ba, Mo, As, Fe, Mn) concentrations in pore water were higher from those in the overlying water column. The difference was most pronounced in the case of Mn and Fe, which increased below SWI up to 800-fold and 1 000-fold, respectively. These two elements had analogous vertical distribution patterns at all sampling sites, with marked peaks just below SWI, in the first 4 cm of sediment. The obtained Fe concentration range in pore water was 3.17-2 775 μg L^{-1}, with the lowest values found at the head of the estuary (K1) and highest in Prokljan Lake (K7). Mn had also broad range, from 17.0 μg L^{-1} to 5 501 μg L^{-1}, with lower values found at sites K1 and K8. The recorded ranges in the supernatant water were 0.422-2.96 μg L^{-1} and 3.18-271 μg L^{-1}.

Similar distribution to that of Fe and Mn was noticed for some other elements, but not in entire estuarine area. For example, Ni followed the described distribution pattern in Prokljan Lake (K7) and Co in Prokljan Lake and at the port site (K36) and former factory site (K20). The concentration ranges in pore water and overlying water were 0.422-5.18 μg L^{-1} for Ni and 0.004-1.58 μg L^{-1} for Co.

The increase of As concentrations just below SWI was observed at all sampling sites except K1, where increase was recorded at depth 12-14 cm. At this site, as well as at K20 and K36, there was a second concentration peak at depths 28-36 cm, 20-22 cm and 8-10 cm. The obtained concentration range was 0.87-30.6 μg L^{-1}.

Aluminium concentrations in the overlying water and pore water were found in the range between 1.55 μg L^{-1} and 71.9 μg L^{-1}, with a general increase trend in downcore direction. At some locations (K8, K20 and K36) concentrations varied along depth but with a gradual increase pattern, while at others (K1 and K7) marked peak was observed at depths higher than 14 cm.

Lithium and Ba were two elements whose concentrations showed lowest variability from site to site, with reported pore water ranges 153-261 μg L^{-1} and 11.9-71.9 μg L^{-1}. However, their distribution showed an opposite trend, Li decreased downcore, whereas Ba increased.

Copper concentrations in pore water and overlying water were ranging between 0.008 μg L^{-1} and 9.70 μg L^{-1}. As for Cu vertical distribution in the estuary, two main trends can be distinguished. In Prokljan Lake (K7) and at the old factory site (K20), highest Cu concentrations were recorded in the bottom water, and they decrease across the SWI and deeper into the sediment. In other parts of the estuary, the Cu concentration peaks were found in the sediment, with differences in peak depths. In the Guduča River (K8) maximum was observed right below the SWI, whereas at the port site (K36) and at the head of the estuary (K1) peaks were located at depths 8-10 cm and 18-20 cm.

Vertical Cr distribution also followed two different patterns. In Prokljan Lake (K7) and Šibenik Bay (K20 and K36), there was a decrease of concentrations immediately below SWI, followed by an increase at depths 10-16 cm and subsequent decrease in downcore direction. Inversely, in the Guduča River (K8) and at the head of the estuary (K1), Cr concentrations increased below SWI. The measured values were in range 0.045-0.494 μg L^{-1}.

In the upper estuary Pb content in pore water was below 1 μg L^{-1}, while in the lower estuary it rose up to 6.48 μg L^{-1}. In the overlying water Pb concentrations ranged between 0.005 μg L^{-1} and 0.811 μg L^{-1}. Vertical distribution differed from site to site, Pb decreased gradually along core at site K7, whereas opposite behaviour was observed at site K8. At sites K1, K20 and K36, distribution was characterized by the marked peaks at depths 20-22 cm, 16-18 cm and 9-10 cm, respectively.

Zinc vertical distribution also differed vastly between sites. The obtained range was 0.751-182 μg L^{-1}. The highest value was observed at site K7, where vertical distribution was characterized by two distinct peaks, the stronger one at depth 14-16 cm, and the weaker one at 26-28 cm. A maximum concentration at site K20 was observed at depth 16-18 cm, with the value 15-fold higher than values in the rest of the core. At site K36, values were varying along the core, with the maximum observed at SWI. Contrary, at the K8 sampling location, vertical distribution was quite uniform, with the obtained range (~1-4 μg L^{-1}). Distribution at site K1 was characterized by much higher values in overlying water than in the pore water.

Molybdenum in the pore water and overlying water from the Krka River estuary was found in the range between 6.27 μg L^{-1} and 221 μg L^{-1}. Profiles from Prokljan Lake and Guduča River were characterized by lower values and lower intra-core variability compared to other sites in estuary where values increased substantially in the downcore direction. In core K1, which is

longer than cores K20 and K36, Mo decrease was observed after reaching the maximum at depth 20-22 cm.

Distributions of V and U were characterized by higher concentrations in the bottom water than in the first centimetres of the pore water. However, both elements varied downward, with values at greater depths exceeding those recorded in the overlying water. Moreover, the concentration ranges were similar, 0.248-14.7 μg L^{-1} for V and 0.974-14.1 μg L^{-1} for U.

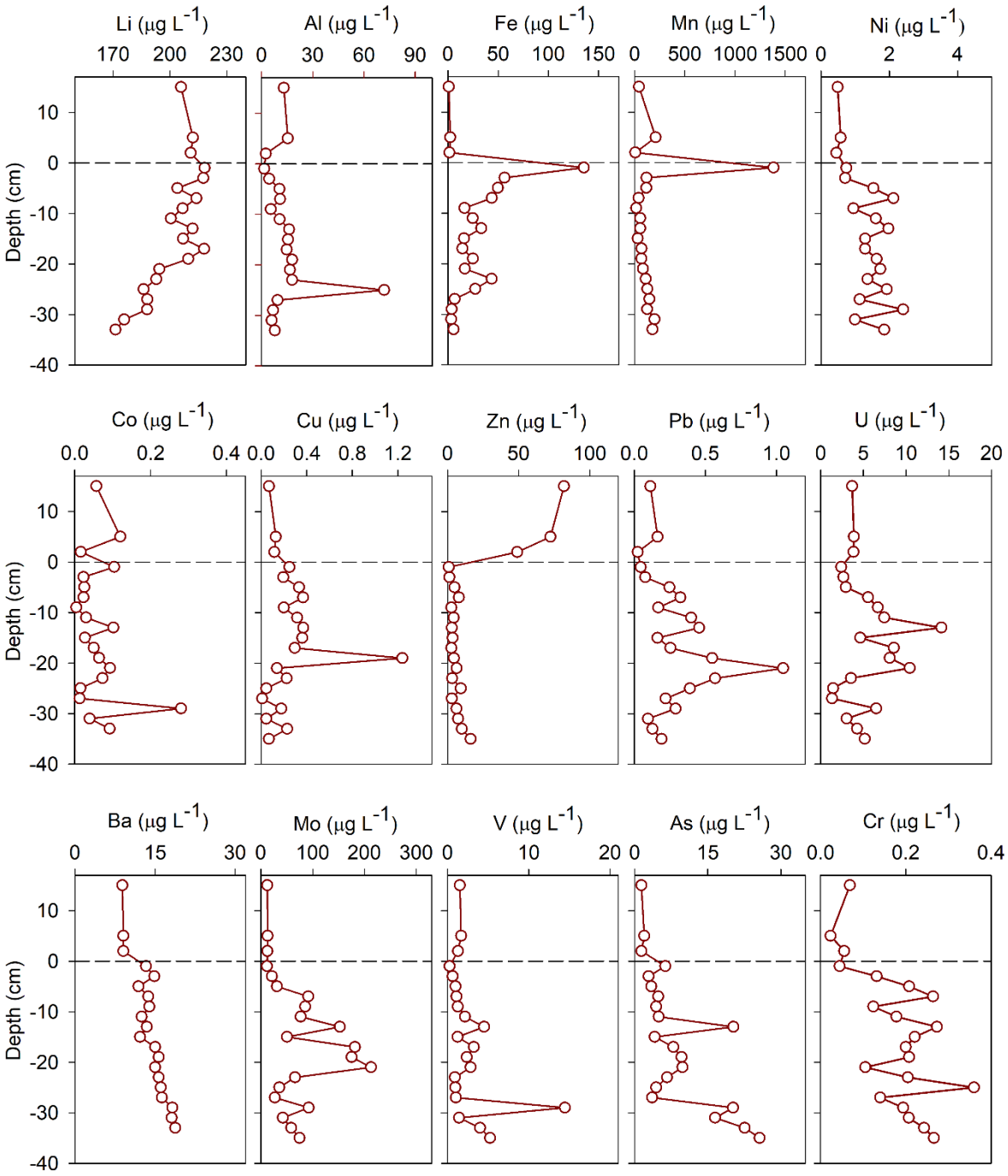

Figure 5.36. Vertical distribution of selected elements (Li, Al, Fe, Mn, Ni, Co, Cu, Zn, Pb, U, Ba, Mo, V, As, Cr) in the sediment pore water (core K1)

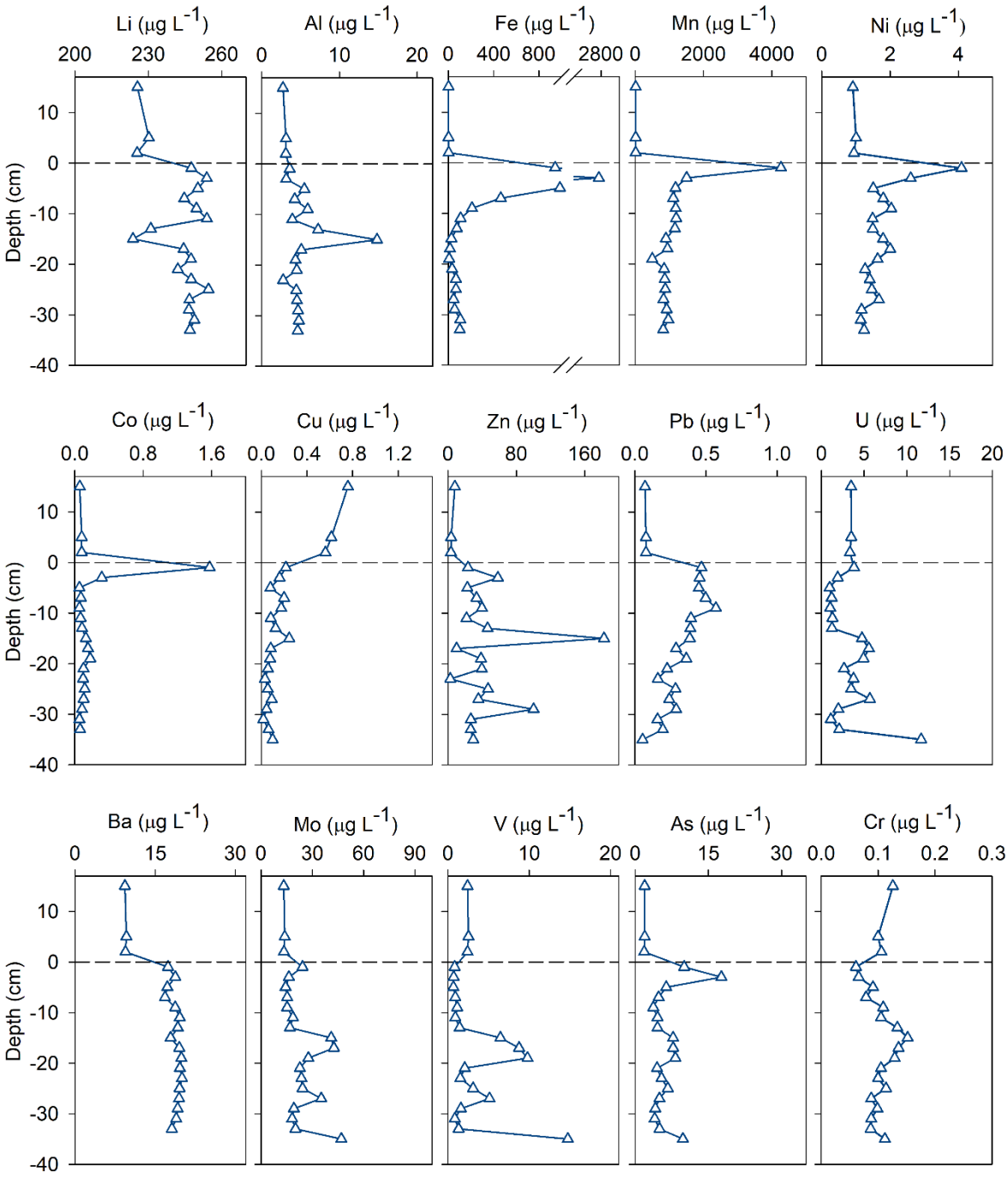

Figure 5.37. Vertical distribution of selected elements (Li, Al, Fe, Mn, Ni, Co, Cu, Zn, Pb, U, Ba, Mo, V, As, Cr) in the sediment pore water (core K7)

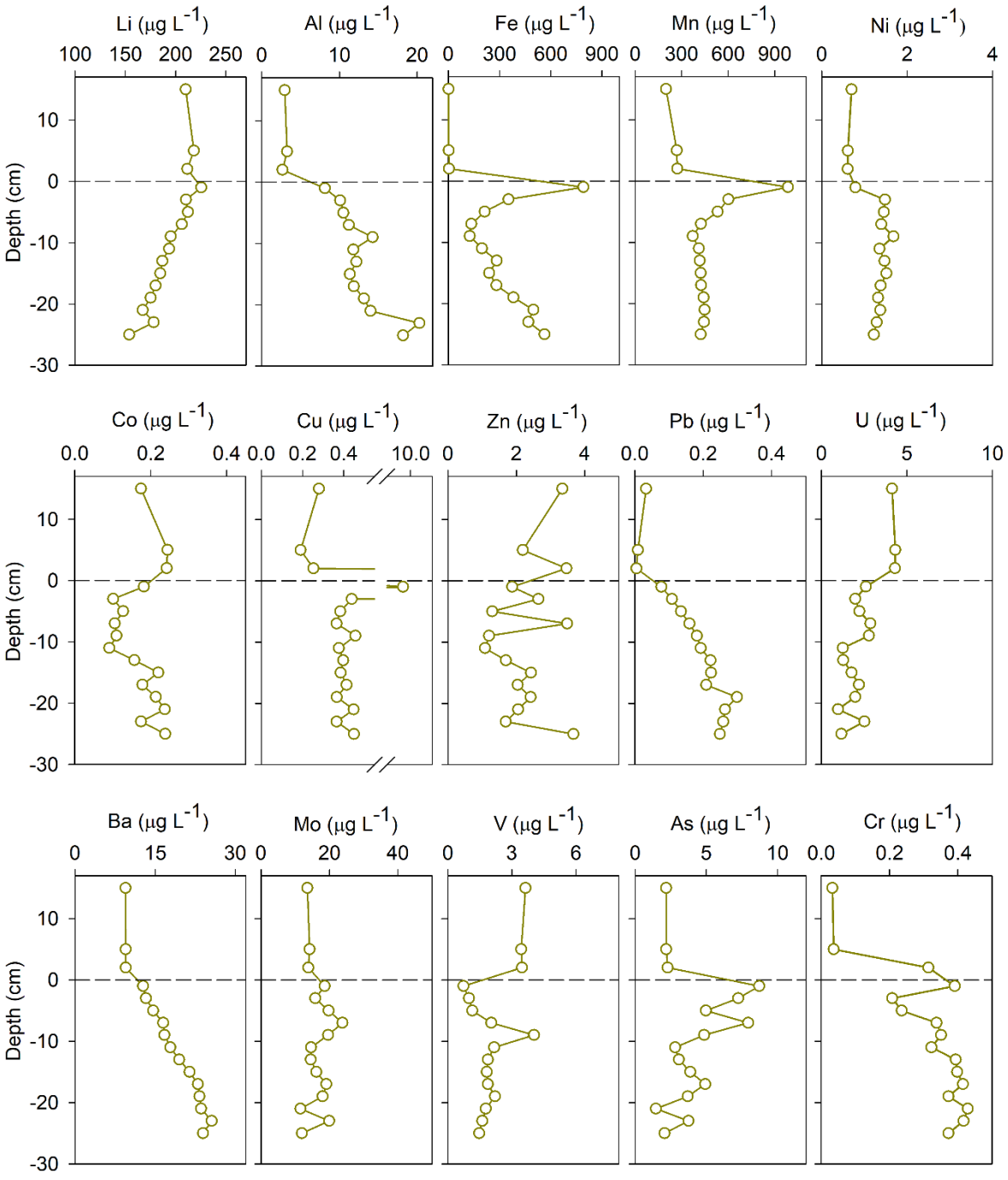

Figure 5.38. Vertical distribution of selected elements (Li, Al, Fe, Mn, Ni, Co, Cu, Zn, Pb, U, Ba, Mo, V, As, Cr) in the sediment pore water (core K8)

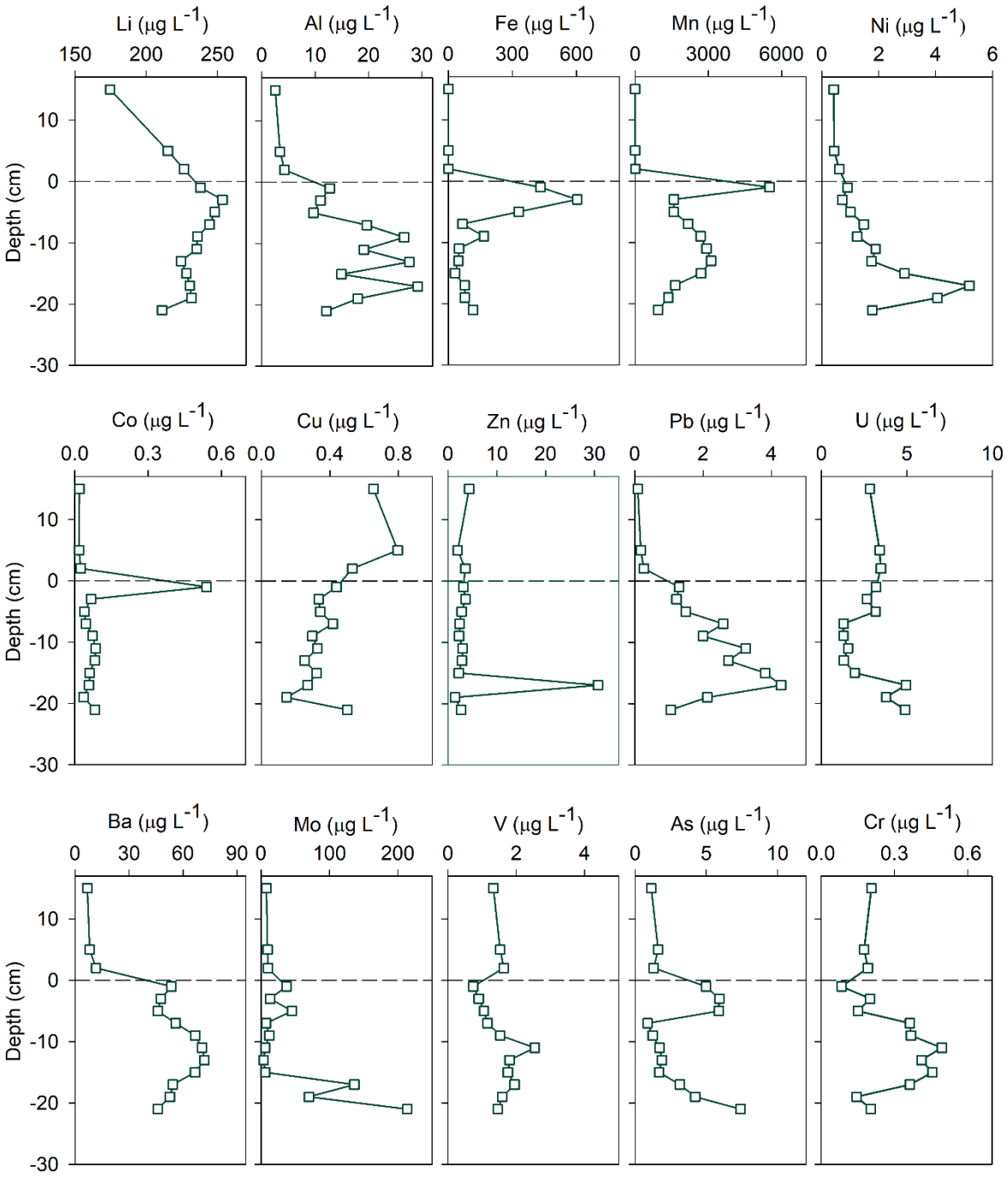

Figure 5.39. Vertical distribution of selected elements (Li, Al, Fe, Mn, Ni, Co, Cu, Zn, Pb, U, Ba, Mo, V, As, Cr) in the sediment pore water (core K20)

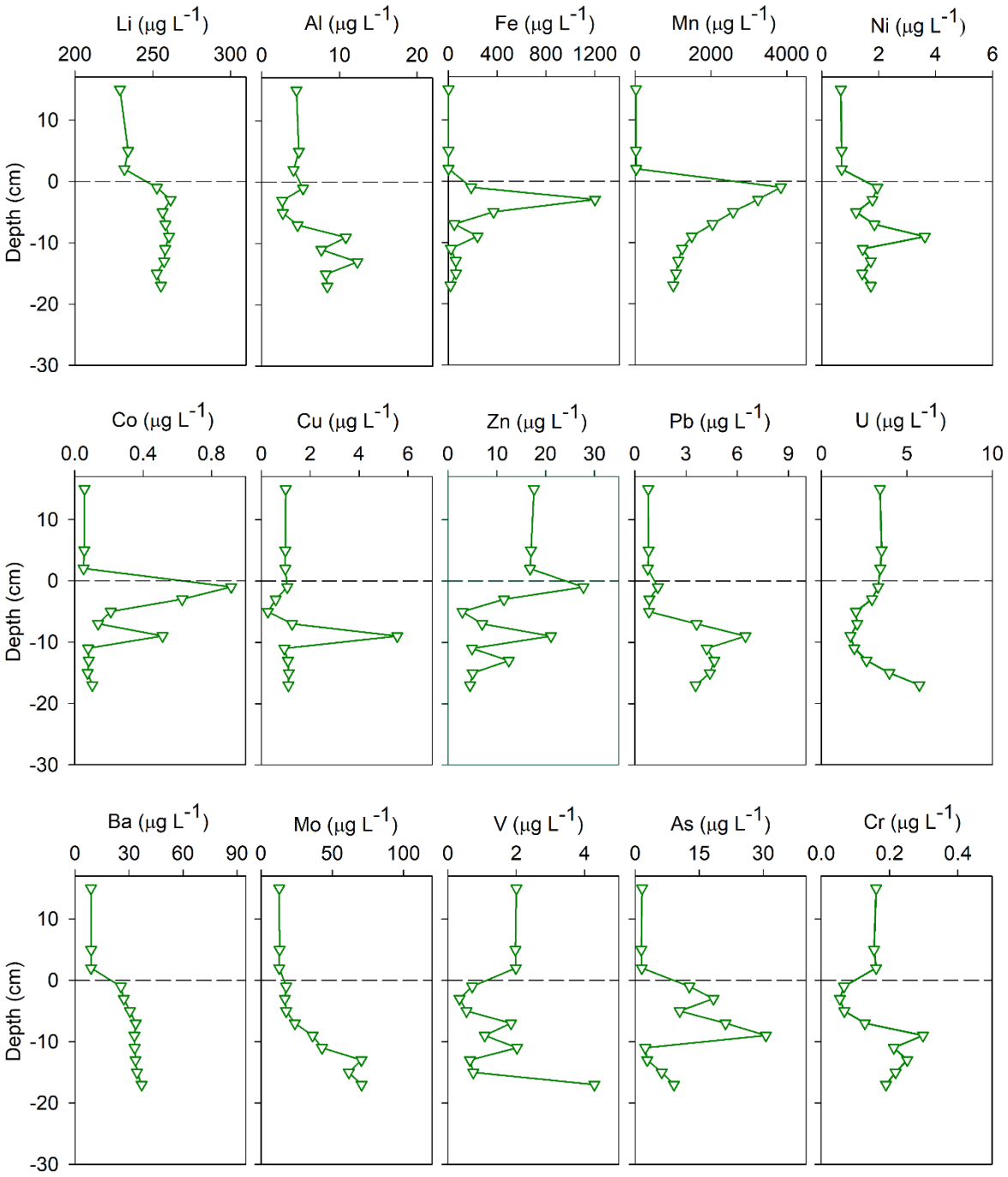

Figure 5.40. Vertical distribution of selected elements (Li, Al, Fe, Mn, Ni, Co, Cu, Zn, Pb, U, Ba, Mo, V, As, Cr) in the sediment pore water (core K36)

6. DISCUSSION

6. DISCUSSION

6.1. Spatial distribution of metals in the surface estuarine sediments

Two general observations can be made according to the spatial distribution of selected metals in the Krka River estuary; (1) terrigenous elements demonstrate distribution pattern with highest values found in sediment from the Guduča mouth, Zaton Bay and K19 sampling location and (2) metals having mostly anthropogenic origins demonstrate distribution patterns with clear distinction between the upper unpolluted estuary and lower estuary affected by multiple anthropogenic sources.

Obtained Fe and Al spatial distributions, as well as those of other terrigenous elements (data not shown), are mostly in line with the previous studies conducted in this area, which show low input of terrigenous material from the Krka River to the estuary and denote Guduča River and Litno Spring (Zaton) as main pathways of detrital material into the estuary (Prohić and Juračić 1989; Juračić and Pravdić 1991; Cukrov 2006; Cukrov and Barišić 2006). However, the high concentrations found in this research at location K19 are unexpected and the origin of this material remains unclear.

The increased concentrations of some elements found in the Šibenik Bay can mostly be attributed to one of the three main sources of the anthropogenic pollution in the area. The former TEF factory clearly affected Mn content in the Krka River estuary, with values reaching 3.2% in the proximity of the ex-factory, which is manifold increase compared to pristine part of the estuary and other location in Adriatic and elsewhere (Table 6.1.). The factory seemed to be a source of other metals as well; Pb, Fe, Ni, Co and in lesser extent of As, Cu, Zn and Hg. The activities in the Port of Šibenik presumably had a major impact on concentrations of Zn, Cd and Cr in the Šibenik Bay, but also contributed to the enhanced levels of As, Cu and Pb. The levels of Zn, Cd and Cr are similar to or even exceed the values reported at contaminated sites such as Rijeka harbour and Toulon Bay (Table 6.1.). Moreover, the highest values of Hg and As, recorded in the shipyard/marina area are as well in the range of coastal and estuarine contaminated sites (Table 6.1.).

The input and behaviour of analysed metals in area of the ex-factory, the port and the marina/shipyard will be discussed in more details in Sections 6.6.4., 6.6.6. and 6.6.7., dealing with sediment cores taken at these locations.

In addition, it can be concluded from the surface sediment metal distribution maps that there is no dispersal of contaminants outside of the estuary to the open sea. The distribution pattern is most probably influenced by multiple factors: closed morphology of the estuary, bottom seawater layer moving landward preventing transport of metal in a seaward direction (Mikac et al. 1989) and fast adsorption of metals to the particles and deposition to the seabed. By the studying adsorption on inorganic solid phases in Krka river water of various salinities (S = 3, 20 and 38) Bilinski et al. (1991) demonstrated the remarkable self-purification ability of the Krka River estuary with respect to Hg, Zn and Pb. The authors postulated that the surface sediments of the Krka River estuary containing calcite and aluminosilicates could be considered a sink for most trace metals. However, as indicated by distribution maps, the bottom seawater layer causes the spread of the contamination in a landward direction.

Table 6.1. Ranges of metal concantrations in the Krka River estuary (surface sediments and cores) and in the costal and estuarine environments in Croatia and other countries in Europe. Values as expressed as μg g^{-1}.

Location	Mn	Co	Ni	Cu	Zn	As	Cr	Pb	Cd	Hg	Reference
Neretva River delta	107-1 318	0.36-17.9	3.63-87.9	5.14-108	10.6-162	-	-	4.36-48.8	0.10-2.01	-	Jurina et al. 2015
Bakar Bay	-	11.5-14.3	56.3-80.7	30.7-89.3	85.5-156	10.3-19	52.8-69.8	41.2-71.5	0.17-0.4	0.33-0.65	Cukrov et al. 2014
Rijeka harbour	-	9.00-16.4	54.8-143	30.6-429	69.8-1 260	9.50-37.7	42.7-117	23.6-637	0.14-4.66	0.10-8.06	Cukrov et al. 2011
Kaštela Bay	-	-	-	-	-	-	-	-	-	14.3-74.0	Kwokal et al. 2002
Marine lake Mir	71-468	0.80-6.90	3.60-19.6	1.59-46.2	5.10-44.0	1.90-13.0	-	2.37-21.6	0.01-0.37	-	Mlakar et al. 2015
Makirina Bay	200-300	7.05-10.8	26.5-37.9	27.6-34.1	47.7-50.6	14.5-17.4	82.1-120	23.7-27.4	0.25-0.33	0.07-0.07	Komar et al. 2015
NP Mljet	-	-	-	6.8-18.9	15.4-53.2	-	-	21.3-82.6	0.09-0.30	0.10-0.38	Cuculić et al. 2009
Toulon Bay	-	-	8.8-37.6	5.8-846	24.3-1 340	6.7-61	8.5-121	14.9-469	0.05-2.90	0.03-27.3	Tessier et al. 2011
Loire estuary	-	-	0.88-68.6	<LOD-84.0	3.87-349	0.53-47.7	2.02-315	1.49-104	0.01-3.33	<LOD-0.37	Coynel et al. 2016
Gulf of Trieste	-	-	88.0-97.0	28.0-35.0	155-175	10.9-15.7	150-171	64.0-76.0	0.16-0.23	0.54-1.24	Acquavita et al. 2010
	-	-	-	-	-	-	-	-	-	0.10-23.3	Covelli et al. 2001
Tiber estuary	-	-	6.22-494	16.0-528	6.18-413	2.65-45.3	8.52-190	3.07-187	0.08-2.22	0.05-1.14	Montouri et al. 2016
Nerbioi–Ibaizabal estuary	66-935	0.3-16	3.4-120	15-571	41-1 260	0.6–220	5.0-134	21-445	0.01-17	-	Fdez-Ortiz de Vallejuelo et al. 2010
Krka River estuary											
surface sediment	128-32 038	2.52-16.1	11.3-63.4	5.25-63.4	37.6-1 201	5.43-39.6	20.7-129	18.0-665	0.11-11.2	0.06-12.4	This study
cores-upper part	127-486	3.33-8.62	20.1-56.6	6.51-25.9	37.6-95.5	4.64-14.4	35.1-98.2	14.5-550	0.34-0.60	0.04-0.19	This study
cores-lower part	148-21 389	3.21-29.5	15.4-97.9	6.39-267	29.6-1 561	8.49-101	32.6-786	17.5-737	0.12-10.4	0.72-57.8	This study

6.2. Metal pollution assessment in the surface estuarine sediments

6.2.1. Enrichment factor

Distinguishing between natural content of metals in sediments and anthropogenic contamination is often a challenging task. Geochemical normalization based on the concentration of a conservative element is a commonly used to compensate for differences in grain size and carbonate content variations, and to identify anomalous metal concentrations. Enrichment factor (EF) is defined as observed metal to conservative element ratio in the sample of interest divided by background metal/conservative element ratio. Several conservative elements can be used, e.g. Al, Fe, Li, Ti. The enrichment factor is expressed as:

$$EF = \frac{\left(\frac{Me}{X}\right)_{Sample}}{\left(\frac{Me}{X}\right)_{Background}}$$

where $(Me/X)_{Sample}$ is the metal to conservative element ratio in the sample of interest and $(Me/X)_{Background}$ is the natural background value of metal to conservative element ratio. In this work, Li was chosen as conservative element due to the better recovery rate than Al, possible anthropogenic input of Al (Prohić 1984) and Fe in the Krka River estuary and involvement of Fe in early diagenesis processes which can change the metal/Fe ratio. As natural background value, deepest layer (34-36 cm) of the K1 core was used. According to previous research (Cukrov et al. 2007), sedimentation in this area is 2 mm y^{-1}. Thus, the chosen layer has been deposited before approximately 180 years, i.e., before industrial development in the study area.

Based on the enrichment factor, pollution can be classified in one of five categories (Sutherland 2000): EF < 2: deficiency to low enrichment; EF 2–5: moderate enrichment; EF 5–20: significant enrichment; EF 20–40: very high enrichment; EF > 40: extremely high enrichment.

The summary (min, max and mean) of the calculated EFs is given in the Table 6.2. and contour plots of selected elements in the Fig 6.1. The obtained enrichment factors for the surface sediments clearly demonstrated differences between the upper part of the estuary – from the last Krka River waterfall to the end of Prokljan Lake and the lower part of the estuary – downstream of Prokljan Lake. In the upper part of the estuary, there was no enrichment (EF < 2) at most of the sampling stations. Down from Prokljan Lake, there was enrichment at all sampling locations, ranging from moderate enrichment to extremely high enrichment, depending on observed element.

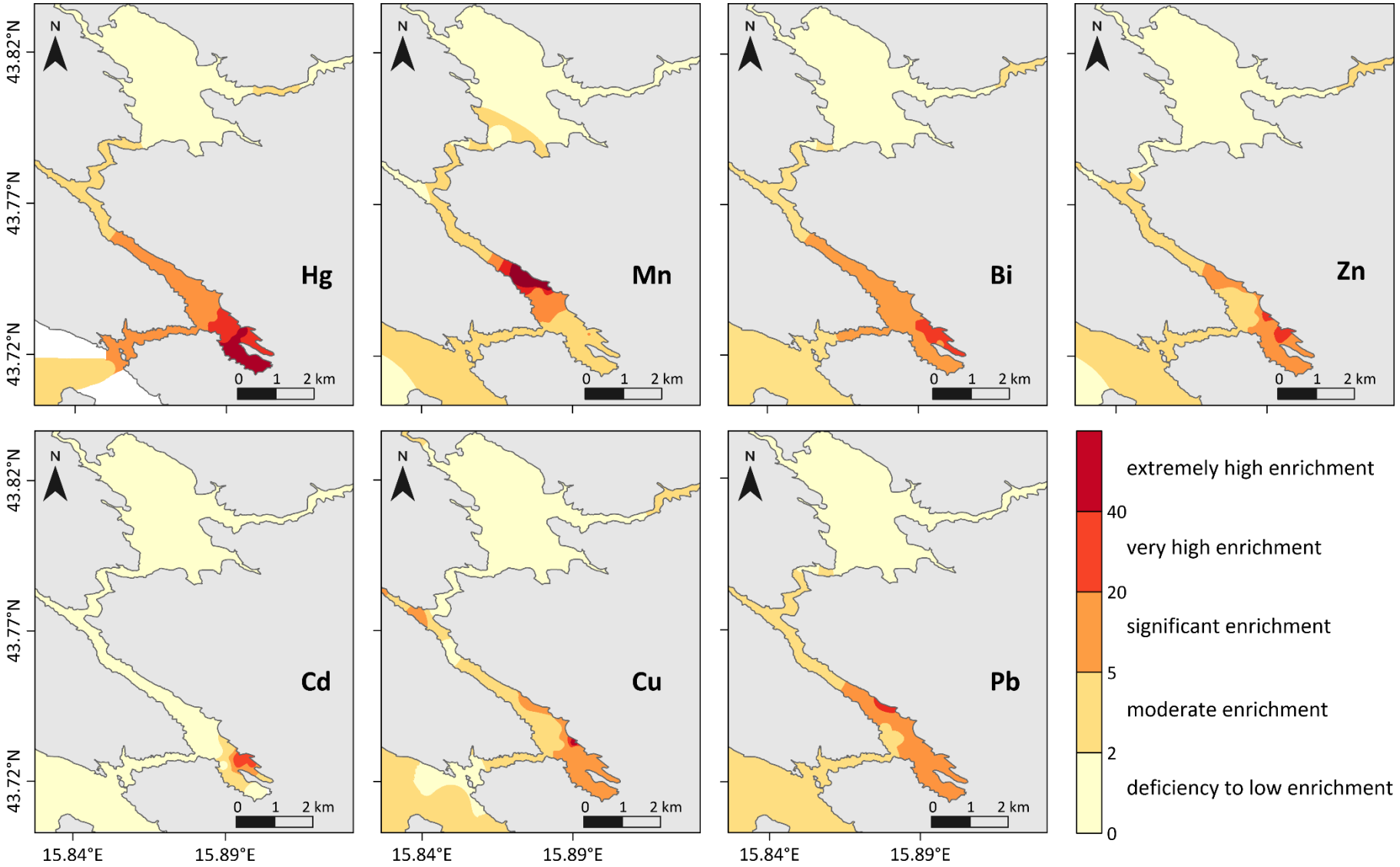

Figure 6.1. Spatial distribution of calculated enrichment factors of selected elements in the surface sediment (0-5 cm) of the Krka estuary

The EF ranges of Fe, Cr, Co and Ni were 0.93-2.73, 0.87-3.64, 0.77-2.49 and 0.83-1.77, respectively. Although Fe, Cr and Co showed values higher than 2, it was the case at only two (Fe, Co) or three (Cr) sampling sites. Therefore, it can be concluded that Fe, Cr, Co and Ni in the surface sediments of the Krka River estuary are dominantly of the natural origin.

Antimony showed moderate enrichment in majority of the sampling locations in the Šibenik Bay, while in other parts of estuary Sb EF values were low, indicating deficiency to low enrichment. Molybdenum, with mean EF value of 1.47, showed no enrichment in most of the estuary. However, at sampling site K24, EF value of 15.3 indicated significant enrichment.

The EF ranges of Ag, U, Ba and As were 0.84-16.6, 0.51-17.1, 0.93-6.32 and 0.85-7.93, with averages 2.77, 2.20, 2.13 and 2.09, respectively. The higher EF values indicating moderate to significant enrichment were found only in the Šibenik Bay area, while in rest of the estuary EF values were <2.

Contamination of surface sediment by Cd was limited to the port area, where EF values indicated very high enrichment (up to 36.6). Unlike Cd, whose enrichment was restricted to the narrow area, following elements were enriched in the most part of the lower estuary: Sn, Cu, Pb, Mn, Zn, Bi and Hg, respectively. Tin, with EF range of 1.06-11.8, has demonstrated moderate to significant enrichment, while Pb, Bi and Zn, with EF ranges 1.18-29.6, 1.36-26.9 and 1.46-38.8 have indicated even very high enrichment in some areas. Very high enrichment is associated with the former Electrode and Ferroalloy Factory (Pb), the port area (Bi, Zn) and the Šibenik waterfront (Zn).

Extremely high enrichment has been recorded for Cu (45.4), Mn (103) and Hg (150.7). These extremely high EF values are linked to the former TEF factory (Mn), the port (Hg), marina/shipyard (Hg) and Šibenik waterfront (Cu). Based on obtained EF values, which indicated high to extremely high enrichment in almost entire Šibenik Bay, Hg is the heaviest pollutant among the measured elements in the Krka River estuary.

Table 6.2. Calculated enrichment factors (EF) and geoaccumulation indices (I_{geo}) for surface sediments (0-5 cm) from the Krka River estuary

	EF			Igeo		
	min	max	mean	min	max	mean
Hg	0.91	151	17.0	-0.66	7.11	2.32
Bi	1.36	26.9	8.25	-0.65	4.47	1.88
Zn	1.46	38.8	5.57	-0.67	4.33	1.29
Mn	0.71	103	5.48	-1.38	6.58	0.88
Pb	1.18	29.6	5.37	-0.42	4.79	1.40
Cu	1.11	45.4	4.98	-1.42	3.24	1.23
Sn	1.06	11.8	3.46	-1.81	2.94	0.97
Ag	0.84	16.6	2.77	-1.53	2.75	0.52
Cd	0.51	36.6	2.73	-2.41	4.24	-0.18
U	0.51	17.1	2.20	-0.76	3.15	0.07
Ba	0.93	6.32	2.13	-1.52	2.33	0.36
As	0.85	7.93	2.09	-0.82	2.05	0.32
Mo	0.35	15.3	1.47	-1.66	1.67	-0.44
Sb	0.54	4.50	1.43	-1.33	1.30	-0.24
Fe	0.93	2.72	1.36	-1.60	0.61	-0.11
Cr	0.87	3.64	1.35	-1.73	0.91	-0.14
Co	0.77	2.49	1.33	-1.54	1.14	-0.16
Ni	0.83	1.77	1.26	-1.95	0.54	-0.20

6.2.2. Geoaccumulation index

Another commonly used criterion for assessing the metal pollution level in sediments is the geoaccumulation index (I_{geo}). It was originally defined by Müller (1979) in order to determine and define metal contamination in sediments by comparing current concentrations with pre-industrial levels. The geoaccumulation index is calculated as follows:

$$I_{geo} = log_2\left(\frac{C_n}{1.5B_n}\right)$$

where C_n is the measured concentration of the examined metal (n) in the sediment and B_n is the geochemical background concentration of the metal (n). A factor 1.5 is introduced to minimise the effect of possible variations in the background values which may be attributed to lithologic variations in the sediments. Background values used for the calculation of I_{geo} are the same as those used for the calculation of EFs, described in the Subchapter 6.2.1.

Müller (1979) established seven classes of I_{geo} values: $I_{geo} \leq 0$, unpolluted; $0 < I_{geo} < 1$, unpolluted to moderately polluted; $1 < I_{geo} < 2$, moderately polluted; $2 < I_{geo} < 3$, moderately to heavily polluted; $3 < I_{geo} < 4$, heavily polluted; $4 < I_{geo} < 5$, heavily to extremely polluted; > 5, extremely polluted.

The highest class (>5) reflects 100-fold enrichment above the background area. In the Krka River estuary these high values were found only for Hg ($I_{geo\text{-}max} = 7.11$) in the shipyard/marina area (Table 6.2.). The rest of the Šibenik Bay was heavily or heavily to extremely polluted with Hg. Therefore, calculation of geoaccumulation index confirmed that Hg is the heaviest pollutant in the Krka River estuary, as already indicated by enrichment factor.

Furthermore, calculated I_{geo} values confirmed other observations made according to EF; (1) there is a clear distinction between lower and upper part of the estuary on the basis of metal contamination and (2) Pb ($I_{geo\text{-}max} = 4.79$), Bi ($I_{geo\text{-}max} = 4.47$), Zn ($I_{geo\text{-}max} = 4.33$), Cu ($I_{geo\text{-}max} = 3.24$), Cd ($I_{geo\text{-}max} = 4.24$) and Mn ($I_{geo\text{-}max} = 6.58$) (Table 6.2.) are major pollutants following Hg in the Krka River estuary.

6.3. Ecotoxicological risk assessment in the surface estuarine sediments

On their own, the data on total metal concentrations in the sediment are not enough to assess potential toxicity for organisms living in or near this ecosystem. For this purpose, interpretive tools such as various sediment quality guidelines (SQGs) are required to predict the biological effect of present metals on benthic organisms (Burton 2002). The ones proposed by Long et al. (1995) are widely in use. Based on ecotoxicological data from North American marine ecosystems, these authors defined two threshold values: the effects-range-low (ERL) and the effects-range-median (ERM), calculated as the 10^{th} and the 50^{th} percentiles of the effect dataset. The ERL value indicates the concentration limit for each pollutant above which negative impacts on organisms are possible, while the ERM value is the concentration limit above which adverse effects on organisms are expected. The ERL and ERM guideline values for trace metals are as follows: Ag (1.0 and 3.7 μg g^{-1}), Cd (1.2 and 9.6 μg g^{-1}), Pb (46.7 and 218 μg g^{-1}), Cr (81 and 370 μg g^{-1}), Ni (20.9 and 51.6 μg g^{-1}), Cu (34 and 270 μg g^{-1}), Zn (150 and 410 μg g^{-1}), As (8.2 and 70 μg g^{-1}) and Hg (0.15 and 0.71 μg g^{-1}).

The percentages of sampling stations in the Krka River estuary corresponding to SQG ranges are given in Fig. 6.2. As it can be seen on the plot, Ni content in the surface sediments exceeded

ERL or ERM value at most of the sampling sites (87%). However, this is interpreted as a natural background, since similar concentrations were found in deeper sediments collected in the Krka River estuary, which were deposited before industrial development in the area. Similar case with the same interpretation was reported by Cukrov et al. (2014) for the sediments of the Bakar Bay, located in the northern part of the eastern Adriatic coast. Moreover, comparable situation is described by the same authors for arsenic. In our case, some sampling points were As was above ERL value can be attributed to the background concentration, while in in the Šibenik Bay values can be attributed to the anthropogenic input. Therefore, negative influence of As to biota is possible in the lower estuary.

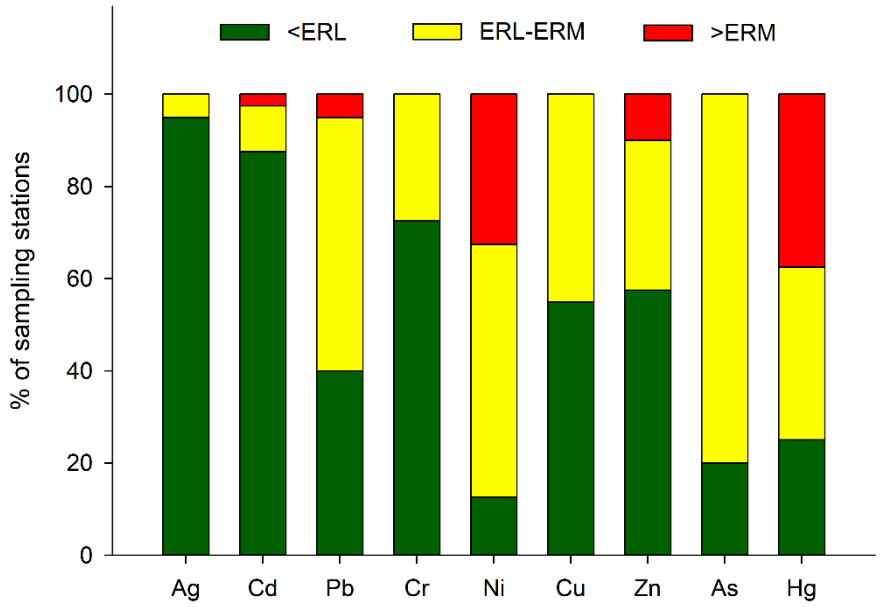

Figure 6.2. Percentages of the sampling stations corresponding to ranges of Sediment Quality Guidelines values (effect-range-low (ERL) and effect-range-median (ERM)) in the surface sediment of the Krka River estuary

Extent of the Hg pollution in the surface sediments of the Krka River estuary is already established through obtained high concentrations and calculated indices (EF, I_{geo}). By comparing its values to ERL and ERM, one can see that sediment from more than 1/3 of sampling sites exceeded ERL value, and the same number of sediment samples exceeded the ERM. Therefore, Hg can be regarded as a main contaminant in terms of toxicity for benthic organism in the Krka River estuary.

Lead concentrations exceeded ERL or ERM at 60% of sampling locations, making Pb an element that represents possible toxic threat on living organism in significant part of the estuary. Regarding Pb concentration, negative effects are expected at two sampling locations; in front of the former factory and in the marina. Another element whose values exceeded ERM is Zn. The concentrations above ERM were found at four locations, along the Šibenik coastline, between the port and the former factory. Zinc concentrations from nearby sampling location did not surpass ERM, but were very close to this value, therefore Zn can also be regarded as toxic threat on organisms in the Šibenik Bay area.

High Cd concentration recorded in the sediment taken in the vicinity of the transhipment port surpass ERM, and sediment from the four surrounding sites exceeded ERL value. However, in the most part of the estuary, Cd concentrations in the surface sediment do not represent threat for living organisms. Chromium and Cu concentrations were below ERL value at 29 and 22 sampling sites, respectively. In the rest of the stations, mainly located in the Šibenik Bay, values exceeded ERL value, meaning negative impact on organisms is possible. Regarding the fact that Ag exceeds ERL at just two sampling sites in the port, it is not likely that it will have an adverse effect to the benthic community.

Considering that multiple contamination is often encountered in natural environments, the mean ERM quotient (m-ERM-Q) method was used to determine the possible biological effect of combined toxicant groups by calculating mean quotients for a range of contaminants using the following equitation:

$$m - ERM - Q = \frac{\sum_{i=1}^{n}(\frac{C_i}{ERM_i})}{n}$$

where C_i is the concentration of a metal in a sediment, ERM_i is the ERM value for metal i, and n is the number of metals. Long et al. (2000) have defined several classes of toxicity probability for biota as: m-ERM-Q < 0.1, 9 % probability of toxicity; 0.11–0.5, 21 % probability of toxicity; 0.51–1.5, 49 % probability of toxicity; and > 1.51, 76 % probability of toxicity.

The mean ERM quotients were calculated using seven studied elements: Ag, Cd, Pb, Cr, Cu, Zn, As and Hg. Considering its naturally elevated concentrations, Ni was omitted from calculation. The m-ERM-Q values in surface sediment of the Krka River estuary varied within the range of 0.07-2.3, with the mean value of 0.36. As shown in Fig. 6.3., majority of the studied area (65%) is within the 0.11-0.5 class, indicating that combination of the studied metals has a toxicity probability of 21%. Higher toxicity is expected in the proximity of anthropogenic

contamination sources; the former Electrode and Ferroalloy Factory, the port and especially the marina/shipyard area where toxicity probability is 76%.

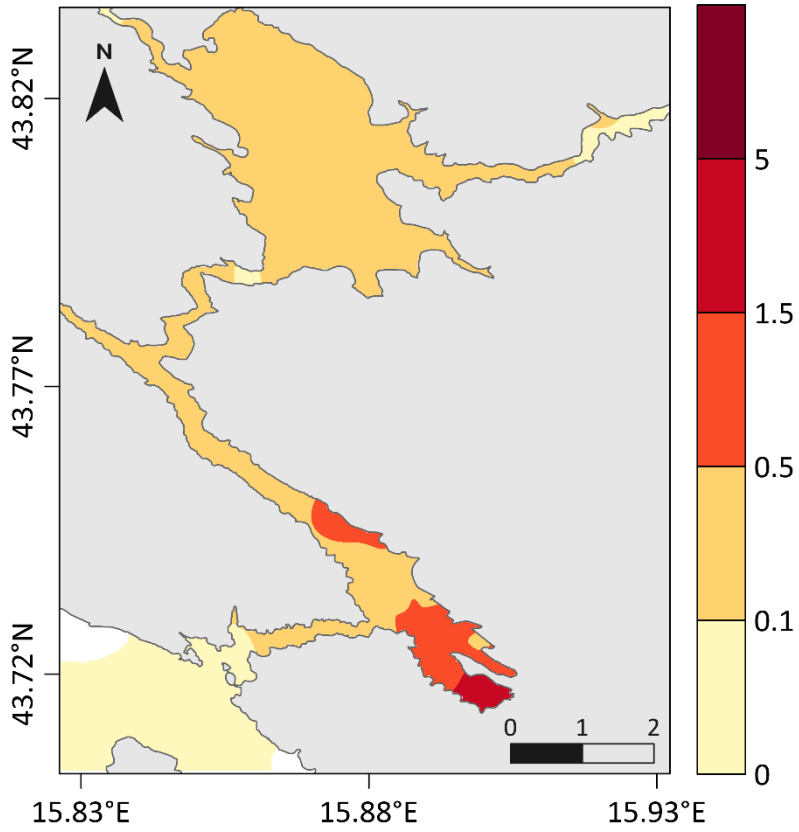

Figure 6.3. Spatial distribution of the mean ERM quotients (m-ERM-Q) in the surface sediment of the Krka River estuary. The classes of toxicity probability for biota are defined as: m-ERM-Q < 0.1, 9 % probability of toxicity; 0.11–0.5, 21 % probability of toxicity; 0.51-1.5, 49 % probability of toxicity; and > 1.51, 76 % probability of toxicity.

6.4. Source identification of metals in the surface estuarine sediments

The surface sediment data were subjected to a Pearson correlation matrix and a principal component analysis (PCA) in order to elucidate different sources of elements and to determine similarities between sampling points. The PCA reduced the number of variables to five principal components (PCs), which were able to explain 98.5% of the data variance (Table 6.3.).

Table 6.3. Eigenvalues, percentage of variance and cumulative variance of the first five principal components (surface sediment data set)

PC	Eigenvalue	% of Variance	Cumulative %
1	14.7	45.9	45.9
2	7.12	22.2	68.1
3	2.92	9.14	77.3
4	2.25	7.02	84.3
5	1.66	5.20	89.5

The first principal component (PC1) was dominated by Al, Ti, Fe, Li, Rb, etc., accounting for 45.9% of the total variance. In sediments, these elements are dominantly of terrigenous origin and rarely influenced by human activities. Nickel, Co and Cr were also included in the PC1. Due to the similar PC loading and significant correlation between Ni, Co and Cr with terrigenous elements ($r > 0.7$, $p < 0.01$) (Table 6.4.), it can be concluded that these metals have a same origin, i.e., Ni, Co and Cr in sediment come from natural source. This finding is in accordance with low EFs calculated in this research, which also indicate natural origin of these elements. However, Cr also demonstrated significant correlation ($r > 0.45$, $p < 0.01$) with some of the contaminants, more precisely, with those elements which had elevated concentrations in the port area (Cd, U, Cu, Zn, As, P). As seen in the spatial distribution, that was also the area where highest Cr content was recorded. Therefore, based on spatial distribution, PCA and correlation, it can be concluded that Cr is predominantly of natural origin in the Krka River estuary with possible anthropogenic input in the port area.

The second principal component (PC2) was loaded by Ag, Cd, Pb, Bi, U, Cu, Zn, Hg, etc., accounting for 22.2% of the total variance. Due to the lack of the correlation of these elements with terrigenous elements, increased EFs and spatial distributions which indicate elevated concentration in proximity of one or more possible anthropogenic sources, it can be concluded that these elements mostly have anthropogenic origin. The position of U, Cd and P separates them from the rest of the contaminants, indicating they have a common origin. Considering highest values were recorded in the port area, they most probably originate from the phosphate ore, as already suggested elsewhere (Cukrov 2006).

The third principal component (PC3) was dominated by Mn and Pb and it accounted for 9.14% of the total variance. The similar PC loading of these two elements and their significant correlation ($r = 0.88$, $p < 0.01$), suggest the common anthropogenic source. As seen on surface distribution maps, a common source of these two elements is the former Electrode and

Ferroalloy Factory. Although Co is mainly of natural origin in the surface sediments of the Krka River estuary, probably there is some anthropogenically induced Co at the K20 sampling station, i.e., in front of the former factory. This conclusion has been made due to its high loading in PC3, significant correlation ($r = 0.61$ and 0.70, $p < 0.01$) with Mn and Pb as well as moderate enrichment in the K20 sample according to EF.

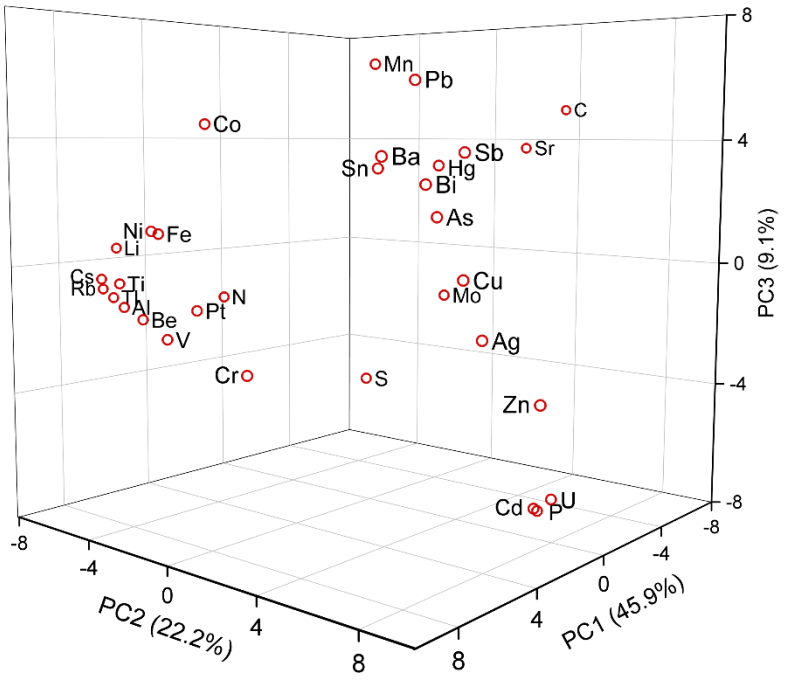

Figure 6.4. 3D loading plot of principal component analysis (PCA) for measured elements in the surface sediment from the Krka River estuary

The different PC loading and lack of the significant ($p < 0.01$) correlations between Hg and the other metals, except As ($r = 0.85$, $p < 0.01$) and in lesser extent Cu ($r = 0.46$, $p < 0.01$), indicates that Hg had a unique anthropogenic source. This is in agreement with the surface distribution maps, which revealed the marina/shipyard area as a main source of Hg and As contamination.

3D score plot (Fig. 6.5.) separated sampling points to the two main groups; (1) the ones dominated by Al and other terrigenous elements, mostly located in the upper estuary and Zaton Bay and (2) the ones distributed along with C and Sr, mostly located at the mouth of the Krka River estuary and in the Šibenik Bay. K20 and K36 diverged from the rest of the sampling points most probably due to the strong anthropogenic influence which resulted in the extremely high concentrations of some elements (e.g. Mn) in these two locations.

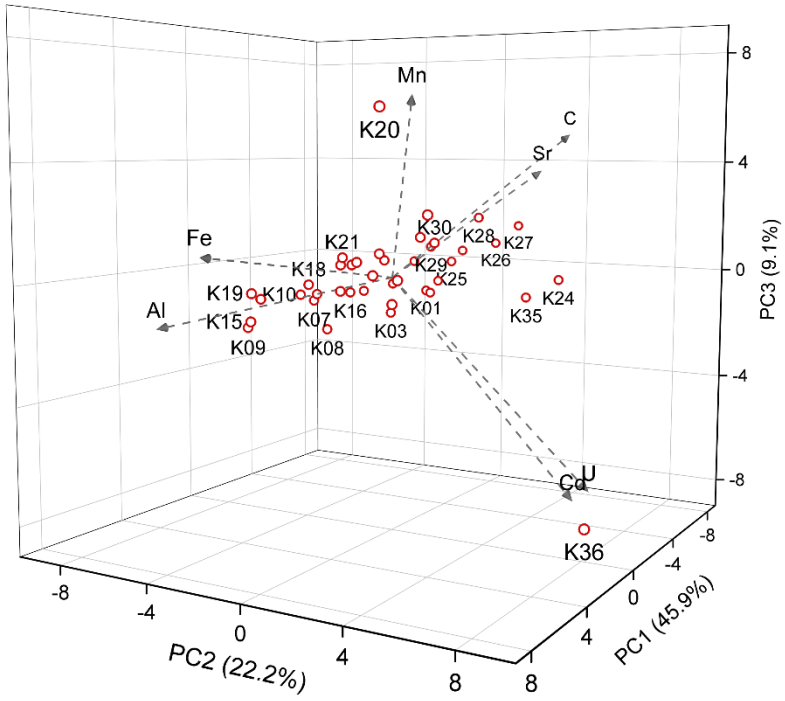

Figure 6.5. 3D score plot of principal component analysis (PCA) results obtained for 40 sampling locations. Red circle symbols represent sampling points. Labels are given for 21 of 40 points, due to clarity reasons.

Table 6.4. Pearson correlation matrix for elements measured in the surface sediment from the Krka River estuary

	Li	Rb	Ag	Cd	Pb	U	Al	Ti	Cr	Mn	Fe	Co	Ni	Cu	Zn	Sr	As	Hg	C	N	S	P
Li	1																					
Rb	**0.93**	1																				
Ag	0.07	0.05	1																			
Cd	-0.18	-0.16	**0.60**	1																		
Pb	0.22	0.15	**0.50**	0.23	1																	
U	-0.22	-0.21	**0.59**	**0.98**	0.24	1																
Al	**0.94**	**0.97**	0.20	0.02	0.27	-0.03	1															
Ti	**0.89**	**0.96**	0.17	-0.10	0.24	-0.13	**0.96**	1														
Cr	**0.67**	**0.72**	**0.61**	**0.48**	**0.48**	**0.45**	**0.83**	**0.78**	1													
Mn	0.15	0.09	0.15	0.01	**0.88**	0.01	0.15	0.14	0.21	1												
Fe	**0.85**	**0.89**	0.31	0.03	**0.45**	-0.01	**0.93**	**0.92**	**0.85**	0.27	1											
Co	**0.75**	**0.70**	0.33	-0.04	**0.70**	-0.06	**0.77**	**0.75**	**0.73**	**0.61**	**0.88**	1										
Ni	**0.87**	**0.89**	0.34	-0.01	**0.47**	-0.05	**0.93**	**0.92**	**0.85**	0.33	**0.95**	**0.91**	1									
Cu	0.07	0.11	**0.80**	**0.43**	**0.60**	**0.47**	0.24	0.27	**0.57**	0.25	0.39	0.38	0.38	1								
Zn	-0.05	-0.07	**0.82**	**0.86**	**0.56**	**0.88**	0.13	0.04	**0.61**	0.25	0.21	0.24	0.21	**0.77**	1							
Sr	-0.39	**-0.51**	0.00	0.10	0.02	0.14	**-0.44**	**-0.47**	-0.28	-0.06	-0.26	-0.14	-0.35	-0.09	0.05	1						
As	0.18	0.16	**0.57**	0.39	**0.56**	0.40	0.30	0.28	**0.55**	0.19	**0.48**	0.39	0.34	**0.66**	**0.56**	0.22	1					
Hg	0.11	0.04	0.36	0.15	0.38	0.17	0.12	0.12	0.30	0.02	0.28	0.20	0.18	**0.46**	0.35	0.27	**0.85**	1				
C	**-0.78**	**-0.86**	-0.14	-0.19	0.00	-0.15	**-0.87**	**-0.83**	**-0.75**	0.11	**-0.72**	**-0.47**	**-0.72**	-0.16	-0.16	**0.44**	-0.17	0.01	1			
N	**0.47**	**0.57**	0.27	-0.02	0.23	-0.08	**0.55**	**0.56**	**0.53**	0.20	**0.50**	**0.46**	**0.60**	0.15	0.06	**-0.58**	0.06	0.02	-0.34	1		
S	-0.01	0.16	0.35	0.23	0.11	0.22	0.17	0.23	0.33	-0.01	0.19	0.04	0.20	**0.42**	0.27	**-0.49**	0.23	0.13	-0.10	**0.65**	1	
P	-0.20	-0.19	**0.57**	**0.99**	0.20	**0.99**	-0.01	-0.13	**0.45**	-0.02	-0.01	-0.06	-0.05	**0.41**	**0.85**	0.14	0.36	0.11	-0.18	-0.07	0.18	1

$p < 0.01$; $p < 0.001$

6.5. Behaviour of trace elements in the estuarine waters

Estuarine waters are characterized by steep physicochemical gradients in e.g. salinity, density, pH and suspended particulate matter concentrations, which strongly influence the geochemical cycling of many elements. The most common approach of examining the behaviour of a chemical constituent in the estuarine mixing zone is to compare their distribution with a salinity, where salinity is an indicator of conservative mixing (Coffey et al. 1997; Tahir et al. 2008). However, reported data on trace metal behaviour in different estuarine systems show that for number of elements both conservative and non-conservative behaviour pattern can be found, indicating dependency of metal behaviour to the local conditions (Chester 1990, Strady et al. 2009; Joung and Shiller 2016). Moreover, the theoretical dilution line (TDL) (straight line between river and seawater end-members) can have negative or positive slope. In many estuarine systems around the world, dissolved constituent-salinity plots show a negative slope, meaning that river end-member is enriched in the trace element concerned relative to the seawater (Regnier and Wollast 1993; Machado et al. 2016). Namely, very often rivers receive emissions from different human activities along its course, becoming the main pathway of transport of the land-based pollution to the sea. On the contrary, in the Krka River estuary concentrations of most of the analysed elements are lower in the freshwater end-member than in the seawater (Figs. 6.6.-6.8.), corresponding to the very low input of trace metals, suspended particulate matter and organic carbon via Krka River (Cindrić et al. 2015).

Lithium, Mo, U, V and As demonstrated a linear relationship with salinity, indicating the conservative behaviour of these elements in the Krka River estuary, i.e. their distribution is attributable to the mixing processes between the river and seawater. The strong positive deviation from the TDL was observed only for As in the surface layer at the K20 sampling site, suggesting the additional As input, most probably of anthropogenic origin. These findings are in a good agreement with previously reported behaviour of Li, Mo, U, V and As in the Krka River estuary (Mikac et al. 2007). In addition, conservative pattern of these elements has been reported for many estuarine systems (Stoffyn-Egli 1982a; Elbaz-Poulichet et al. 1996; Windom et al. 2000; von Strandmann et al. 2008; Strady et al. 2009; Murphy et al. 2014; Fiket et al. 2018; Pavoni et al. 2020).

Barium concentration slightly increased in seaward direction from ~7 μg L^{-1} to ~8.5 μg L^{-1}, but positive deviation from the TDL was observed for surface and FSI layer samples from the Guduča River. According to Coffey et al. (1997), the behaviour of Ba in estuarine waters is governed by release from the fresh riverine particulate matter in the low to mid salinity ranges.

Considering that Guduča River is a main supplier of particulate matter to the estuary (Juračić and Pohić 1991), the observed release can be attributed to ion exchange between seawater major cations and Ba bound on the riverine suspended particulate matter (Moore and Shaw 2008). Moreover, estuarine sediments may act as an additional source of Ba, through desorption mechanism or by benthic dissolution of marine barite (Joung and Shiller 2014), as it will be discussed in Sections 6.6.1. and 6.7.1.

Generally, dissolved Fe exhibits non-conservative behaviour during estuarine mixing, where dominant mechanism for the river-borne Fe removal is salt-induced flocculation. In contrast to the usual observations, there is an increase in concentrations with salinity in the Krka River estuary, as well as marked positive departure from the TDL. Most prominent deviation from the TDL is observed in the Šibenik Bay (the port area), where maximum was found at the FSI layer, what is also seen in other parts of the estuary. This Fe behaviour pattern in the Krka River estuary was previously reported by Elbaz-Poulichet et al. (1991), where authors suggest colloidal concentration increase at the interface as possible explanation for observed enrichment.

Nickel and Al exhibited nearly conservative behaviour, with values rising from the freshwater end-member (0.1 μg L^{-1} and 0.4 μg L^{-1}) to the seawater end-member (0.4 μg L^{-1} and 1.7 μg L^{-1}). Aluminium exhibited positive deviation from the TDL in near-bottom (K20, K36) and surface (K36) samples from Šibenik Bay, indicating an additional Al supply. On contrary, the dissolved Ni showed highest positive deviation from the TDL in surface layer of the Guduča River. Even though there is no universal pattern of dissolved Ni behaviour in estuaries, generally either conservative behaviour or addition is observed, where main sources of additional dissolved Ni are desorption from the particulate matter and remobilization from the sediment (Martino 2000). Nickel concentrations in the SPM are high in the Krka River estuary, due to the Ni abundance in flysch and flysch-like source rocks (Juračić 1987). Therefore, additional dissolved Ni found in the surface layer of the Guduča River can be assigned to the desorption from the particles.

Notwithstanding the significant Mn enrichment of sediment from the Šibenik Bay and partly Prokljan Lake, it seems that dissolution of the Mn oxyhydroxides in the sediment and subsequent Mn diffusion across the SWI, does not have a significant influence on the content of Mn in the water column. In addition, highest increase in Mn concentration was found in the near-bottom sample from the head of the estuary, i.e. a sampling location with the lowest Mn content in the sediment. This observation can be explained by diffusive flux of Mn from the

sediment pore water to the overlying water and low levels of oxygen at the bottom which prevented the fast Mn oxidation. The high Mn flux and low oxygen levels were also reported in the Guduča River, but the increase in Mn concentration was not observed due to the sampling depth (1 m above the bottom).

The dissolved Cr and Co were the only two elements for which higher concentrations were observed in the freshwater end-member (~0.2 μg L^{-1} and ~0.02 μg L^{-1}) than in the seawater end-member (~0.1 μg L^{-1} and ~0.01 μg L^{-1}). Notwithstanding a conservative behaviour of dissolved Cr in most estuaries, both positive and negative departure from the TDL are observed in the Krka River estuary. The highest increase of Cr concentrations in relation to salinity was recorded in the Šibenik Bay, suggesting additional input from anthropogenic sources. The dissolved Co demonstrated a non-conservative behaviour, with removal observed in the Guduča River and at the head of the estuary and release in Prokljan Lake and Šibenik Bay.

The obtained results show that dissolved Zn clearly displayed a non-conservative behaviour, with the strongly positive departure from the TDL recorded at all sampling locations, but in the different layers of the water column. For example, at the head of the estuary Zn addition is detected in the seawater layer, while in the Guduča River it was detected in the surface layer. Considering the Zn enrichment found in the surface sediment of the port area and the highest dissolved Zn concentration detected in the near-bottom sample at the same site, it may be concluded that contaminated sediment is a source of additional Zn input. However, evidently this is not the only Zn supply route. Possible sources are nautical marina and ″diffusive″ inputs of communal waters from the Šibenik (although majority of wastewater is channelized to a collector) (Cindrić et al. 2015). The addition of Zn in the surface layer and removal in the seawater layer observed at the Guduča River presumably may be linked to the SPM and the changes in the pH, i.e. the sudden decline below the halocline. According to the literature, Zn exhibits strong accumulation within the SPM, with recorded values commonly much higher than in dissolved or sediment fraction (Juračić and Pravdić 1991; Beck et al. 2013; Marcovecchio et al. 2016). Moreover, there is a strong relationship between Zn adsorbed to SPM and pH, with a significant metal release with increasing pH and removal with decreasing pH, respectively (Marcovecchio et al. 2016).

The dissolved Cu concentration exhibited a non-conservative behaviour in the Krka River estuary, with the positive deviation from the TDL observed in surface (brackish) and FSI layer at all sites but the head of the estuary. The most prominent increase in Cu concentrations is

registered in the Šibenik Bay, at the site K36 which was sampled in July. Observed increase was about 4-fold in relation to the seawater end member. The similar Cu behaviour pattern was reported by Elbaz-Poulichet et al. (1991) and Cindrić et al. (2015). The latter linked increased Cu concentrations to the anthropogenic input, more precisely to the release from antifouling paints. During summer season, nautical traffic in the estuary increases substantially due to the intensive touristic activities. Therefore, high concentrations measured during the summer season in the Šibenik Bay support the postulation of nautical traffic of pleasure/recreational boats as the primary source of additional Cu in the estuarine waters.

Contrary to Cu, Pb presented strong positive departure from the TDL for bottommost samples from the Šibenik Bay. The additional Pb supply originates presumably from bay sediments which are significantly enriched in Pb, i.e. from the diffusive flux from the pore water to the overlying water.

Although there is no data on Cd concentrations from the head of the estuary, based on the data obtained at other locations, it can be seen that Cd has had a near-conservative behaviour, with the increasing trend in seaward direction. The highest Cd concentration was measured in the K36 bottom sample (i.e. in the port area), most probably resulting from desorption from the contaminated sediment. As already seen from the surface sediment distribution maps, pollution with Cd in the estuary is connected to the point-source. More precisely, to the Port of Šibenik, a port specialized for bulk cargo transhipment, mainly of Cd-rich phosphate ores and fertilizers.

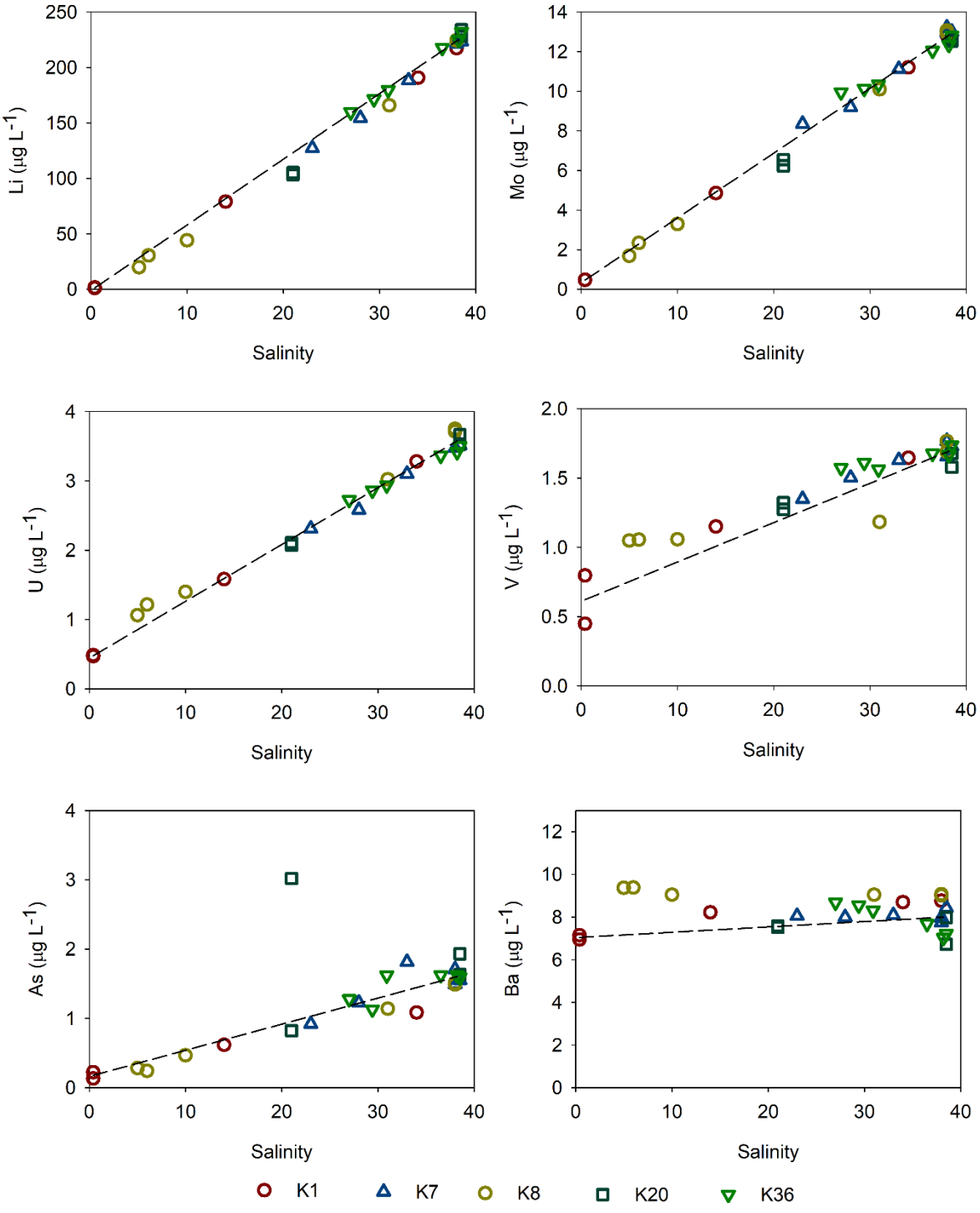

Figure 6.6. Dissolved element (Li, Mo, U, V, As, Ba) distribution along the salinity gradient. The dashed line represents theoretical dilution line.

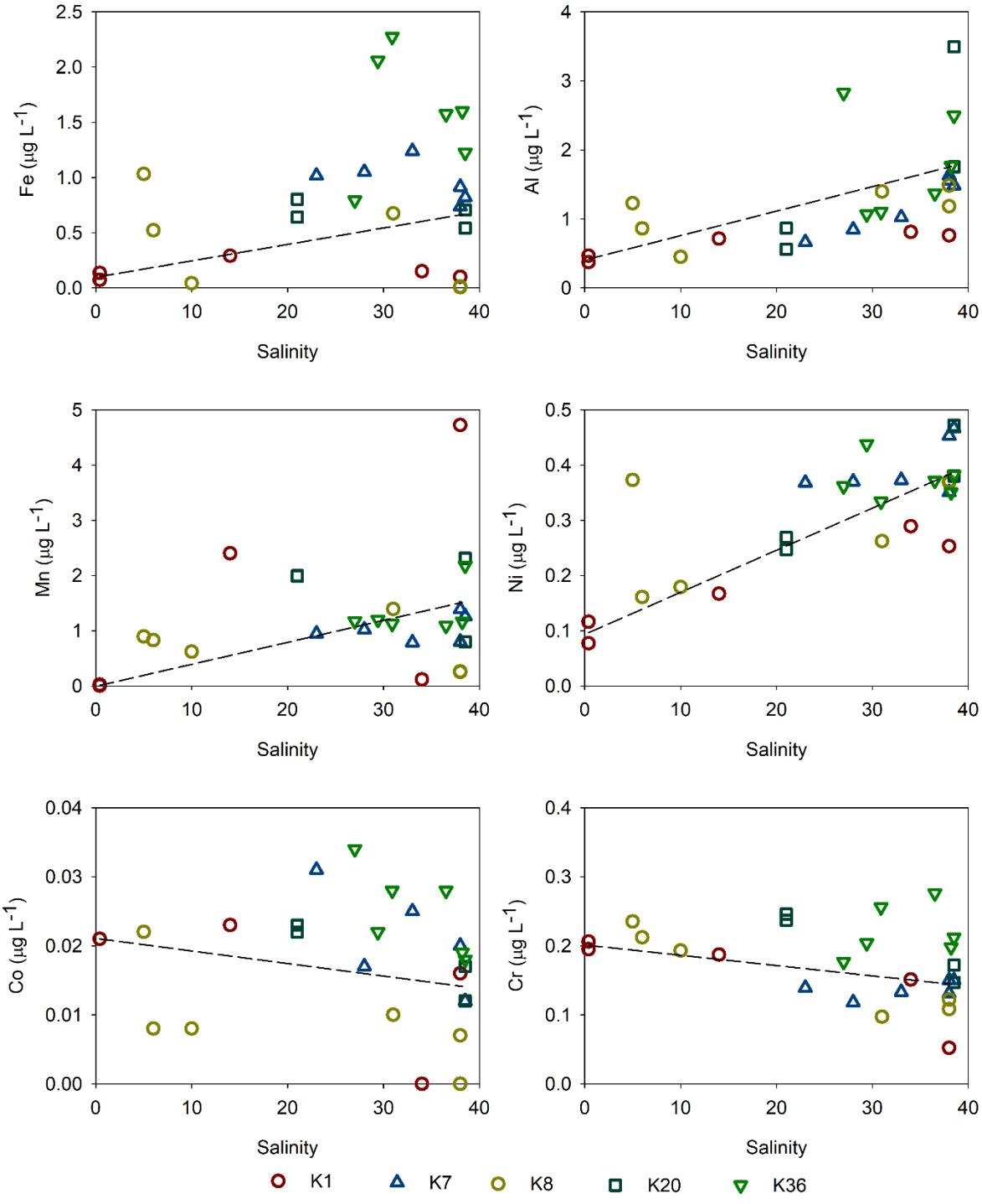

Figure 6.7. Dissolved element (Fe, Al, Mn, Ni, Co, Cr) distribution along the salinity gradient. The dashed line represents theoretical dilution line.

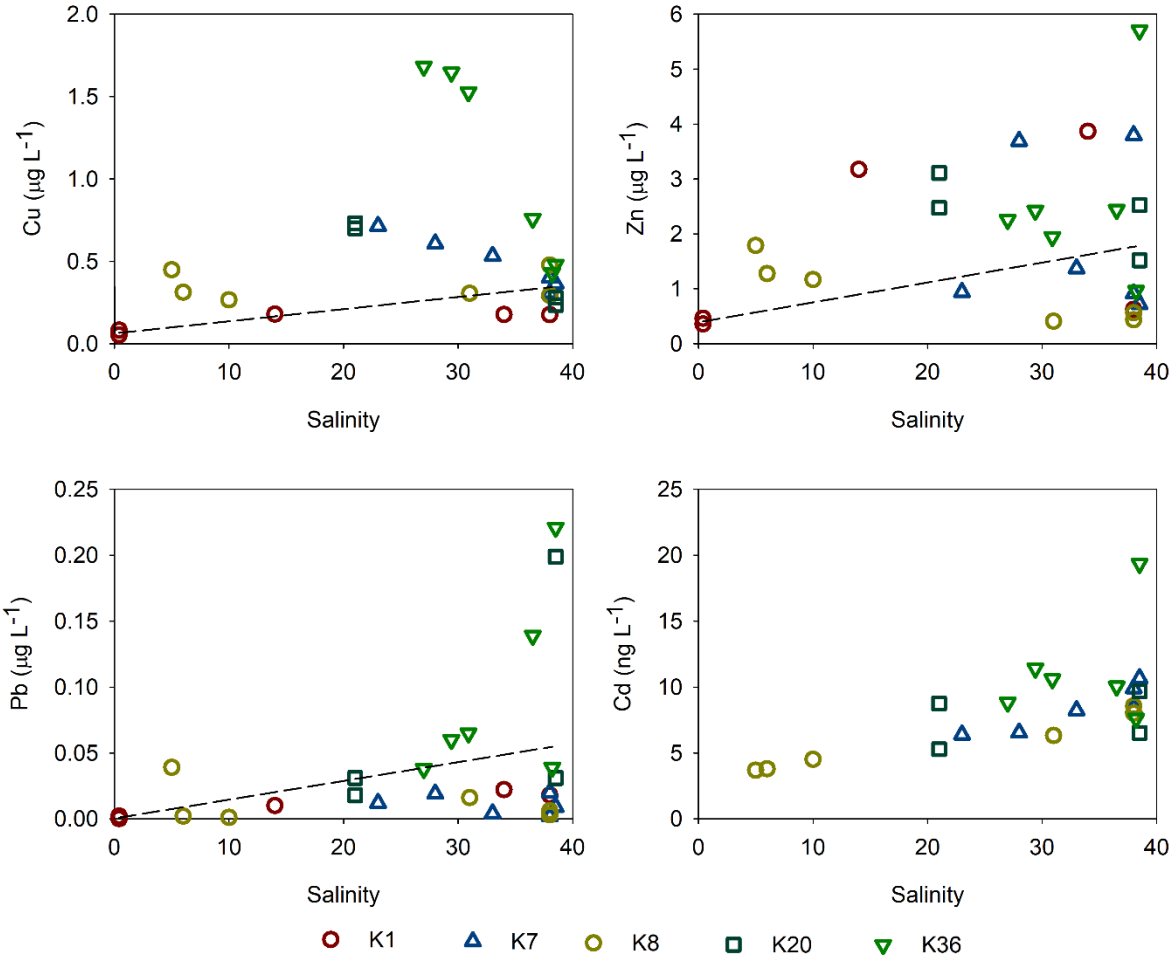

Figure 6.8. Dissolved element (Cu, Zn, Pb, Cd) distribution along the salinity gradient. The dashed line represents theoretical dilution line.

6.6. Vertical distribution of metals in the estuarine sediments

The principal component analysis was performed on the seven sediment cores sampled in the Krka River estuary: K1 – the head of the estuary, K7 – Prokljan Lake, K8 – the Guduča River, K20 – the former Electrode and Ferroalloy Factory, K22 – the Research Station Martinska, K32 – the nautical marina/shipyard and K36 – the port. The data set included major, minor and trace elements and grain size fractions (<2µm, <63µm, >63µm). The PCA showed that 87% of the variance was explained by the first four components (35.4%, 27.2%, 13.5% and 10.9% for PC1, PC2, PC3 and PC4, respectively) (Table 6.5.).

Table 6.5. Eigenvalues, percentage of variance and cumulative variance of the first four principal components (sediment cores data set)

PC	Eigenvalue	% of Variance	Cumulative %
1	12.4	35.4	35.4
2	9.53	27.2	62.6
3	4.73	13.5	76.1
4	3.80	10.9	87.0

The elements that are found in elevated content in the former factory area projected strongly at PC1, while those from the port area projected strongly at PC3 and those from the marina/shipyard area projected strongly at PC4. The lithogenic elements (Li, Al, Fe, Ti, Cs, Rb…) had large positive loading in PC2. The 3D score plot showed that samples from the upper estuary, the Research Station Martinska and deepest layer of the nautical marina/shipyard are spread across the PC2 (Fig. 6.9.), indicating that main factor governing the sediment composition is the share of the terrigenous elements. Sediment from the Guduča River had highest positive loadings in PC2, which agrees with its status of the main supplier of the terrigenous material to the estuary. The negative loadings in PC2 of the samples from the head of the estuary and the Research Station Martinska and bottom layers of the marina/shipyard core, coupled with their association with the coarser fraction, suggested there are mostly governed by carbonates. Furthermore, the 3D biplot clearly showed that samples from the former factory area, the port and most of the samples from the marina/shipyard area are not merely influenced by input of particulate material, but by input from the anthropogenic sources. The three locations are well separated based on the main contaminants, e.g., Cd and Zn in the port area, Hg and As in the marina/shipyard area and Mn in the area of the ex-factory.

The general classification of the upper estuary as uncontaminated and the lower estuary as an area impacted by anthropogenic pollution, is confirmed by the mean EFs calculated for each core (Table 6.6., Fig 6.10.). As seen in the Fig. 6.10., mean EFs of the cores K1, K7 and K8 mostly do not exceed the value 2 which indicates moderate enrichment, whereas cores from the Šibenik Bay exhibited even extremely high significant enrichment in Mn, Zn and Hg.

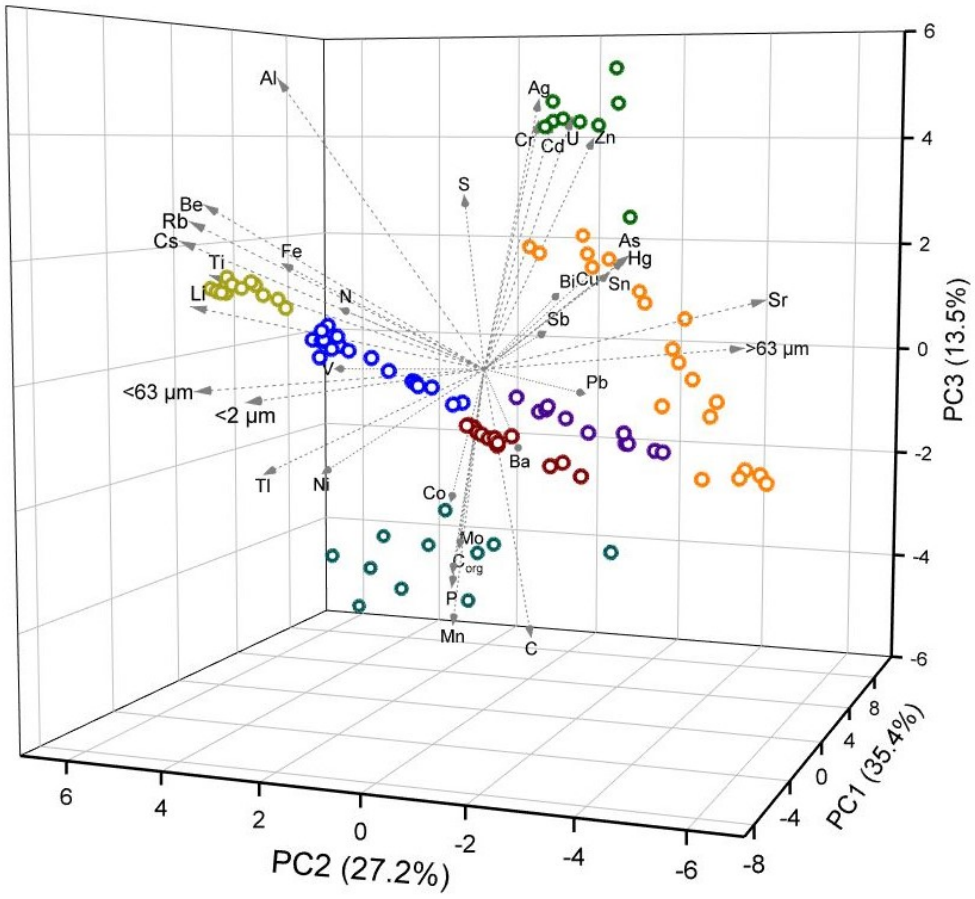

Figure 6.9. 3D biplot of principal component analysis (PCA) results obtained for total of 100 samples (open circles) from seven sediment cores: K1 (red), K7 (blue), K8 (ochre), K20 (dark green), K22 (purple), K32 (orange) and K36 (green).

However, vertical distribution of an element in the sediment core is not influenced only by input of the particulate material, grain size or human impact, but may be affected by the processes of the early diagenesis. To compensate for granulometric and mineralogical effects on metal contents and to help in elucidating the natural (terrigenous and diagenetic) and anthropogenic contribution of metals in sediment a geochemical normalization was performed. As in calculation of the EFs, Li has been chosen as normalizer over Al or Fe. The possible anthropogenic Al input (Prohić 1984) is confirmed by the PCA analysis and can be seen from its position between lithogenic and the "port contaminants" at the 3D biplot, i.e., Al had strong positive loadings both in PC2 (lithogenic elements) and PC3 (the "port contaminants"). The downcore distribution of Li-normalized ratios of metals (M/Li) in sediment cores from the Krka River estuary is given in Figs. 6.11.-6.17., and Pearson correlation matrix in Appendices 14.-20. The facilitate the interpretation of results, the background M/Li ratio was added to the graphs. As previously described, the element concentrations measured in the deepest layer (34-36 cm)

of the K1 core were used as the background values. The (right) deviation of M/Li ratios in the sediment cores from the background M/Li ratio indicates an enrichment, either because of natural or anthropogenic causes. The vertical distribution of metals and their possible sources will be discussed in more details in the following sections.

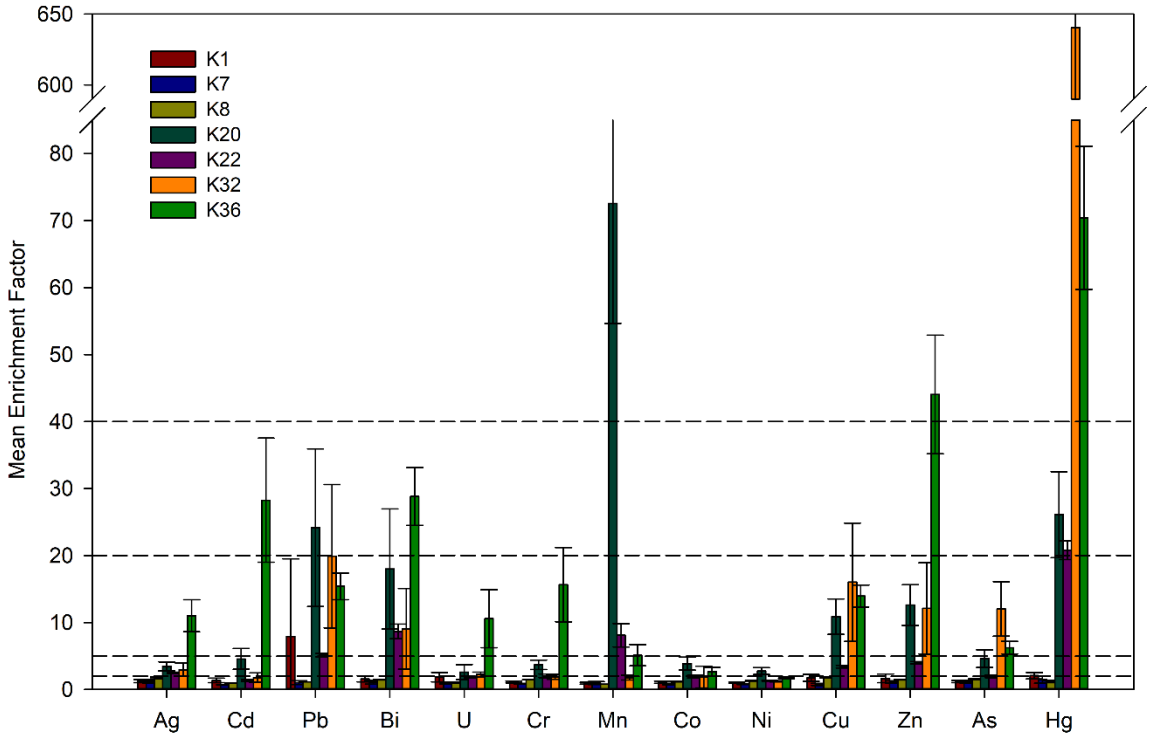

Figure 6.10. The mean enrichment factors of selected elements (Ag, Cd, Pb, Bi, U, Cr, Mn, Co, Ni, Cu, Zn, As, Hg) for the cores from the Krka River estuary (K1, K7, K8, K20, K22, K32, K36). Dashed horizontal lines represent boundaries between enrichment classes.

Table 6.6. The mean enrichment factors calculated for the sediment cores from the Krka River estuary

	K1	K7	K8	K20	K22	K32	K36
Be	1.01	0.96	1.42	1.36	0.94	1.03	1.76
Rb	0.95	0.91	1.47	0.67	0.95	0.93	0.87
Mo	2.47	0.63	1.05	7.30	1.11	1.63	3.03
Ag	1.27	1.22	1.72	3.46	2.50	2.97	11.0
Cd	1.38	0.70	0.97	4.58	1.33	1.79	28.3
Sn	1.34	0.94	1.20	7.96	5.42	11.2	10.1
Sb	1.64	0.90	1.14	11.9	2.26	15.2	6.14
Cs	0.98	0.98	1.34	0.82	0.99	0.97	0.93
Tl	1.04	0.90	1.36	2.25	0.90	1.08	1.17
Pb	7.92	1.04	1.15	24.2	5.15	19.9	15.4
Bi	1.59	1.09	1.46	18.0	8.68	9.08	28.8
U	1.86	0.90	1.06	2.62	1.82	2.25	10.6
Al	0.98	0.90	1.24	1.18	1.10	1.10	2.31
Ti	1.12	0.92	1.24	1.36	1.17	1.30	1.33
V	1.12	0.82	1.35	2.40	1.17	1.42	2.22
Cr	1.14	0.89	1.49	3.70	2.07	1.90	15.7
Mn	0.95	0.98	0.79	72.6	8.11	1.79	5.13
Fe	1.07	0.86	1.33	1.77	1.16	1.51	1.82
Co	1.09	0.83	1.21	3.87	1.94	1.88	2.68
Ni	1.05	0.81	1.31	2.76	1.31	1.23	1.77
Cu	1.74	0.78	1.81	10.9	3.41	16.0	14.0
Zn	1.67	1.12	1.48	12.6	4.01	12.1	44.0
Sr	1.43	1.15	0.74	2.39	6.26	8.53	6.20
Ba	1.23	0.88	1.27	10.6	2.83	4.63	6.74
As	1.20	1.09	1.57	4.61	1.97	12.0	6.26
Hg	2.07	1.48	1.19	26.1	20.8	641	70.4

6.6.1. The head of the estuary

The spatial distribution of metals and metalloids in the surface sediment of the Krka River estuary revealed the unpolluted character of the upper estuary. Likewise, the vertical distribution of the analysed elements at the head of the estuary mostly reflects the natural variability of the background values. According to the calculated EFs, Pb is the only element which shows significant enrichment in this area. Two strong peaks appear in the sediment column, at depths 8-10 cm and 20-22 cm, with concentrations much higher than background values observed in this area, as well in other parts of the Adriatic (Dolenec et al. 1998; Felja et al. 2016). Moreover, these values are in range or even higher than values reported in some contaminated sites, such as Rijeka and Toulon harbour (Table 6.1.). According to the

sedimentation rate of 2 mm $year^{-1}$ reported by Cukrov et al. (2007) for this part of the estuary, the observed peak at 8-10 cm may be attributed to the time period ~1970-1980. This finding is in accordance to the Pb concentration maxima found between 1960 and 1980 AD, commonly reported in the aquatic sediments from the northern hemisphere (Cossa et al. 2018). The proximity of the K1 location to the road and the sharp decline in Pb levels in layers above this maximum indicate the anthropogenic origin due to the Pb emissions by burning of the leaded gasoline. The deeper and the stronger peak can most probably be attributed to the beginning of the industrialization of the Skradin area in the late -19th century. Namely, at the head of the estuary a calcium carbide factory started to operate in 1897. However, production did not least long, because factory disappeared in flames in 1899 (Raos 2018).

Molybdenum and U demonstrated moderate enrichment and departure from the background M/Li ratio between depth 2 cm and 24 cm, and 4 cm to 16 cm, respectively. These elements are redox-sensitive elements, i.e. they are known to be soluble under oxidizing conditions, and to precipitate when euxinic conditions are encountered. While previously it was thought that under the sulfidic conditions Mo^{VI} reduces to the Mo^{IV} and precipitates as highly insoluble $Mo^{IV}S_2$ phase (Crusius et al. 1996; Helz et al. 1996), more recently different removal mechanism was proposed. Namely, in the oxidized water Mo is found in the form of the highly inactive molybdate ($Mo^{VI}O_4^{2-}$), while in the sulfidic environment oxygen atoms in molybdate can be replaced with sulphur atoms, creating a complex ($Mo^{VI}O_nS_4^{2-}$) that makes the Mo compound more likely to bound to particulate Fe or organic matter, and thus to be removed from the pore water (Erickson and Helz 2000). Uranium in the oxic water, found in the form U^{VI}, forms highly soluble complexes with carbonate species ($UO_2(CO_3^{-2})_3^{-4}$) which dominates the speciation in most natural waters. In anoxic pore water, U^{VI} is reduced to U^{IV}, followed by adsorption or precipitation, possibly as uraninite ($U^{IV}O_2$) at depth of the dissolution of the Fe oxyhydroxides or below (Crusius et al. 1996; Morford and Emerson 1999; Zheng et al. 2002). Considering that enhanced levels of Mo and U in the solid phase co-occurs with the presence of the sulphide in the pore water, it may be postulated that observed enrichment is result of authigenic formation of the solid phase. According to Zhang et al. (2000), the threshold value for authigenic Mo formation, presumably by co-precipitation of Mo-Fe-S phase is ~0.1 μM, meaning that sulphide levels at the head of the estuary were high enough for the Mo authigenesis.

Cadmium is also known to be sensitive to redox changes. Unlike, U and possibly Mo, it does not change oxidation state, but has the strong tendency to form highly insoluble CdS in the presence of trace levels of H_2S (Rosenthal et al. 1995). Therefore, the increase in solid phase

Cd concentrations at depth ~10 cm can be attributed to the natural process of Cd removal from suboxic pore water through precipitation of CdS. The analogue explanation can be given for Cu and Zn (Billon et al. 2001), which showed marked peaks of element/Li ratios at the same depth (~10 cm).

Furthermore, the deviations of the Fe/Li, Ni/Li, Co/Li and As/Li ratios from the background M/Li ratio at depth ~20 cm may be due to the formation of the metal sulphide minerals rather than to the anthropogenic input, considering that these elements did not show enrichment in the sediment core K1. Iron is usually the predominant sulphide-generating metal (Billon et al. 2001), and the rest may occur by coprecipitation and/or adsorption to FeS_x solid phases and/or formation of discrete metal sulphide phases (Huerta-Diaz et al. 1998; Billon et al. 2001; Duan et al. 2019). The correlation matrix showed a significant correlation between Fe and Ni, Ci and As ($r = 0.89\text{-}0.97$, $p < 0.001$) (Appendix 14.). The fact that dissolved sulphide was not detected in the pore water at this depth may be due to the rapid removal from the pore water by reaction with metal cations.

The Cr/Li ratio had a similar distribution pattern as those of Ni/Li and Co/Li. However, its behaviour in the aquatic sediments is somewhat different. In the environment, Cr is found manly in the two oxidations states - Cr(III) and Cr(VI). Under oxic conditions, dissolved species hydrogen chromate ($HCr^{VI}O_4^-$) and chromate ($Cr^{VI}O_4^{2-}$) prevail in the sediment, with their relative abundance depending on the pH. Under reducing conditions, mainly in the presence of Fe(II) and HS^-, Cr(VI) is reduced to Cr(III), which forms insoluble hydroxide and oxide compounds and make strong complexes with minerals and organic matter (Gorny et al. 2016; Byrne et al. 2017; Rosales et al. 2017).

The occurrence of the diagenetic barite is typically linked to the deeper parts of the sediment column where complete sulphate exhaustion results in dissolution of barite. The dissolved Ba^{2+} diffuses upward into the sulphate-bearing zone, leading to formation of an authigenic barium front just above the SMTZ (Gingele et al. 1999; Zindorf et al. 2019). However, it has been suggested that authigenic barite mobilization and precipitation can also occur in the uppermost sediment layers, in the suboxic environments where sulphate reduction takes place, but pore water is not completely depleted in SO_4^{2-} (McManus et al. 1998; Griffith and Paytan 2012). The precipitation of the diagenetic barite occurs beneath the SWI, where dissolved Ba^{2+} interreacts with the sulphate diffusing from the overlying water column (Magnall et al. 2016). Therefore, barium peak at depth ~10 cm presumably may be attributed to the early diagenetic processes.

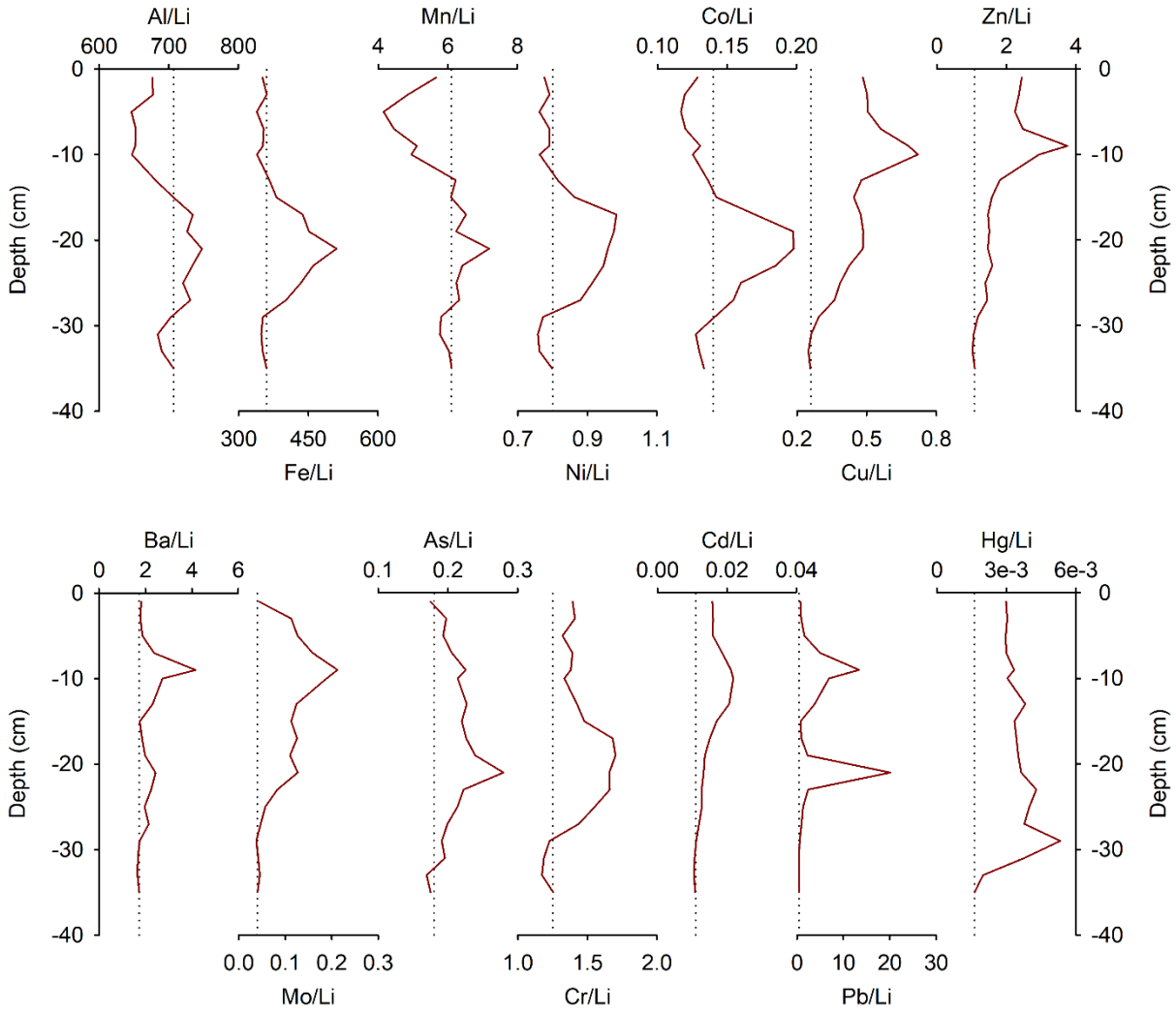

Figure 6.11. The downcore distribution of Li-normalized ratios of metals (Al, Fe, Mn, Ni, Co, Cu, Zn, Ba, Mo, As, Cr, Cd, Pb, Hg) in sediment core K1. Dashed vertical line represents background M/Li ratio.

6.6.2. Prokljan Lake

The vertical distribution of analysed elements in Prokljan Lake generally had an upward increasing trend. However, the element/Li ratios and comparison with the background element/Li ratio suggest that for most of the elements observed increase can be attributed to the natural variation due to the change in the input of the terrigenous material. The unpolluted character of Prokljan Lake has been confirmed by EFs, which suggested depletion to low enrichment of analysed metals and metalloids, except the Hg, which was moderately enriched

in two subsamples. Besides for the Hg, the M/Li ratios of Pb, Cu and Zn indicated that these elements are at least partly of anthropogenic origin. The same conclusion is given in the previous research of sediments in the Krka River estuary for Cu and Pb, but Zn is attributed to the natural variation of the source rock and Zn carriers, such as Fe and Mn oxides and organic matter (Prohić and Juračić 1989). However, not only the Zn content obtained in this research was ~2-fold higher than reported by Prohić and Juračić (1989), but the vertical distribution was different, unlike for Cu and Pb which showed similar distribution trend with the difference in the depth at which the concentration increase begun.

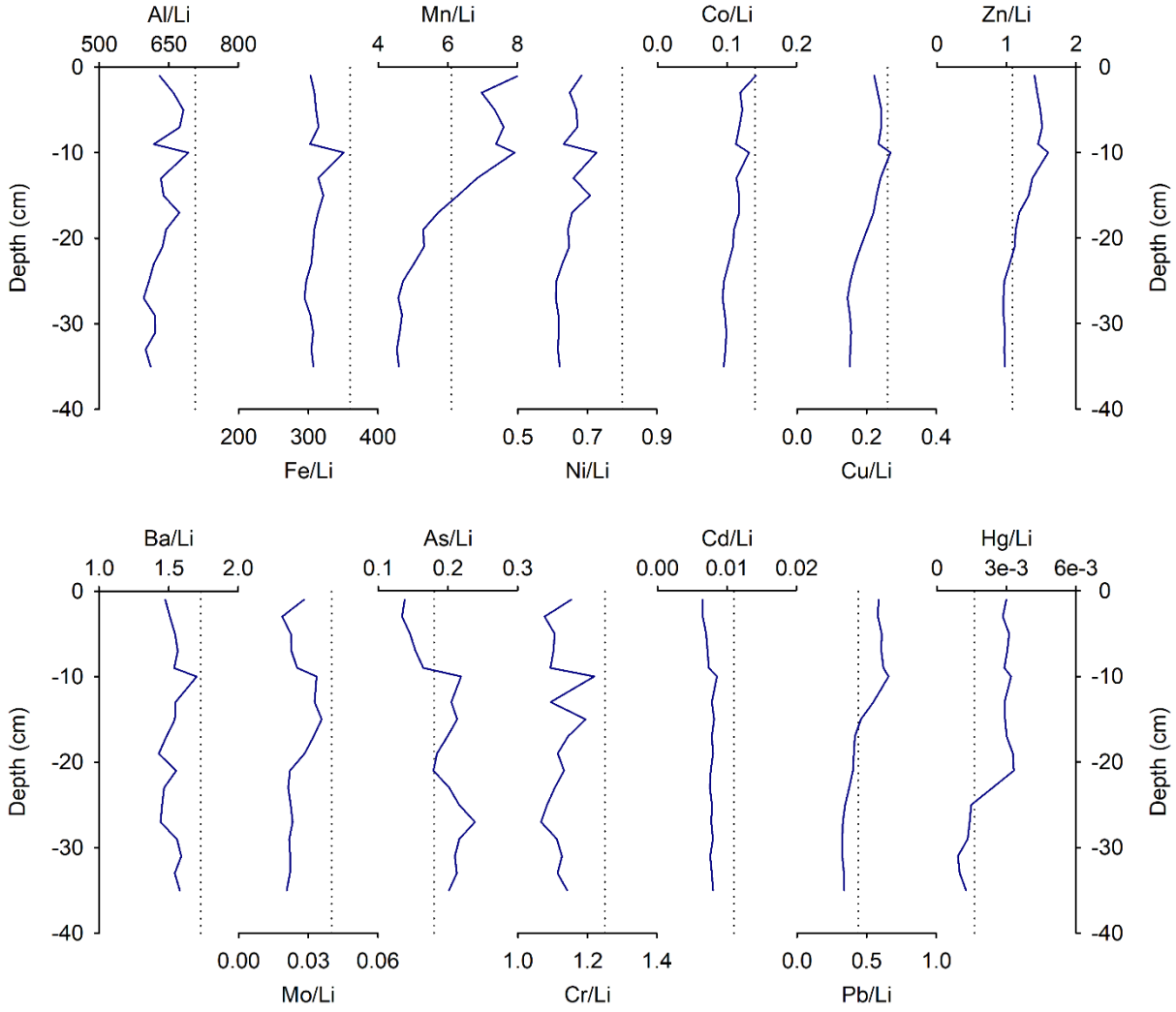

Figure 6.12. The downcore distribution of Li-normalized ratios of metals (Al, Fe, Mn, Ni, Co, Cu, Zn, Ba, Mo, As, Cr, Cd, Pb, Hg) in sediment core K7. Dashed vertical line represents background M/Li ratio.

The early diagenesis processes could increase Mn levels at the top of the core through oxidation of reduced Mn which diffused across the SWI and then precipitates as oxides (Guédron et al.

2020), yet in the case of Pokljan Lake, the increase in upper part of the core can as well be attributed to the anthropogenic input, as analysis of the surface sediment revealed the upstream spreading of the Mn from its source, the former TEF factory. Slight departure from the element/Li ratios at depth below 10 cm for some elements co-occurs with the detection of sulphide in the pore water and increase of solid S concentration, indicating a possible formation of sulphide minerals. Although sulphide concentration is lower than observed at the head of the estuary, it is still high enough for the formation of authigenic Mo (Zheng et al. 2000) and Cd (Rosenthal et al. 1995) solid phases, for instance.

The correlation matrix revealed the significant correlation between almost all analysed elements and C_{org} and absence of the correlation with the fine fraction, even the significant negative correlation with the fraction < 2 μm (Appendix 15.), implying that in Prokljan Lake organic matter is the main active adsorptive phase for metals and metalloids.

6.6.3. The Guduča River

The vertical distribution of granulometric, mineralogical and geochemical composition in the sediment from the Guduča River indicate uniform sedimentation in the last ~50-65 years. The approximate age was calculated using sedimentation rate of 4-5 mm $year^{-1}$ reported for the Guduča River mouth by Cukrov et al. (2007). The levels of lithogenic elements (e.g. Al and Fe) in the Guduča River sediments are higher than those recorded in Prokljan Lake and particularly at the head of the estuary. However, as previously explained, this distribution is outcome of the differences between particulate material carried by Krka River and Guduča River, respectively. The higher amount of the terrigenous material in the Guduča River can also be seen from the comparison between mineralogical composition of the sediments from the two sites, i.e. from the higher abundance of silicate minerals in the Guduča River.

Likewise, the concentrations of elements which are often considered as contaminants, such as Ni, Cr, Co, Pb, Cu and As, are higher in the Guduča River compared to the head of the estuary. However, low calculated enrichment factor (< 2) coupled with significant correlation with lithogenic elements (Appendix 16.) imply the natural origin of these metals. Lead and Cu nevertheless can be in some extent of anthropogenic origin, regarding the higher amount observed in sediment than in the source rocks (flysch and Eocene limestone) (Prohić and Juračić 1989). Cadmium, which is classified as highly toxic metal and frequently enriched in the sediments which are under anthropogenic pressure, was found in the range of the background

value, as at other locations in the upper estuary. Contrary to the other two locations in the upper estuary, Cd did not show slight enrichment in the area of the detected sulphide, suggesting that at the Guduča River there was no formation of the CdS. However, vertical distributions of Mo, Mo/Li, total S and ΣHS^- indicate formation of authigenic Mo solid phase at depth ~10 cm.

Slight and constant increase of Zn and Hg concentrations towards the top of the core, accompanied by the lack of the significant correlation with lithogenic elements (Appendix 16.) suggest possible anthropogenic input of these elements in the Guduča River. However, the recorded levels are still quite low and there is no enrichment with respect to these elements according to the calculated enrichment factor.

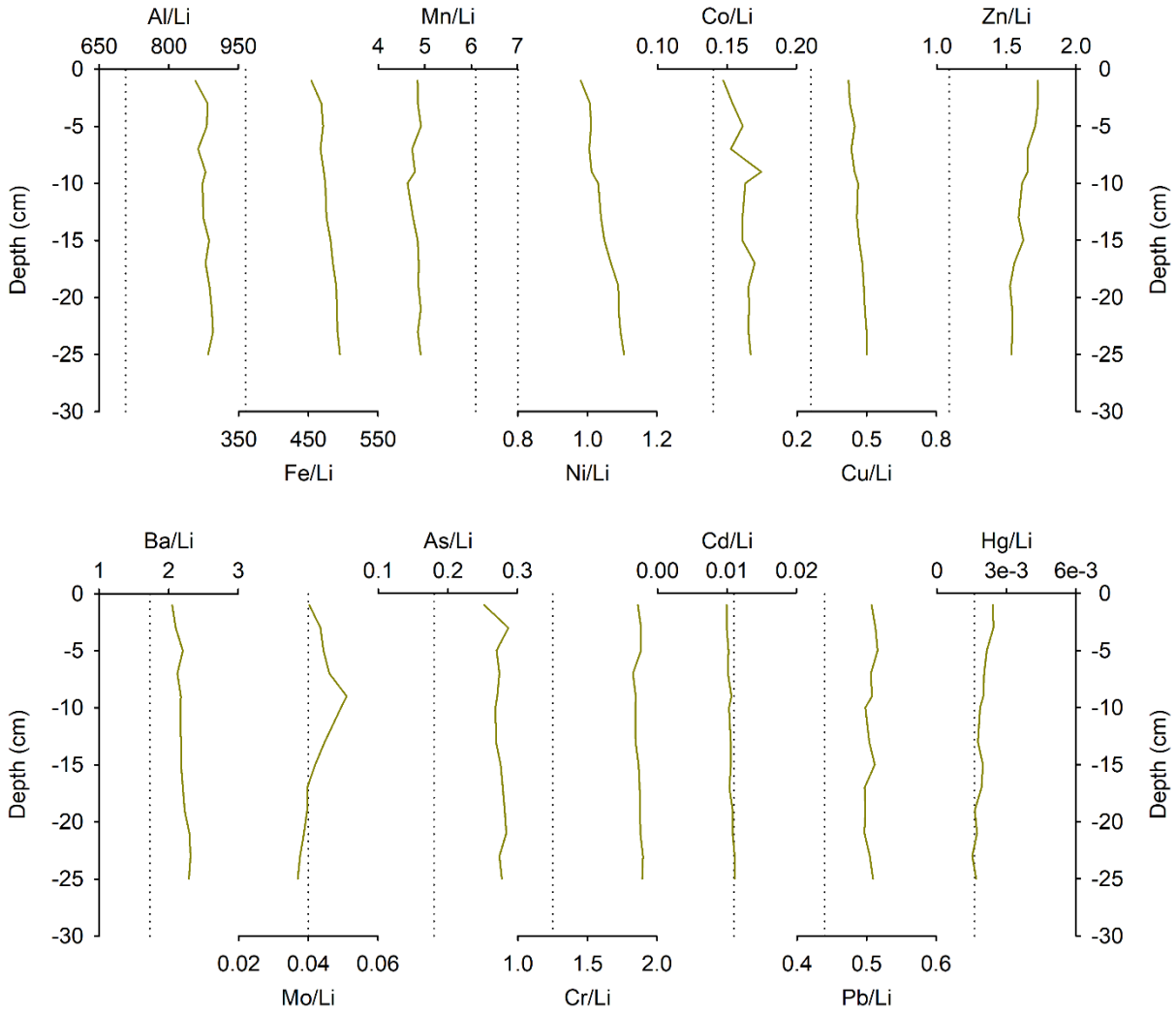

Figure 6.13. The downcore distribution of Li-normalized ratios of metals (Al, Fe, Mn, Ni, Co, Cu, Zn, Ba, Mo, As, Cr, Cd, Pb, Hg) in sediment core K8. Dashed vertical line represents background M/Li ratio.

6.6.4. The former Electrode and Ferroalloy Factory

The former Electrode and Ferroalloy Factory caused severe environmental degradation of its surroundings, which is evident from the contamination of the soil (Oreščanin et al. 2004, 2009) and sediment (Cukrov et al. 2008) by metals, and sediment contamination by organic pollutants (Mandić et al. 2018). As seen in previous Sections (6.1.-6.4.), there is evidence of negative impact on the estuarine surface sediments although the plant is out of production for more than 25 years. Evidently, elevated metal concentrations were observed along the core K20, which was sampled in the vicinity of the former TEF factory. As expected, sediment from the core K20 was highly enriched in Mn, with the mean EF (72.6) corresponding to the extremely high significant enrichment. Very high significant enrichment was observed for Pb and Hg, while significant enrichment was recorded for Bi, Cu, Zn, Mo, Sn, Sb and Ba. Moreover, Ag, Cd, U, Cr, Co, Ni, V, Sr and As showed a moderate enrichment (Fig. 6.10., Table 6.6.). The metallurgical slag as source of the enhanced levels of some metals was confirmed by determining its elemental composition (Table 6.7.). Primary, it was the source of Mn, but also Co, Mo, U, As. According to the slag analysis by Oreščanin et al. (2004), it could be as well the source of Pb, V, Cr, Cu, Zn.

Table 6.7. Elemental composition of the slag ([a]This study, [b]Oreščanin et al. 2004, [c]Ecoina 2002) and soil ([b]Oreščanin et al. 2004) from the former Electrode and Ferroalloy Factory area. Manganese, Al, Ba and Fe are expressed in %, and other elements in μg g^{-1}.

Element	Slag[a]	Slag[b]	Soil[b]	Slag[c]
Mn	12.4	1.0	13.0	16
Al	6.62	-	-	7.2
Ba	2.03	-	-	0.28
Fe	1.02	63.6	4.4	-
Sr	3 230	17.0	465	-
Pb	16.8	250	198	<50
U	15.2	-	-	-
Mo	7.39	-	-	<50
V	32.9	110	257	57
Cr	30.9	700	152	<50
Cu	63.2	410	172	64
Zn	70.3	1 480	612	<100
Co	45.6	-	-	57
As	22.9	-	-	<20

In any case, dust emitted directly from the factory to the air and slag deposited on the grounds of the factory where main long-term anthropogenic input of contaminants to the sediment, as well as to the other environmental compartments. However, the vertical distribution of analysed metals is not only governed by anthropogenic input, but partly with early diagenesis processes. Sulphide, the end-product of the sulphate reduction, was present in pore water at concentrations higher than 100 μM, may contribute to the formation of the metal solid phase through reduction of metal oxyanions (Sitte et al. 2010), such as those of uranium, or through precipitation of metal cations as sulphides (Billon et al. 2001; Sitte et al. 2010), such as those of Cd, Cu or Zn.

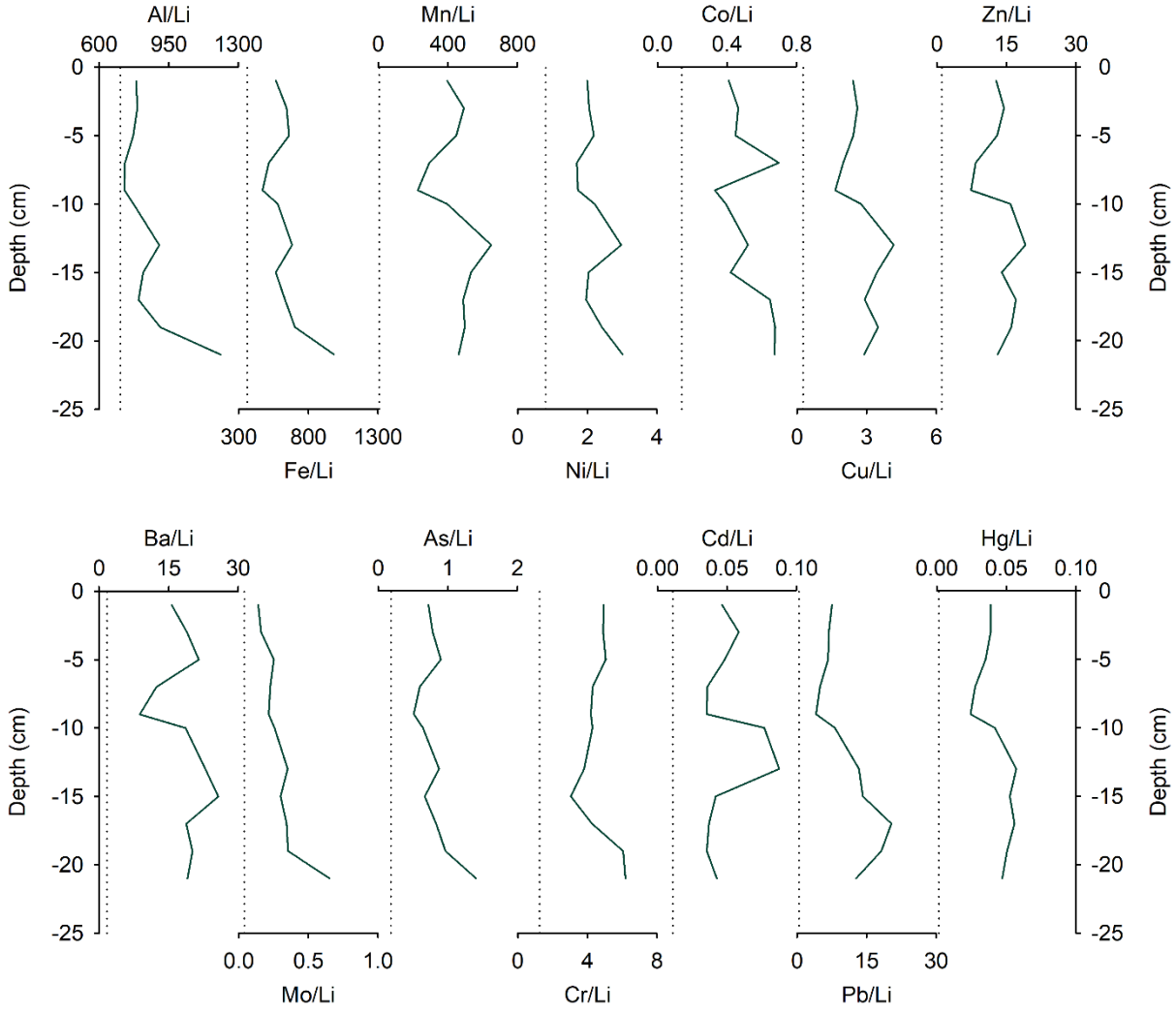

Figure 6.14. The downcore distribution of Li-normalized ratios of metals (Al, Fe, Mn, Ni, Co, Cu, Zn, Ba, Mo, As, Cr, Cd, Pb, Hg) in sediment core K20. Dashed vertical line represents background M/Li ratio.

It is difficult to make historical interpretation of the sediment core at this site due to uncertainty in estimated sedimentation rates for the Šibenik Bay. Previously reported values varied from

almost no existing recent sedimentation (Juračić 1987), across less than 1 mm $year^{-1}$ (Cukrov et al. 2007), to 5.2 mm $year^{-1}$ (Bogner 2001). However, the obtained sedimentation rates are questionable because of the significant mixing of sediment by bioturbation (Juračić 1987, Bogner 2001). In addition, owing to the large amounts of slag that can be found in sediment near the location of the former TEF factory, it is not possible to assume continuous sedimentation and discuss the historical input of contaminants. Nevertheless, a decrease in concentrations of most of the analysed metals is observed in the upper layers of the sediment core, indicating a possibility that removal of the source of the pollution has been recorded in the sediment.

6.6.5. The Research Station Martinska

The concentrations of analysed metals at the Martinska site are significantly lower than at the TEF factory site, notwithstanding that the two sites are less than 1 km apart. Evidently, the contaminants are dominantly transported in the upstream direction from its source (Šibenik city) and not towards the opposite estuarine bank, as already evidenced from the surface distribution of the analysed elements. The marked difference in metal distribution between two banks was not observed only in the sediment but is also established in the estuarine surface water layer (Cindrić 2015).

Despite the fact that obtained values are not as high as those obtained from the sediment sampled in the vicinity of the former factory, for some elements there are much higher than those measured in the upper estuary. The mean Hg, Mn and Pb contents, in particular, were ~10-times, 5-times and 3-times higher than those measured in the upper estuary (K1 core excluded in the case of Pb). The anthropogenic contribution of these elements in the sediment at location Research Station Martinska is evident from the mean calculated EFs (Fig. 6.10., Table 6.6.). Namely, Hg demonstrates very high significant enrichment, whereas Mn and Pb demonstrate significant enrichment. Sediment is moreover moderately enriched by Ag, Cu, Zn, Cr and Ba. Most of the analysed elements had a similar vertical distribution pattern (Li, Al, Fe, Ni, Cu, Zn, Mo, V, Pb), which was characterized by downcore gradual increase up to the maximum value in the layer 8-9 cm, and subsequent decrease in the last two subsamples. This pattern was in agreement with the distribution trend of the fine fraction (< 63 μm), and was opposite to the distribution trend of the mean grain size, which suggest the impact of the grain size distribution on the metal concentrations along sediment core. The influence is confirmed

by correlation matrix. Namely, both lithogenic elements and some of the eco-toxic elements were significantly correlated ($r = 0.88\text{-}0.92$, $p < 0.001$) with the granulometric fraction < 63 μm (Appendix 18.). The lack of correlation between C_{org} and metals, implies that metal variations were mainly related to the grain size distribution, and are not connected to the organic matter.

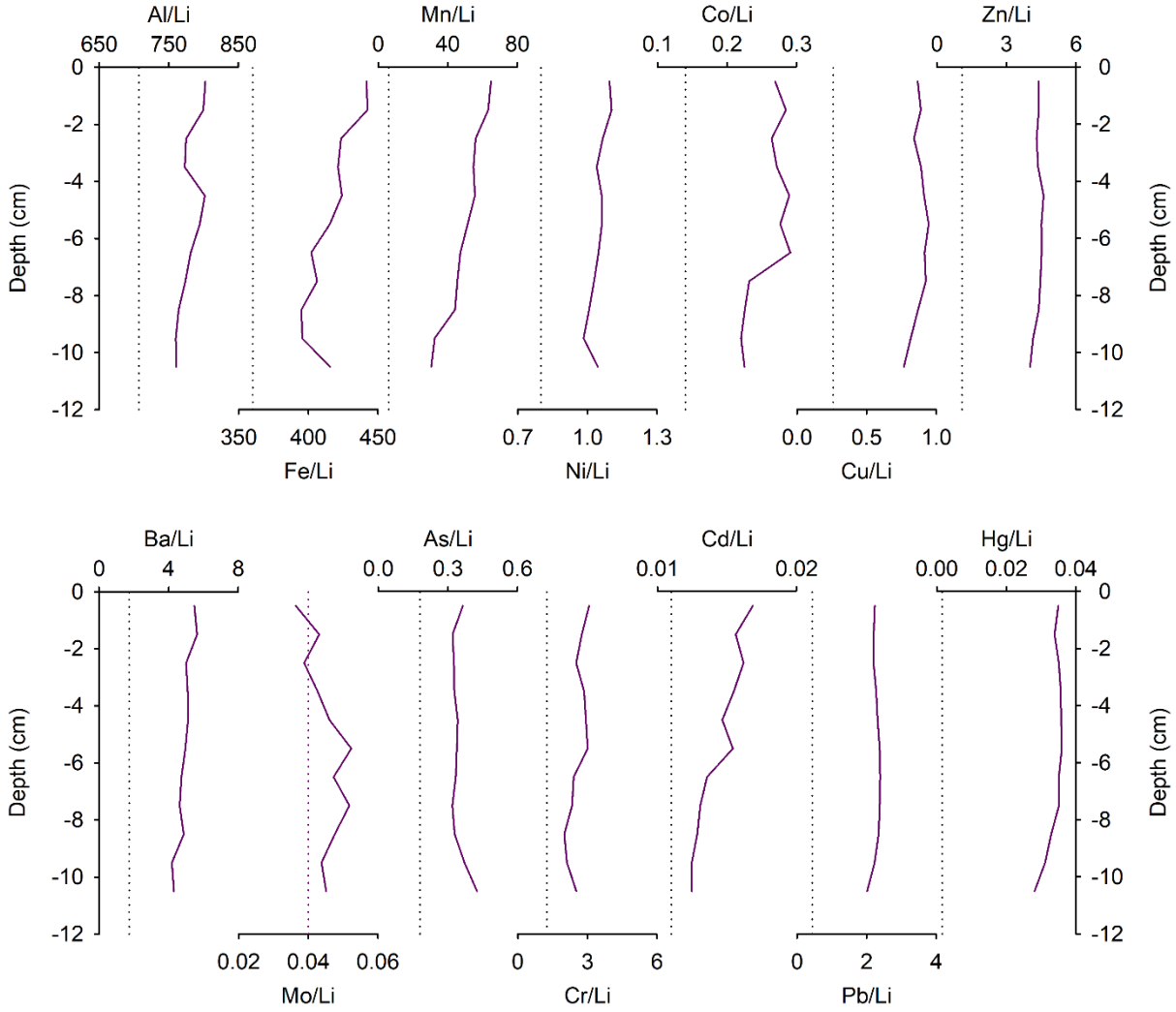

Figure 6.15. The downcore distribution of Li-normalized ratios of metals (Al, Fe, Mn, Ni, Co, Cu, Zn, Ba, Mo, As, Cr, Cd, Pb, Hg) in sediment core K22. Dashed vertical line represents background M/Li ratio.

6.6.6. The nautical marina/shipyard area

In the southeast part of the Šibenik Bay, known as St Peter's Cove, surface sediment is heavily enriched in number of trace metals, as discussed in Subchapters 6.1.-6.4. The results of the

analysed elements in the K32 sediment core confirm contamination of this area and illustrate historical trend of metal accumulation.

By far the most significant metal contaminant in the nautical marina/shipyard area is Hg, with concentrations reaching almost 60 μg g^{-1}, corresponding to the extremely high significant enrichment (EF = 641). According to the ^{210}Pb and ^{137}Cs sediment age estimation (Fig. 5.31.), a significant increase in Hg values occurred around 1950, coinciding with the beginning of the operation of the naval repair shipyard. The connection between shipyard activities and elevated sediment Hg concentrations has been reported previously (Fairely et al. 1998; Cardellicchio et al. 2006; Canário et al. 2007). During shipbuilding and repairing processes, a huge volume of wastes and contaminants are released (Celebi and Vardar 2008; Rahman and Karim 2015), often leading to severe seabed contamination and negative impact on marine sediments in local waters. Among the contaminants commonly found near shipyards are toxic metals, tributyltin (TBT), PAH and other chlorinated organic components (Chiu et al. 2006; OECD 2010). A continuous increase in Hg concentrations at this site can be observed until the mid-70s, followed by invariable values for the next 25 years. Subsequently, the decrease in Hg concentrations occurred, most probably due to the decline of the shipyard business during the late 90s and early 2000s. The reasons for the increase of Hg content in the uppermost 2 cm of core section remain unclear. However, some authors (Rasmussen 1994; Canário et al. 2005; Chatterjee et al. 2009) suggest that increased concentrations in the surface layer can result from post depositional diagenetic processes that remobilize Hg from the deeper sediments, causing upward migration in the sediment column.

The extremely high Hg concentrations were limited to the narrow area surrounding the repair shipyard, nonetheless, the observed values were in range with some of the most contaminated sites regarding Hg in the Adriatic, such as Kaštela Bay where sediments were contaminated due to the uncontrolled effluent of a PVC chlor-alkali plant and the Gulf of Trieste where high Hg concentrations in the sediment were a consequence of long-term mining activity (Idrija mine, Slovenia) (Table 6.1.).

The area is heavily contaminated by arsenic, as well. The mean As concentrations in the sediment core K32 is 10-times higher than the mean of the K1 sediment core, and up to 3-times higher compared to the other anthropogenically impacted sites in the Šibenik Bay. The impact of the human activities moreover is evident from the calculated EFs, which indicated significant enrichment of the cove by As. The vertical distribution trend is very similar to that of Hg, suggesting that the start of the shipbuilding activities affected not only Hg content in the

sediment, but also the content of other metals, among which As. The perfect positive relationship between these two elements ($r = 1.00$, $p < 0.001$) confirms the common historical input. The possible sources are fossil fuels combustion and the antifouling paints, as both elements were used as biocides in paints in the past (Llewellyn 1972; Almeida et al. 2007; Sarı et al. 2013).

Sediment from the nautical marina/shipyard area is moreover significantly enriched by Zn, Cu and Pb. The mean measured values are up to 8-fold, 10-fold and 11-fold higher than those recorded in the sediment cores form the upper estuary. The contamination of coastal sediments by these metals is often observed in areas which are under the negative impact of the shipyards and harbours (Eklund et al. 2010; Cukrov et al. 2011; Alyazichi et al. 2015; Valero et al. 2019). Copper and Zn contamination results from the use of Cu and Zn-based antifouling paints which are applied to the hulls of boats and to other submerged structures to prevent the growth of fouling organisms (Singh and Turner 2009; Turner 2010; Lagerström et al. 2016). The leaching of metals from the paints, in particular in harbours and marinas, lead to the elevated concentrations in the water and to the accumulation of metals in the sediment. Furthermore, large quantities of the antifouling paint particles are produced in boatyards and shipyards during the boat maintenance and cleaning activities, such as scraping and various types of blasting. The generated particles readily enter the nearby coastal environment with wastewater washdown or as airborne dust and are subsequently transported to the sediment where they may pose a hazard to the deposit feeders (Turner 2010; Lagerström et al. 2016). Although Pb may also be found in the composition of the antifouling paints (Paradas and Filho 2007; Costa et al. 2016), its primary source is the combustion of the diesel fuels by ships (Yang et al. 2014; Andrade et al. 2017; Valero et al. 2020). The vertical distribution of the Cu/Li, Zn/Li and Pb/Li ratios showed background values in the bottom 8 cm of the sediment core, followed by sharp increase towards the top of the core with the beginning of the shipyard activities, as observed in the case of Hg and As. Unlike the latter two, maximum content of Cu, Zn and Pb was not at the depth 8-9 cm, but closer to the sediment surface, as a result of the current use of the Cu-based antifouling paints.

The significant enrichment in Ba in the top 9 cm of the core is most likely connected to the diesel fuel (Sutherland 2000; Cukrov et al. 2011). Although the rest of the elements follow the similar vertical distribution pattern, with slight to more prominent increment in respect to the background values in the upper part of the core, the calculated EFs indicate low enrichment either moderate enrichment at certain depths.

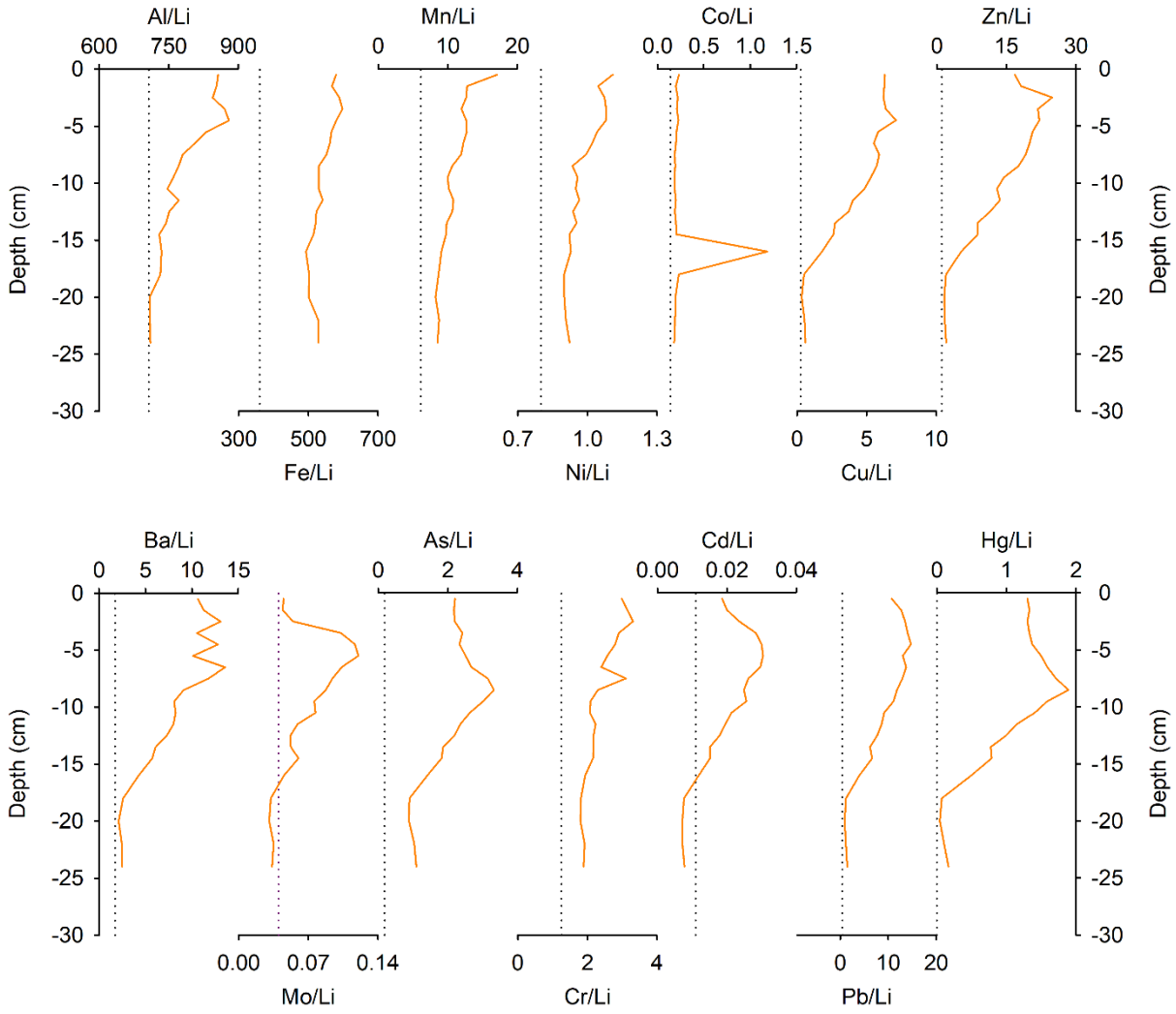

Figure 6.16. The downcore distribution of Li-normalized ratios of metals (Al, Fe, Mn, Ni, Co, Cu, Zn, Ba, Mo, As, Cr, Cd, Pb, Hg) in sediment core K32. Dashed vertical line represents background M/Li ratio.

The upcore increasing trend observed for terrigenous elements (Al, Li, Fe), supported by the results of the radionuclide analysis (data not shown) and mineralogical composition, indicate the increased input of terrigenous material in the upper part of core. As there is no know possible natural source of terrigenous material in the area, it may originate from the land reclamation of the Mandalina peninsula. Although both terrigenous elements and those that have been identified as contaminants have upcore increasing trend, the M/Li ratios indicate that terrigenous material is not the source of the elevated metal content in the sediment. The departure of Al/Li ratio from the background ratio in the upper part of the core suggest its additional anthropogenic source, as already seen from the PCA analysis of the complete sediment cores data set.

Unlike sediment core K22, there is no significant correlation between fine fraction and metals in the sediment core K32, except the one of the Cr and fraction < 63 μm ($r = 0.60$, $p < 0.01$) (Appendix 19.). Instead, lithogenic and eco-toxic elements demonstrated significant correlation between each other, and with C_{org}, implying that in the marina/shipyard area metals are dominantly connected to the organic matter.

6.6.7. The Port of Šibenik

In addition to the ex-factory and the nautical marina/shipyard, the Port of Šibenik is a significant source of contamination for the estuarine environment, as already demonstrated by the surface sediment distribution maps and as reported in previous research (Mikac et al. 2007; Cukrov et al. 2008).

According to the sedimentation rate of 4-5 mm $year^{-1}$ in the port area reported by Cukrov (2006), the sediment core K36 represents approximately the last 40 years. With that stated and taken in account the long history of port activities at this location, the elevated concentrations of different metals along the entire core are not unexpected. The mean concentrations of the K36 core were manifold higher than those obtained at sampling locations in the upper estuary, specifically, Hg was ~29-times higher, Zn up to 23-times higher, Cd ~20-times higher, Cr up to 11-times higher, Pb and Cu up to 7-times higher, U and Ba up to 5-times higher and As up to 4-times higher, respectively. The proportion of the anthropogenic impact on the sediment can clearly be seen from the calculated mean EFs. Mercury and Zn, which showed extremely high enrichment, are heaviest pollutants in the port area, followed by Cd, which exhibited very high significant enrichment. Sediment core K36 is moreover significantly enriched by Ag, Pb, U, Cr, Mn, Cu, As and Ba. Most certainly, a part of the observed contamination can be attributed to the raw phosphates and artificial fertilizers, the main type of cargo handled in the Port of Šibenik. Namely, the phosphate rocks used to manufacture phosphate fertilizers contain various amounts of accompanying elements, such as Cd and U, which are transferred to fertilizers and can even become more concentrated during production processes. In addition to U and Cd, fertilizers may contain Zn, As, Cr, Cu, Pb, Hg, Ni and V. Concentrations of these elements may vary considerably, both in the raw phosphate and in fertilizers, depending on the source rock (Table 6.8.).

Table 6.8. Mean metal concentrations in phosphate rock deposit ([a]Kongshaug et al. 1992) and range and mean concentrations in European phosphate fertilizers (414 samples comprised of NPK's, phosphate rock and processed phosphates sampled from 26 countries, including Croatia) ([b]Verbeeck et al. 2020).

	Metal concentration (μg g^{-1})									
Phosphate rock[a]	U	Cd	Zn	As	Cr	Pb	Hg	Ni	V	Cu
Russia		0.1		1	13	3	0.01	2	100	
Morocco		30		11	225	7	0.04	26	87	
North Africa		60		16	105	6	0.05	33	300	
Middle East		9		6	129	4	0.05	29	122	
Fertilizers[b]										
Europe (n=414)										
Min	0.04	0.07	4.2	0.18	0.31	0.09		0.63	0.09	1.78
Max	242	51	12 800	110	429	179		151	365	866
Mean	41	6.26	251	5.5	70	4.2		16	62	33

The soil contamination mainly by Cd and U as a consequence of phosphate fertilizers use is reported around the world (Giuffré de López Camelo et al. 1997; Schipper et al. 2011; Schnug and Haneklaus 2014; AlKhader 2015). The contamination of the port sediment by the raw phosphates and fertilizers is supported by detected apatite minerals in all analysed layers in the core K36, evidencing the input of dry bulk cargo into the estuarine environment during transhipment. Moreover, significant correlation between P and Cd ($r = 0.88$, $p < 0.01$), Cd and U ($r = 0.81$, $p < 0.01$) and P and U ($r = 0.79$, $p < 0.05$) (Appendix 20.) indicate that the three come from the common source. Based on correlation matrix, the raw phosphates and fertilizers are the main source of only Cd and U, whereas other elements most probably originate from several sources, e.g. from the untreated wastewater of the Šibenik city which was in the past discharged into the estuary at this location.

Furthermore, none of the analysed elements showed significant correlation with the fine fraction, while significant correlation with C_{org} was observed only for Hg ($r = 0.85$, $p < 0.01$) and Pb ($r = 0.69$, $p < 0.05$) (Appendix 20.). The weaker correlation of Al to Li ($r = 0.71$, $p < 0.05$) and Rb ($r = 0.73$, $p < 0.05$) (Appendix 20.) suggest the possibility that at least part of the Al content in sediment is not of natural, but anthropogenic origin.

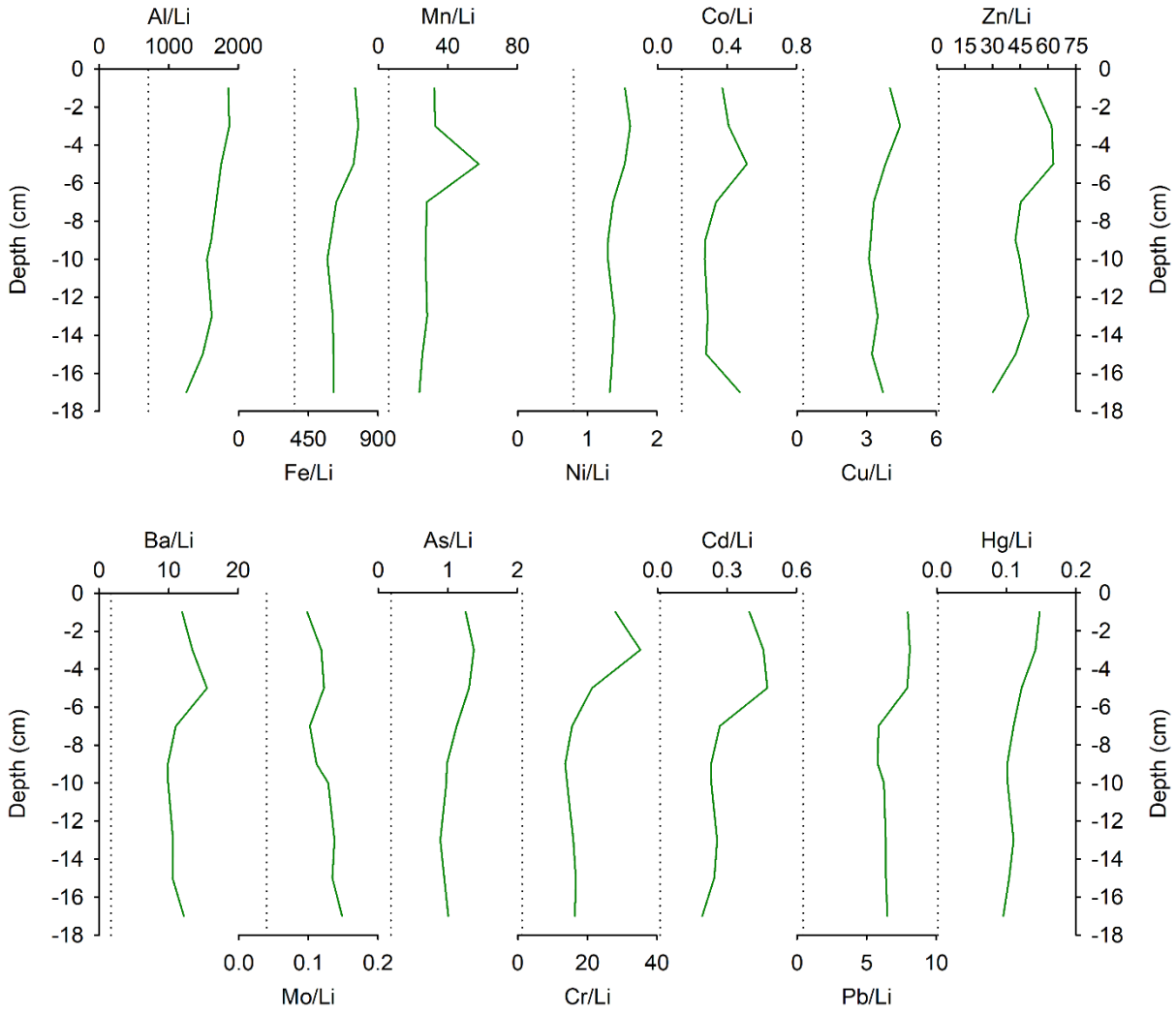

Figure 6.17. The downcore distribution of Li-normalized ratios of metals (Al, Fe, Mn, Ni, Co, Cu, Zn, Ba, Mo, As, Cr, Cd, Pb, Hg) in sediment core K36. Dashed vertical line represents background M/Li ratio.

The enrichment of some elements in the upper part of the core can rather be attributed to the early diagenetic reactions in the sediment than to the increased anthropogenic input in more recent times. For example, the marked Mn/Li peak observed at depth 4-6 cm (Fig. 6.17.) is presumably result of the downward diffusion of dissolved Mn^{2+} and subsequent formation of the solid phase. Namely, under reducing conditions where manganese concentrations reach sufficiently high levels, some of the divalent manganese may precipitate out of pore water as a pure or mixed carbonate phases and phosphate phases, or in lesser extent as sulphide phases (Burdige 1993; Ingri et al. 2011; Gorny et al. 2016; Dellwig et al. 2018).

6.7. Metal dynamics in the pore water and at the sediment-water interface

Pore water is known to be a sensitive indicator for describing the type and extension of diagenetic processes, which control the metal partitioning between solid and dissolved phase (van den Berg et al. 2000; Gavriil and Angelidis, 2006). A major driver of metal partitioning and recycling in the estuarine and coastal sediments is microbially driven oxidation of OM and associated reductive dissolution of Fe and Mn oxyhydroxides (Tankere-Muller et al. 2007; Santos-Echeandia et al. 2009; Prajith et al. 2016; Jokinen et al. 2020), which typically occurs within a few centimetres from the SWI. In these environments, sediments are characterized by compression of the redox zones which results in very thin oxic layer (< 1 cm), which often remains undetected due to the pore water sampling resolution. This type of behaviour was observed also in the Krka River estuary, where dissolved Fe and Mn profiles displayed a very sharp increase below the SWI at all sampling sites, but the mobilization intensity varied between sites. In Prokljan Lake and in the Šibenik Bay, Mn was released to the pore water shallower (0-2 cm) than Fe (2-4 cm), following the ideal redox sequence in the coastal sediments (Jørgensen and Kasten 2006), whereas at the head of the estuary and in the Guduča River the maximums occurred at the same layer (0-2 cm). The suboxic layer of the sediment, marked by high concentrations of dissolved Fe and Mn, is often characterized by increased levels of other metals, released to the pore water by reductive dissolution of their carrier phases (Fe and Mn oxyhydroxides, biogenic material). For instance, high increase of dissolved Co below SWI in Prokljan Lake and Šibenik Bay concurs with Mn peaks, and most probably can be related to the mobilization of the Mn, as adsorption of Co by MnO_2 is well documented in the literature (Murray and Dillard 1979). The early diagenetic processes may moreover liberate dissolved As, which was adsorbed onto or coprecipitated with Fe oxyhydroxides (Dang et al. 2015; Gorny et al. 2016), as observed at all sites except the head of the estuary. More details on metal distribution in pore water for each sampling station are given below. The Pearson correlation matrix for pore water parameters measured in cores K1, K7, K8, K20 and K36 are given in Appendices 22.–26.

Along dissolved Fe and Mn, the other diagenetic tracers (NH_4^+, PO_4^{3-}, ΣHS^-, DIC) displayed fairly similar patterns, consistent with the classical diagenetic zonation. The OM mineralization is reflected in the pore water profiles as progressive gradual increase in NH_4^+ and PO_4^{3-}, observed at all sampling sites, and release of DIC into pore water at the Guduča River and in the Šibenik Bay. Moreover, the occurrence of dissolved sulphide in the pore water consistently coincide with drawdown of the Fe^{2+}. Namely, the dissolved Fe diffused from suboxic zone

downward reacts with sulphide produced by sulphate reduction bacteria in anoxic layer of the sediment, and forms insoluble phases.

The mineralization products of early diagenesis processes may accumulate in the pore water. If accumulation is at or near the SWI and pore water concentrations are in excess of those in the overlying water, it will result in diffusive fluxes from the sediment to the bottom water across the SWI. The benthic diffusive fluxes of metals from sediment to the water column may be equivalent or even higher than riverine influxes in many coastal area (Santos-Echeandia et al. 2009; Duan et al. 2019). To calculate diffusive fluxes of metals across the SWI Fick's first law of diffusion was used:

$$Flux = -\Phi D_{sed} \frac{\partial C}{\partial x}$$

where Φ is porosity, D_{sed} is diffusion coefficient in the pore water volume of sediment and ($\partial C/\partial x$) is the concentration gradient at the SWI. The porosity was calculated based on water content and bulk density (Storms et al. 1991) and was > 0.7 at the top of the core at all sampling locations. Therefore, following empirical equitation was used to calculate the D_{sed} (Ullman and Sandstrom 1987):

$$D_{sed} = \Phi^2 D \ (\Phi > 0.7)$$

where D is the diffusion coefficient in water adjusted to in situ temperature using the Stokes–Einstein equation. The values for D for each element were taken from Li and Gregory (1974). The D value for V was assumed to be equal to the one of Mo (MoO_4^{2-}) (Scholz et al. 2011). The concentration gradient was estimated from the concentration difference between the uppermost pore water sample and the bottom water divided by the depth of the uppermost pore water sample (2 cm). The positive fluxes are directed into the sediment, while negative fluxes indicate release of the metal from the sediment to the overlying water column. In general, a negative flux was observed for most of the considered elements in the Krka River estuary (Table 6.9.), suggesting that sediment is acting as a source of metals for the overlying water column. The fluxes of Mn and Fe across the SWI were much higher than the ones estimated for other metals, but consistent with literature reported magnitudes (Sondi et al. 2017; Petranich et al. 2018; Duan et al. 2019). The impact of benthic diffusive flux on dissolved Mn and Fe concentrations is clearly evident in the upper part of the estuary, where recorded concentration in supernatant water were up to hundreds (Fe) and thousands (Mn) of times higher than those recorded in the seawater layer of the water column. In the Šibenik Bay, the influence of benthic

flux on supernatant concentrations in not recorded for Fe, while for Mn it was much less prominent than in the upper part of the estuary. The observed difference between lower and upper estuary may be attributed to the residence time increasing in upward direction and consequent lower oxygen saturation rates in bottom waters of the upper estuary. In the Šibenik Bay, the bottom layer contains water rich in oxygen which came recently from the adjacent open sea (Legović et al. 1991b), causing the oxidation and precipitation of diffusing Fe and Mn.

Table 6.9. Fluxes of dissolved metals across the sediment-water interface at five sampling locations in the Krka River estuary. A negative flux indicates diffusion from the sediment to the overlying water column, while positive flux indicates the importation of dissolved metal to the sediment from the water column.

Element	Diffusive flux (ng cm^{-2} y^{-1})				
	K1	K7	K8	K20	K36
Li	-544	-1 659	-1 026	-567	-1 398
Al	35.4	-18.8	-201	-209	-41.2
Fe	-7 203	-50 909	-41 692	-15 290	-8 949
Mn	-66 243	-205 541	-33 686	-174 608	-164 601
Co	-4.73	-81.0	3.17	-18.3	-41.8
Ni	-14.5	-155	-8.73	-9.30	-55.1
Cu	-7.09	18.8	-500	3.27	-3.87
Zn	2 543	-1 053	82.7	14.3	-520
Pb	-1.58	-28.1	-5.16	-49.2	-38.6
Cr	0.89	3.68	-6.15	5.80	6.87
Ba	-271	-512	-205	-1 763	-955
Mo	59.4	-783	-336	-1 266	-307
V	73.8	113	192	42.0	82.4
U	44.8	-13.9	51.1	5.61	3.58
As	-318	-537	-412	-158	-652

The behavior of metals in the sediment column and at the SWI is very complex, because their partitioning between solid and dissolved phases may be influenced by many factors, such as content of organic carbon and Fe/Mn oxyhydroxides, pH and redox conditions, and salinity. A common approach in describing the solid-solution interactions is using the partition coefficient K_d (L kg^{-1}), which is calculated as the ratio between metal concentration in solid phase (C_s) (mg kg^{-1}) and in dissolved phase (C_d) (mg L^{-1}) (Wang and Wang 2017; Duan et al. 2019; Liu et al. 2019). Sediment-pore water partition coefficients, especially their logarithms ($logK_d$), may be seen as a measure of the reactivity, transport and fate of compounds in pore water (Emili et al. 2016). In general, low values of partitioning coefficient are related to those metals that may feasibly transfer from the sediment to the water, therefore have a potentially higher

bioavailability and toxicity than those with high values. The mean $logK_d$ values of selected elements in the sediment cores from the Krka River estuary are given in the Table 6.10.

Table 6.10. The average $LogK_d$ values for metals in the sediment cores of the Krka River estuary

	$logK_d$														
	Li	Mo	Pb	U	Al	V	Cr	Mn	Fe	Co	Ni	Cu	Zn	Ba	As
K1	2.22	1.65	5.28	2.70	6.78	4.62	5.57	2.53	5.59	4.58	4.25	4.93	4.16	3.54	2.63
K7	2.31	1.56	5.15	2.51	6.95	4.24	5.85	2.32	4.86	4.14	4.07	4.81	3.36	3.65	2.93
K8	2.42	2.11	5.25	3.15	6.55	4.98	5.38	2.57	4.54	4.57	4.72	4.04	4.49	3.79	3.49
K20	2.02	1.88	5.29	2.99	6.26	4.96	6.00	3.64	4.90	4.77	4.66	5.12	5.03	3.91	3.59
K36	2.00	1.94	4.92	3.48	6.76	4.71	6.69	2.56	5.49	4.55	4.30	4.96	4.96	4.00	3.43
Total	2.25	1.95	5.10	3.11	6.56	4.68	5.71	2.97	5.33	4.90	4.41	5.00	4.30	3.77	3.36

In general, there was no significant difference for the $logK_d$ values with depth, indicating a steady equilibrium between the dissolved and solid phase. Moreover, the prominent difference between the sampling locations was not observed. However, the differences were apparent among metals since the $logK_d$ values varied from 1.15 for Mo in the layer 28-30 cm of the K1 core to 7.15 for Cr in the layer 2-4 cm of the K36 core. Average $logK_d$ decreased in following order: Al > Cr > Fe > Pb > Cu > Co > V > Ni > Zn > Ba > As > U > Mn > Li > Mo. The $logK_d$ values > 5 indicate elements or compounds with affinity to the solid phase of the sediment and low geochemical mobility in the water; values in the range $3 < logK_d < 4$ characterize chemicals more easily released from solid phases and $logK_d$ values < 3 chemicals present preferentially in the liquid phase (Nabelkova and Komínková 2012; Sedeño-Díaz et al. 2020). Therefore, $logK_d$ values of Fe, Al, Pb and Cr suggest that these elements are highly stable in the sediments, while $logK_d$ values of Li, Mo, and partly of U, Mn and As indicate the greater the partitioning of the metal towards the soluble phase.

Considering that partition coefficients of a particular metal depend on the pH of the system and the nature and concentration of sorbents associated with the sediment (Alison and Alison 2005), correlation was made in order to evaluate the dependence of $logK_d$ values of various metals on sediment pore water pH, Eh and sorbents such as organic matter and Fe minerals (Appendix 21.). For the calculation, logarithmic values of C_{org} and total Fe in solid phase were used. The $logK_d$ values of Mo, U, Al, Cr, and As slightly decreased as the pH increased, showing a significant negative correlation ($p < 0.001$) with pH. On contrary, the $logK_d$ values of Pb, Mn and Fe demonstrated a significant positive correlation with the pH (Pb and Mn $p < 0.001$; Fe p

< 0.01). A significant positive correlation with $logFe_{solid}$ was observed for As, Ni, Mo, Li, U, and Ba ($p < 0.001$) and for V and Zn ($p < 0.01$), suggesting that Fe minerals are important adsorbents of these elements in the sediment. Moreover, the organic matter was proved to be an important adsorbent phase in the sediment, as evidenced from the significant positive correlation between $logC_{org}$ and $logK_d$ values of Ba, Mo, As, Zn, U, Mn, Ni and Cu ($p < 0.001$) and Cr ($p < 0.01$). Another parameter which influences the metal mobility in the sediment, and thus the partition coefficient, is the Eh. The correlation matrix showed significant negative correlation between Eh and U, Mn, Zn, Ba, As ($p < 0.001$) and Co ($p < 0.01$).

6.7.1. The head of the estuary

Iron and Mn behaviour in the sediment is strongly influenced by redox conditions in sediment, as confirmed by their significant correlation ($r = 0.73$, $p < 0.001$) with pore water Eh. At the head of the estuary a clear subsurface maximum of dissolved Fe and Mn was observed at depth 0-2 cm. As previously discussed, Fe and Mn oxyhydroxides were reduced by bacterial activities during the degradation of organic matter, subsequently releasing dissolved Fe and Mn into pore water. Although peaks of dissolved Mn generally appear above Fe since Mn reduction is favoured thermodynamically (Froelich et al. 1979), in core K1 there were observed in the same layer, probably due to compression of redox zones and sediment core slicing resolution (2 cm) which did not allow to distinguish apart zone of Mn and Fe reduction. The upward diffusion of dissolved Mn and Fe caused a benthic diffusive flux from the sediment to the overlying water column, considerably impacting the Fe and especially Mn content in the bottom water. The calculated Mn flux was ~2-3 times lower than in Prokljan Lake and Šibenik Bay, yet the concentrations in bottom water were order of magnitude higher due to the low oxygen concentration in the bottom water at the head of the estuary, which prevented fast reprecipitation of Mn oxyhydroxides. However, the increased concentrations were limited to the near-bottom water, and did not had an effect on the Mn content in the entire water column. The appearance of sulphide below the peaks of Mn and Fe marks the anoxic layer of the sediment, where downward Fe and Mn flux is limited by formation of new minerals, most likely Fe sulphides and Mn carbonates (Burdige 1993; Duan et al. 2019). The carbonate precipitation as dominant Mn consumption mechanism in the pore water is supported with findings of Prohić and Kniewald (1987), who demonstrated that Mn is predominantly bound to the carbonate fraction of the Krka River estuary sediments.

Although Fe and Mn oxyhydroxides are known to adsorb a large range of metals (Burdige 1993), which is also suggested at the head of the estuary by the coupling relationship between metals (Cr, Co, Ni, As) and Fe ($r = 0.89\text{-}0.97$, $p < 0.001$) and Mn ($r = 0.75\text{-}0.89$, $p < 0.001$) in solid sediment fraction, the significant correlation between dissolved concentrations in pore water was not observed. The lack of significant correlation combined with the pore water profiles indicated that distribution of analysed metals was not primary controlled by the reductive dissolution of the Fe and Mn oxyhydroxides.

However, the marked peaks of dissolved metals (Co, Cu, Pb, V, As) were observed in anoxic layer, at depth below 10 cm, which is quite unexpected due to the high insolubility of these metals with sulphide (Dang et al. 2015; Duan et al. 2019). Though unusual, this type of behaviour was recorded elsewhere, and linked to: (i) metal binding with dissolved organic matter (DOM) (Santos-Echeandia et al. 2009; Lourino-Cabana et al. 2014; Dang et al. 2015; Duan et al. 2019; Jokinen et al. 2020), thus reducing their solubility despite the sulphide presence; (ii) the formation of dissolved metal polysulfide complexes (Huerta-Diaz et al. 1998; Wang and Tessier 2009; Dang et al. 2015; Duan et al. 2019; Jokinen et al. 2020); (iii) metal-sulphide-DOM ternary interactions and (Hoffmann et al. 2012; Dang et al. 2015; Duan et al. 2019; Jokinen et al. 2020) (iv) the dissolution of less reactive Fe and Mn oxyhydroxides deeper in the sediment, in the zone of sulphate reduction (Mucci et al. 2000; Rigaud et al. 2013; Tapia and Audry 2013; Egger et al. 2016; Jokinen et al. 2020). Moreover, peaks of Cr, which tends to precipitate and/or to be adsorbed onto minerals (especially aluminosilicates) in anoxic sediments (Gorny et al. 2016), also appeared in the pore water of the anoxic part of the sediment. Rigaud et al. (2013) recorded the co-occurrence of the dissolved and solid Cr peaks in the sediment and suggested that solid/liquid equilibrium has a strong control of the pore water Cr content. This covariation was observed at the head of the estuary, and also in Prokljan Lake. In addition, as many authors evidence, Cr mobility in the sediment is greatly affected by the complexation with the dissolved organic matter (DOM) which increases its solubility under reducing conditions in the pore water (Rigaud et al. 2013; Duan et al. 2019; Jokinen et al. 2020).

Despite the fact that Al oxyhydroxides, alongside Fe and Mn oxyhydroxides, are effective scavengers of metals (e.g. Cu, Cd, Zn, Mn) in the sediment (Goldbreg et al. 1996), and that Al has a potentially important role in the early diagenesis of the silicate minerals (Stoffyn-Egli 1982b), the available pore water Al data sets are scarce, consequently the Al behaviour in the pore water is not well established as those of Fe and Mn. The dissolved Al is released from detrital (lithogenic) mineral phases (Dixit et al. 2001), in marine sediments the source of Al is

most likely the dissolution of relatively unstable amorphous Al oxyhydroxides or other highly weathered aluminosilicate material (Stoffyn-Egli 1982b; Michalopoulos and Aller 1995). However, Stoffyn-Egli (1982b) points out that Al content in the pore water is result of the of kinetic equilibrium between several reactions involving various minerals (some of them probably metastable in the sediment), rather than the result of thermodynamic equilibrium with aluminium oxyhydroxides or aluminosilicate minerals. Moreover, due to the high dissolved SiO_2 concentrations, author suggest that minerals most likely to control dissolved Al in marine sediments are aluminosilicate minerals. In any case, as pore water Al concentrations build up above some threshold level, they induce the formation of a new authigenic phase (Burdige 2006), a process often referred to as reverse weathering (Michalopoulos and Aller 1995; Dixit et al. 2001). Moreover, dissolved Al derived from detrital material, is known to decrease silica solubility by incorporation into the matrix of deposited biogenic silica (Dixit et al. 2001; Burdige 2006). These processes remove Al from solution in a way that close coupling of dissolution, reprecipitation and incorporation reaction inhibits the build-up of dissolved Al. Yet, the dissolved Al peaks were recorded in the North Atlantic sediments, usually in the upper 10 cm of the sediment (Stoffyn-Egli 1982b). The above described processes may impact the dissolved Al in the sediment of the Krka River estuary as well. At the head of the estuary, a marked increase of dissolved Al is observed in the layer 24-26 cm, characterized by the rapid removal in both upward and downward direction.

Uranium and Mo behaviour in the sediment pore water is described in the Section 6.7.1. In briefly, they are redox-sensitive elements, known to be present in oxidized waters as highly soluble species ($Mo^{VI}O_4^{2-}$ and $UO_2(CO_3^{-2})_3^{-4}$), and removed from the pore water by precipitation or adsorption when conditions turn anoxic (U) or euxinic (Mo). The similarity of their behaviour in the pore water is evident from the significant correlation ($r = 0.86$-0.93, $p < 0.001$) observed at all sites except the Šibenik Port. Although U and Mo are supposed to be removed from the pore water in the anoxic sediments, at all sites, except the Guduča River, the presence of dissolved U and Mo peaks was observed in the anoxic zone. This atypical behaviour however has been previously reported for estuarine and marine sediments (Chaillou et al. 2002; Audry et al. 2006; Dang et al. 2018). Several possible explanations for release of dissolved U in deep sediments were proposed, including re-oxygenation of the sediment during core slicing or possible presence of authigenic colloidal phases in the dissolved phase that could cross the 0.2 μm pore size filters (Chaillou et al. 2002). Audry et al. (2006) and Dang et al. (2018) reject the hypothesis of sampling artefacts, suggesting that U release into deep anoxic sediments is a

result of the set of biogeochemical processes, such as biotic and abiotic oxidation of previously accumulated solid U and formation of stable uranyl carbonate or organic-U complexes that enhance U solubility (Dang et al. 2018).

In the marine sediments, Ba may be associated with various particulate phases, some of which are biologically associated (organic matter, carbonates, opal and barite) and some may not be directly related to biological activity (terrigenous material, Fe and Mn oxyhydroxides) (Dehairs et al. 1980; Gingele and Dahmke 1994; McManus et al. 1998; Gonneea and Paytan 2006). The microbial oxidation of the organic matter and consequent sulphate consumption, causes barite dissolution, releasing Ba into the pore water (McManus et al. 1998; Schenau et al. 2001). The slight gradual increase of dissolved Ba from the SWI downward was observed at the head of the estuary, as well as at other sites in the Krka River estuary. The pore water concentrations exceeded the bottom water Ba values, resulting in the concentration gradient across the SWI and the diffusive Ba flux from sediment to the overlying column. The diffused Ba may be reprecipitated with sulphate forming barite (Liguori et al. 2016). The strong positive correlation of Ba and DOC ($r = 0.72$, $p < 0.001$), DIC ($r = 0.74$, $p < 0.001$) and PO_4^{3-} ($r = 0.88$, $p < 0.001$) indicates that substantial fraction of released Ba is derived from biogenic barite or organic matter bound Ba (Dehairs et al. 1980; Dang et al. 2015).

In general, Li showed downcore decreasing trend at all sites, indicating Li uptake by sediment during early diagenesis. Scholz et al. (2010) suggest, based on the Li data (^{7}Li and Li concentrations) of shallow pore waters from the Nile deep-sea fan and the eastern Black Sea, that the downcore Li decrease in pore water is attributed to adsorption rather than structural incorporation into clay minerals.

6.7.2. Prokljan Lake

Prokljan Lake, as well as the rest of the Krka River estuary, is characterized by the build-up of the dissolved Mn and Fe concentrations in first centimetres below the SWI, reflecting the reductive dissolution of Mn and Fe oxyhydroxides during OM mineralization. The dissolved Fe maximum was observed at higher depth (2-4 cm) than Mn maximum (0-2 cm), following the ideal redox sequence in marine sediments (Jørgensen and Kasten 2006). Contrary to the head of the estuary, the release of dissolved Fe and Mn into pore water was accompanied by the release of other metals (Co, Ni, As) as well. The pore water distribution of Co and Ni, and their significant correlation to Mn ($r = 0.95$ and $r = 0.87$, $p < 0.001$), suggest that these elements

are mainly associated with Mn oxyhydroxides, thus released into pore water when Mn oxyhydroxides are reduced. The coupling of Co and Ni to Mn is in agreement with previously reported work (Shaw et al. 1990; Audry et al. 2006; Lesven et al. 2008; Santos-Echeandia et al. 2009; Sondi et al. 2017). Moreover, many authors have reported that As mobility in the subsurface sediments is closely linked to Fe cycling (Rigaud et al. 2013, Tapia and Audry 2013; Dang et al. 2014; Sondi et al. 2017; Fiket et al. 2019). Thus, strong positive correlation between As and Fe ($r = 0.80$, $p < 0.001$) and co-occurrence of dissolved As and Fe peaks below the SWI suggest that As was associated (adsorbed and/or coprecipitated) with Fe oxyhydroxides and released to the pore water during reductive dissolution from Fe oxyhydroxides, or rather reductive desorption as some suggest (Tapia and Audry 2013).

The distribution of dissolved Zn in the estuary showed a substantial intra-site variation. In Prokljan lake, instead of being removed below the zone of Fe reduction due to the extremely fast ZnS precipitation kinetics even at trace levels of sulphide present (Morse and Luther 1999; Duan et al. 2019), several peaks of dissolved Zn were observed along the depth. As already described for other elements (Co, Cu, Pb, V, As), the metal-DOM interactions (Charriau et al. 2011; Jokinen et al. 2020) and the formation of dissolved metal-(poly)sulphide complexes (Wang and Tessier 2009; Duan et al. 2019) may also increase Zn solubility. However, Zn had a strong positive correlation ($r = 0.82$, $p < 0.001$) with Al, implying that common process may control their distribution in Prokljan Lake pore water, possibly the dissolution of highly weathered aluminosilicate material (Stoffyn-Egli 1982b; Michalopoulos and Aller 1995).

6.7.3. The Guduča River

Low oxygen levels in the bottom part of the water column resulted in the further compression of redox zones in the sediment from the Guduča River, likewise observed at the head of the estuary. The release of dissolved Fe and Mn, corresponding to the reduction of Fe and Mn oxyhydroxides in the suboxic layer of the sediment, was observed in the uppermost pore water sample (0-2 cm). Similarly to the head of the estuary, the release of Co and Ni associated to the Mn oxyhydroxides was not observed at the SWI. However, the release of the dissolved As was recorded at the top of the core, contrary to the As behaviour at the head of the estuary, but in accordance to other sampling sites in the estuary and many studies around the world who observed a strong relationship between reduction of Fe oxyhydroxides and remobilization of As (Rigaud et al. 2013, Tapia and Audry 2013; Dang et al. 2014; Sondi et al. 2017; Fiket et al.

2019). In addition, the reductive dissolution of Fe is known to have a strong influence on the Cr remobilization during early diagenetic processes in the sediment (Rigaud et al. 2013; Gorny et al. 2016). Yet, in the Krka River estuary the release of the Cr into pore water at the depth of the Fe reduction was observed only in the sediment from the Guduča River, suggesting that the dissolution of Fe oxyhydroxides in not playing a key role on the Cr mobility in the Krka River estuary. The mobility is possibly controlled by the solid/liquid equilibrium as suggested by Rigaud et al. (2013) or by the complexation with DOM (Rigaud et al. 2013; Gorny et al. 2016; Duan et al. 2019; Jokinen et al. 2020). Furthermore, in the Guduča River the build-up of dissolved Cu concentrations at the SWI was observed. Considering that Cu is known to be bioactive metal, its release into pore water is attributed to the association with biogenic material and the degradation of OM by microbial community present in the sediment (Shaw et al. 1990; Audry et al. 2006; Gavriil and Angelidis 2006; Santos-Echeandia et al. 2009; Duan et al. 2019). However, due to the compressed redox zonation it is difficult to distinguish with certainty which carrier phase (biogenic material, Fe and Mn oxyhydroxides) contributed the most to the release of metal into pore water.

6.7.4. The former Electrode and Ferroalloy Factory

The established behaviour of dissolved Fe and Mn in the sediment of the Krka River estuary characterized by marked peaks in the first centimetres below the SWI is observed at the former TEF factory sampling site as well. As in other locations where bottom waters are not largely depleted in oxygen (Prokljan Lake, the Šibenik Port), the two peaks were found in separate layers and it was possible to decipher between Mn and Fe as carrier phases of metals. The reductive dissolution of Mn oxyhydroxides led to release of Co at the SWI, as often reported in literature (Shaw et al. 1990; Audry et al. 2006; Lesven et al. 2008; Santos-Echeandia et al. 2009; Rigaud et al. 2013; Dang et al. 2015; Sondi et al. 2017). Common dissolution pathway of these two elements in the sediment core K20 is confirmed by the strong significant correlation ($r = 0.85$, $p < 0.001$). However, the release of Ni associated to Mn oxyhydroxides was not observed at this site, such in the case of Prokljan Lake. The build-up of dissolved As concentrations below the SWI may be attributed to the reduction of Fe oxyhydroxides, as observed both in this study and elsewhere (Rigaud et al. 2013; Tapia and Audry 2013; Dang et al. 2014; Sondi et al. 2017; Fiket et al. 2019), although correlation between the Fe and As ($r = 0.59$, $p < 0.05$) was not as strong as that observed between Mn and Co.

Subsequently to the suboxic layer lies the zone where predominant pathway of organic matter mineralization is bacterial reduction of seawater sulphate to sulphide (Jørgensen et al. 2019). The dissolved sulphide concentration recorded at this site were much higher than in the rest of the estuary, which is not surprising given that the factors controlling sulphide concentrations are the availability of dissolved sulphate and organic matter. As sulphate is being resupplied from the bottom seawater, sulphate concentrations are in the same range at all stations in estuary, whereas C_{org} content found at the former factory sites was considerably higher than at other sampling locations. In this sediment zone, dissolved Fe diffused downwards from the suboxic layer precipitated out of pore water as sulphide phase. Dissolved Mn, however, was not completely removed, but the second, less prominent increase was observed. Manganese removal is controlled by carbonates (Burdige 1993; Kalnejais et al. 2015; Wang and Wang 2017) rather than sulphides, considering that the affinity of Mn for sulphides is relatively poor (Morse and Luther 1999; Billon et al. 2001; Gao et al. 2009).

The enhanced concentrations of some metals (Pb, V, Cr, Ni) were found in the sulfidic zone of the sediment, as already observed in the sediment cores from other sampling locations in the estuary. Considering that correlation matrix revealed strong positive correlation of all four metals with DOC ($r = 0.74\text{-}0.87$, $p < 0.001$), and also correlation between dissolved sulphide and V ($r = 0.72$, $p < 0.05$), Cr ($r = 0.86$, $p < 0.001$) and Pb ($r = 0.62$, $p < 0.05$), the increased concentrations can be attributed, as described above, to the formation of metal-DOM complexes (Santos-Echeandia et al. 2009; Rigaud et al. 2013; Lourino-Cabana et al. 2014; Dang et al. 2015; Duan et al. 2019; Jokinen et al. 2020), metal-polysulphide complexes (Huerta-Diaz et al. 1998; Wang and Tessier 2009; Dang et al. 2015; Duan et al. 2019; Jokinen et al. 2020) or to the metal-sulphide-DOM ternary interactions and (Hoffmann et al. 2012; Dang et al. 2015; Duan et al. 2019; Jokinen et al. 2020).

6.7.5. The Port of Šibenik

The dissolved Fe and Mn behaviour in the sediment from the Port of Šibenik followed the distribution pattern observed in Prokljan Lake and at the ex-factory site, hence Mn peak was observed in the first sediment layer below the SWI, whereas Fe maximum was observed in the subsequent layer. The well-known association between Mn and Co in the literature (Shaw et al. 1990; Audry et al. 2006; Lesven et al. 2008; Santos-Echeandia et al. 2009; Rigaud et al. 2013; Dang et al. 2015; Sondi et al. 2017) was observed at this site too, reflected in the co-occurrence

of the subsurface peaks and strong positive correlation between the two ($r = 0.84$, $p < 0.01$). Moreover, the release of As into pore water was recorded at the depth of Fe maximum as often observed both in this study and others (Rigaud et al. 2013, Tapia and Audry 2013; Dang et al. 2014; Sondi et al. 2017; Fiket et al. 2019). However, this was not the strongest As peak, therefore strong correlation was not observed between Fe and As ($r = 0.34$). Another metal that demonstrated a build-up in the pore water just below the SWI was Zn, which in known to be bioactive metal and its release is attributed to the OM mineralization (Tapia and Audry 2013; Duan et al. 2019).

In the Šibenik Port the most important diagenesis reactivity zone in the sediment seemed to be well below the zone of the surface OM mineralization and the zone of the Fe and Mn oxyhydroxides reductive dissolution. Namely, the strong release of Co, As and Zn but also other analysed metals (Ni, Cu, Pb, V and Cr) was observed at the depth ~10 cm. Distribution pattern of DOC and diagenesis tracers (PO_4^{3-}, NH_4^+, ΣHS^-) implied that there is significant net production of DOM at that depth. The strong correlation was found between Ni, Cu, As and DOC ($r = 0.75$-0.77, $p < 0.05$, $r = 0.81$, $p < 0.01$) and NH_4^+ ($r = 0.72$-0.75, $p < 0.05$), respectively. The positive correlation was moreover found among Pb, Cr and DIC ($r = 0.75$ and $r = 0.71$, $p < 0.05$), as well as among Pb, Cr and PO_4^{3-} ($r = 0.98$ and $r = 0.97$, $p < 0.001$). Therefore, increased dissolved metals concentrations found at depth ~10 cm may be attributed to the OM degradation processes.

7. CONCLUSIONS

7. CONCLUSIONS

In this work surface distribution of metals in the sediment of the Krka River estuary were studied, accompanied with identification of their sources and contamination assessment. The sediment cores were studied to assess the historical trends and main diagenetic processes controlling the mobility of metals in the sediment and across the SWI. Results may be summarized as follows:

- The spatial distribution of terrigenous elements in the surface sediment of the Krka River estuary indicates the Guduča River and Litno Spring in the Zaton Bay as main input pathways of the terrigenous particulate material.
- While upper estuary is rather pristine, the significant enrichment in a number of metals was observed in the sediment of the Šibenik Bay as a consequence of anthropogenic pollution from the three main sources: the former Electrode and Ferroalloy Factory, the Port of Šibenik and nautical marina/repair shipyard. The obtained results show that metal contamination in the lower estuary is more significant and widespread than previously considered, with concentrations of some metals (e.g. Hg, Pb, Zn, Mn, Cd, Cu, As) comparable to heavily polluted European coastal and estuarine sites.
- According to the metal distribution maps, there is no dispersal of contaminants outside of the estuary to the open sea. The distribution pattern is most probably influenced by multiple factors: closed morphology of the estuary, bottom seawater layer moving landward preventing transport of metals in a seaward direction and fast adsorption of metals to the particles and deposition to the seabed. However, a fraction of metals is being transported upstream from its source in the Šibenik Bay due to the bottom water movement.
- The probability of harmful effects of multiple contamination of sediment to the living organisms was evaluated according to the mean ERM quotient. Major part of the Krka River estuary has a toxicity probability of 21%, whereas closer to the contamination sources toxicity is 49% or even 76%.
- The sediment vertical profiles proved to be valuable archives for studying historical input of contaminants in the environment. This is the case especially in the cores which are deep enough to reach the pre-contamination level, such as the core sampled in the marina/shipyard. The sudden increase in number of metals co-occurred with the beginning of the repair shipyard activities, as evidenced by the ^{210}Pb and ^{137}Cs sediment dating results. At the head of the estuary, a short industrial episode at the end of the 19th

century, impacted the sediment quality through significant increase of Pb concentrations.

- However, the historical interpretation should be made with caution because metals may be enriched in sediment as a result of early diagenetic processes. For example, dissolved metals may react with sulphide produced by sulphate reduction during the mineralization of the organic matter, and form discreate metal sulphide phases or coprecipitate and/or be adsorbed to iron sulphide solid phases, which result in the peaks of metal solid phase at a certain depth, as seen in the core from the head of the estuary. Furthermore, Mn enrichment in the upper part of core form the port area may be attributed to the downward diffusion of dissolved Mn^{2+} and subsequent precipitation out of pore water as a pure or mixed carbonate phases and phosphate phases, or in lesser extent as sulphide phases.
- The diagenetic tracers (Fe^{2+}, Mn^{2+}, NH_4^+, PO_4^{3-}, ΣHS^-, DIC) displayed vertical distribution pattern consistent with the classical diagenetic zonation, but with compressed redox zones, due to very thin oxic layer. For instance, reduction of Mn oxyhydroxides at all studied sites in the estuary occurred in the top two centimetres of sediment and reduction of Fe oxyhydroxides was observed either in the same or the subsequent sediment layer.
- Metal partitioning and recycling in the pore water was mainly affected by the microbially mediated oxidation of organic matter and associated reductive dissolution of Fe and Mn oxyhydroxides. Namely, the build-up of dissolved Mn, Fe and other metals in the pore water was observed in the first centimetres below the SWI, reflecting the Fe and Mn oxyhydroxides reduction and release of adsorbed metals.
- Even the small concentrations of dissolve sulphide caused the removal of metal from the pore water most likely due to the formation of the highly insoluble solid phases. However, the marked peaks of dissolved metals were observed in the anoxic sediment of the Krka River estuary. This unusual behaviour may be due to the metal-DOM, metal-polysulphide and metal-sulphide-DOM interactions and/or the dissolution of less reactive Fe and Mn oxyhydroxides deeper in the sediment, in the zone of sulphate reduction.
- According to calculated benthic diffusive fluxes of most of the considered elements, sediment in the Krka River estuary is acting as a source of metals for the overlying water column. The impact of the diffusive flux is especially evident in the upper part of the

estuary where recorded concentration in supernatant water were up to hundreds (Fe) and thousands (Mn) of times higher than those recorded in the seawater layer of the water column at depths more distant to the SWI. The reason for this is the lower oxygen saturation rate in the upper part of the estuary, preventing the fast oxidation and precipitation of diffusing Fe and Mn.

8. REFERENCES

8. REFERENCES

Acquavita, A., Predonzani, S., Mattassi, G., Rossin, P., Tamberlich, F., Falomo, J. and Valić, I. (2010): Heavy metal contents and distribution in coastal sediments of the Gulf of Trieste (Northern Adriatic Sea, Italy). Water, Air, & Soil Pollution, 211, 95-111.

AlKhader, A. (2015): The impact of phosphorus fertilizers on heavy metals content of soils and vegetables grown on selected farms in Jordan. Agrotechnol, 5, 137.

Aller, R.C. (1994): Bioturbation and Remineralization of Sedimentary Organic-Matter - Effects of Redox Oscillation. Chemical Geology, 114, 331-345.

Allison, J.D. and Allison, T.L. (2005): Partition coefficients for metals in surface water, soil, and waste. Rep. EPA/600/R-05, 74.

Almeida, E., Diamantino, T.C. and de Sousa, O. (2007): Marine paints: the particular case of antifouling paints. Progress in Organic Coatings, 59, 2-20.

Alyazichi, Y.M., Jones, B.G. and McLean, E. (2015): Source identification and assessment of sediment contamination of trace metals in Kogarah Bay, NSW, Australia. Environmental Monitoring and Assessment, 187, 20.

Amato, E.D., Simpson, S.L., Remaili, T.M., Spadaro, D.A., Jarolimek, C.V. and Jolley, D.F. (2016): Assessing the Effects of Bioturbation on Metal Bioavailability in Contaminated Sediments by Diffusive Gradients in Thin Films (DGT). Environmental Science & Technology, 50, 3055-3064.

Aminot, A. and Kérouel, R. (2004) Hydrologie des écosystèmes marins: paramètres et analyses. Editions Quae, 335 pp.

Andrade, R., Hatje, V., Masqué, P., Zurbrick, C.M., Boyle, E.A. and Santos, W. (2017): Chronology of anthropogenic impacts reconstructed from sediment records of trace metals and Pb isotopes in Todos os Santos Bay (NE Brazil). Marine Pollution Bulletin, 125, 459-471.

Apak, R. (2002): Adsorption of heavy metal ions on soil surfaces and similar substances. In: Encyclopedia of Surface and Colloid Science, A.T. Hubbard, (Ed.), Marcel Dekker, New York, 385-417.

Arndt, S., Jorgensen, B.B., LaRowe, D.E., Middelburg, J.J., Pancost, R.D. and Regnier, P. (2013): Quantifying the degradation of organic matter in marine sediments: A review and synthesis. Earth-Science Reviews, 123, 53-86.

Atkinson, C.A., Jolley, D.F. and Simpson, S.L. (2007): Effect of overlying water pH, dissolved oxygen, salinity and sediment disturbances on metal release and sequestration from metal contaminated marine sediments. Chemosphere, 69, 1428-1437.

Audry, S., Blanc, G., Schäfer, J., Chaillou, G. and Robert, S. (2006): Early diagenesis of trace metals (Cd, Cu, Co, Ni, U, Mo, and V) in the freshwater reaches of a macrotidal estuary. Geochimica Et Cosmochimica Acta, 70, 2264-2282.

Audry, S., Grosbois, C., Bril, H., Schafer, J., Kierczak, J. and Blanc, G. (2010): Post-depositional redistribution of trace metals in reservoir sediments of a mining/smelting-impacted watershed (the Lot River, SW France). Applied Geochemistry, 25, 778-794.

Bak, F. and Pfennig, N. (1987): Chemolithotrophic growth of Desulfovibrio sulfodismutans sp. nov. by disproportionation of inorganic sulfur compounds. Archives of Microbiology, 147, 184-189.

Baldock, J.A., Masiello, C.A., Gelinas, Y. and Hedges, J.I. (2004): Cycling and composition of organic matter in terrestrial and marine ecosystems. Marine Chemistry, 92, 39-64.

Beck, M., Böning, P., Schückel, U., Stiehl, T., Schnetger, B., Rullkötter, J. and Brumsack, H.-J. (2013): Consistent assessment of trace metal contamination in surface sediments and suspended particulate matter: A case study from the Jade Bay in NW Germany. Marine Pollution Bulletin, 70, 100-111.

Benjamin, M.M. and Lawler, D.F. (2013) Water quality engineering: Physical/chemical treatment processes. John Wiley & Sons, 912 pp.

Benoit, J.M., Shull, D.H., Harvey, R.M. and Beal, S.A. (2009): Effect of Bioirrigation on Sediment-Water Exchange of Methylmercury in Boston Harbor, Massachusetts. Environmental Science & Technology, 43, 3669-3674.

Berner, R.A. (1980) Early diagenesis: a theoretical approach. Princeton University Press, 241 pp.

Bianchi, T.S. (2007) Biogeochemistry of estuaries. Oxford University Press New York, 706 pp.

Bilinski, H., Kozar, S., Plavšić, M., Kwokal, Ž. and Branica, M. (1991): Trace metal adsorption on inorganic solid phases under estuarine conditions. Marine Chemistry, 32, 225-233.

Bilinski, H., Kwokal, Ž. and Branica, M. (1992): Processes affecting the fate of mercury in the Krka River Estuary. Water Research, 26, 1243-1253.

Bilinski, H., Kwokal, Ž., Plavšić, M., Wrischer, M. and Branica, M. (2000): Mercury distribution in the water column of the stratified Krka river estuary (Croatia): importance of natural organic matter and of strong winds. Water Research, 34, 2001-2010.

Billon, G., Ouddane, B., Laureyns, J. and Boughriet, A. (2001): Chemistry of metal sulfides in anoxic sediments. Physical Chemistry Chemical Physics, 3, 3586-3592.

Bogner, D. (2001): Površinski sedimenti i sedimentacija na djelu sjevernojadranskog hrvatskog šelfa. Disertacija, Sveučilište u Zagrebu, 203 pp.

Bogner, D., Ujević, I., Zvonarić, T. and Barić, A. (2004): Distribution of selected trace metals in coastal surface sediments from the middle and south adriatic sea. Fresenius Environmental Bulletin, 13, 1281-1287.

Bonacci, O. and Ljubenkov, I. (2005): Nove spoznaje o hidrologiji rijeke Krke. Hrvatske Vode, 13, 52, 265-281.

Bonacci, O., Jukić, D. and Ljubenkov, I. (2006): Definition of catchment area in karst: case of the rivers Krčić and Krka, Croatia. Hydrological Sciences Journal-Journal Des Sciences Hydrologiques, 51, 682-699.

Bonacci, O., Andrić. I. and Roje-Bonacci, T. (2017): Hydrological analysis of Skradinski Buk tufa waterfall (Krka River, Dinaric karst, Croatia). Environmental Earth Sciences, 76, 669.

Boudreau, B.P. (1984): On the Equivalence of Nonlocal and Radial-Diffusion Models for Porewater Irrigation. Journal of Marine Research, 42, 731-735.

Boudreau, B.P. (1996): The diffusive tortuosity of fine-grained unlithified sediments. Geochimica Et Cosmochimica Acta, 60, 3139-3142.

Bourg, A. (1988): Metals in aquatic and terrestrial systems: Sorption, speciation, and mobilization. In: Chemistry and biology of solid waste, (Ed.), Springer, 3-32.

Bradl, H.B. (2004): Adsorption of heavy metal ions on soils and soils constituents. Journal of Colloid and Interface Science, 277, 1-18.

Buljan, M. (1969): Neka hidrografska svojstva estuarnih područja rijeka Krke i Zrmanje. Krš Jugoslavije, 6, 303-331.

Burdige, D.J. (1993): The Biogeochemistry of Manganese and Iron Reduction in Marine-Sediments. Earth-Science Reviews, 35, 249-284.

Burdige, D.J. (2006) Geochemistry Of Marine Sediments. Princeton University Press, 624 pp.

Burdige, D.J. (2007): Preservation of organic matter in marine sediments: Controls, mechanisms, and an imbalance in sediment organic carbon budgets? Chemical Reviews, 107, 467-485.

Burns, R.J.and Burns, V.M. (1981): Authigenic oxides. In: The Sea, 7. The Oceanic Lithosphere, C. Emiliani, (Ed.), Wiley-Interscience, New York, 875-914.

Burton, E.D., Phillips, I.R. and Hawker, D.W. (2006): Factors controlling the geochemical partitioning of trace metals in estuarine sediments. Soil & Sediment Contamination, 15, 253-276.

Burton Jr, G.A. (2002): Sediment quality criteria in use around the world. Limnology, 3, 65-76.

Byrne, P., Taylor, K.G., Hudson-Edwards, K.A. and Barrett, J.E. (2017): Speciation and potential long-term behaviour of chromium in urban sediment particulates. Journal of Soils and Sediments, 17, 2666-2676.

Caetano, M., Madureira, M.J. and Vale, C. (2003): Metal remobilisation during resuspension of anoxic contaminated sediment: short-term laboratory study. Water Air and Soil Pollution, 143, 23-40.

Cai, W.J. and Sayles, F.L. (1996): Oxygen penetration depths and fluxes in marine sediments. Marine Chemistry, 52, 123-131.

Caille, N., Tiffreau, C., Leyval, C. and Morel, J.L. (2003): Solubility of metals in an anoxic sediment during prolonged aeration. Science of the Total Environment, 301, 239-250.

Campanha, M.B., Moreira, A.B. and Bisinoti, M.C. (2012): Metal fluxes at the sediment-water interface in rivers in the Turvo/Grande drainage basin, So Paulo State, Brazil. Journal of Soils and Sediments, 12, 1508-1516.

Canário, J., Vale, C. and Caetano, M. (2005): Distribution of monomethylmercury and mercury in surface sediments of the Tagus Estuary (Portugal). Marine Pollution Bulletin, 50, 1142-1145.

Canário, J., Prego, R., Vale, C. and Branco, V. (2007): Distribution of mercury and monomethylmercury in sediments of Vigo Ria, NW Iberian Peninsula. Water, Air, and Soil Pollution, 182, 21-29.

Canfield, D.E. and Thamdrup, B. (2009): Towards a consistent classification scheme for geochemical environments, or, why we wish the term 'suboxic' would go away. Geobiology, 7, 385-392.

Cantwell, M.G., Burgess, R.M. and Kester, D.R. (2002): Release and phase partitioning of metals from anoxic estuarine sediments during periods of simulated resuspension. Environmental Science & Technology, 36, 5328-5334.

Cardellicchio, N., Buccolieri, A., Di Leo, A. and Spada, L. (2006): Heavy metals in marine sediments from the Mar Piccolo of Taranto (Ionian Sea, southern Italy). Annali di Chimica: Journal of Analytical, Environmental and Cultural Heritage Chemistry, 96, 727-741.

Cauwet, G. (1991): Carbon inputs and biogeochemical processes at the halocline in a stratified estuary: Krka River, Yugoslavia. Marine Chemistry, 32, 269-283.

Celebi, U.B. and Vardar, N. (2008): Investigation of VOC emissions from indoor and outdoor painting processes in shipyards. Atmospheric Environment, 42, 5685-5695.

Chaillou, G., Anschutz, P., Lavaux, G., Schäfer, J. and Blanc, G. (2002): The distribution of Mo, U, and Cd in relation to major redox species in muddy sediments of the Bay of Biscay. Marine Chemistry, 80, 41-59.

Chapman, P.M. and Wang, F.Y. (2001): Assessing sediment contamination in estuaries. Environmental Toxicology and Chemistry, 20, 3-22.

Charriau, A., Lesven, L., Gao, Y., Leermakers, M., Baeyens, W., Ouddane, B. and Billon, G. (2011): Trace metal behaviour in riverine sediments: role of organic matter and sulfides. Applied Geochemistry, 26, 80-90.

Chatterjee, M., Canario, J., Sarkar, S., Branco, V., Bhattacharya, A. and Satpathy, K. (2009): Mercury enrichments in core sediments in Hugli–Matla–Bidyadhari estuarine complex, north-eastern part of the Bay of Bengal and their ecotoxicological significance. Environmental geology, 57, 1125.

Chen, L.-J., Zhu, M.-X., Yang, G.-P. and Huang, X.-L. (2013): Reductive reactivity of iron (III) oxides in the East China Sea sediments: characterization by selective extraction and kinetic dissolution. PloS one, 8, e80367.

Chester, R. (1990) Marine geochemistry. Unwin Hyman Ltd London, 698 pp.

Chiu, S., Ho, K., Chan, S., So, O. and Lai, K. (2006): Characterization of contamination in and toxicities of a shipyard area in Hong Kong. Environmental Pollution, 142, 512-520.

Ciceri, G., Maran, S., Martinotti, W. and Queirazza, G. (1992): Geochemical Cycling of Heavy-Metals in a Marine Coastal Area - Benthic Flux Determination from Pore Water Profiles and Insitu Measurements Using Benthic Chambers. Hydrobiologia, 235, 501-517.

Ciffroy, P., Monnin, L., Garnier, J.M., Ambrosi, J.P. and Radakovitch, O. (2019): Modelling geochemical and kinetic processes involved in lead (Pb) remobilization during resuspension events of contaminated sediments. Science of the Total Environment, 679, 159-171.

Cindrić, A.-M., Garnier, C., Oursel, B., Pižeta, I. and Omanović, D. (2015): Evidencing the natural and anthropogenic processes controlling trace metals dynamic in a highly stratified estuary: The Krka River estuary (Adriatic, Croatia). Marine Pollution Bulletin, 94, 199-216.

Cindrić, A.-M., Marcinek, S., Garnier, C., Salaün, P., Cukrov, N., Oursel, B., Lenoble, V. and Omanović, D. (2020): Evaluation of diffusive gradients in thin films (DGT) technique for speciation of trace metals in estuarine waters-A multimethodological approach. Science of the Total Environment, 137784.

Ciutat, A., Gerino, M. and Boudou, A. (2007): Remobilization and bioavailability of cadmium from historically contaminated sediments: Influence of bioturbation by tubificids. Ecotoxicology and Environmental Safety, 68, 108-117.

Coffey, M., Dehairs, F., Collette, O., Luther, G., Church, T. and Jickells, T. (1997): The behaviour of dissolved barium in estuaries. Estuarine, Coastal and Shelf Science, 45, 113-121.

Cossa, D., Fanget, A.-S., Chiffoleau, J.-F., Bassetti, M.-A., Buscail, R., Dennielou, B., Briggs, K., Arnaud, M., Guédron, S. and Berne, S. (2018): Chronology and sources of trace elements

accumulation in the Rhône pro-delta sediments (Northwestern Mediterranean) during the last 400 years. Progress in oceanography, 163, 161-171.

Costa, L.D.F., Mirlean, N., Wasserman, J.C. and Wallner-Kersanach, M. (2016): Variability of labile metals in estuarine sediments in areas under the influence of antifouling paints, southern Brazil. Environmental Earth Sciences, 75, 580.

Covelli, S., Faganeli, J., Horvat, M. and Brambati, A. (2001): Mercury contamination of coastal sediments as the result of long-term cinnabar mining activity (Gulf of Trieste, northern Adriatic sea). Applied Geochemistry, 16, 541-558.

Covelli, S., Faganeli, J., De Vittor, C., Predonzani, S., Acquavita, A. and Horvat, M. (2008): Benthic fluxes of mercury species in a lagoon environment (Grado Lagoon, Northern Adriatic Sea, Italy). Applied Geochemistry, 23, 529-546.

Covelli, S., Langone, L., Acquavita, A., Piani, R. and Emili, A. (2012): Historical flux of mercury associated with mining and industrial sources in the Marano and Grado Lagoon (northern Adriatic Sea). Estuarine, Coastal and Shelf Science, 113, 7-19.

Coynel, A., Gorse, L., Curti, C., Schafer, J., Grosbois, C., Morelli, G., Ducassou, E., Blanc, G., Maillet, G.M. and Mojtahid, M. (2016): Spatial distribution of trace elements in the surface sediments of a major European estuary (Loire Estuary, France): Source identification and evaluation of anthropogenic contribution. Journal of Sea Research, 118, 77-91.

Crusius, J., Calvert, S., Pedersen, T. and Sage, D. (1996): Rhenium and molybdenum enrichments in sediments as indicators of oxic, suboxic and sulfidic conditions of deposition. Earth and Planetary Science Letters, 145, 65-78.

Crusius, J., Bothner, M.H. and Sommerfield, C.K. (2004): Bioturbation depths, rates and processes in Massachusetts Bay sediments inferred from modeling of Pb-210 and Pu239+240 profiles. Estuarine Coastal and Shelf Science, 61, 643-655.

Cuculić, V., Cukrov, N., Barišić, D. and Mlakar, M. (2006): Uranium in sediments, mussels (Mytilus sp.) and seawater of the Krka river estuary. Journal of Environmental Radioactivity, 85, 59-70.

Cuculić, V., Cukrov, N., Kwokal, Ž. and Mlakar, M. (2009): Natural and anthropogenic sources of Hg, Cd, Pb, Cu and Zn in seawater and sediment of Mljet National Park, Croatia. Estuarine, Coastal and Shelf Science, 81, 311-320.

Cukrov, N. (2006): Estuarij rijeke Krke, klopka za radionuklide. Diseracija, Sveučilište u Zagrebu, 111 pp.

Cukrov, N. and Barišić, D. (2006): Spatial distribution of K-40 and Th-232 in recent sediments of the Krka River Estuary. Croatica Chemica Acta, 79, 115-118.

Cukrov, N., Barišić, D. and Juračić, M. (2007): Calculated sedimentation rate in the Krka River Estruary using vertical Diostribution of 137Cs. CIESM congress, 38.

Cukrov, N., Frančišković-Bilinski, S., Mikac, N. and Roje, V. (2008): Natural and anthropogenic influences recorded in sediments from the Krka river estuary (Eastern Adriatic coast), evaluated by statistical methods. Fresenius Environmental Bulletin, 17, 855-863.

Cukrov, N., Mlakar, M., Cuculić, V. and Barišić, D. (2009): Origin and transport of U-238 and Ra-226 in riverine, estuarine and marine sediments of the Krka River, Croatia. Journal of Environmental Radioactivity, 100, 497-504.

Cukrov, N., Frančišković-Bilinski, S., Hlača, B. and Barišić, D. (2011): A recent history of metal accumulation in the sediments of Rijeka harbor, Adriatic Sea, Croatia. Marine Pollution Bulletin, 62, 154-167.

Cukrov, N., Frančišković-Bilinski, S. and Bogner, D. (2014): Metal contamination recorded in the sediment of the semi-closed Bakar Bay (Croatia). Environmental geochemistry and health, 36, 195-208.

Dang, D.H. (2014): Dynamique sédimentaire et mécanismes de transferts des métaux/métalloïdes dans un écosystème contaminé: la Rade de Toulon. Thèse, Université de Toulon, 281 pp.

Dang, D.H., Tessier, E., Lenoble, V., Durrieu, G., Omanović, D., Mullot, J.-U., Pfeifer, H.-R., Mounier, S. and Garnier, C. (2014): Key parameters controlling arsenic dynamics in coastal sediments: an analytical and modeling approach. Marine Chemistry, 161, 34-46.

Dang, D.H., Lenoble, V., Durrieu, G., Omanović, D., Mullot, J.U., Mounier, S. and Garnier, C. (2015): Seasonal variations of coastal sedimentary trace metals cycling: Insight on the effect of manganese and iron (oxy)hydroxides, sulphide and organic matter. Marine Pollution Bulletin, 92, 113-124.

Dang, D.H., Evans, R.D., Wang, W., Omanović, D., El Houssainy, A., Lenoble, V., Mullot, J.-U., Mounier, S. and Garnier, C. (2018): Uranium isotope geochemistry in modern coastal sediments: Insights from Toulon Bay, France. Chemical Geology, 481, 133-145.

Dellwig, O., Schnetger, B., Meyer, D., Pollehne, F., Häusler, K. and Arz, H.W. (2018): Impact of the major Baltic inflow in 2014 on manganese cycling in the Gotland Deep (Baltic Sea). Frontiers in Marine Science, 5, 248.

Dixit, S., Van Cappellen, P. and van Bennekom, A.J. (2001): Processes controlling solubility of biogenic silica and pore water build-up of silicic acid in marine sediments. Marine Chemistry, 73, 333-352.

Dolenec, T., Faganeli, J. and Pirc, S. (1998): Major, minor and trace elements in surficial sediments from the open Adriatic Sea: a regional geochemical study. Geologia Croatica, 51, 59-73.

Dou, Y.G., Li, J., Zhao, J.T., Hu, B.Q. and Yang, S.Y. (2013): Distribution, enrichment and source of heavy metals in surface sediments of the eastern Beibu Bay, South China Sea. Marine Pollution Bulletin, 67, 137-145.

Du Laing, G., De Vos, R., Vandecasteele, B., Lesage, E., Tack, F.M. and Verloo, M.G. (2008): Effect of salinity on heavy metal mobility and availability in intertidal sediments of the Scheldt estuary. Estuarine, Coastal and Shelf Science, 77, 589-602.

Duan, L.Q., Song, J.M., Liang, X.M., Yin, M.L., Yuan, H.M., Li, X.G., Ren, C.Z., Zhou, B., Kang, X.M. and Yin, X.B. (2019): Dynamics and diagenesis of trace metals in sediments of the Changjiang Estuary. Science of the Total Environment, 675, 247-259.

Dzombak, D.A. and Morel, F.M.M. (1987): Adsorption of Inorganic Pollutants in Aquatic Systems. Journal of Hydraulic Engineering-Asce, 113, 430-475.

Ecoina (2002): Studija ekološke sanacije zaostalih sastojaka iz proizvodnje ferolegura i ugljeno grafitnih elektroda, Retrived from http://www.tef.hr/stranica/9/razgradnja-i-ekoloska-sanacija.html.

Egger, M., Lenstra, W., Jong, D., Meysman, F.J., Sapart, C.J., Van der Veen, C., Röckmann, T., Gonzalez, S. and Slomp, C.P. (2016): Rapid sediment accumulation results in high methane effluxes from coastal sediments. PloS one, 11, e0161609.

Eggleton, J. and Thomas, K.V. (2004): A review of factors affecting the release and bioavailability of contaminants during sediment disturbance events. Environment International, 30, 973-980.

Ehlers, L.J. and Luthy, R.G. (2003): Contaminant bioavailability in soil and sediment. Environmental Science & Technology, 37, 295a-302a.

Eklund, B., Elfström, M., Gallego, I., Bengtsson, B.-E. and Breitholtz, M. (2010): Biological and chemical characterization of harbour sediments from the Stockholm area. Journal of Soils and Sediments, 10, 127-141.

Elbaz-Poulichet, F., Guan, D.M. and Martin, J.-M. (1991): Trace metal behaviour in a highly stratified Mediterranean estuary: the Krka (Yugoslavia). Marine Chemistry, 32, 211-224.

Elbaz-Poulichet, F., Garnier, J.-M., Guan, D., Martin, J.-M. and Thomas, A. (1996): The conservative behaviour of trace metals (Cd, Cu, Ni and Pb) and As in the surface plume of stratified estauries: Example of the Rhône River (France). Estuarine, Coastal and Shelf Science, 42, 289-310.

Emerson, D. (2000): Microbial oxidation of Fe (II) and Mn (II) at circumneutral pH. In: Environmental Microbe-Metal Interactions, (Ed.), American Society of Microbiology, 31-52.

Emili, A., Acquavita, A., Covelli, S., Spada, L., Di Leo, A., Giandomenico, S. and Cardellicchio, N. (2016): Mobility of heavy metals from polluted sediments of a semi-enclosed basin: in situ benthic chamber experiments in Taranto's Mar Piccolo (Ionian Sea, Southern Italy). Environmental Science and Pollution Research, 23, 12582-12595.

Erickson, B.E. and Helz, G.R. (2000): Molybdenum (VI) speciation in sulfidic waters:: stability and lability of thiomolybdates. Geochimica Et Cosmochimica Acta, 64, 1149-1158.

Fairbanks, R.G. (1989): A 17,000-Year Glacio-Eustatic Sea-Level Record - Influence of Glacial Melting Rates on the Younger Dryas Event and Deep-Ocean Circulation. Nature, 342, 637-642.

Fairey, R., Roberts, C., Jacobi, M., Lamerdin, S., Clark, R., Downing, J., Long, E., Hunt, J., Anderson, B. and Newman, J. (1998): Assessment of sediment toxicity and chemical concentrations in the San Diego Bay region, California, USA. Environmental Toxicology and Chemistry: An International Journal, 17, 1570-1581.

Farley, K.J., Dzombak, D.A. and Morel, F.M.M. (1985): A Surface Precipitation Model for the Sorption of Cations on Metal-Oxides. Journal of Colloid and Interface Science, 106, 226-242.

Fdez-Ortiz de Vallejuelo, S., Arana, G., de Diego, A. and Madariaga, J.M. (2010): Risk assessment of trace elements in sediments: the case of the estuary of the Nerbioi–Ibaizabal River (Basque Country). Journal of Hazardous Materials, 181, 565-573.

Felja, I., Romić, M., Romić, D., Bakić, H., Pikelj, K. and Juračić, M. (2016): Application of empirical model to predict background metal concentration in mixed carbonate-alumosilicate sediment (Adriatic Sea, Croatia). Marine Pollution Bulletin, 106, 190-199.

Fiket, Ž., Pikelj, K., Ivanić, M., Barišić, D., Vdović, N., Dautović, J., Žigovečki Gobac, Ž., Mikac, N., Bermanec, V., Sondi, I. and Kniewald, G. (2017): Origin and composition of sediments in a highly stratified karstic estuary: An example of the Zrmanja River estuary (eastern Adriatic). Regional Studies in Marine Science, 16, 67-78.

Fiket, Ž., Ivanić, M., Turk, M.F., Mikac, N. and Kniewald, G. (2018): Distribution of trace elements in waters of the Zrmanja River estuary (eastern Adriatic coast, Croatia). Croatica Chemica Acta, 91, 29-42.

Fiket, Ž., Fiket, T., Ivanić, M., Mikac, N. and Kniewald, G. (2019): Pore water geochemistry and diagenesis of estuary sediments—an example of the Zrmanja River estuary (Adriatic coast, Croatia). Journal of Soils and Sediments, 19, 2048-2060.

Filgueiras, A., Lavilla, I. and Bendicho, C. (2002): Chemical sequential extraction for metal partitioning in environmental solid samples. Journal of Environmental Monitoring, 4, 823-857.

Froelich, P.N., Klinkhammer, G.P., Bender, M.L., Luedtke, N.A., Heath, G.R., Cullen, D., Dauphin, P., Hammond, D., Hartman, B. and Maynard, V. (1979): Early Oxidation of Organic-Matter in Pelagic Sediments of the Eastern Equatorial Atlantic - Suboxic Diagenesis. Geochimica Et Cosmochimica Acta, 43, 1075-1090.

Gagnon, C., Mucci, A. and Pelletier, E. (1996): Vertical distribution of dissolved sulphur species in coastal marine sediments. Marine Chemistry, 52, 195-209.

Gao, Y., Leermakers, M., Gabelle, C., Divis, P., Billon, G., Ouddane, B., Fischer, J.C., Wartel, M. and Baeyens, W. (2006): High-resolution profiles of trace metals in the pore waters of riverine sediment assessed by DET and DGT. Science of the Total Environment, 362, 266-277.

Gao, Y., Lesven, L., Gillan, D., Sabbe, K., Billon, G., De Galan, S., Elskens, M., Baeyens, W. and Leermakers, M. (2009): Geochemical behavior of trace elements in sub-tidal marine sediments of the Belgian coast. Marine Chemistry, 117, 88-96.

Gavriil, A. and Angelidis, M. (2006): Metal diagenesis in a shallow semi-enclosed marine system in the Aegean Sea, Greece. Estuarine, Coastal and Shelf Science, 70, 487-498.

Gill, G.A., Bloom, N.S., Cappellino, S., Driscoll, C.T., Dobbs, C., McShea, L., Mason, R. and Rudd, J.W.M. (1999): Sediment-water fluxes of mercury in Lavaca Bay, Texas. Environmental Science & Technology, 33, 663-669.

Gingele, F. and Dahmke, A. (1994): Discrete barite particles and barium as tracers of paleoproductivity in South Atlantic sediments. Paleoceanography, 9, 151-168.

Gingele, F., Zabel, M., Kasten, S., Bonn, W. and Nürnberg, C. (1999): Biogenic barium as a proxy for paleoproductivity: Methods and limitations of application. In: Use of Proxies in Paleoceanography, (Ed.), Springer, 345-364.

Giuffré de López Camelo, L., de Miguez, S.R. and Marbán, L. (1997): Heavy metals input with phosphate fertilizers used in Argentina. Science of the Total Environment, 204, 245-250.

Goldberg, S., Davis, J. and Hem, J. (1996): The surface chemistry of aluminum oxides and hydroxides. In: The environmental chemistry of aluminum, G. Sposito, (Ed.), Lewis Publishers, New York, 271-331.

Gonneea, M.E. and Paytan, A. (2006): Phase associations of barium in marine sediments. Marine Chemistry, 100, 124-135.

Gorny, J., Billon, G., Noiriel, C., Dumoulin, D., Lesven, L. and Made, B. (2016): Chromium behavior in aquatic environments: a review. Environmental Reviews, 24, 503-516.

Griffith, E.M. and Paytan, A. (2012a): Barite in the ocean–occurrence, geochemistry and palaeoceanographic applications. Sedimentology, 59, 1817-1835.

Griffith, E.M. and Paytan, A. (2012b): Barite in the ocean - occurrence, geochemistry and palaeoceanographic applications. Sedimentology, 59, 1817-1835.

Gržetić, Z., Precali, R., Degobbis, D. and Škrivanić, A. (1991): Nutrient enrichment and phytoplankton response in an Adriatic karstic estuary. Marine Chemistry, 32 (2–4), 313-331.

Guédron, S., Audry, S., Acha, D., Bouchet, S., Point, D., Condom, T., Heredia, C., Campillo, S., Baya, A. and Groleau, A. (2020): Diagenetic production, accumulation and sediment-water exchanges of methylmercury in contrasted sediment facies of Lake Titicaca (Bolivia). Science of the Total Environment, 138088.

Hadžija, O., Juračić, M., Luić, M., Tonković, M. and Jeričević, B. (1985): The carbohydrates in relation to mineralogic and granulometric composition of surface sediments in the Karst estuary (River Krka estuary, Yugoslavia). Estuarine, Coastal and Shelf Science, 21, 701-709.

Hammerschmidt, C.R. and Fitzgerald, W.F. (2008): Sediment-water exchange of methylmercury determined from shipboard benthic flux chambers. Marine Chemistry, 109, 86-97.

He, Y., Men, B., Yang, X.F. and Wang, D.S. (2015): Bioturbation/bioirrigation effect on thallium released from reservoir sediment by different organism types. Science of the Total Environment, 532, 617-624.

Helios-Rybicka, E. and Förstner, U. (1986): Effect of oxyhydrate coatings on the binding energy of metals by clay minerals. In: Sediments and water interactions, (Ed.), Springer, 381-385.

Hensen, C., Zabel, M. and Schulz, H.N. (2006): Benthic cycling of oxygen, nitrogen and phosphorus. In: Marine Geochemistry, (Ed.), Springer, 207-240.

Ho, H.H., Swennen, R., Cappuyns, V., Vassilieva, E., Van Gerven, T. and Tran, T.V. (2013): Speciation and Mobility of Selected Trace Metals (As, Cu, Mn, Pb and Zn) in Sediment with Depth in Cam River-Mouth, Haiphong, Vietnam. Aquatic Geochemistry, 19, 57-75.

Hoang, T.K., Probst, A., Orange, D., Gilbert, F., Elger, A., Kallerhoff, J., Laurent, F., Bassil, S., Duong, T.T. and Gerino, M. (2018): Bioturbation effects on bioaccumulation of cadmium in the wetland plant Typha latifolia: A nature-based experiment. Science of the Total Environment, 618, 1284-1297.

Hoffmann, M., Mikutta, C. and Kretzschmar, R. (2012): Bisulfide reaction with natural organic matter enhances arsenite sorption: insights from X-ray absorption spectroscopy. Environmental Science & Technology, 46, 11788-11797.

Honeyman, B.D. and Santschi, P.H. (1987): The Effect of Particle Concentration on the Rate of Thorium Adsorption. Abstracts of Papers of the American Chemical Society, 193, 61-Geoc.

Huang, Y.X., Zhang, D.F., Xu, Z.H., Yuan, S.J., Li, Y.S. and Wang, L. (2017): Effect of overlying water pH, dissolved oxygen and temperature on heavy metal release from river sediments under laboratory conditions. Archives of Environmental Protection, 43, 28-36.

Huerta-Diaz, M.A., Tessier, A. and Carignan, R. (1998): Geochemistry of trace metals associated with reduced sulfur in freshwater sediments. Applied Geochemistry, 13, 213-233.

Hulth, S., Aller, R.C., Canfield, D.E., Dalsgaard, T., Engstrom, P., Gilbert, F., Sundback, K. and Thamdrup, B. (2005): Nitrogen removal in marine environments: recent findings and future research challenges. Marine Chemistry, 94, 125-145.

Ingri, J., Pekka, L., Dauvalter, V., Rodushkin, I. and Peinerud, E. (2011): Manganese redox cycling in Lake Imandra: impact on nitrogen and the trace metal sediment record. Biogeosciences Discussions, 8.

Jokinen, S.A., Jilbert, T., Tiihonen-Filppula, R. and Koho, K. (2020): Terrestrial organic matter input drives sedimentary trace metal sequestration in a human-impacted boreal estuary. Science of the Total Environment, 717, 137047.

Jørgensen, B.B. (2006): Bacteria and Marine Biogeochemistry. In: Marine Geochemistry, (Ed.), Springer, 169-206.

Jørgensen, B.B. and Kasten, S. (2006): Sulfur cycling and methane oxidation. In: Marine geochemistry, (Ed.), Springer, 271-309.

Jørgensen, B.B., Findlay, A.J. and Pellerin, A. (2019): The Biogeochemical Sulfur Cycle of Marine Sediments. Frontiers in Microbiology, 10.

Joung, D. and Shiller, A.M. (2014): Dissolved barium behavior in Louisiana Shelf waters affected by the Mississippi/Atchafalaya River mixing zone. Geochimica Et Cosmochimica Acta, 141, 303-313.

Joung, D. and Shiller, A.M. (2016): Temporal and spatial variations of dissolved and colloidal trace elements in Louisiana Shelf waters. Marine Chemistry, 181, 25-43.

Juračić, M. (1987): Mehanizmi sedimentacije u nekim estuarijama Jadrana, svojstva recentnih sedimenata i suspendirane tvari. Disertacija, Sveučilište u Zagrebu, 103 pp.

Juračić, M. and Pravdić, V. (1991): The role of suspended matter in assessing the assimilative capacity case study of two estuaries in the Adriatic Sea. Chemistry and Ecology, 5, 241-248.

Juračić, M. and Prohić, E. (1991): Mineralogy, Sources of Particles, and Sedimentation in the Krka River Estuary(Croatia). Geološki Vjesnik, 44.

Jurina, I., Ivanić, M., Vdović, N., Troskot-Čorbić, T., Lojen, S., Mikac, N. and Sondi, I. (2015): Deposition of trace metals in sediments of the deltaic plain and adjacent coastal area (the Neretva River, Adriatic Sea). Journal of Geochemical Exploration, 157, 120-131.

Kalnejais, L.H., Martin, W.R. and Bothner, M.H. (2010): The release of dissolved nutrients and metals from coastal sediments due to resuspension. Marine Chemistry, 121, 224-235.

Kalnejais, L.H., Martin, W.R. and Bothner, M.H. (2015): Porewater dynamics of silver, lead and copper in coastal sediments and implications for benthic metal fluxes. Science of the Total Environment, 517, 178-194.

Kelderman, P. and Osman, A.A. (2007): Effect of redox potential on heavy metal binding forms in polluted canal sediments in Delft (The Netherlands). Water Research, 41, 4251-4261.

Kennish, M.J. (2016) Encyclopedia of Estuaries. Springer.

Komar, D., Dolenec, M., Lambaša Belak, Ž., Slavica Matešić, S., Lojen, S., Kniewald, G., Vrhovnik, P., Dolenec, T. and Rogan Šmuc, N. (2015): Geochemical characterization and environmental status of Makirina Bay sediments (northern Dalmatia, Republic of Croatia). Geologia Croatica, 68, 79-92.

Kongshaug, G., Bockman, O., Kaarstad, O. and Morka, H. (1992): Inputs of trace elements to soils and plants. The Norwegian Academy of Science and Letters, Proc. Chemical Climatology and Geomedical Problems, Nnrsk Hydro, Oslo, Norway, 1992, 185-216.

Krämer, M. and Cypionka, H. (1989): Sulfate formation via ATP sulfurylase in thiosulfate-and sulfite-disproportionating bacteria. Archives of Microbiology, 151, 232-237.

Kristensen, E. (2000): Organic matter diagenesis at the oxic/anoxic interface in coastal marine sediments, with emphasis on the role of burrowing animals. Hydrobiologia, 426, 1-24.

Kristensen, E., Penha-Lopes, G., Delefosse, M., Valdemarsen, T., Quintana, C.O. and Banta, G.T. (2012): What is bioturbation? The need for a precise definition for fauna in aquatic sciences. Marine Ecology Progress Series, 446, 285-302.

Kwokal, Ž., Frančišković-Bilinski, S., Bilinski, H. and Branica, M. (2002): A comparison of anthropogenic mercury pollution in Kaštela Bay (Croatia) with pristine estuaries in Ore (Sweden) and Krka (Croatia). Marine Pollution Bulletin, 44, 1152-1157.

Lagerström, M., Norling, M. and Eklund, B. (2016): Metal contamination at recreational boatyards linked to the use of antifouling paints—investigation of soil and sediment with a field portable XRF. Environmental Science and Pollution Research, 23, 10146-10157.

Legović, T., Gržetić, Z. and Žutić, V. (1991a): Subsurface temperature maximum in a stratified estuary. Marine Chemistry, 32, 163-170.

Legović, T., Petricioli, D. and Žutić, V. (1991b): Hypoxia in a pristine stratified estuary (Krka, Adriatic Sea). Marine Chemistry, 32, 347-359.

Legović, T., Žutić, V., Gržetić, Z., Cauwet, G., Precali, R. and Viličié, D. (1994): Eutrophication in the Krka estuary. Marine Chemistry, 46, 203-215.

Lerman, A. (1978): Chemical Exchange across Sediment-Water Interface. Annual Review of Earth and Planetary Sciences, 6, 281-303.

Lesven, L., Gao, Y., Billon, G., Leermakers, M., Ouddane, B., Fischer, J.C. and Baeyens, W. (2008): Early diagenetic processes aspects controlling the mobility of dissolved trace metals in three riverine sediment columns. Science of the Total Environment, 407, 447-459.

Liu, S., Wang, Z., Zhang, Y., Liu, Y., Yuan, W., Zhang, T., Liu, Y., Li, P., He, L. and Chen, J. (2019): Distribution and partitioning of heavy metals in large anthropogenically impacted river, the Pearl River, China. Acta Geochimica, 38, 216-231.

Llewellyn, O. (1972): Marine antifouling compositions and their applications. The Annals of occupational hygiene, 15, 393-396.

Long, E.R., MacDonald, D.D., Smith, S.L. and Calder, F.D. (1995): Incidence of adverse biological effects within ranges of chemical concentrations in marine and estuarine sediments. Environmental management, 19, 81-97.

Long, E.R., MacDonald, D.D., Severn, C.G. and Hong, C.B. (2000): Classifying probabilities of acute toxicity in marine sediments with empirically derived sediment quality guidelines. Environmental Toxicology and Chemistry: An International Journal, 19, 2598-2601.

Louis, Y., Garnier, C., Lenoble, V., Mounier, S., Cukrov, N., Omanović, D. and Pižeta, I. (2009): Kinetic and equilibrium studies of copper-dissolved organic matter complexation in water column of the stratified Krka River estuary (Croatia). Marine Chemistry, 114, 110-119.

Lourino-Cabana, B., Billon, G., Lesven, L., Sabbe, K., Gillan, D.-C., Gao, Y., Leermakers, M. and Baeyens, W. (2014): Monthly variation of trace metals in North Sea sediments. From experimental data to modeling calculations. Marine Pollution Bulletin, 87, 237-246.

Lyons, W.B. and Fitzgerald, W.F. (1980): Trace-Metal Fluxes to Nearshore Long-Island-Sound Sediments. Marine Pollution Bulletin, 11, 157-161.

Machado, A.A.S., Spencer, K., Kloas, W., Toffolon, M. and Zarfl, C. (2016): Metal fate and effects in estuaries: A review and conceptual model for better understanding of toxicity. Science of the Total Environment, 541, 268-281.

Magnall, J.M., Gleeson, S., Stern, R., Newton, R., Poulton, S. and Paradis, S. (2016): Open system sulphate reduction in a diagenetic environment–Isotopic analysis of barite (δ34S and δ18O) and pyrite (δ34S) from the Tom and Jason Late Devonian Zn–Pb–Ba deposits, Selwyn Basin, Canada. Geochimica Et Cosmochimica Acta, 180, 146-163.

Mamužić, P. (1971): Osnovna geološka karta SFRJ 1:100.000, list Šibenik K33–8. Institut za geološka istraživanja, Zagreb (1962-1965). Savezni geološki institut, Beograd.

Mandić, J., Tronczyński, J. and Kušpilić, G. (2018): Polycyclic aromatic hydrocarbons in surface sediments of the mid-Adriatic and along the Croatian coast: Levels, distributions and sources. Environmental Pollution, 242, 519-527.

Marcinek, S., Santinelli, C., Cindrić, A.-M., Evangelista, V., Gonnelli, M., Layglon, N., Mounier, S., Lenoble, V. and Omanović, D. (2020): Dissolved organic matter dynamics in the pristine Krka River estuary (Croatia). Marine Chemistry, 225, 103848.

Marcovecchio, J.E., Botté, S.E. and Severini, M.D.F. (2016): Distribution and behavior of zinc in estuarine environments: an overview on Bahía Blanca estuary (Argentina). Environmental Earth Sciences, 75, 1168.

Martinčić, D., Kwokal, Ž., Stoeppler, M. and Branica, M. (1989): Trace-Metals in Sediments from the Adriatic Sea. Science of the Total Environment, 84, 135-147.

Martinčić, D., Kwokal, Ž. and Branica, M. (1990): Distribution of Zinc, Lead, Cadmium and Copper between Different Size Fractions of Sediments .2. The Krka River Estuary and the Kornati-Islands (Central Adriatic Sea). Science of the Total Environment, 95, 217-225.

Martino, M. (2000): Complexation and particle-water interactions of nickel in estuaries. Dissertation, University of Plymouth, 223 pp.

McLean, J. and Bledsoe, B. (1992): Behavior of metals in soils. EPA Ground Water Issue. Environmental Protection Agency, Washington. EPA.

McManus, J., Berelson, W.M., Klinkhammer, G.P., Johnson, K.S., Coale, K.H., Anderson, R.F., Kumar, N., Burdige, D.J., Hammond, D.E., Brumsack, H.J., McCorkle, D.C. and Rushdi, A. (1998): Geochemistry of barium in marine sediments: Implications for its use as a paleoproxy. Geochimica Et Cosmochimica Acta, 62, 3453-3473.

Metzger, E., Simonucci, C., Viollier, E., Sarazin, G., Prevot, F., Elbaz-Poulichet, F., Seidel, J.L. and Jezequel, D. (2007a): Influence of diagenetic processes in Thau lagoon on cadmium behavior and benthic fluxes. Estuarine Coastal and Shelf Science, 72, 497-510.

Metzger, E., Simonucci, C., Viollier, E., Sarazin, G., Prevot, F. and Jezequel, D. (2007b): Benthic response to shellfish farming in Thau lagoon: Pore water signature. Estuarine Coastal and Shelf Science, 72, 406-419.

Michalopoulos, P. and Aller, R.C. (1995): Rapid clay mineral formation in Amazon delta sediments: reverse weathering and oceanic elemental cycles. Science, 270, 614-617.

Middelburg, J.J., Soetaert, K., Herman, P.M.J. and Heip, C.H.R. (1996): Denitrification in marine sediments: A model study. Global Biogeochemical Cycles, 10, 661-673.

Mikac, N., Kwokal, Ž., May, K. and Branica, M. (1989): Mercury Distribution in the Krka River Estuary (Eastern Adriatic Coast). Marine Chemistry, 28, 109-126.

Mikac, N., Kwokal, Ž., Martinčić, D. and Branica, M. (1996): Uptake of mercury species by transplanted mussels Mytilus galloprovincialis under estuarine conditions (Krka river estuary). Science of the Total Environment, 184, 173-182.

Mikac, N. and Kwokal, Ž. (1997): Distribution of mercury species in the water column of the stratified Krka River Estuary. Croatica Chemica Acta, 70, 271-288.

Mikac, N., Roje, V., Cukrov, N. and Foucher, D. (2006): Mercury in aquatic sediments and soils from Croatia. Arhiv za higijenu rada i toksikologiju, 57, 325.

Mikac, N., Roje, V., Dautović, J., Cukrov, N. and Kniewald, G. (2007): Raspodela metala i metaloida u sedimentu i vodi ušća rijeke Krke. Zbornik radova rijeka Krka i Nacionalni park „Krka, 823-838.

Mlakar, M., Fiket, Ž., Geček, S., Cukrov, N. and Cuculić, V. (2015): Marine lake as in situ laboratory for studies of organic matter influence on speciation and distribution of trace metals. Continental Shelf Research, 103, 1-11.

Montuori, P., Aurino, S., Garzonio, F., Nardone, A. and Triassi, M. (2016): Estimation of heavy metal loads from Tiber River to the Tyrrhenian Sea and environmental quality assessment. Environmental Science and Pollution Research, 23, 23694-23713.

Moore, W.S. and Shaw, T.J. (2008): Fluxes and behavior of radium isotopes, barium, and uranium in seven Southeastern US rivers and estuaries. Marine Chemistry, 108, 236-254.

Morford, J.L. and Emerson, S. (1999): The geochemistry of redox sensitive trace metals in sediments. Geochimica Et Cosmochimica Acta, 63, 1735-1750.

Morse, J.W. and Luther, G.W. (1999): Chemical influences on trace metal-sulfide interactions in anoxic sediments. Geochimica Et Cosmochimica Acta, 63, 3373-3378.

Muller, G. (1979): Schwermetalle in den sedimenten des Rheins-Veranderungen seit. Umschav, 79, 133-149.

Murphy, J. and Riley, J.P. (1962): A modified single solution method for the determination of phosphate in natural waters. Analytica Chimica Acta, 27, 31-36.

Murphy, M.J., von Strandmann, P.A.P., Porcelli, D. and Ingri, J. (2014): Li isotope behaviour in the low salinity zone during estuarine mixing. Procedia Earth and Planetary Science, 10, 204-207.

Murray, J.W. and Dillard, J.G. (1979): The oxidation of cobalt (II) adsorbed on manganese dioxide. Geochimica Et Cosmochimica Acta, 43, 781-787.

Nabelkova, J. and Kominkova, D. (2012): Trace metals in the bed sediment of small urban streams. The Open Environmental & Biological Monitoring Journal, 5.

Nadilo, B. (2003): Kanalizacijski sustav grada Šibenika. Građevinar, 55, 599-603.

Nia, Y. (2011): Utilisation d'un échantillonneur passif (DGT) pour l'évaluation de la remobilisation des métaux dans les sédiments : expérimentation et modélisation. Thèse, l'Université Paul-Cézanne, 174 pp.

NRC (2003) Bioavailability of contaminants in soils and sediments: processes, tools, and applications. The National Academies Press, Washington, DC, 432 pp.

OECD (2010): Environmental and climate change issues in the shipbuilding industry, Organisation for Economic Co-operation and Development.

Omanović, D., Kwokal, Ž., Goodwin, A., Lawrence, A., Banks, C., Compton, R. and Komorsky-Lovrić, Š. (2006): Trace metal detection in Šibenik Bay, Croatia: cadmium, lead and copper with anodic stripping voltammetry and manganese via sonoelectrochemistry. A case study. Journal of the Iranian Chemical Society, 3, 128-139.

Oreščanin, V., Barišić, D., Mikelić, L., Lovrenčić, I., Rubčić, M., Rožmarić-Macefat, M. and Lulić, S. (2004): Environmental contamination assessment of the surroundings of the ex-Šibenik's ferro-manganese Smelter, Croatia. Journal of Environmental Science and Health Part a-Toxic/Hazardous Substances & Environmental Engineering, 39, 2493-2506.

Oreščanin, V., Mikelić, I.L., Mikelić, L., Rubčić, M. and Lulić, S. (2009): The influence of past metallurgical activity on the concentration of heavy metals in the soil/grass system in Šibenik (Croatia). International journal of environment and pollution, 37, 437-449.

Pađan, J., Marcinek, S., Cindrić, A.-M., Layglon, N., Lenoble, V., Salaün, P., Garnier, C. and Omanović, D. (2019): Improved voltammetric methodology for chromium redox speciation in estuarine waters. Analytica Chimica Acta, 1089, 40-47.

Pađan, J., Marcinek, S., Cindrić, A.-M., Layglon, N., Garnier, C., Salaün, P., Cobelo-García, A. and Omanović, D. (2020): Determination of sub-picomolar levels of platinum in the pristine Krka River estuary (Croatia) using improved voltammetric methodology. Environmental Chemistry, 17, 77-84.

Paradas, W.C. and Amado Filho, G.M. (2007): Are metals of antifouling paints transferred to marine biota? Brazilian Journal of Oceanography, 55, 51-56.

Pavoni, E., Crosera, M., Petranich, E., Adami, G., Faganeli, J. and Covelli, S. (2020): Partitioning and mixing behaviour of trace elements at the Isonzo/Soča River mouth (Gulf of Trieste, northern Adriatic Sea). Marine Chemistry, 103800.

Pedrosa-Pamies, R., Parinos, C., Sanchez-Vidal, A., Gogou, A., Calafat, A., Canals, M., Bouloubassi, I. and Lampadariou, N. (2015): Composition and sources of sedimentary organic matter in the deep eastern Mediterranean Sea. Biogeosciences, 12, 7379-7402.

Peng, J.F., Song, Y.H., Yuan, P., Cui, X.Y. and Qiu, G.L. (2009): The remediation of heavy metals contaminated sediment. Journal of Hazardous Materials, 161, 633-640.

Pennafirme, S., Lima, I., Bitencourt, J., Crapez, M. and Lopes, R. (2015): Organic matter biodegradation by bacterial consortium under metal stress. In: Biodegradation and Bioremediation of Polluted Systems-New Advances and Technologies, (Ed.), InTech: Ch Rijeka, 04.

Petranich, E., Croce, S., Crosera, M., Pavoni, E., Faganeli, J., Adami, G. and Covelli, S. (2018): Mobility of metal (loid) s at the sediment-water interface in two tourist port areas of the Gulf of Trieste (northern Adriatic Sea). Environmental Science and Pollution Research, 25, 26887-26902.

Plavšić, M., Kwokal, Ž., Strmečki, S., Peharec, Ž., Omanović, D. and Branica, M. (2009): Determination of the copper complexing ligands in the Krka river estuary. Fresenius Environ. Bull, 18, 327-334.

Prajith, A., Rao, V.P. and Chakraborty, P. (2016): Distribution, provenance and early diagenesis of major and trace metals in sediment cores from the Mandovi estuary, western India. Estuarine, Coastal and Shelf Science, 170, 173-185.

Prohić, E. (1984): Raspodjela elemenata u tragovima u recentnim sedimentima estuarija Krke. Disertacija, Sveučilište u Zagrebu, Zagreb, 200 pp.

Prohić, E. and Kniewald, G. (1987): Heavy-Metal Distribution in Recent Sediments of the Krka River Estuary - an Example of Sequential Extraction Analysis. Marine Chemistry, 22, 279-297.

Prohić, E. and Juračić, M. (1989): Heavy-Metals in Sediments - Problems Concerning Determination of the Anthropogenic Influence - Study in the Krka River Estuary, Eastern Adriatic Coast, Yugoslavia. Environmental Geology and Water Sciences, 13, 145-151.

Rahman, A. and Karim, M.M. (2015): Green shipbuilding and recycling: Issues and Challenges. International Journal of Environmental Science and Development, 6, 838.

Raos, N. (2018): Povijest proizvodnje kalcijeva karbida u Hrvatskoj (1897.–1945.). Kemija u industriji: Časopis kemičara i kemijskih inženjera Hrvatske, 67, 235-240.

Rasmussen, P.E. (1994): Current methods of estimating atmospheric mercury fluxes in remote areas. Environmental Science & Technology, 28, 2233-2241.

Reeder, R.J., Schoonen, M.A. and Lanzirotti, A. (2006): Metal speciation and its role in bioaccessibility and bioavailability. Reviews in Mineralogy and Geochemistry, 64, 59-113.

Regnier, P. and Wollast, R. (1993): Distribution of trace metals in suspended matter of the Scheldt estuary. Marine Chemistry, 43, 3-19.

Remaili, T.M., Simpson, S.L., Amato, E.D., Spadaro, D.A., Jarolimek, C.V. and Jolley, D.F. (2016): The impact of sediment bioturbation by secondary organisms on metal bioavailability, bioaccumulation and toxicity to target organisms in benthic bioassays: Implications for sediment quality assessment. Environmental Pollution, 208, 590-599.

Remaili, T.M., Yin, N.Y., Bennett, W.W., Simpson, S.L., Jolley, D.F. and Welsh, D.T. (2018): Contrasting effects of bioturbation on metal toxicity of contaminated sediments results in misleading interpretation of the AVS-SEM metal-sulfide paradigm. Environmental Science-Processes & Impacts, 20, 1285-1296.

Riba, I., Garcia-Luque, E., Blasco, J. and Delvalls, T.A. (2003): Bioavailability of heavy metals bound to estuarine sediments as a function of pH and salinity values. Chemical Speciation and Bioavailability, 15, 101-114.

Ridgway, J. and Shimmield, G. (2002): Estuaries as repositories of historical contamination and their impact on shelf seas. Estuarine Coastal and Shelf Science, 55, 903-928.

Rigaud, S., Radakovitch, O., Couture, R.M., Deflandre, B., Cossa, D., Garnier, C. and Garnier, J.M. (2013): Mobility and fluxes of trace elements and nutrients at the sediment-water interface of a lagoon under contrasting water column oxygenation conditions. Applied Geochemistry, 31, 35-51.

Rivera-Duarte, I. and Russell Flegal, A. (1997): Porewater gradients and diffusive benthic fluxes of Co, Ni, Cu, Zn, and Cd in San Francisco Bay. Croatica Chemica Acta, 70, 389-417.

Robbins, J.A. (1978): Geochemical and geophysical applications of radioactive lead. In: Biogeochemistry of Lead in the Environment, J.O. Nriagu, (Ed.), Elsevier Scientific, Amsterdam, 285-393.

Rosales, R.M., Faz, A., Gómez-Garrido, M., Muñoz, M.A., Murcia, F.J., González, V. and Acosta, J.A. (2017): Geochemical speciation of chromium related to sediments properties in the riverbed contaminated by tannery effluents. Journal of Soils and Sediments, 17, 1437-1448.

Rosenthal, Y., Lam, P., Boyle, E.A. and Thomson, J. (1995): Authigenic Cadmium Enrichments in Suboxic Sediments - Precipitation and Postdepositional Mobility. Earth and Planetary Science Letters, 132, 99-111.

Ross, S.M. (1994): Retention, transformation and mobility of toxic metals in soils. In: Toxic metals in soil-plant systems, S.M. ROSS, (Ed.), Wiley, New York, 63-152.

Rullkötter, J. (2006): Organic matter: the driving force for early diagenesis. In: Marine geochemistry, (Ed.), Springer, 125-168.

Sakellari, A., Plavšić, M., Karavoltsos, S., Dassenakis, M. and Scoullos, M. (2011): Assessment of copper, cadmium and zinc remobilization in Mediterranean marine coastal sediments. Estuarine Coastal and Shelf Science, 91, 1-12.

Santos-Echeandia, J., Prego, R., Cobelo-Garcia, A. and Millward, G.E. (2009): Porewater geochemistry in a Galician Ria (NW Iberian Peninsula): Implications for benthic fluxes of dissolved trace elements (Co, Cu, Ni, Pb, V, Zn). Marine Chemistry, 117, 77-87.

Santschi, P., Hohener, P., Benoit, G. and Buchholtztenbrink, M. (1990): Chemical Processes at the Sediment Water Interface. Marine Chemistry, 30, 269-315.

Sarı, E., Ünlü, S., Apak, R., Balcı, N. and Koldemir, B. (2013): Mercury distribution in the sediments of ambarlı port area, Sea of Marmara (Turkey). Chemistry and Ecology, 29, 28-43.

Saulnier, I. and Mucci, A. (2000): Trace metal remobilization following the resuspension of estuarine sediments: Saguenay Fjord, Canada. Applied Geochemistry, 15, 191-210.

Schaller, J. (2014): Bioturbation/bioirrigation by Chironomus plumosus as main factor controlling elemental remobilization from aquatic sediments? Chemosphere, 107, 336-343.

Schenau, S., Prins, M., De Lange, G. and Monnin, C. (2001): Barium accumulation in the Arabian Sea: Controls on barite preservation in marine sediments. Geochimica Et Cosmochimica Acta, 65, 1545-1556.

Schipper, L.A., Sparling, G.P., Fisk, L., Dodd, M., Power, I. and Littler, R.A. (2011): Rates of accumulation of cadmium and uranium in a New Zealand hill farm soil as a result of long-term use of phosphate fertilizer. Agriculture, ecosystems & environment, 144, 95-101.

Schnug, E. and Haneklaus, N. (2014): Uranium, the hidden treasure in phosphates. Procedia Engineering, 83, 265-269.

Scholz, F., Hensen, C., De Lange, G.J., Haeckel, M., Liebetrau, V., Meixner, A., Reitz, A. and Romer, R.L. (2010): Lithium isotope geochemistry of marine pore waters–insights from cold seep fluids. Geochimica Et Cosmochimica Acta, 74, 3459-3475.

Scholz, F., Hensen, C., Noffke, A., Rohde, A., Liebetrau, V. and Wallmann, K. (2011): Early diagenesis of redox-sensitive trace metals in the Peru upwelling area–response to ENSO-related oxygen fluctuations in the water column. Geochimica Et Cosmochimica Acta, 75, 7257-7276.

Schulz, H.D. (2006): Quantification of early diagenesis: dissolved constituents in pore water and signals in the solid phase. In: Marine geochemistry, (Ed.), Springer, 73-124.

Sedeño-Díaz, J.E., López-López, E., Mendoza-Martínez, E., Rodríguez-Romero, A.J. and Morales-García, S.S. (2020): Distribution Coefficient and Metal Pollution Index in Water and Sediments: Proposal of a New Index for Ecological Risk Assessment of Metals. Water, 12, 29.

Seitzinger, S.P. (1988): Denitrification in Fresh-Water and Coastal Marine Ecosystems - Ecological and Geochemical Significance. Limnology and Oceanography, 33, 702-724.

Sempéré, R. and Cauwet, G. (1995): Occurrence of organic colloids in the stratified estuary of the Krka River (Croatia). Estuarine, Coastal and Shelf Science, 40, 105-114.

Shaw, T.J., Gieskes, J.M. and Jahnke, R.A. (1990): Early diagenesis in differing depositional environments: the response of transition metals in pore water. Geochimica Et Cosmochimica Acta, 54, 1233-1246.

Shepard, F.P. (1954): Nomenclature based on sand-silt-clay ratios. Journal of sedimentary Research, 24, 151-158.

Shull, D.H. (2009): Bioturbation. Encyclopedia of Ocean Sciences, 220, 395-400.

Silburn, B., Kroger, S., Parker, E.R., Sivyer, D.B., Hicks, N., Powell, C.F., Johnson, M. and Greenwood, N. (2017): Benthic pH gradients across a range of shelf sea sediment types linked to sediment characteristics and seasonal variability. Biogeochemistry, 135, 69-88.

Singh, N. and Turner, A. (2009): Leaching of copper and zinc from spent antifouling paint particles. Environmental Pollution, 157, 371-376.

Sitte, J., Akob, D.M., Kaufmann, C., Finster, K., Banerjee, D., Burkhardt, E.-M., Kostka, J.E., Scheinost, A.C., Büchel, G. and Küsel, K. (2010): Microbial links between sulfate reduction and metal retention in uranium-and heavy metal-contaminated soil. Applied and Environmental Microbiology, 76, 3143-3152.

Smith, K.S. (1999): Metal sorption on mineral surfaces: an overview with examples relating to mineral deposits. The Environmental Geochemistry of Mineral Deposits. Part B: Case Studies and Research Topics, 6, 161-182.

Soetaert, K., Hofmann, A.F., Middelburg, J.J., Meysman, F.J.R. and Greenwood, J. (2007): The effect of biogeochemical processes on pH. Marine Chemistry, 105, 30-51.

Sondi, I., Mikac, N., Vdović, N., Ivanić, M., Furdek, M. and Škapin, S.D. (2017): Geochemistry of recent aragonite-rich sediments in Mediterranean karstic marine lakes: Trace elements as pollution and palaeoredox proxies and indicators of authigenic mineral formation. Chemosphere, 168, 786-797.

Song, Z., Li, P., Ding, L., Li, Z., Zhu, W., He, T. and Feng, X. (2018): Environmental mercury pollution by an abandoned chlor-alkali plant in Southwest China. Journal of Geochemical Exploration, 194, 81-87.

Sposito, G. (1984) The surface chemistry of soils. Oxford university press, 234 pp.

Sposito, G. (1987): Distinguishing adsorption from surface precipitation. In: Geochemical Processes at Mineral Surfaces, J. Davis &K. Hayes, (Ed.), ACS Publications, 217-228.

Stoffyn-Egli, P. (1982a): Conservative behaviour of dissolved lithium in estuarine waters. ECSS, 14, 577-587.

Stoffyn-Egli, P. (1982b): Dissolved aluminium in interstitial waters of recent terrigenous marine sediments from the North Atlantic Ocean. Geochimica Et Cosmochimica Acta, 46, 1345-1352.

Storms, M.A., Natland, J.H. et al**.** (1991): Proceedings of the Ocean Drilling Program, Initial Reports, Vol. 132.

Strady, E., Blanc, G., Schäfer, J., Coynel, A. and Dabrin, A. (2009): Dissolved uranium, vanadium and molybdenum behaviours during contrasting freshwater discharges in the Gironde Estuary (SW France). Estuarine, Coastal and Shelf Science, 83, 550-560.

Stumm, W. (1992) Processes at the Mineral-water and Particle-water Interfaces in Natural Systems, pp. 448. Wiley New York.

Stumm, W. and Morgan, J.J. (1970) Aquatic chemistry; an introduction emphasizing chemical equilibria in natural waters. Wiley-Interscience, New York, 583 pp.

Stumm, W. and Morgan, J. (1996) Aquatic Chemistry–chemical equilibria and rates in natural waters 3rd edition. Wiley-Interscience, New York.

Sunda, W.G. and Kieber, D.J. (1994): Oxidation of humic substances by manganese oxides yields low-molecular-weight organic substrates. Nature, 367, 62-64.

Sundby, B. (2006): Transient state diagenesis in continental margin muds. Marine Chemistry, 102, 2-12.

Surić, M. (2005): Submerged Karst - Dead or Alive? Examples from the Eastern Adriatic Coast (Croatia). Geoadria, 10, 5-19.

Sutherland, R. (2000): Bed sediment-associated trace metals in an urban stream, Oahu, Hawaii. Environmental geology, 39, 611-627.

Svensen, C., Viličić, D., Wassmann, P., Arashkevich, E. and Ratkova, T. (2007): Plankton distribution and vertical flux of biogenic matter during high summer stratification in the Krka estuary (Eastern Adriatic). Estuarine, Coastal and Shelf Science, 71, 381–390.

Svetličić, V., Žutić, V. and Tomaić, J. (1991): Estuarine transformation of organic matter: single coalescence events of estuarine surface active particles. Marine Chemistry, 32, 253-267.

Šurija, B. and Branica, M. (1995): Distribution of Cd, Pb, Cu and Zn in carbonate sediments from the Krka river estuary obtained by sequential extraction. Science of the Total Environment, 170, 101-118.

Tahir, N.M., Suratman, S., Shazili, N.A.M., Ariffin, M.M., Amin, M.S.M., Ariff, N.F.M.N.I. and Sulaiman, W.N.H.W. (2008): Behaviour of water quality parameters during ebb tide in Dungun river estuary, Terengganu. Journal of Sustainability Science and Management, 3, 1-10.

Tan, W.-f., Lu, S.-j., Liu, F., Feng, X.-h., He, J.-z. and Koopal, L.K. (2008): Determination of the point-of-zero charge of manganese oxides with different methods including an improved salt titration method. Soil Science, 173, 277-286.

Tankere-Muller, S., Zhang, H., Davison, W., Finke, N., Larsen, O., Stahl, H. and Glud, R.N. (2007): Fine scale remobilisation of Fe, Mn, Co, Ni, Cu and Cd in contaminated marine sediment. Marine Chemistry, 106, 192-207.

Tapia, J. and Audry, S. (2013): Control of early diagenesis processes on trace metal (Cu, Zn, Cd, Pb and U) and metalloid (As, Sb) behaviors in mining-and smelting-impacted lacustrine environments of the Bolivian Altiplano. Applied Geochemistry, 31, 60-78.

Tessier, A. and Campbell, P.G.C. (1987): Partitioning of Trace-Metals in Sediments - Relationships with Bioavailability. Hydrobiologia, 149, 43-52.

Tessier, E., Garnier, C., Mullot, J.-U., Lenoble, V., Arnaud, M., Raynaud, M. and Mounier, S. (2011): Study of the spatial and historical distribution of sediment inorganic contamination in the Toulon bay (France). Marine Pollution Bulletin, 62, 2075-2086.

Thamdrup, B., Glud, R.N. and Hansen, J.W. (1994): Manganese Oxidation and in-Situ Manganese Fluxes from a Coastal Sediment. Geochimica Et Cosmochimica Acta, 58, 2563-2570.

Theng, B.K.G. (1979) Formation and Properties of Clay-Polymer Complexes. Elsevier Science, 359 pp.

Truesdale, V.W. and Smith, C.J. (1975): The formation of molybdosilicic acids from mixed solutions of molybdate and silicate. Analyst, 100, 203-212.

Turner, A. (2010): Marine pollution from antifouling paint particles. Marine Pollution Bulletin, 60, 159-171.

Ullman, W.J. and Sandstrom, M.W. (1987): Dissolved Nutrient Fluxes from the Nearshore Sediments of Bowling Green Bay, Central Great-Barrier-Reef Lagoon (Australia). Estuarine Coastal and Shelf Science, 24, 289-303.

UNEP (2013): Global Mercury Assessment 2013: Sources, Emissions, Releases and Environmental Transport, UNEP Chemicals Branch, Geneva, Switzerland.

Valdes, J., Vargas, G., Sifeddine, A., Ortlieb, L. and Guinez, M. (2005): Distribution and enrichment evaluation of heavy metals in Mejillones Bay (23 degrees S), Northern Chile: Geochemical and statistical approach. Marine Pollution Bulletin, 50, 1558-1568.

Valero, A., Umbría-Salinas, K., Wallner-Kersanach, M., de Andrade, C.F., Yabe, M.J.S., Contreira-Pereira, L., Wasserman, J.C., Kuroshima, K.N. and Zhang, H. (2020): Potential availability of trace metals in sediments in southeastern and southern Brazilian shipyard areas

using the DGT technique and chemical extraction methods. Science of the Total Environment, 710, 136216.

van den Berg, G.A., Loch, J.P.G., van der Heijdt, L.M. and Zwolsman, J.J.G. (2000): Redox processes in recent sediments of the river Meuse, The Netherlands. Biogeochemistry, 48, 217-235.

Verbeeck, M., Salaets, P. and Smolders, E. (2020): Trace element concentrations in mineral phosphate fertilizers used in Europe: A balanced survey. Science of the Total Environment, 712, 136419.

Vesper, D.J. (2019): Contamination of cave waters by heavy metals. In: Encyclopedia of caves, (Ed.), Elsevier, 320-325.

Vidal-Dura, A., Burke, I.T., Stewart, D.I. and Mortimer, R.J.G. (2018): Reoxidation of estuarine sediments during simulated resuspension events: Effects on nutrient and trace metal mobilisation. Estuarine Coastal and Shelf Science, 207, 40-55.

Violante, A., Cozzolino, V., Perelomov, L., Caporale, A. and Pigna, M. (2010): Mobility and bioavailability of heavy metals and metalloids in soil environments. Journal of soil science and plant nutrition, 10, 268-292.

Vojvodić, V. and Ćosović, B. (1992): The hydrophobic fraction of organic matter in the Krka River Estuary. Marine Chemistry, 39, 251-267.

von der Heyden, B.P. and Roychoudhury, A.N. (2015): Application, Chemical Interaction and Fate of Iron Minerals in Polluted Sediment and Soils. Current Pollution Reports, 1, 265-279.

von Strandmann, P.A.P., James, R.H., van Calsteren, P., Gíslason, S.R. and Burton, K.W. (2008): Lithium, magnesium and uranium isotope behaviour in the estuarine environment of basaltic islands. Earth and Planetary Science Letters, 274, 462-471.

Wang, F. and Tessier, A. (2009): Zero-valent sulfur and metal speciation in sediment porewaters of freshwater lakes. Environmental Science & Technology, 43, 7252-7257.

Wang, L.-F., Yang, L.-Y., Kong, L.-H., Li, S., Zhu, J.-R. and Wang, Y.-Q. (2014): Spatial distribution, source identification and pollution assessment of metal content in the surface sediments of Nansi Lake, China. Journal of Geochemical Exploration, 140, 87-95.

Wang, W.H. and Wang, W.X. (2017): Trace metal behavior in sediments of Jiulong River Estuary and implication for benthic exchange fluxes. Environmental Pollution, 225, 598-609.

Warnken, K.W., Gill, G.A., Griffin, L.L. and Santschi, P.H. (2001): Sediment-water exchange of Mn, Fe, Ni and Zn in Galveston Bay, Texas. Marine Chemistry, 73, 215-231.

Warren, L.A. and Haack, E.A. (2001): Biogeochemical controls on metal behaviour in freshwater environments. Earth-Science Reviews, 54, 261-320.

Weiner, E.R. (2008) Applications of environmental aquatic chemistry: a practical guide. CRC Press, 456 pp.

Wentworth, C.K. (1922): A scale of grade and class terms for clastic sediments. The journal of geology, 30, 377-392.

Whitby, L.M. and Schnitzer, M. (1978): Humic and Fulvic Acids in Sediments and Soils of Agricultural Watersheds. Canadian Journal of Soil Science, 58, 167-178.

Williams, M.R., Millward, G.E., Nimmo, M. and Fones, G. (1998): Fluxes of Cu, Pb and Mn to the northeastern Irish Sea: The importance of sedimental and atmospheric inputs. Marine Pollution Bulletin, 36, 366-375.

Windom, H., Smith, R., Niencheski, F. and Alexander, C. (2000): Uranium in rivers and estuaries of globally diverse, smaller watersheds. Marine Chemistry, 68, 307-321.

Xie, M.W., Simpson, S.L. and Wang, W.X. (2019): Bioturbation effects on metal release from contaminated sediments are metal-dependent. Environmental Pollution, 250, 87-96.

Yang, J., Zhang, B., Peng, X., Wang, H., Li, Z., Cai, W. and Fang, H. (2014): Sediment Quality Assessment for Heavy Metal Contamination in the Dongzhai Harbor (Hainan Island, China) with Pollution Indice Approach. The Open Chemical Engineering Journal, 8.

Yuan-Hui, L. and Gregory, S. (1974): Diffusion of ions in sea water and in deep-sea sediments. Geochimica Et Cosmochimica Acta, 38, 703-714.

Zhang, C., Yu, Z.G., Zeng, G.M., Jiang, M., Yang, Z.Z., Cui, F., Zhu, M.Y., Shen, L.Q. and Hu, L. (2014): Effects of sediment geochemical properties on heavy metal bioavailability. Environment International, 73, 270-281.

Zheng, Y., Anderson, R.F., Van Geen, A. and Kuwabara, J. (2000): Authigenic molybdenum formation in marine sediments: a link to pore water sulfide in the Santa Barbara Basin. Geochimica Et Cosmochimica Acta, 64, 4165-4178.

Zheng, Y., Anderson, R.F., van Geen, A. and Fleisher, M.Q. (2002): Remobilization of authigenic uranium in marine sediments by bioturbation. Geochimica Et Cosmochimica Acta, 66, 1759-1772.

Zhong, H. and Wang, W.X. (2006): Influences of aging on the bioavailability of sediment-bound Cd and Zn to deposit-feeding sipunculans and soldier crabs. Environmental Toxicology and Chemistry: An International Journal, 25, 2775-2780.

Zhong, H., Kraemer, L. and Evans, D. (2012): Effects of aging on the digestive solubilization of Cu from sediments. Environmental Pollution, 164, 195-203.

Zhu, X.L., Shan, B.Q., Tang, W.Z., Li, S.S. and Rong, N. (2016): Distributions, fluxes, and toxicities of heavy metals in sediment pore water from tributaries of the Ziya River system, northern China. Environmental Science and Pollution Research, 23, 5516-5526.

Zindorf, M., März, C., Wagner, T., Gulick, S.P., Strauss, H., Benowitz, J., Jaeger, J., Schnetger, B., Childress, L. and LeVay, L. (2019): Deep Sulfate-Methane-Transition and sediment diagenesis in the Gulf of Alaska (IODP Site U1417). Marine Geology, 417, 105986.

Žutić, V. and Legović, T. (1987): A film of organic matter at the fresh-water/sea-water interface of an estuary. Nature, 328, 612-614.

Internet References

Internet Reference 1: TEF d.d. Povijest TEF-a - stup šibenskog industrijskog razvoja u 20. stoljeću. Tef. http://tef.hr/stranica/5/povijest-tef-a-stup-sibenskog-industrijskog-razvoja-u-20-stoljecu.html. Last accessed 6 August 2020.

Internet Reference 2: TEF d.d. TEF danas - između ekološke sanacije, rješavanja dužničko-vjerovničkih odnosa i valorizacije dijelova prostora. Tef. http://tef.hr/stranica/5/povijest-tef-a-stup-sibenskog-industrijskog-razvoja-u-20-stoljecu.html. Last accessed 6 August 2020.

Internet Reference 3: Port of Šibenik Authority. History of the Port of Šibenik. Portauthority-sibenik. https://www.portauthority-sibenik.hr/en/port_of_sibenik/povijest.asp. Last accessed 7 August 2020.

Internet Reference 4: Leksikografski zavod Miroslav Krleža. (9 November 2016, updated 30 November 2019). NCP − Remontno brodogradilište Šibenik d. o. o. Tehnika.lzmk. https://tehnika.lzmk.hr/ncp-%E2%88%92-remontno-brodogradiliste-sibenik/. Last accessed 7 August 2020.

Internet References 5: D-Marin. Mandalina. D-marin. https://www.d-marin.com/hr/marine/mandalina/. Last accessed 7 August 2020.

9. APPENDICES

9. APPENDICES

Appendix 1. Chemical composition of the 40 surface sediment samples (0-5) (K01-K40) from the Krka River estuary. Values are expressed in μg g^{-1}.

	K01	K02	K03	K04	K05	K06	K07	K08	K09	K10	K11	K12	K13	K14	K15	K16	K17	K18	K19	K20
Li	27.6	25.9	32.4	27.3	41.0	51.4	60.7	38.0	58.5	64.0	25.8	63.2	37.2	69.0	56.3	41.4	46.1	60.5	71.3	50.9
Be	0.924	0.883	1.15	0.869	1.24	1.0	1.80	1.69	2.17	1.94	0.780	1.82	1.12	2.13	2.31	1.53	1.72	1.90	2.23	1.97
Rb	34.8	35.4	46.5	30.1	44.1	55.4	68.2	68.4	90.2	72.5	27.5	69.2	41.7	80.7	88.1	60.2	59.8	69.5	83.3	57.1
Mo	2.31	2.71	3.72	1.46	1.31	1.27	1.74	2.67	2.56	0.904	0.701	1.42	0.895	1.19	1.38	1.10	2.98	1.33	1.56	3.37
Ag	0.203	0.181	0.229	0.188	0.210	0.245	0.244	0.253	0.298	0.262	0.161	0.283	0.217	0.352	0.415	0.268	0.352	0.377	0.432	0.706
Cd	0.468	0.471	0.530	0.434	0.444	0.426	0.433	0.532	0.426	0.369	0.203	0.383	0.255	0.382	0.383	0.280	0.441	0.384	0.452	0.960
Sn	2.80	3.54	3.17	2.77	2.77	2.71	3.08	2.36	3.19	4.28	2.38	3.98	2.77	5.55	6.65	3.23	19.79	5.62	6.74	9.80
Sb	0.264	0.331	0.301	0.350	0.564	0.436	0.593	0.335	0.512	0.582	0.348	0.426	0.384	0.454	0.436	0.336	0.547	0.512	0.684	1.64
Cs	3.12	3.04	3.88	2.79	4.20	4.98	6.21	5.08	7.13	6.54	2.49	6.06	3.68	7.16	6.64	4.69	5.00	6.10	7.18	5.16
Tl	0.395	0.421	0.554	0.425	0.488	0.500	0.703	0.688	0.821	0.702	0.316	0.657	0.409	0.818	0.834	0.631	0.676	0.707	0.819	0.716
Pb	18.0	18.0	23.6	21.7	29.8	35.0	38.5	19.9	30.4	47.2	24.5	52.1	38.4	82.3	78.3	45.8	64.3	83.3	117	665
Bi	0.250	0.241	0.328	0.223	0.284	0.291	0.394	0.282	0.377	0.523	0.221	0.513	0.386	0.984	0.709	0.383	0.658	1.04	1.66	3.80
U	2.47	2.40	2.19	2.19	2.05	2.09	2.23	2.66	2.55	1.67	1.83	2.65	1.94	2.22	2.42	2.62	3.50	2.45	2.49	3.69
Al	21666	21025	27130	18939	27948	33003	40700	36247	49234	43109	16948	41421	25733	49204	50933	33211	38883	44543	52861	38615
Ti	806	708	1002	696	856	1058	1207	1282	1814	1263	525	1352	872	1610	1911	1340	1555	1499	1733	1322
V	50.6	50.0	65.6	43.9	56.7	67.3	80.3	80.8	108	76.0	35.1	77.2	49.4	87.4	102	70.6	80.1	77.7	92.4	89.2
Cr	43.0	43.7	56.9	38.3	49.7	56.5	69.2	72.8	92.5	72.6	30.1	69.0	44.7	83.8	94.8	59.6	70.4	77.2	91.6	88.1
Mn	128	147	195	184	336	329	478	166	467	752	501	686	584	1014	329	261	454	1130	1689	32038
Fe	11211	11239	14938	10016	15090	17185	21074	21080	27382	22569	10074	21613	14080	26533	30140	19620	25300	24037	28405	27603
Co	3.51	3.56	5.03	3.62	4.91	5.28	7.21	6.01	8.70	7.56	3.53	7.67	5.42	9.65	9.04	6.71	8.26	8.90	11.0	16.1
Ni	25.4	26.4	35.5	22.2	30.3	34.0	46.3	44.1	57.0	47.5	19.5	45.4	30.2	57.0	58.3	37.5	44.8	52.0	63.4	63.2
Cu	16.6	20.6	30.8	12.0	15.8	15.1	17.3	27.2	24.0	20.3	9.27	20.6	14.6	30.6	88.3	24.5	73.0	30.1	39.8	89.8
Zn	76.0	70.2	99.7	66.0	86.6	82.0	96.8	70.0	101	108	52.0	106	74.9	151	133	75.8	125	146	191	495
Sr	331	380	318	355	435	486	500	237	398	631	1865	934	1807	694	498	614	819	1006	653	733
Ba	57.0	57.5	76.1	50.9	71.8	95.2	97.8	89.8	119	109	52.4	104	76.3	139	170	91.5	127	136	166	477
As	5.43	6.26	7.72	7.49	7.73	8.49	9.93	9.16	13.6	10.0	6.87	11.5	7.51	10.2	18.0	12.0	16.9	10.6	11.8	19.9
Pt	0.016	0.018	0.020	0.018	0.022	0.023	0.026	0.024	0.029	0.029	0.016	0.028	0.023	0.032	0.034	0.029	0.039	0.026	0.031	0.026
Hg	0.058	0.070	0.092	0.224	0.140	0.166	0.117	0.056	0.091	0.181	0.124	0.242	0.187	0.397	0.297	0.160	0.329	0.448	0.675	1.15
C	10.1	9.65	8.76	10.2	9.27	8.79	7.76	8.66	7.09	7.55	9.65	7.95	8.95	7.27	6.46	7.72	8.85	7.94	7.28	9.88
N	0.251	0.210	0.230	0.180	0.198	0.172	0.171	0.340	0.235	0.176	0.105	0.161	0.139	0.197	0.175	0.104	0.192	0.177	0.215	0.239
S	0.626	0.715	0.891	0.625	0.460	0.447	0.415	0.907	0.502	0.358	0.330	0.447	0.346	0.363	0.552	0.329	0.896	0.416	0.456	0.511
P	0.040	0.040	0.049	0.033	0.043	0.044	0.050	0.057	0.063	0.061	0.050	0.060	0.049	0.076	0.083	0.050	0.084	0.083	0.094	0.164

Appendix 1. (continued)

	K21	K22	K23	K24	K25	K26	K27	K28	K29	K30	K31	K32	K33	K34	K35	K36	K37	K38	K39	K40
Li	53.1	52.4	49.8	11.4	22.6	15.6	12.1	25.6	32.8	36.4	42.0	50.3	44.5	42.5	15.9	28.3	45.1	47.6	52.9	43.2
Be	1.71	1.70	1.76	0.423	0.728	0.522	0.513	0.882	1.16	1.28	1.44	1.60	1.68	1.69	0.930	1.87	1.54	1.59	1.67	1.39
Rb	60.8	62.1	59.2	8.27	29.3	15.4	7.07	26.1	35.7	43.1	45.9	53.7	60.8	68.4	17.4	32.2	53.2	56.2	62.6	50.8
Mo	1.63	1.44	1.94	7.03	1.66	0.717	0.737	1.13	1.13	1.70	1.52	2.66	2.23	2.08	1.04	2.43	1.83	1.57	1.61	1.14
Ag	0.496	0.495	0.830	0.902	0.176	0.159	0.091	0.231	0.276	0.649	0.627	0.626	0.869	0.675	0.471	1.57	1.77	0.801	0.741	0.465
Cd	0.473	0.458	0.542	0.582	0.141	0.159	0.112	0.321	0.241	0.739	0.953	0.906	2.70	1.36	3.84	11.2	1.32	0.648	0.574	0.413
Sn	7.73	7.56	12.2	4.14	2.31	1.44	0.733	14.39	4.19	8.61	12.2	12.4	11.8	12.7	3.85	8.13	11.4	9.71	9.04	7.10
Sb	0.798	0.613	0.823	0.622	0.353	0.289	0.306	1.25	0.492	0.964	0.882	1.33	0.823	1.24	0.545	1.33	0.670	0.834	0.640	0.491
Cs	5.33	5.36	5.21	0.81	2.47	1.32	0.70	2.15	3.06	3.68	3.80	4.45	4.76	5.17	1.55	2.72	4.41	4.73	5.04	4.18
Tl	0.604	0.600	0.591	0.196	0.282	0.182	0.129	0.294	0.350	0.450	0.475	0.584	0.552	0.570	0.282	0.453	0.575	0.542	0.585	0.498
Pb	123	108	132	93.2	21.5	19.0	21.1	45.0	57.1	130	152	231	144	159	78.5	192	165	149	117	85.4
Bi	1.90	1.79	2.37	0.652	0.195	0.249	0.145	0.579	0.922	2.62	2.35	2.73	3.62	4.03	1.42	3.10	5.04	3.78	3.06	1.50
U	2.40	2.23	3.31	5.01	2.81	2.25	2.43	3.18	2.68	3.44	4.00	4.30	5.61	3.98	8.22	25.02	3.12	2.97	2.99	2.31
Al	40501	39254	39000	8432	18257	9778	5453	17264	22999	28517	33175	35222	41191	38117	19992	32450	34064	35469	37143	30076
Ti	1295	1375	1364	434	856	397	174	603	799	905	1096	1276	1337	1272	470	875	1224	1329	1326	1059
V	73.1	73.0	76.3	31.6	41.7	25.3	19.7	39.5	51.8	60.6	71.2	83.2	85.7	94.2	48.4	89.6	74.0	78.3	76.1	59.6
Cr	80.5	79.7	82.6	31.3	45.0	26.3	20.7	46.0	51.9	64.2	75.5	80.6	90.2	88.6	49.1	129.34	85.5	80.5	83.0	65.5
Mn	3643	2161	1723	309	226	215	216	610	897	895	850	623	746	603	350	866	1027	1263	1365	1454
Fe	23977	23357	24050	6474	11075	8124	11865	14735	17624	18637	22141	25063	24642	26342	12438	19025	22542	22752	23241	18751
Co	10.2	9.51	10.2	2.52	3.90	3.23	4.03	6.28	7.23	7.39	8.26	7.64	8.03	8.41	3.68	6.18	8.33	9.11	9.78	8.11
Ni	55.9	52.7	55.2	16.1	29.7	16.5	11.3	27.6	36.4	38.9	41.7	43.9	51.8	58.2	20.0	38.2	49.9	51.8	55.1	44.5
Cu	46.3	44.0	62.0	133	12.4	8.17	5.25	19.3	25.9	54.2	65.7	90.9	76.7	92.5	32.7	112	92.0	74.0	55.8	36.0
Zn	198	187	243	474	40.7	37.6	47.8	98.2	123	241	300	341	497	389	280	1201	367	281	224	143
Sr	887	969	982	585	1565	1334	1929	1989	1769	1516	1485	1516	931	736	1934	1143	827	1074	1095	1137
Ba	208	193	224	124	64.0	37.7	33.1	85.2	103	203	202	223	218	219	116	280	278	234	198	153
As	12.4	12.1	14.7	9.78	8.90	8.14	9.75	8.47	8.92	18.6	23.4	39.6	16.9	17.2	22.1	22.4	20.2	15.4	14.4	10.4
Pt	0.025	0.028	0.028	0.019	0.018	0.008	0.012	0.015	0.018	0.028	0.031	0.026	0.027	0.029	0.017	0.029	0.038	0.025	0.032	0.025
Hg	0.864	0.950	1.36	0.434	0.108	0.125	0.199	0.552	0.521	2.35	6.28	12.4	2.42	2.33	0.964	1.88	2.13	2.18	1.64	0.784
C	8.82	8.66	8.92	10.6	9.69	10.4	12.0	10.5	9.62	9.59	9.15	9.09	8.51	8.22	9.75	7.39	9.16	9.02	8.81	8.86
N	0.225	0.195	0.227	0.081	0.144	0.072	0.077	0.120	0.146	0.181	0.169	0.164	0.191	0.165	0.093	0.175	0.282	0.227	0.223	0.188
S	0.504	0.448	0.578	0.514	0.408	0.248	0.337	0.373	0.359	0.520	0.391	0.632	0.595	0.638	0.408	0.701	0.774	0.538	0.516	0.400
P	0.112	0.115	0.191	0.287	0.023	0.023	0.028	0.059	0.072	0.186	0.271	0.159	0.677	0.280	1.345924	4.280937	0.235	0.151	0.130	0.099

Appendix 2. Chemical composition of the water samples from the K1 sampling location (wc – water column, sw – supernatant water, pw – pore water, numbers in the sample name indicate water depth, distance from the bottom, and sediment layer from which pore water was extracted). Values are expressed in μg L^{-1}.

	Li	Rb	Mo	Sb	Cs	Tl	Pb	U	Al	Ti	V	Cr	Mn	Fe	Co	Ni	Cu	Zn	Sr	Ba	As
wc 0.2 m	0.975	0.777	0.466	0.023	0.001	0.031	0.002	0.470	0.372	0.016	0.448	0.195	0.022	0.072	0.021	0.077	0.052	0.357	336	7.14	0.131
wc 2 m	1.60	1.19	0.470	0.026	0.002	0.025	<0.005	0.485	0.465	0.003	0.797	0.206	0.005	0.136	0.021	0.116	0.082	0.459	348	6.94	0.222
wc 3.4 m	78.9	43.4	4.86	0.099	0.105	0.025	0.010	1.58	0.713	0.035	1.15	0.187	2.40	0.290	0.023	0.167	0.179	3.17	3110	8.22	0.617
wc 4.4 m	191	107	11.2	0.228	0.261	0.029	0.022	3.28	0.811	0.000	1.65	0.151	0.116	0.151	<0.005	0.289	0.176	3.87	7220	8.69	1.08
wc 6.7 m	217	123	12.8	0.253	0.305	0.032	0.018	3.74	0.759	0.000	1.69	0.052	4.72	0.100	0.016	0.253	0.175	0.621	8383	8.76	1.49
sw 15 cm	206	115	12.4	0.289	0.297	0.024	0.113	3.68	13.1	0.017	1.51	0.069	43.9	0.656	0.057	0.486	0.069	81.8	8035	8.87	1.39
sw 5 cm	212	121	12.8	0.297	0.312	0.022	0.164	3.88	15.4	0.034	1.67	0.024	210	2.09	0.120	0.576	0.127	72.3	8227	9.04	1.99
sw 2 cm	211	115	12.5	0.259	0.280	0.020	0.024	3.86	2.50	0.017	1.28	0.056	6.61	1.39	0.016	0.447	0.115	48.9	8028	9.04	1.41
pw 0-2 cm	218	131	11.6	0.202	0.320	0.009	0.046	2.39	1.55	0.082	0.248	0.045	1385	135	0.104	0.743	0.247	0.751	8277	13.3	6.29
pw 2-4 cm	218	128	21.4	0.176	0.328	0.009	0.077	2.66	4.51	0.518	0.614	0.132	119	56.3	0.023	0.706	0.194	1.14	8063	14.8	2.88
pw 4-6 cm	204	120	30.8	0.243	0.286	0.008	0.248	2.95	10.5	1.23	0.985	0.208	117	49.6	0.025	1.54	0.333	4.79	7788	11.9	3.45
pw 6-8 cm	214	126	91.3	0.639	0.348	0.008	0.324	5.55	10.8	1.23	1.09	0.264	41.4	43.7	0.023	2.12	0.368	7.82	7944	13.7	4.87
pw 8-0 cm	207	123	85.6	0.883	0.343	0.005	0.169	6.70	5.43	0.433	1.26	0.124	17.0	16.4	0.004	0.950	0.198	2.52	7814	13.9	4.44
pw 10-12 cm	200	114	76.8	1.07	0.277	0.006	0.400	7.45	10.6	1.40	2.15	0.178	56.1	24.6	0.030	1.61	0.315	4.23	7857	12.5	4.95
pw 12-14 cm	212	130	153	5.12	0.343	0.009	0.457	14.1	16.1	2.00	4.50	0.273	56.2	33.0	0.102	1.97	0.369	2.92	7741	13.4	20.3
pw 14-16 cm	207	122	50.3	0.943	0.266	0.007	0.163	4.63	15.5	1.45	1.24	0.221	30.7	15.9	0.027	1.29	0.361	3.42	7681	12.2	4.14
pw 16-18 cm	218	133	182	5.68	0.304	0.008	0.254	8.57	14.7	1.02	3.24	0.200	69.7	14.2	0.050	1.29	0.294	2.55	8021	15.0	7.96
pw 18-20 cm	210	128	175	6.29	0.291	0.007	0.548	8.08	18.0	1.35	2.35	0.208	67.2	24.7	0.064	1.63	1.24	4.34	7593	15.7	9.63
pw 20-22 cm	194	118	213	6.00	0.238	0.006	1.05	10.4	16.6	0.690	2.84	0.105	83.5	16.7	0.093	1.74	0.137	6.23	7476	15.0	9.83
pw 22-24 cm	193	118	65.9	2.15	0.219	0.006	0.568	3.55	17.9	1.34	0.904	0.205	112	43.5	0.073	1.36	0.224	3.11	7429	15.7	6.66
pw 24-26 cm	186	113	35.6	1.10	0.192	0.008	0.391	1.46	71.9	2.22	0.968	0.360	127	27.1	0.015	1.93	0.044	9.21	7194	16.1	4.42
pw 26-28 cm	188	115	26.8	1.02	0.152	0.006	0.221	1.32	9.40	0.618	1.01	0.140	147	6.58	0.013	1.13	0.008	2.83	7422	16.3	3.61
pw 28-30 cm	188	125	92.3	7.91	0.172	0.009	0.291	6.51	6.71	0.330	14.5	0.194	125	3.54	0.280	2.41	0.175	6.10	6937	18.2	20.2
pw 30-32 cm	176	111	42.3	4.53	0.125	0.007	0.097	3.03	5.85	0.316	1.41	0.207	199	3.17	0.039	0.996	0.044	7.27	6826	18.1	16.5
pw 32-34 cm	171	113	58.5	7.49	0.126	0.008	0.128	4.26	7.79	0.456	4.00	0.243	179	5.49	0.092	1.85	0.228	9.82	6664	18.8	22.6
pw 34-32 cm	162	109	74.7	10.2	0.117	0.021	0.193	5.16	8.38	0.548	5.22	0.266	206	5.84	0.110	2.52	0.067	16.1	6286	19.1	25.6

Appendix 3. Chemical composition of the water samples from the K7 sampling location (wc – water column, sw – supernatant water, pw – pore water, numbers in the sample name indicate water depth, distance from the bottom, and sediment layer from which pore water was extracted). Values are expressed in μg L^{-1}.

	Li	Rb	Mo	Sb	Cs	Tl	Pb	U	Al	Ti	V	Cr	Mn	Fe	Co	Ni	Cu	Zn	Sr	Ba	As
wc 0.5 m	127	71.2	8.36	0.21	0.19	1.10	0.01	2.31	0.66	0.01	1.35	0.14	0.95	1.02	0.03	0.37	0.71	0.94	5019	8.05	0.92
wc 1.6 m	154	88.8	9.20	0.25	0.22	0.24	0.02	2.58	0.85	0.03	1.50	0.12	1.02	1.05	0.02	0.37	0.61	3.69	5890	8.00	1.23
wc 2.3 m	188	111	11.1	0.30	0.27	0.11	0.00	3.10	1.02	0.00	1.63	0.13	0.79	1.24	0.03	0.37	0.53	1.37	7344	8.09	1.81
wc 3.2 m	222	128	13.2	0.34	0.33	0.07	0.00	3.48	1.63	0.01	1.77	0.13	1.39	0.91	0.02	0.45	0.40	0.91	8454	7.97	1.49
wc 6 m	222	131	13.0	0.36	0.33	0.05	0.02	3.48	1.56	0.01	1.65	0.15	0.80	0.74	0.02	0.35	0.31	3.80	8562	7.74	1.71
wc 15 m	223	130	13.0	0.35	0.32	0.03	0.01	3.51	1.48	0.03	1.73	0.15	1.26	0.82	0.01	0.47	0.36	0.72	8487	8.44	1.55
sw 15 cm	226	131	13.2	0.37	0.38	0.03	0.07	3.47	2.71	0.04	2.40	0.13	15.8	1.09	0.06	0.91	0.76	7.80	8471	9.32	1.96
sw 5 cm	230	132	13.8	0.37	0.39	0.03	0.08	3.49	3.12	0.07	2.52	0.10	16.1	1.19	0.08	1.00	0.61	3.55	8553	9.58	1.95
sw 2 cm	225	128	13.3	0.35	0.37	0.02	0.08	3.35	3.09	0.08	2.39	0.11	18.3	2.62	0.08	0.94	0.56	3.35	8573	9.40	1.87
pw 0-2 cm	248	154	24.2	0.63	0.48	0.01	0.47	3.80	3.59	0.14	0.82	0.06	4268	944	1.58	4.09	0.21	23.2	8803	17.4	10.1
pw 2-4 cm	254	154	16.3	0.30	0.43	0.00	0.46	1.91	3.13	0.15	0.71	0.07	1508	2775	0.32	2.60	0.16	58.2	8768	18.7	17.7
pw 4-6 cm	250	160	14.3	0.27	0.43	0.00	0.45	0.98	5.47	0.30	0.67	0.09	1184	987	0.05	1.51	0.08	22.5	8658	17.3	6.36
pw 6-8 cm	245	153	15.2	0.29	0.39	0.01	0.50	1.19	4.23	0.37	0.90	0.08	1115	462	0.07	1.80	0.20	33.3	8534	16.8	4.83
pw 8-0 cm	250	153	15.2	0.34	0.40	0.01	0.57	1.02	5.91	0.58	1.13	0.11	1189	207	0.05	2.03	0.17	39.6	8953	18.7	3.73
pw 10-12 cm	254	163	18.6	0.35	0.40	1.11	0.40	1.30	3.92	0.46	0.90	0.11	1200	108	0.07	1.49	0.08	21.5	8642	19.6	4.58
pw 12-14 cm	231	146	16.8	0.38	0.37	0.21	0.39	1.23	7.25	0.39	1.44	0.13	1164	74.3	0.08	1.50	0.12	46.2	8215	19.2	4.60
pw 14-16 cm	224	142	41.0	1.55	0.34	0.11	0.39	4.75	14.8	0.42	6.46	0.15	902	26.9	0.13	1.79	0.24	183	7606	17.9	7.80
pw 16-18 cm	244	158	42.6	1.91	0.37	0.06	0.29	5.57	5.09	0.28	8.77	0.14	950	14.2	0.15	2.00	0.08	9.92	8408	19.5	7.78
pw 18-20 cm	247	160	27.6	1.73	0.38	0.04	0.36	4.92	4.35	0.26	9.80	0.13	503	7.10	0.18	1.64	0.08	38.4	8521	19.9	8.25
pw 20-22 cm	242	155	22.7	1.15	0.34	0.03	0.23	2.64	4.51	0.18	2.07	0.11	850	31.4	0.10	1.27	0.06	39.5	8407	19.6	4.50
pw 22-24 cm	247	165	23.6	1.57	0.35	0.02	0.16	3.75	2.74	0.22	1.52	0.10	869	65.4	0.10	1.40	0.03	2.53	8673	20.0	5.41
pw 24-26 cm	255	165	24.2	1.52	0.33	0.01	0.29	3.48	4.43	0.17	3.10	0.11	882	65.8	0.12	1.46	0.06	46.8	8376	19.5	6.70
pw 26-28 cm	247	166	35.2	2.39	0.34	0.01	0.24	5.68	4.52	0.24	5.11	0.09	830	44.1	0.10	1.67	0.09	35.5	8273	19.5	4.98
pw 28-30 cm	247	156	19.1	0.99	0.32	0.01	0.29	1.98	4.67	0.29	1.59	0.10	924	55.0	0.08	1.17	0.04	100	8284	19.2	4.12
pw 30-32 cm	249	160	18.1	0.84	0.33	0.00	0.16	1.10	4.78	0.16	0.84	0.09	969	105	0.05	1.14	0.02	26.6	8553	18.9	4.00
pw 32-34 cm	247	160	20.1	1.24	0.35	0.00	0.20	2.08	4.63	0.13	1.31	0.09	822	100	0.06	1.24	0.06	26.4	8506	18.1	5.02
pw 34-32 cm	249	168	46.9	4.20	0.41	0.00	0.06	11.7	3.54	0.23	14.7	0.11	524	49.6	0.11	1.93	0.10	29.5	7978	17.4	9.81

Appendix 4. Chemical composition of the water samples from the K8 sampling location (wc – water column, sw – supernatant water, pw – pore water, numbers in the sample name indicate water depth, distance from the bottom, and sediment layer from which pore water was extracted). Values are expressed in μg L^{-1}.

	Li	Rb	Mo	Sb	Cs	Tl	Pb	U	Al	Ti	V	Cr	Mn	Fe	Co	Ni	Cu	Zn	Sr	Ba	As
wc 0.5 m	19.7	12.1	1.68	0.057	0.032	0.066	0.039	1.06	1.23	0.051	1.05	0.235	0.896	1.03	0.022	0.373	0.448	1.79	987	9.36	0.280
wc 2 m	30.5	18.6	2.34	0.063	0.050	0.053	0.002	1.22	0.860	0.041	1.06	0.212	0.829	0.522	0.008	0.161	0.312	1.27	1455	9.38	0.241
wc 2.9 m	44.1	26.7	3.29	0.075	0.070	0.044	0.001	1.40	0.450	0.021	1.06	0.193	0.619	0.042	0.008	0.179	0.266	1.17	1988	9.04	0.464
wc 3.1 m	166	94.9	10.1	0.192	0.236	0.032	0.016	3.02	1.40	0.046	1.18	0.097	1.39	0.674	0.010	0.262	0.305	0.409	6480	9.04	1.14
wc 4 m	224	122	12.94	0.261	0.330	0.030	0.003	3.71	1.18	0.700	1.69	0.108	0.262	0.011	0.000	0.368	0.293	0.562	8270	9.01	1.49
wc 6 m	225	123	13.05	0.267	0.337	0.029	0.006	3.75	1.48	0.049	1.77	0.122	0.251	0.006	0.007	0.371	0.477	0.434	8244	9.07	1.51
sw 15 cm	210	113	13.53	0.371	0.295	0.016	0.033	4.14	2.94	0.032	3.64	0.033	199	0.494	0.174	0.697	0.279	3.35	8030	9.43	2.19
sw 5 cm	218	119	14.19	0.379	0.315	0.015	0.009	4.32	3.26	0.071	3.44	0.037	269	1.10	0.244	0.613	0.190	2.19	8152	9.48	2.18
sw 2 cm	211	112	13.81	0.365	0.286	0.010	0.005	4.30	2.65	0.053	3.47	0.314	272	2.96	0.242	0.608	0.253	3.47	8069	9.46	2.28
pw 0-2 cm	226	136	18.60	0.142	0.360	0.009	0.078	2.61	8.13	0.290	0.727	0.391	984	791	0.182	0.789	9.701	1.88	8361	12.7	8.72
pw 2-4 cm	210	127	15.84	0.162	0.323	0.008	0.109	1.98	10.1	0.799	0.982	0.208	600	353	0.101	1.48	0.439	2.65	7944	13.3	7.25
pw 4-6 cm	212	131	19.75	0.281	0.338	0.008	0.135	2.23	10.5	1.20	1.14	0.236	531	212	0.127	1.46	0.383	1.29	8031	14.6	4.97
pw 6-8 cm	206	132	23.77	0.654	0.343	0.007	0.160	2.87	11.2	1.21	2.03	0.338	424	134	0.105	1.39	0.365	3.49	8080	16.5	7.95
pw 8-0 cm	195	124	19.57	0.669	0.308	0.007	0.182	2.78	14.3	1.26	4.04	0.351	371	124	0.110	1.68	0.457	1.20	7844	16.7	4.85
pw 10-12 cm	193	123	14.61	0.246	0.286	0.007	0.193	1.25	11.8	1.08	2.17	0.323	410	196	0.091	1.35	0.376	1.08	7862	17.8	2.82
pw 12-14 cm	187	120	14.52	0.279	0.271	0.007	0.222	1.28	12.2	0.803	1.87	0.394	417	282	0.157	1.47	0.397	1.70	7882	19.5	3.07
pw 14-16 cm	185	122	16.17	0.393	0.270	0.005	0.223	1.77	11.3	0.938	1.81	0.398	423	238	0.220	1.52	0.385	2.43	7938	21.4	3.88
pw 16-18 cm	180	121	19.09	0.499	0.259	0.005	0.209	2.20	11.8	0.771	1.87	0.415	425	281	0.178	1.38	0.414	2.04	7805	23.0	4.92
pw 18-20 cm	175	117	18.00	0.497	0.241	0.005	0.299	1.98	13.2	1.05	2.20	0.373	442	381	0.213	1.32	0.366	2.42	7762	23.3	3.70
pw 20-22 cm	167	117	11.50	0.171	0.213	0.005	0.264	0.974	14.0	0.706	1.77	0.429	447	498	0.237	1.37	0.448	2.05	7549	23.6	1.46
pw 22-24 cm	178	123	19.91	0.554	0.249	0.005	0.259	2.52	20.3	1.32	1.60	0.417	443	469	0.174	1.29	0.365	1.69	7801	25.6	3.75
pw 24-26 cm	154	108	11.92	0.205	0.192	0.006	0.249	1.17	18.2	0.66	1.46	0.373	423	563	0.238	1.22	0.450	3.67	6905	24.0	2.08

Appendix 5. Chemical composition of the water samples from the K20 sampling location (wc – water column, sw – supernatant water, pw – pore water, numbers in the sample name indicate water depth, distance from the bottom, and sediment layer from which pore water was extracted). Values are expressed in μg L^{-1}.

	Li	Rb	Mo	Sb	Cs	Tl	Pb	U	Al	Ti	V	Cr	Mn	Fe	Co	Ni	Cu	Zn	Sr	Ba	As
wc 0.5 m	103	63.0	6.23	0.168	0.142	0.862	0.031	2.07	0.865	0.082	1.28	0.246	1.99	0.804	0.022	0.269	0.732	2.47	4187	7.58	3.02
wc 2.5m	105	65.5	6.54	0.168	0.150	0.349	0.018	2.11	0.561	0.034	1.32	0.237	2.00	0.641	0.023	0.247	0.701	3.11	4282	7.52	0.823
wc 5 m	228	136	12.7	0.330	0.317	0.281	0.031	3.67	1.75	0.027	1.58	0.172	0.800	0.541	0.012	0.380	0.279	2.53	8562	6.72	1.93
wc 32 m	234	132	12.5	0.338	0.322	0.191	0.199	3.53	3.49	0.020	1.68	0.147	2.31	0.706	0.017	0.472	0.235	1.52	8454	7.98	1.63
sw 15 cm	175	102	9.60	0.257	0.238	0.147	0.086	2.83	2.52	0.018	1.33	0.206	3.18	0.529	0.019	0.422	0.655	4.31	6668	6.79	1.13
sw 5 cm	215	127	11.7	0.326	0.303	0.128	0.176	3.40	3.40	0.016	1.52	0.176	5.11	0.433	0.017	0.438	0.797	1.96	8074	8.10	1.62
sw 2 cm	226	129	12.6	0.365	0.331	0.112	0.266	3.48	4.25	0.013	1.64	0.192	6.89	0.422	0.025	0.613	0.531	3.52	8429	11.6	1.30
pw 0-2 cm	238	159	39.4	0.447	0.422	0.140	1.30	3.20	12.7	0.327	0.743	0.084	5501	431	0.539	0.900	0.439	3.11	8705	53.5	4.97
pw 2-4 cm	253	162	15.6	0.258	0.455	0.065	1.22	2.66	11.0	0.248	0.902	0.201	1593	603	0.066	0.725	0.334	3.57	8848	47.7	5.91
pw 4-6 cm	248	157	47.4	0.279	0.441	0.037	1.49	3.17	9.64	0.412	1.05	0.151	1578	329	0.040	1.01	0.343	2.76	8610	45.9	5.89
pw 6-8 cm	244	151	9.84	0.322	0.437	0.022	2.59	1.30	19.7	0.903	1.16	0.364	2173	65.2	0.045	1.47	0.417	2.34	8344	55.8	0.870
pw 8-0 cm	236	145	14.2	0.587	0.445	0.016	2.00	1.29	26.6	1.39	1.53	0.368	2684	166	0.072	1.24	0.298	2.24	8290	66.7	1.23
pw 10-12 cm	235	143	8.77	0.849	0.473	0.013	3.25	1.56	19.1	3.87	2.55	0.494	2921	50.4	0.085	1.89	0.328	2.94	8380	70.6	1.71
pw 12-14 cm	224	141	6.27	0.852	0.477	0.009	2.74	1.30	27.6	4.41	1.80	0.411	3113	47.3	0.081	1.75	0.252	2.85	8270	71.9	1.89
pw 14-16 cm	228	144	8.35	1.07	0.495	0.006	3.81	1.95	14.9	3.71	1.76	0.456	2701	29.8	0.061	2.91	0.322	2.15	8169	66.6	1.68
pw 16-18 cm	230	150	141	3.29	0.499	0.001	4.29	4.94	29.2	2.88	1.96	0.364	1633	75.8	0.058	5.18	0.270	30.7	8150	54.3	3.15
pw 18-20 cm	232	148	73.2	3.38	0.507	0.001	2.12	3.79	18.0	1.06	1.59	0.145	1361	76.4	0.036	4.06	0.146	1.39	8062	52.8	4.22
pw 20-22 cm	211	132	221	5.38	0.482	0.003	1.05	4.89	12.1	0.600	1.46	0.204	944	114	0.082	1.78	0.503	2.64	7161	45.9	7.41

Appendix 6. Chemical composition of the water samples from the K36 sampling location (wc – water column, sw – supernatant water, pw – pore water, numbers in the sample name indicate water depth, distance from the bottom, and sediment layer from which pore water was extracted). Values are expressed in μg L^{-1}.

	Li	Rb	Mo	Sb	Cs	Tl	Pb	U	Al	Ti	V	Cr	Mn	Fe	Co	Ni	Cu	Zn	Sr	Ba	As
wc 0.5 m	160	91.3	9.96	0.253	0.231	1.45	0.038	2.73	2.83	0.037	1.57	0.177	1.17	0.794	0.034	0.362	1.68	2.26	6117	8.68	1.28
wc 2.5 m	172	100	10.1	0.256	0.244	0.340	0.060	2.86	1.07	0.043	1.61	0.204	1.20	2.06	0.022	0.438	1.65	2.42	6611	8.55	1.13
wc 3 m	180	105	10.3	0.273	0.260	0.172	0.065	2.94	1.10	0.024	1.56	0.256	1.13	2.28	0.028	0.334	1.53	1.95	6814	8.32	1.62
wc 3.5 m	218	120	12.1	0.328	0.308	0.110	0.139	3.37	1.37	0.055	1.68	0.276	1.09	1.58	0.028	0.372	0.759	2.44	8191	7.69	1.63
wc 6 m	225	124	12.4	0.329	0.311	0.074	0.039	3.42	1.77	0.022	1.67	0.198	1.17	1.60	0.019	0.351	0.430	0.965	8547	7.03	1.63
wc 13 m	232	127	12.8	0.342	0.325	0.055	0.221	3.50	2.50	0.031	1.74	0.212	2.18	1.23	0.018	0.382	0.480	5.71	8561	7.21	1.59
sw 15 cm	229	129	12.7	0.365	0.334	0.043	0.784	3.43	4.46	0.037	2.01	0.161	23.1	0.634	0.057	0.671	0.993	17.6	8698	8.84	1.63
sw 5 cm	234	131	13.0	0.383	0.348	0.041	0.811	3.52	4.77	0.045	1.98	0.155	23.0	0.580	0.055	0.698	0.977	17.0	8646	8.86	1.46
sw 2 cm	232	127	12.7	0.358	0.346	0.031	0.755	3.45	4.08	0.029	1.99	0.161	32.2	0.831	0.051	0.703	0.977	16.8	8552	8.79	1.57
pw 0-2 cm	253	156	17.5	0.444	0.498	0.010	1.35	3.32	5.31	0.092	0.707	0.067	3836	186	0.915	1.95	1.06	27.7	9313	25.5	12.7
pw 2-4 cm	261	155	16.7	0.388	0.444	0.002	0.856	2.95	2.63	0.063	0.337	0.055	3235	1202	0.628	1.78	0.586	11.5	9220	27.0	18.4
pw 4-6 cm	256	159	17.6	0.352	0.469	0.024	0.833	2.02	2.70	0.077	0.544	0.068	2582	369	0.210	1.21	0.260	2.92	9139	30.4	10.5
pw 6-8 cm	258	167	23.7	0.576	0.522	0.029	3.62	2.09	4.60	0.277	1.85	0.128	2039	48.4	0.136	1.85	1.26	6.96	9066	33.7	21.2
pw 8-0 cm	260	167	36.0	0.566	0.584	0.011	6.48	1.70	10.8	0.387	1.08	0.298	1490	238	0.513	3.62	5.56	21.1	8833	32.9	30.6
pw 10-12 cm	258	162	42.7	0.522	0.561	0.002	4.22	1.93	7.67	0.493	2.02	0.213	1238	20.1	0.078	1.44	0.935	4.90	8665	33.1	2.39
pw 12-14 cm	257	160	70.4	0.633	0.581	0.000	4.65	2.64	12.3	0.572	0.644	0.252	1136	60.3	0.081	1.72	1.08	12.4	8662	33.5	2.84
pw 14-16 cm	253	158	61.6	0.701	0.598	0.001	4.40	3.97	8.25	0.481	0.739	0.218	1077	63.0	0.075	1.42	1.11	5.03	8530	34.4	6.22
pw 16-18 cm	255	158	70.5	0.976	0.619	0.004	3.56	5.74	8.43	0.408	4.29	0.190	1005	17.0	0.102	1.72	1.10	4.50	8489	37.0	9.10

Appendix 7. Chemical composition of the K1 sediment core. Sample names indicate the sediment layer depth. Values are expressed in μg g^{-1}.

	K1																	
	0-2	**2-4**	**4-6**	**6-8**	**8-10**	**10-12**	**12-14**	**14-16**	**16-18**	**18-20**	**20-22**	**22-24**	**24-26**	**26-28**	**28-30**	**30-32**	**32-34**	**34-36**
Li	26.5	28.1	30.6	28.5	25.5	27.7	29.2	33.1	34.7	33.4	27.4	34.9	36.0	32.6	35.1	36.4	36.6	36.5
Be	0.760	0.786	0.879	0.790	0.689	0.749	0.823	0.952	1.03	1.02	0.81	1.04	1.01	0.903	0.956	0.957	0.994	1.02
Rb	32.4	34.2	35.6	33.5	29.6	31.5	33.7	39.3	45.4	43.5	31.6	43.5	45.9	41.8	44.5	45.5	46.3	47.0
Mo	1.15	3.17	3.87	4.53	5.42	5.25	3.63	3.74	4.37	3.69	3.48	2.90	2.05	1.53	1.32	1.52	1.66	1.48
Ag	0.196	0.217	0.234	0.226	0.202	0.204	0.176	0.183	0.188	0.187	0.156	0.202	0.203	0.166	0.166	0.170	0.178	0.175
Cd	0.418	0.449	0.487	0.530	0.538	0.604	0.602	0.562	0.524	0.456	0.363	0.443	0.459	0.390	0.390	0.387	0.385	0.395
Sn	2.07	2.12	2.11	2.08	1.94	2.42	1.84	2.02	2.24	2.14	1.92	2.16	1.99	1.68	1.74	1.77	1.76	1.73
Sb	0.377	0.501	0.574	0.570	0.699	0.928	0.707	0.735	0.774	0.835	0.874	0.763	0.636	0.463	0.441	0.444	0.439	0.444
Cs	2.87	3.07	3.24	3.01	2.62	2.80	2.99	3.49	3.87	3.62	2.54	3.62	3.90	3.50	3.74	3.85	3.88	3.94
Tl	0.355	0.385	0.423	0.426	0.401	0.434	0.427	0.471	0.486	0.448	0.363	0.457	0.478	0.434	0.458	0.469	0.476	0.483
Pb	19.7	25.1	48.4	141	341	191	111	25.8	32.3	76.6	550	83.6	47.8	31.1	20.8	15.3	15.4	16.1
Bi	0.198	0.208	0.302	0.235	0.266	0.230	0.210	0.241	0.227	0.204	0.166	0.222	0.212	0.166	0.150	0.146	0.147	0.152
U	1.68	2.84	3.68	3.71	3.92	4.22	4.26	4.39	3.96	3.18	2.58	2.76	2.35	1.92	1.97	2.02	1.95	1.88
Al	17935	19002	19761	18616	16591	17917	19867	23387	25516	24267	20470	25600	25930	23792	24639	24867	25244	25788
Ti	957	984	1024	998	922	942	1018	1208	1375	1322	1149	1385	1375	1183	1120	1123	1113	1156
V	40.3	46.2	49.7	48.5	44.7	47.9	51.6	60.3	68.2	63.5	52.4	65.3	65.1	54.9	51.3	52.6	52.8	55.1
Cr	36.9	39.6	40.4	39.7	35.1	36.9	41.6	48.9	58.4	56.9	45.4	57.9	55.9	46.8	43.0	43.2	42.9	45.7
Mn	150	136	127	127	130	137	182	201	227	208	197	224	225	206	203	210	221	223
Fe	9302	10114	10357	10086	8958	9397	10673	12605	15207	15071	13987	16062	15621	13084	12331	12668	12859	13121
Co	3.41	3.36	3.57	3.43	3.33	3.47	3.98	4.71	5.91	6.60	5.42	6.45	5.76	5.03	4.94	4.64	4.76	4.87
Ni	20.6	22.2	23.3	22.6	20.1	21.1	23.8	28.6	34.1	32.6	26.3	33.0	32.9	28.7	27.1	27.5	27.9	29.1
Cu	12.8	14.1	15.5	16.0	17.3	20.0	13.9	14.7	16.5	16.2	13.3	14.8	13.9	11.8	10.3	9.48	9.13	9.37
Zn	64.7	66.2	68.9	70.5	95.5	81.5	52.8	52.4	51.2	50.4	40.2	55.8	50.4	47.4	41.3	38.6	37.6	39.8
Sr	369	435	411	442	567	519	395	341	315	279	241	314	322	304	287	300	300	296
Ba	48.1	50.0	57.1	67.6	106	75.7	67.2	58.1	64.3	66.4	66.6	78.3	70.5	69.9	61.3	60.7	60.6	63.2
As	4.64	5.54	5.90	5.86	5.74	5.92	6.62	7.27	7.86	8.00	7.66	7.76	7.69	6.49	6.70	7.11	6.20	6.39
Hg	0.079	0.085	0.091	0.085	0.085	0.084	0.112	0.111	0.119	0.117	0.100	0.150	0.144	0.123	0.187	0.137	0.073	0.060
C	14.6	14.5	13.9	14.1	14.3	14.2	13.5	12.9	12.0	10.7	9.18	11.5	12.2	12.3	12.2	12.3	12.2	12.1
Corg	0.779	1.13	0.881	0.548	0.633	0.725	0.786	0.364	0.381	0.376	0.270	0.687	0.570	0.573	0.481	0.565	0.642	0.507
N	0.223	0.231	0.222	0.214	0.194	0.186	0.135	0.133	0.111	0.091	0.065	0.108	0.100	0.097	0.093	0.096	0.094	0.097
S	0.415	0.556	0.621	0.636	0.624	0.615	0.629	0.708	0.731	0.669	0.511	0.657	0.667	0.642	0.585	0.641	0.629	0.623
P	0.041	0.037	0.034	0.033	0.034	0.030	0.027	0.028	0.029	0.028	0.026	0.031	0.029	0.027	0.027	0.027	0.026	0.027

Appendix 8. Chemical composition of the K7 sediment core. Sample names indicate the sediment layer depth. Values are expressed in μg g^{-1}.

	K7																	
	0-2	**2-4**	**4-6**	**6-8**	**8-10**	**10-12**	**12-14**	**14-16**	**16-18**	**18-20**	**20-22**	**22-24**	**24-26**	**26-28**	**28-30**	**30-32**	**32-34**	**34-36**
Li	60.5	61.8	59.7	58.1	60.5	53.9	60.6	60.0	58.5	58.5	54.4	51.2	49.7	48.5	47.9	46.3	43.2	42.9
Be	1.60	1.63	1.57	1.52	1.61	1.40	1.59	1.69	1.62	1.61	1.46	1.40	1.34	1.29	1.31	1.26	1.16	1.15
Rb	70.4	71.5	70.1	68.3	72.2	65.8	70.4	71.2	69.4	68.9	64.1	59.9	58.3	56.1	56.0	54.4	51.4	51.2
Mo	1.70	1.15	1.34	1.31	1.52	1.81	1.98	2.14	1.88	1.66	1.20	1.09	1.11	1.12	1.04	1.03	0.953	0.887
Ag	0.277	0.276	0.273	0.272	0.273	0.252	0.248	0.432	0.387	0.368	0.341	0.361	0.307	0.306	0.322	0.316	0.306	0.296
Cd	0.395	0.403	0.418	0.418	0.446	0.461	0.474	0.489	0.457	0.467	0.417	0.386	0.389	0.374	0.382	0.351	0.337	0.342
Sn	3.10	2.87	2.90	2.67	2.82	2.70	2.67	2.68	2.60	2.54	2.38	2.32	2.07	2.01	2.01	1.96	1.84	1.82
Sb	0.646	0.675	0.710	0.690	0.752	0.772	0.772	0.732	0.663	0.738	0.578	0.545	0.494	0.457	0.439	0.423	0.388	0.385
Cs	6.22	6.32	6.30	6.16	6.43	6.22	6.30	6.35	6.18	6.17	5.74	5.35	5.22	5.04	5.02	4.87	4.60	4.60
Tl	0.735	0.745	0.731	0.716	0.740	0.619	0.738	0.717	0.691	0.689	0.637	0.598	0.582	0.567	0.567	0.544	0.527	0.518
Pb	35.4	35.9	36.3	35.2	37.5	35.5	33.2	27.5	24.3	23.9	21.9	19.2	17.2	15.9	15.6	15.1	14.6	14.5
Bi	0.347	0.355	0.362	0.351	0.371	0.354	0.319	0.265	0.235	0.224	0.201	0.183	0.170	0.164	0.160	0.155	0.147	0.145
U	2.03	2.30	2.55	2.46	2.76	3.05	3.02	2.76	2.60	2.51	2.34	2.38	2.45	2.49	2.43	2.36	2.24	2.33
Al	38138	40792	40641	39112	37332	37303	38353	38333	39316	37688	34627	31643	30183	28870	29721	28763	25940	26165
Ti	1707	1813	1793	1645	1546	1503	1585	1803	1816	1804	1672	1560	1424	1463	1491	1426	1244	1228
V	73.6	76.8	77.4	75.2	76.1	76.3	78.5	83.5	79.6	75.1	69.1	61.1	57.9	54.5	56.2	54.6	49.1	48.5
Cr	69.8	66.6	66.0	64.0	66.1	65.7	66.3	71.7	66.9	65.2	61.7	56.7	53.9	51.7	53.3	52.2	48.2	48.9
Mn	486	431	438	442	446	427	415	378	335	310	289	257	234	222	225	214	196	197
Fe	18350	19085	18552	18267	18280	18904	19050	19295	18353	18046	16690	15572	14759	14272	14522	14212	13156	13162
Co	8.54	7.34	7.27	6.83	6.82	7.10	6.88	7.05	6.87	6.43	5.90	5.23	4.76	4.54	4.65	4.59	4.22	4.09
Ni	41.3	40.1	39.9	39.0	38.2	39.1	40.0	42.5	38.3	37.7	35.3	32.2	30.4	29.5	29.6	28.6	26.6	26.6
Cu	13.4	14.3	14.4	14.1	14.2	14.5	14.5	13.7	12.9	11.8	9.97	8.53	7.64	7.02	7.28	7.22	6.63	6.51
Zn	85.1	89.3	88.8	88.0	88.0	86.3	83.4	79.3	69.4	66.4	61.0	53.7	48.4	46.4	46.1	45.5	42.1	42.0
Sr	530	496	495	474	470	452	447	454	451	454	475	461	478	503	544	576	584	553
Ba	89.3	93.3	92.2	90.9	93.1	91.7	93.8	92.7	86.8	83.7	84.5	75.2	72.2	69.9	74.8	73.7	66.7	67.7
As	8.35	8.28	8.67	8.91	9.96	11.8	12.4	12.8	11.6	10.8	9.76	10.3	10.7	11.6	10.4	9.72	9.20	8.63
Hg	0.182	0.176	0.186	0.176	0.176	0.173	0.177	0.177	0.176	0.192	0.181	0.124	0.074	0.069	0.064	0.042	0.043	0.054
C	8.59	8.52	8.39	8.29	8.16	8.14	8.04	8.13	8.17	8.27	8.44	8.61	8.76	8.93	8.94	9.08	9.18	9.28
Corg	0.740	0.854	1.18	1.13	1.24	1.04	1.05	0.971	0.822	0.847	0.620	0.578	0.660	0.576	0.579	0.620	0.590	0.608
N	0.210	0.211	0.202	0.199	0.188	0.181	0.171	0.158	0.149	0.141	0.127	0.119	0.113	0.113	0.113	0.113	0.112	0.119
S	0.317	0.358	0.411	0.404	0.424	0.520	0.573	0.598	0.577	0.529	0.426	0.410	0.417	0.427	0.425	0.467	0.459	0.444
P	0.049	0.049	0.048	0.046	0.045	0.044	0.042	0.041	0.039	0.039	0.037	0.036	0.035	0.033	0.033	0.032	0.032	0.030

Appendix 9. Chemical composition of the K8 sediment core. Sample names indicate the sediment layer depth. Values are expressed in μg g^{-1}.

	K8												
	0-2	**2-4**	**4-6**	**6-8**	**8-10**	**10-12**	**12-14**	**14-16**	**16-18**	**18-20**	**20-22**	**22-24**	**24-26**
Li	47.9	47.5	47.8	50.1	49.4	51.8	50.5	49.8	50.6	51.2	50.0	51.7	50.7
Be	1.85	1.88	1.86	1.95	1.92	2.05	1.99	1.96	2.02	2.06	2.02	2.09	2.06
Rb	87.4	87.2	87.8	91.8	90.7	96.2	95.8	94.4	97.6	100	99.0	103	102
Mo	1.93	2.06	2.12	2.31	2.52	2.56	2.26	2.09	2.01	2.03	1.94	1.94	1.87
Ag	0.448	0.454	0.433	0.431	0.410	0.412	0.397	0.393	0.391	0.395	0.392	0.391	0.387
Cd	0.476	0.472	0.488	0.507	0.525	0.533	0.532	0.526	0.524	0.554	0.540	0.574	0.562
Sn	2.69	3.09	2.71	2.81	2.76	2.84	2.81	2.77	2.82	2.86	2.83	2.97	2.86
Sb	0.624	0.651	0.675	0.655	0.662	0.742	0.708	0.661	0.707	0.733	0.754	0.738	0.708
Cs	6.78	6.76	6.78	7.05	7.00	7.40	7.31	7.23	7.37	7.51	7.37	7.73	7.58
Tl	0.829	0.824	0.834	0.857	0.847	0.906	0.900	0.898	0.924	0.948	0.937	0.979	0.968
Pb	24.3	24.4	24.7	25.4	25.1	25.8	25.5	25.5	25.2	25.5	24.8	26.1	25.8
Bi	0.281	0.283	0.283	0.297	0.293	0.309	0.313	0.302	0.313	0.318	0.311	0.328	0.323
U	2.52	2.86	2.99	2.94	2.85	3.02	2.90	2.63	2.54	2.59	2.47	2.56	2.44
Al	41055	41972	42153	43247	43421	45233	44152	44117	44516	45469	44616	46268	44819
Ti	1731	1780	1958	2072	2095	2016	1974	1875	2112	2143	2010	1865	1783
V	92.6	95.5	99.1	100	99.7	105	103	101	104	106	104	107	106
Cr	89.2	89.5	90.1	91.5	91.2	95.6	93.2	92.9	94.9	96.2	94.0	98.2	95.9
Mn	232	230	235	237	237	240	240	241	247	249	246	251	249
Fe	21760	22256	22528	23417	23316	24571	24039	23967	24572	25099	24554	25421	25093
Co	7.06	7.31	7.71	7.65	8.62	8.45	8.14	8.01	8.60	8.48	8.28	8.55	8.46
Ni	47.0	47.8	48.3	50.4	50.0	53.4	52.5	52.2	54.1	55.8	54.4	56.6	56.0
Cu	20.2	20.3	21.5	21.8	22.1	24.0	23.1	23.3	24.4	25.0	24.6	25.9	25.4
Zn	82.7	82.1	81.6	82.8	81.6	83.6	80.2	80.7	78.9	78.2	77.1	79.8	77.9
Sr	321	334	351	323	314	297	298	290	277	273	278	262	261
Ba	98.2	99.9	105	106	107	113	110	108	112	114	115	120	116
As	12.1	13.6	12.9	13.7	13.4	13.9	13.6	13.7	14.1	14.4	14.2	14.2	14.1
Hg	0.116	0.116	0.103	0.103	0.099	0.097	0.090	0.099	0.098	0.084	0.087	0.079	0.086
C	8.29	8.12	7.84	7.69	7.36	7.28	7.24	7.35	7.07	7.05	6.98	6.88	6.93
Corg	0.544	0.562	0.522	0.244	0.304	0.332	0.356	0.427	1.95	1.79	1.72	1.86	1.19
N	0.334	0.300	0.270	0.262	0.251	0.248	0.236	0.246	0.236	0.223	0.226	0.230	0.232
S	0.531	0.656	0.734	0.805	0.818	0.804	0.759	0.760	0.681	0.668	0.653	0.627	0.608
P	0.060	0.056	0.053	0.054	0.053	0.056	0.057	0.059	0.059	0.061	0.062	0.063	0.064

Appendix 10. Chemical composition of the K20 sediment core. Sample names indicate the sediment layer depth. Values are expressed in μg g^{-1}.

	K20										
	0-2	**2-4**	**4-6**	**6-8**	**8-10**	**10-12**	**12-14**	**14-16**	**16-18**	**18-20**	**20-22**
Li	35.9	31.0	31.5	42.2	51.2	41.0	33.0	39.6	36.2	27.4	15.3
Be	1.28	1.28	1.17	1.16	1.25	1.38	1.57	1.54	1.49	1.20	0.753
Rb	29.2	25.0	24.7	27.0	29.5	31.2	30.9	44.0	38.5	27.9	14.6
Mo	4.99	4.94	7.92	9.56	11.0	10.5	11.6	11.9	12.5	9.71	9.95
Ag	0.596	0.498	0.486	0.509	0.509	0.613	0.695	0.792	0.716	0.519	0.267
Cd	1.66	1.81	1.52	1.51	1.82	3.14	2.88	1.66	1.34	0.972	0.651
Sn	12.1	13.2	11.0	11.5	10.5	13.8	17.2	16.4	14.3	12.0	6.95
Sb	2.62	3.24	3.01	3.23	3.66	5.83	8.40	5.69	6.82	5.65	3.71
Cs	3.03	2.65	2.62	2.88	3.21	3.27	3.17	4.46	3.71	2.73	1.48
Tl	0.761	0.720	0.747	0.752	0.901	1.26	2.12	1.32	1.06	0.864	0.530
Pb	271	212	211	209	211	334	441	562	737	499	195
Bi	1.90	1.48	1.38	1.61	1.98	3.14	4.15	6.17	3.75	2.31	0.87
U	3.23	3.55	4.05	3.91	3.87	4.26	4.78	5.19	4.90	4.57	4.60
Al	28233	24520	24255	30787	37269	31651	29726	32464	28880	24873	18487
Ti	1496	1327	1313	1619	1949	1739	1431	1469	1408	1248	960
V	129	110	112	155	203	157	129	118	105	95.2	69.2
Cr	177	152	159	181	215	176	125	120	154	166	94.5
Mn	14225	15225	14089	12365	11641	16165	21389	21066	17650	13607	7058
Fe	20387	19946	20790	21806	24081	23743	22532	22378	22872	19268	15029
Co	14.7	14.4	14.1	29.5	16.9	16.1	17.1	16.6	23.4	18.5	10.3
Ni	71.6	63.4	68.8	71.5	88.3	90.3	97.9	80.3	71.0	66.1	46.0
Cu	86.9	80.7	76.4	84.1	84.5	113	138	136	106	95.9	44.2
Zn	461	450	410	353	380	650	631	554	618	441	201
Sr	545	578	564	518	431	541	613	664	737	746	693
Ba	563	587	676	522	449	764	756	1016	681	551	291
As	25.8	24.2	28.2	25.1	26.0	26.3	28.8	26.3	30.0	26.5	21.4
Hg	1.39	1.20	1.10	1.17	1.25	1.71	1.89	2.08	2.02	1.38	0.719
C	22.4	22.8	21.7	18.5	17.9	23.1	27.3	21.5	18.6	16.3	12.5
Corg	14.8	21.0	14.3	8.11	8.54	16.8	16.3	9.58	10.0	6.42	2.39
N	0.307	0.281	0.235	0.222	0.218	0.302	0.386	0.367	0.248	0.179	0.087
S	0.933	0.850	0.613	0.654	0.618	0.719	0.798	0.822	0.850	0.814	0.697
P	0.073	0.049	2.29	3.38	3.73	2.02	1.54	1.53	1.69	1.72	1.44

Appendix 11. Chemical composition of the K22 sediment core. Sample names indicate the sediment layer depth. Values are expressed in μg g^{-1}.

	K22										
	0-1	**1-2**	**2-3**	**3-4**	**4-5**	**5-6**	**6-7**	**7-8**	**8-9**	**9-10**	**10-11**
Li	25.4	26.6	28.2	28.1	29.6	32.4	35.2	34.8	37.7	35.4	29.1
Be	0.695	0.708	0.768	0.758	0.777	0.841	0.925	0.897	0.965	0.881	0.733
Rb	30.8	32.3	34.3	34.2	36.2	39.7	43.1	42.8	45.4	42.8	35.8
Mo	0.93	1.14	1.09	1.20	1.37	1.69	1.66	1.80	1.79	1.55	1.31
Ag	0.312	0.312	0.341	0.357	0.372	0.408	0.435	0.419	0.438	0.388	0.309
Cd	0.429	0.415	0.456	0.435	0.435	0.499	0.478	0.455	0.484	0.441	0.363
Sn	7.07	7.47	7.64	7.72	7.90	9.59	8.56	8.61	8.34	7.91	6.64
Sb	0.597	0.635	0.667	0.857	0.768	0.881	0.963	1.02	1.10	1.08	0.92
Cs	2.70	2.82	3.00	2.98	3.18	3.50	3.81	3.77	4.02	3.72	3.11
Tl	0.301	0.307	0.325	0.325	0.345	0.380	0.411	0.409	0.441	0.437	0.375
Pb	56.8	58.5	62.0	64.0	68.7	76.9	84.2	82.7	88.5	78.8	58.7
Bi	0.822	0.828	0.921	0.994	1.12	1.36	1.45	1.50	1.45	1.20	0.839
U	2.40	2.45	2.57	2.70	2.87	3.05	3.23	3.17	3.31	3.29	3.01
Al	20414	21226	21816	21729	23766	25703	27539	26942	28775	26885	22146
Ti	983	1050	1074	1044	1094	1179	1246	1248	1373	1271	1079
V	44.1	47.8	47.5	47.4	53.4	58.4	62.7	60.3	65.7	63.8	54.5
Cr	78.0	73.1	70.7	80.2	87.0	97.2	84.8	81.4	75.3	74.7	73.2
Mn	1647	1676	1574	1537	1646	1661	1662	1580	1660	1144	885
Fe	11239	11746	11926	11844	12568	13442	14172	14144	14876	13995	12100
Co	6.84	7.56	7.44	7.64	8.58	8.95	10.26	8.07	8.49	7.78	6.55
Ni	27.8	29.3	30.0	29.2	31.5	34.4	36.9	35.8	37.9	34.8	30.4
Cu	22.1	23.6	23.6	25.1	27.0	30.6	32.3	32.2	32.7	28.9	22.4
Zn	112	117	121	123	137	146	159	156	166	147	117
Sr	1649	1706	1571	1530	1558	1507	1474	1328	1369	1593	1727
Ba	139	149	141	143	151	161	167	161	183	148	125
As	9.27	8.49	9.19	9.22	10.1	10.9	11.8	11.1	12.4	13.1	12.4
Hg	0.889	0.899	0.988	1.00	1.06	1.16	1.24	1.22	1.24	1.10	0.82
C	10.9	11.0	10.9	10.9	10.7	10.4	10.3	10.5	10.2	10.3	10.4
Corg	1.30	1.45	1.59	1.92	1.06	1.68	1.94	1.56	0.960	1.02	1.11
N	0.144	0.147	0.152	0.155	0.151	0.154	0.158	0.166	0.151	0.130	0.108
S	0.274	0.279	0.292	0.304	0.341	0.369	0.371	0.388	0.412	0.402	0.372
P	0.120	0.124	0.129	0.124	0.121	0.120	0.115	0.117	0.112	0.081	0.061

Appendix 12. Chemical composition of the K32 sediment core. Sample names indicate the sediment layer depth. Values are expressed in μg g^{-1}.

	K32																			
	0-1	**1-2**	**2-3**	**3-4**	**4-5**	**5-6**	**6-7**	**7-8**	**8-9**	**9-10**	**10-11**	**11-12**	**12-13**	**13-14**	**14-15**	**15-17**	**17-19**	**19-21**	**21-23**	**23-25**
Li	40.8	39.2	34.6	35.6	37.5	38.3	34.0	31.9	30.5	29.0	28.5	25.9	24.5	25.0	24.0	23.4	19.8	18.7	17.0	17.8
Be	1.45	1.43	1.17	1.11	1.16	1.11	1.00	0.885	0.843	0.795	0.755	0.727	0.656	0.657	0.645	0.602	0.516	0.488	0.453	0.476
Rb	50.2	48.6	41.7	42.9	45.3	45.6	40.2	38.0	36.9	33.8	34.1	30.0	29.3	30.2	29.0	28.3	24.2	22.8	20.6	21.8
Mo	1.84	1.73	1.88	3.66	4.38	4.60	3.52	3.00	2.67	2.20	2.20	1.53	1.28	1.31	1.44	1.06	0.639	0.575	0.594	0.597
Ag	0.776	0.752	0.726	0.754	0.801	0.722	0.603	0.567	0.470	0.368	0.359	0.328	0.298	0.284	0.267	0.227	0.160	0.138	0.126	0.137
Cd	0.758	0.783	0.813	1.01	1.12	1.16	1.01	0.832	0.758	0.741	0.608	0.505	0.438	0.378	0.362	0.276	0.151	0.134	0.122	0.138
Sn	36.5	37.6	32.6	32.9	32.4	28.2	25.3	17.8	14.3	12.3	11.3	13.2	9.34	9.12	7.89	6.33	4.37	3.87	3.69	4.00
Sb	10.5	7.19	30.7	7.83	29.9	9.95	4.96	4.11	2.91	2.27	2.48	5.75	1.88	1.60	1.68	0.850	0.429	0.432	0.414	0.453
Cs	4.36	4.17	3.60	3.76	3.98	4.00	3.54	3.37	3.25	3.01	2.98	2.61	2.57	2.65	2.50	2.48	2.07	1.95	1.77	1.85
Tl	0.492	0.488	0.467	0.495	0.510	0.515	0.485	0.458	0.445	0.427	0.422	0.386	0.377	0.377	0.361	0.341	0.293	0.276	0.256	0.270
Pb	438	498	467	500	553	498	466	414	361	323	262	224	189	155	160	92.8	23.9	17.5	20.1	26.0
Bi	2.14	2.09	1.97	2.53	2.87	2.47	2.05	1.63	1.06	0.859	0.788	0.599	0.534	2.033	0.397	0.256	0.119	0.107	0.096	0.107
U	2.84	2.84	3.09	4.04	4.36	4.40	4.06	3.95	3.97	3.58	3.42	3.07	2.88	2.93	2.79	2.67	2.47	2.48	2.46	2.54
Al	34928	33417	29193	31026	33001	31781	27365	24855	23553	22019	21307	19995	18418	18605	17482	17165	14479	13287	12046	12650
Ti	1742	1622	1617	1544	1799	1574	1428	1347	1229	1146	1183	1133	942	988	917	865	800	750	668	729
V	87.4	80.9	75.1	82.8	92.7	94.5	83.1	73.7	71.5	62.7	62.2	56.4	50.8	50.6	49.5	47.0	38.0	33.7	33.1	33.6
Cr	122	123	114	103	105	98.5	81.4	98.9	70.3	60.5	59.1	57.9	53.3	54.4	51.7	45.2	35.9	33.7	32.6	33.6
Mn	695	500	436	426	474	486	415	379	324	289	289	279	261	246	233	212	171	154	148	151
Fe	23650	22248	20347	21306	21792	21673	19079	17586	16194	15364	15112	14031	12826	13034	12335	11524	9936	9380	8962	9412
Co	9.46	7.75	7.53	7.46	8.53	7.89	6.78	5.93	5.87	5.29	5.34	5.12	4.62	5.01	4.89	27.69	4.55	3.65	3.21	3.21
Ni	45.2	41.0	37.1	38.5	40.5	39.8	34.7	31.7	28.6	27.7	27.1	25.0	23.0	23.8	22.1	21.7	17.8	16.9	15.4	16.4
Cu	257	246	215	227	267	223	188	188	175	154	138	104	91.2	68.3	62.7	42.2	9.88	6.39	9.17	10.8
Zn	687	712	861	777	830	790	680	611	539	420	370	353	283	219	212	124	39.6	30.3	29.6	36.6
Sr	1371	1355	1494	1530	1499	1555	1702	1746	1835	1798	1851	1960	1921	1952	1920	2035	2112	2007	2143	2127
Ba	433	442	453	375	481	387	461	376	278	235	236	208	179	152	137	99.3	51.2	39.4	41.6	44.3
As	89.9	85.1	75.9	86.2	87.5	95.9	90.7	100	101	87.4	75.0	61.1	53.7	46.5	43.5	32.9	17.7	16.5	17.5	19.4
Hg	53.1	52.1	45.0	47.5	51.4	57.4	53.9	54.6	57.8	46.0	40.2	29.8	24.5	19.4	18.9	11.6	1.42	0.830	1.78	3.03
C	10.3	10.4	10.5	10.3	10.3	10.2	10.4	10.4	10.4	10.4	10.6	10.8	10.8	10.5	10.5	10.5	10.5	10.5	10.6	10.6
Corg	1.21	1.07	0.846	0.854	0.485	0.962	1.36	0.741	0.602	0.777	1.02	0.747	0.582	0.515	0.399	0.477	0.265	0.182	0.160	0.153
N	0.271	0.255	0.216	0.218	0.223	0.215	0.180	0.169	0.137	0.132	0.124	0.119	0.108	0.099	0.099	0.087	0.073	0.065	0.062	0.066
S	0.437	0.455	0.515	0.699	0.820	0.787	0.737	0.675	0.610	0.581	0.578	0.537	0.492	0.489	0.510	0.452	0.355	0.352	0.349	0.370
P	0.164	0.163	0.148	0.157	0.155	0.135	0.111	0.091	0.066	0.064	0.069	0.057	0.051	0.050	0.045	0.039	0.033	0.033	0.032	0.032

Appendix 13. Chemical composition of the K36 sediment core. Sample names indicate the sediment layer depth. Values are expressed in μg g^{-1}.

	K36								
	0-2	**2-4**	**4-6**	**6-8**	**8-10**	**10-12**	**12-14**	**14-16**	**16-18**
Li	23.9	22.3	21.9	28.4	32.2	32.2	31.6	30.7	27.3
Be	1.45	1.46	1.44	1.36	1.36	1.31	1.31	1.26	1.07
Rb	26.4	25.1	24.0	31.4	36.0	37.2	36.4	34.5	30.0
Mo	2.35	2.65	2.67	2.90	3.59	4.13	4.35	4.13	4.05
Ag	1.41	1.67	1.51	1.44	1.52	1.51	1.46	1.30	1.07
Cd	9.47	10.2	10.4	7.64	7.42	7.47	8.14	7.54	5.27
Sn	11.8	12.0	11.0	13.9	13.5	14.2	13.3	18.9	10.8
Sb	1.59	1.63	2.57	1.64	2.02	2.25	2.20	2.44	2.09
Cs	2.37	2.28	2.14	2.80	3.27	3.35	3.27	3.13	2.71
Tl	0.400	0.413	0.386	0.413	0.455	0.461	0.456	0.445	0.397
Pb	190	181	173	166	187	201	202	196	177
Bi	2.79	2.19	2.06	2.90	3.80	4.04	4.48	4.40	3.81
U	14.2	19.9	21.7	13.0	11.3	11.4	12.6	13.3	12.1
Al	44309	41750	38285	47755	51758	49801	51119	45690	34183
Ti	1072	1054	980	1212	1319	1238	1278	1237	1104
V	85.2	86.3	84.3	87.3	94.3	95.5	102	98.9	94.2
Cr	670	786	466	442	436	455	504	512	448
Mn	771	727	1261	788	879	872	889	777	646
Fe	17982	17234	16239	17909	19026	18427	19227	18794	16740
Co	8.92	9.14	11.2	9.58	8.83	8.74	9.15	8.58	12.9
Ni	36.7	36.1	33.6	38.8	41.6	41.6	43.9	41.8	36.1
Cu	95.8	99.3	83.3	94.0	102.15	99.7	110.25	99.1	101
Zn	1269	1384	1375	1286	1363	1439	1561	1307	827
Sr	1176	1338	1492	1367	1284	1269	1361	1425	1621
Ba	285	300	339	313	318	319	336	324	333
As	30.0	30.6	28.5	32.0	31.7	31.4	28.2	29.1	27.5
Hg	3.53	3.17	2.67	3.14	3.26	3.28	3.49	3.19	2.61
C	11.6	10.3	9.1	10.1	10.8	11.1	11.2	11.1	11.1
Corg	3.49	2.21	1.56	2.05	2.80	3.41	2.77	2.18	1.63
N	0.235	0.195	0.166	0.203	0.233	0.234	0.232	0.209	0.171
S	0.768	0.809	0.941	1.09	1.14	1.26	1.32	1.17	1.06
P	0.158	0.185	0.209	0.159	0.138	0.159	0.146	0.168	0.101

Appendix 14. Pearson correlation matrix for sediment parameters measured in the core K1 from the Krka River estuary

	Li	Rb	Mo	Cd	Pb	U	Al	Cr	Mn	Fe	Co	Ni	Cu	Zn	As	Hg	OC	S	P	<2	<63	>63
Li	1																					
Rb	**0.98**	1																				
Mo	-0.55	-0.58	1																			
Cd	-0.40	-0.46	**0.78**	1																		
Pb	-0.59	**-0.61**	0.50	0.07	1																	
U	-0.40	-0.47	**0.91**	**0.92**	0.24	1																
Al	**0.97**	**0.97**	-0.54	-0.46	-0.47	-0.42	1															
Cr	**0.65**	**0.68**	-0.11	-0.14	-0.22	-0.04	**0.78**	1														
Mn	**0.84**	**0.85**	-0.52	-0.44	-0.26	-0.41	**0.93**	**0.77**	1													
Fe	**0.73**	**0.75**	-0.29	-0.38	-0.12	-0.27	**0.87**	**0.94**	**0.88**	1												
Co	**0.67**	**0.71**	-0.24	-0.36	-0.07	-0.23	**0.82**	**0.93**	**0.86**	**0.97**	1											
Ni	**0.81**	**0.84**	-0.28	-0.28	-0.30	-0.20	**0.92**	**0.96**	**0.89**	**0.97**	**0.94**	1										
Cu	-0.56	-0.56	**0.89**	**0.77**	0.35	**0.80**	-0.53	0.01	-0.52	-0.23	-0.17	-0.22	1									
Zn	**-0.74**	**-0.73**	**0.71**	**0.64**	0.27	0.57	**-0.80**	-0.49	**-0.83**	**-0.67**	**-0.63**	**-0.65**	**0.77**	1								
As	0.57	0.55	0.03	-0.09	0.10	0.09	**0.70**	**0.87**	**0.75**	**0.89**	**0.89**	**0.86**	0.00	-0.53	1							
Hg	0.45	0.44	-0.26	-0.17	-0.18	-0.15	0.50	0.50	0.47	0.52	0.54	0.51	-0.14	-0.36	0.58	1						
OC	-0.35	-0.36	0.00	0.17	-0.29	0.02	-0.46	-0.49	-0.58	-0.57	**-0.61**	-0.55	0.09	0.45	**-0.66**	-0.28	1					
S	0.56	0.51	0.31	0.38	-0.27	0.45	0.53	0.58	0.41	0.48	0.44	**0.61**	0.20	-0.11	**0.61**	0.28	-0.34	1				
P	**-0.62**	-0.56	0.16	0.18	-0.08	0.08	**-0.65**	-0.42	**-0.72**	-0.58	-0.58	-0.57	0.37	**0.68**	**-0.68**	-0.35	**0.63**	-0.52	1			
<2	**0.72**	**0.74**	-0.48	**-0.64**	-0.03	-0.51	**0.82**	**0.62**	**0.84**	**0.80**	**0.80**	**0.76**	-0.55	**-0.79**	**0.70**	0.46	**-0.65**	0.33	**-0.79**	1		
<63	0.54	**0.59**	-0.51	**-0.75**	-0.26	**-0.63**	0.52	0.24	0.33	0.38	0.33	0.39	-0.57	-0.46	0.15	0.18	-0.20	0.11	-0.22	**0.65**	1	
>63	-0.54	**-0.59**	0.51	**0.75**	0.26	**0.63**	-0.52	-0.24	-0.33	-0.38	-0.33	-0.39	0.57	0.46	-0.15	-0.18	0.20	-0.11	0.22	**-0.65**	-1.00	1

p < 0.01, **p < 0.001**

Appendix 15. Pearson correlation matrix for sediment parameters measured in the core K7 from the Krka River estuary

	Li	Rb	Mo	Cd	Pb	U	Al	Cr	Mn	Fe	Co	Ni	Cu	Zn	As	Hg	OC	S	P	<2	<63	>63
Li	1																					
Rb	**0.99**	1																				
Mo	**0.73**	**0.76**	1																			
Cd	**0.79**	**0.83**	**0.90**	1																		
Pb	**0.87**	**0.88**	0.59	**0.63**	1																	
U	0.32	0.38	**0.63**	**0.72**	0.38	1																
Al	**0.97**	**0.98**	**0.71**	**0.79**	**0.89**	0.36	1															
Cr	**0.96**	**0.97**	**0.84**	**0.85**	**0.85**	0.38	**0.96**	1														
Mn	**0.89**	**0.90**	**0.65**	**0.64**	**0.99**	0.33	**0.90**	**0.89**	1													
Fe	**0.96**	**0.98**	**0.81**	**0.86**	**0.90**	0.48	**0.98**	**0.98**	**0.91**	1												
Co	**0.93**	**0.94**	**0.74**	**0.70**	**0.91**	0.25	**0.94**	**0.96**	**0.95**	**0.94**	1											
Ni	**0.96**	**0.97**	**0.81**	**0.83**	**0.89**	0.39	**0.97**	**0.99**	**0.92**	**0.99**	**0.97**	1										
Cu	**0.93**	**0.95**	**0.75**	**0.79**	**0.96**	0.48	**0.96**	**0.94**	**0.96**	**0.98**	**0.94**	**0.96**	1									
Zn	**0.91**	**0.93**	**0.66**	**0.70**	**0.99**	0.41	**0.94**	**0.91**	**0.99**	**0.95**	**0.94**	**0.94**	**0.99**	1								
As	0.11	0.14	**0.61**	**0.61**	-0.09	**0.74**	0.08	0.19	-0.07	0.21	0.00	0.17	0.10	-0.01	1							
Hg	**0.94**	**0.95**	**0.72**	**0.82**	**0.84**	0.35	**0.95**	**0.95**	**0.86**	**0.95**	**0.91**	**0.95**	**0.92**	**0.89**	0.11	1						
OC	**0.74**	**0.78**	**0.59**	**0.70**	**0.87**	**0.62**	**0.78**	**0.72**	**0.83**	**0.79**	**0.70**	**0.76**	**0.87**	**0.87**	0.10	**0.71**	1					
S	0.10	0.14	**0.62**	**0.60**	-0.08	**0.70**	0.13	0.21	-0.07	0.23	0.01	0.18	0.17	0.02	**0.81**	0.15	0.21	1				
P	**0.89**	**0.88**	0.52	0.54	**0.97**	0.18	**0.90**	**0.85**	**0.97**	**0.88**	**0.94**	**0.89**	**0.92**	**0.96**	-0.20	**0.83**	**0.76**	-0.22	1			
<2	**-0.81**	**-0.82**	-0.53	**-0.61**	**-0.80**	-0.25	**-0.77**	**-0.78**	**-0.79**	**-0.78**	**-0.76**	**-0.79**	**-0.80**	**-0.82**	0.06	**-0.74**	**-0.77**	0.00	**-0.79**	1		
<63	-0.30	-0.31	-0.35	-0.46	0.00	-0.17	-0.23	-0.33	-0.02	-0.27	-0.12	-0.28	-0.17	-0.10	-0.34	-0.29	-0.17	-0.47	-0.01	0.47	1	
>63	0.30	0.31	0.35	0.46	0.00	0.17	0.23	0.33	0.02	0.27	0.12	0.28	0.17	0.10	0.34	0.29	0.17	0.47	0.01	-0.47	-1.00	1

$p < 0.01$, $p < 0.001$

Appendix 16. Pearson correlation matrix for sediment parameters measured in the core K8 from the Krka River estuary

	Li	Rb	Mo	Cd	Pb	U	Al	Cr	Mn	Fe	Co	Ni	Cu	Zn	As	Hg	OC	S	P	<2	<63	>63
Li	1																					
Rb	**0.87**	1																				
Mo	0.15	-0.29	1																			
Cd	**0.88**	**0.95**	-0.12	1																		
Pb	**0.91**	**0.80**	0.16	**0.87**	1																	
U	-0.18	-0.54	**0.80**	-0.42	-0.08	1																
Al	**0.94**	**0.94**	-0.01	**0.94**	**0.88**	-0.29	1															
Cr	**0.92**	**0.97**	-0.16	**0.93**	**0.86**	-0.40	**0.97**	1														
Mn	**0.80**	**0.97**	-0.38	**0.92**	**0.74**	-0.61	**0.90**	**0.93**	1													
Fe	**0.92**	**0.98**	-0.12	**0.96**	**0.86**	-0.39	**0.98**	**0.97**	**0.95**	1												
Co	**0.80**	**0.78**	0.17	**0.85**	**0.73**	-0.21	**0.86**	**0.81**	**0.79**	**0.86**	1											
Ni	**0.89**	**0.99**	-0.24	**0.95**	**0.81**	-0.49	**0.96**	**0.97**	**0.97**	**0.99**	**0.82**	1										
Cu	**0.87**	**0.98**	-0.24	**0.95**	**0.80**	-0.49	**0.95**	**0.97**	**0.98**	**0.98**	**0.85**	**0.99**	1									
Zn	-0.35	**-0.72**	0.63	-0.64	-0.25	**0.73**	-0.54	-0.56	**-0.79**	-0.65	-0.53	**-0.71**	**-0.71**	1								
As	**0.74**	**0.80**	-0.06	**0.75**	0.66	-0.23	**0.86**	**0.79**	**0.77**	**0.87**	**0.73**	**0.84**	**0.81**	-0.61	1							
Hg	**-0.81**	**-0.93**	0.16	**-0.96**	**-0.79**	0.36	**-0.91**	**-0.89**	**-0.91**	**-0.93**	**-0.81**	**-0.93**	**-0.93**	**0.70**	**-0.74**	1						
OC	0.44	**0.72**	-0.64	0.57	0.25	**-0.73**	0.58	0.67	**0.80**	0.64	0.50	**0.71**	**0.72**	**-0.80**	0.60	-0.61	1					
S	0.20	-0.16	**0.87**	0.00	0.27	**0.75**	0.12	-0.08	-0.20	0.04	0.27	-0.09	-0.09	0.38	0.17	-0.01	-0.53	1				
P	0.42	**0.74**	**-0.76**	0.61	0.32	**-0.90**	0.51	0.64	**0.74**	0.59	0.29	**0.68**	0.67	**-0.72**	0.38	-0.56	**0.75**	**-0.75**	1			
<2	0.65	**0.80**	-0.28	**0.70**	0.58	-0.42	**0.76**	**0.76**	**0.79**	**0.79**	**0.69**	**0.79**	**0.82**	-0.64	0.66	**-0.72**	0.65	-0.05	0.54	1		
<63	-0.05	0.07	-0.08	0.03	0.04	0.19	0.07	0.02	0.04	0.08	0.05	0.07	0.11	-0.18	0.09	-0.18	-0.04	0.17	-0.09	0.52	1	
>63	0.05	-0.07	0.08	-0.03	-0.04	-0.19	-0.07	-0.02	-0.04	-0.08	-0.05	-0.07	-0.11	0.18	-0.09	0.18	0.04	-0.17	0.09	-0.52	-1.00	1

p < 0.01, **p < 0.001**

Appendix 17. Pearson correlation matrix for sediment parameters measured in the core K20 from the Krka River estuary

	Li	Rb	Mo	Cd	Pb	U	Al	Cr	Mn	Fe	Co	Ni	Cu	Zn	As	Hg	OC	S	P	<2	<63	>63
Li	1																					
Rb	0.58	1																				
Mo	0.21	0.46	1																			
Cd	0.48	0.32	0.12	1																		
Pb	0.05	**0.76**	0.59	0.01	1																	
U	-0.20	0.44	**0.84**	-0.05	0.72	1																
Al	**0.96**	0.67	0.39	0.54	0.18	-0.01	1															
Cr	**0.75**	0.12	-0.18	0.21	-0.22	-0.60	0.62	1														
Mn	0.31	**0.81**	0.30	0.59	0.65	0.43	0.42	-0.15	1													
Fe	**0.90**	0.72	0.37	0.68	0.31	0.04	**0.91**	0.58	0.61	1												
Co	0.48	0.37	0.32	0.01	0.31	0.08	0.43	0.39	0.18	0.46	1											
Ni	0.72	0.58	0.40	**0.85**	0.23	0.12	**0.82**	0.37	0.67	**0.87**	0.21	1										
Cu	0.43	**0.84**	0.47	0.63	0.66	0.49	0.58	-0.04	**0.94**	0.68	0.26	**0.79**	1									
Zn	0.38	**0.76**	0.32	0.72	0.66	0.33	0.47	0.07	**0.88**	0.71	0.19	0.72	**0.87**	1								
As	0.39	0.65	0.38	0.36	0.64	0.30	0.41	0.23	0.69	0.67	0.37	0.58	0.64	**0.74**	1							
Hg	0.40	**0.92**	0.51	0.49	**0.83**	0.54	0.54	-0.05	**0.91**	0.67	0.29	0.65	**0.93**	**0.91**	0.71	1						
OC	0.22	0.17	-0.47	0.70	-0.10	-0.41	0.15	0.17	0.52	0.40	-0.15	0.42	0.35	0.57	0.31	0.28	1					
S	-0.19	0.38	-0.27	0.01	0.51	0.02	-0.12	-0.23	0.46	-0.08	-0.08	-0.05	0.36	0.43	0.14	0.48	0.31	1				
P	0.52	0.03	0.57	0.03	-0.13	0.15	0.50	0.45	-0.23	0.41	0.48	0.31	-0.03	-0.18	0.14	-0.10	-0.45	**-0.83**	1			
<2	**0.81**	0.23	0.22	0.11	-0.12	-0.23	0.72	**0.81**	-0.07	0.66	0.51	0.42	0.04	-0.01	0.31	0.01	-0.07	-0.54	**0.79**	1		
<63	0.71	0.55	**0.76**	0.43	0.29	0.41	**0.84**	0.30	0.38	0.73	0.44	**0.78**	0.60	0.36	0.39	0.50	-0.19	-0.34	0.71	0.61	1	
>63	-0.71	-0.55	**-0.76**	-0.43	-0.29	-0.41	**-0.84**	-0.30	-0.38	-0.73	-0.44	**-0.78**	-0.60	-0.36	-0.39	-0.50	0.19	0.34	-0.71	-0.61	**-1.00**	1

p < 0.01, **p < 0.001**

Appendix 18. Pearson correlation matrix for sediment parameters measured in the core K22 from the Krka River estuary

	Li	Rb	Mo	Cd	Pb	U	Al	Cr	Mn	Fe	Co	Ni	Cu	Zn	As	Hg	OC	S	P	<2	<63	>63
Li	1																					
Rb	**1.00**	1																				
Mo	**0.93**	**0.95**	1																			
Cd	0.58	0.58	0.58	1																		
Pb	**0.97**	**0.97**	**0.94**	0.72	1																	
U	**0.95**	**0.95**	**0.92**	0.38	**0.88**	1																
Al	**0.99**	**0.99**	**0.95**	0.64	**0.99**	**0.93**	1															
Cr	0.21	0.23	0.43	0.54	0.36	0.25	0.31	1														
Mn	-0.02	-0.03	0.04	0.67	0.20	-0.27	0.08	0.39	1													
Fe	**0.99**	**0.99**	**0.95**	0.62	**0.98**	**0.92**	**1.00**	0.26	0.06	1												
Co	0.62	0.63	0.66	**0.75**	**0.74**	0.54	0.70	0.63	0.50	0.66	1											
Ni	**0.98**	**0.98**	**0.95**	0.65	**0.98**	**0.91**	**0.99**	0.30	0.10	**0.99**	0.72	1										
Cu	**0.92**	**0.93**	**0.95**	**0.76**	**0.98**	**0.83**	**0.96**	0.47	0.30	**0.95**	**0.80**	**0.96**	1									
Zn	**0.96**	**0.96**	**0.94**	0.71	**1.00**	**0.88**	**0.99**	0.37	0.22	**0.98**	**0.77**	**0.98**	**0.99**	1								
As	**-0.74**	**-0.74**	**-0.76**	**-0.75**	**-0.84**	-0.59	**-0.76**	-0.35	-0.45	**-0.76**	-0.59	**-0.76**	**-0.86**	**-0.83**	1							
Hg	**0.87**	**0.88**	**0.87**	**0.85**	**0.96**	**0.74**	**0.91**	0.47	0.41	**0.90**	**0.82**	**0.91**	**0.98**	**0.96**	**-0.90**	1						
OC	-0.14	-0.11	-0.03	0.33	0.00	-0.19	-0.11	0.35	0.39	-0.12	0.38	-0.06	0.10	-0.02	-0.19	0.17	1					
S	**0.92**	**0.92**	**0.90**	0.31	**0.83**	**0.98**	**0.89**	0.22	-0.33	**0.90**	0.42	**0.88**	**0.78**	**0.83**	-0.55	0.67	-0.32	1				
P	-0.22	-0.23	-0.16	0.56	0.00	-0.46	-0.14	0.30	**0.94**	-0.15	0.33	-0.12	0.10	0.00	-0.35	0.25	0.51	-0.52	1			
<2	**0.84**	**0.84**	**0.78**	0.24	**0.75**	**0.94**	**0.81**	0.21	-0.39	**0.80**	0.40	**0.77**	0.68	**0.75**	-0.46	0.60	-0.38	**0.94**	-0.54	1		
<63	**0.89**	**0.89**	**0.88**	0.63	**0.91**	**0.89**	**0.91**	0.52	0.08	**0.89**	**0.74**	**0.89**	**0.89**	**0.92**	-0.71	**0.88**	-0.11	**0.85**	-0.10	**0.87**	1	
>63	**-0.89**	**-0.89**	**-0.88**	-0.63	**-0.91**	**-0.89**	**-0.91**	-0.52	-0.08	**-0.89**	**-0.74**	**-0.89**	**-0.89**	**-0.92**	0.71	**-0.88**	0.11	**-0.85**	0.10	**-0.87**	-1.00	1

p < 0.01, **p < 0.001**

Appendix 19. Pearson correlation matrix for sediment parameters measured in the core K32 from the Krka River estuary

	Li	Rb	Mo	Cd	Pb	U	Al	Cr	Mn	Fe	Co	Ni	Cu	Zn	As	Hg	OC	S	P	<2	<63	>63
Li	1																					
Rb	**1.00**	1																				
Mo	**0.77**	**0.74**	1																			
Cd	**0.92**	**0.90**	**0.94**	1																		
Pb	**0.97**	**0.96**	**0.85**	**0.97**	1																	
U	**0.67**	**0.64**	**0.97**	**0.89**	**0.79**	1																
Al	**0.99**	**0.99**	**0.76**	**0.91**	**0.96**	**0.65**	1															
Cr	**0.96**	**0.97**	**0.66**	**0.84**	**0.93**	0.55	**0.97**	1														
Mn	**0.96**	**0.97**	**0.65**	**0.82**	**0.89**	0.52	**0.96**	**0.95**	1													
Fe	**0.99**	**0.99**	**0.77**	**0.92**	**0.97**	**0.66**	**1.00**	**0.97**	**0.97**	1												
Co	0.17	0.17	0.06	0.07	0.08	0.00	0.16	0.13	0.15	0.13	1											
Ni	**0.99**	**0.99**	**0.75**	**0.90**	**0.96**	**0.63**	**1.00**	**0.97**	**0.97**	**1.00**	0.16	1										
Cu	**0.98**	**0.98**	**0.80**	**0.94**	**0.99**	**0.72**	**0.98**	**0.95**	**0.93**	**0.98**	0.09	**0.98**	1									
Zn	**0.96**	**0.95**	**0.83**	**0.96**	**0.99**	**0.75**	**0.96**	**0.94**	**0.89**	**0.97**	0.08	**0.95**	**0.98**	1								
As	**-0.97**	**-0.97**	**-0.66**	**-0.85**	**-0.93**	-0.54	**-0.98**	**-0.97**	**-0.95**	**-0.98**	-0.11	**-0.98**	**-0.95**	**-0.93**	1							
Hg	**0.92**	**0.90**	**0.83**	**0.94**	**0.95**	**0.81**	**0.89**	**0.85**	**0.84**	**0.90**	0.04	**0.88**	**0.95**	**0.92**	**-0.84**	1						
OC	**0.82**	**0.80**	**0.57**	**0.75**	**0.77**	0.51	**0.78**	**0.73**	**0.79**	**0.80**	0.13	**0.79**	**0.78**	**0.75**	**-0.75**	**0.82**	1					
S	**0.67**	**0.64**	**0.97**	**0.89**	**0.78**	**0.97**	**0.65**	0.55	0.52	**0.66**	0.06	**0.64**	**0.71**	**0.75**	-0.54	**0.78**	0.52	1				
P	**0.94**	**0.95**	**0.69**	**0.84**	**0.92**	0.55	**0.97**	**0.97**	**0.93**	**0.97**	0.12	**0.97**	**0.94**	**0.93**	**-0.98**	**0.79**	**0.71**	0.56	1			
<2	-0.44	-0.41	**-0.71**	**-0.63**	-0.53	**-0.72**	-0.44	-0.30	-0.38	-0.45	-0.01	-0.43	-0.50	-0.50	0.33	-0.55	-0.45	**-0.70**	-0.38	1		
<63	0.51	0.53	0.08	0.29	0.42	-0.01	0.52	**0.60**	0.55	0.52	-0.10	0.54	0.48	0.44	**-0.61**	0.35	0.35	-0.01	0.55	0.44	1	
>63	-0.51	-0.53	-0.08	-0.29	-0.42	0.01	-0.52	**-0.60**	-0.55	-0.52	0.10	-0.54	-0.48	-0.44	**0.61**	-0.35	-0.35	0.01	-0.55	-0.44	**-1.00**	1

p < 0.01, **p < 0.001**

Appendix 20. Pearson correlation matrix for sediment parameters measured in the core K36 from the Krka River estuary

	Li	Rb	Mo	Cd	Pb	U	Al	Cr	Mn	Fe	Co	Ni	Cu	Zn	As	Hg	OC	S	P	<2	<63	>63
Li	1																					
Rb	**0.99**	1																				
Mo	**0.82**	**0.83**	1																			
Cd	-0.67	-0.62	-0.72	1																		
Pb	0.56	0.62	0.60	-0.10	1																	
U	**-0.86**	**-0.83**	-0.65	**0.81**	-0.43	1																
Al	0.71	0.73	0.29	-0.02	0.53	-0.52	1															
Cr	-0.60	-0.56	-0.54	0.62	0.07	0.49	-0.17	1														
Mn	-0.21	-0.19	-0.20	0.53	-0.11	0.52	0.03	-0.30	1													
Fe	**0.82**	**0.83**	0.52	-0.25	0.71	-0.69	**0.90**	-0.15	-0.23	1												
Co	-0.37	-0.41	0.01	-0.32	-0.55	0.20	**-0.83**	-0.29	0.06	-0.76	1											
Ni	**0.92**	**0.94**	0.73	-0.40	0.72	-0.73	**0.84**	-0.32	-0.20	**0.95**	-0.61	1										
Cu	0.66	0.68	0.67	-0.48	0.64	-0.65	0.47	0.03	-0.58	0.71	-0.29	0.75	1									
Zn	0.20	0.26	-0.02	0.58	0.45	0.16	0.72	0.15	0.48	0.51	-0.75	0.47	0.11	1								
As	-0.14	-0.17	0.30	-0.40	-0.41	0.18	-0.70	-0.38	0.05	-0.55	**0.84**	-0.34	-0.16	-0.60	1							
Hg	0.37	0.41	0.03	0.20	0.64	-0.38	0.79	0.34	-0.23	**0.80**	**-0.87**	0.64	0.52	0.62	**-0.87**	1						
OC	0.37	0.42	0.06	0.08	0.69	-0.46	0.67	0.20	-0.17	0.64	-0.70	0.50	0.40	0.45	**-0.88**	**0.85**	1					
S	**0.90**	**0.91**	**0.89**	-0.59	0.48	-0.64	0.55	-0.71	0.04	0.61	-0.15	**0.82**	0.54	0.26	0.14	0.14	0.11	1				
P	-0.52	-0.47	-0.54	**0.88**	-0.13	0.79	-0.01	0.35	0.65	-0.26	-0.31	-0.33	-0.64	0.59	-0.20	0.00	-0.11	-0.35	1			
<2	-0.61	-0.61	-0.79	0.56	-0.63	0.50	-0.15	0.17	0.35	-0.49	0.08	-0.57	-0.67	0.13	-0.18	-0.08	-0.11	-0.50	0.52	1		
<63	-0.43	-0.42	-0.69	0.54	-0.45	0.34	0.10	0.16	0.30	-0.24	-0.11	-0.34	-0.48	0.30	-0.37	0.17	0.11	-0.35	0.45	**0.96**	1	
>63	0.43	0.42	0.69	-0.54	0.45	-0.34	-0.10	-0.16	-0.30	0.24	0.11	0.34	0.48	-0.30	0.37	-0.17	-0.11	0.35	-0.45	**-0.96**	-1.00	1

p < 0.01, **p < 0.001**

Appendix 21. Pearson correlation matrix for logK_d values of various metals, Eh and pH in the sediment pore water and logarithmic values of C_{org} and Fe in solid fraction of sediment

	Li	Mo	Pb	U	Al	V	Cr	Mn	Fe	Co	Ni	Cu	Zn	Ba	As	pH	Eh	logFe	logOC
Li	1																		
Mo	-0.01	1																	
Pb	-0.27	-0.01	1																
U	-0.22	**0.64**	**-0.36**	1															
Al	0.05	-0.13	-0.30	0.21	1														
V	-0.20	**0.60**	0.04	**0.70**	0.08	1													
Cr	**-0.55**	0.14	-0.26	**0.57**	**0.54**	**0.43**	1												
Mn	**-0.34**	0.26	**0.37**	-0.11	**-0.79**	-0.01	-0.29	1											
Fe	-0.07	**-0.32**	-0.04	**-0.37**	**-0.32**	**-0.66**	**-0.33**	**0.33**	1										
Co	-0.20	**0.32**	0.26	0.12	**-0.56**	0.14	-0.25	**0.70**	**0.31**	1									
Ni	0.17	**0.62**	0.01	**0.35**	-0.11	**0.49**	0.02	0.16	-0.30	0.23	1								
Cu	-0.15	**0.32**	-0.07	0.24	-0.08	0.13	0.22	0.28	0.19	**0.43**	0.13	1							
Zn	**-0.48**	**0.59**	0.18	**0.52**	-0.21	**0.51**	**0.31**	**0.41**	-0.16	0.27	**0.47**	0.10	1						
Ba	**-0.48**	**0.63**	0.04	**0.61**	-0.12	**0.53**	**0.53**	**0.39**	-0.26	0.28	**0.35**	0.22	**0.74**	1					
As	-0.02	**0.78**	-0.17	**0.60**	-0.22	**0.47**	0.18	0.29	-0.18	**0.43**	**0.63**	**0.39**	**0.55**	**0.60**	1				
pH	-0.06	**-0.43**	**0.45**	**-0.54**	**-0.60**	-0.27	**-0.49**	**0.48**	**0.35**	0.20	-0.18	0.00	-0.11	-0.29	**-0.41**	1			
Eh	**0.37**	-0.21	**0.36**	**-0.42**	0.18	-0.12	-0.22	**-0.40**	-0.15	**-0.38**	-0.11	-0.19	**-0.40**	**-0.41**	**-0.46**	0.16	1		
logFe	**0.43**	**0.55**	**-0.42**	**0.46**	-0.01	**0.36**	0.13	-0.05	**-0.38**	-0.07	**0.58**	0.07	**0.32**	**0.45**	**0.62**	**-0.50**	-0.10	1	
logOC	**-0.35**	**0.68**	-0.11	**0.47**	-0.20	**0.44**	**0.38**	**0.47**	-0.19	**0.31**	**0.45**	**0.45**	**0.56**	**0.74**	**0.66**	-0.16	**-0.48**	**0.39**	1

$p < 0.01$, $p < 0.001$

Appendix 22. Pearson correlation matrix for pore water parameters measured in the core K1 from the Krka River estuary

	Mo	Pb	U	Al	V	Cr	Mn	Fe	Co	Ni	Cu	Zn	Ba	As	pH	Eh	DOC	DIC	PO_4^{3-}	NH_4^+	$Si(OH)_4$	SO_4^{2-}
Mo	1																					
Pb	**0.71**	1																				
U	**0.86**	0.54	1																			
Al	0.03	0.31	-0.12	1																		
V	0.27	0.07	0.34	-0.14	1																	
Cr	0.03	0.03	0.04	**0.64**	0.14	1																
Mn	-0.36	-0.32	-0.32	-0.20	-0.15	-0.49	1															
Fe	-0.32	-0.18	-0.23	-0.11	-0.39	-0.43	**0.80**	1														
Co	0.22	0.13	0.28	-0.21	**0.90**	-0.05	0.19	-0.06	1													
Ni	0.33	0.34	0.35	0.26	**0.63**	**0.64**	-0.34	-0.42	0.52	1												
Cu	0.44	0.22	0.36	-0.05	-0.05	0.04	-0.10	0.10	-0.02	0.05	1											
Zn	0.00	0.03	-0.08	0.23	0.29	**0.59**	-0.19	-0.45	0.20	**0.73**	-0.22	1										
Ba	0.00	-0.09	-0.18	0.02	0.48	0.24	-0.07	-0.49	0.45	0.36	-0.26	**0.63**	1									
As	0.23	-0.03	0.34	-0.19	**0.65**	0.31	-0.02	-0.38	**0.66**	**0.60**	-0.09	**0.62**	**0.70**	1								
pH	0.21	0.17	0.28	0.13	0.19	0.34	-0.22	-0.19	0.09	0.40	0.06	0.14	0.18	0.23	1							
Eh	-0.46	-0.41	-0.26	-0.33	-0.15	-0.54	**0.73**	**0.73**	0.04	-0.38	-0.40	-0.36	-0.32	-0.23	-0.03	1						
DOC	0.16	0.03	0.13	0.05	0.43	0.52	-0.24	-0.57	0.35	0.57	-0.14	**0.76**	**0.72**	**0.79**	0.15	-0.52	1					
DIC	-0.42	-0.42	-0.45	-0.08	0.29	0.17	0.29	-0.01	0.38	0.22	-0.11	0.55	**0.74**	0.56	-0.05	-0.03	0.49	1				
PO_4^{3-}	-0.27	-0.24	-0.35	0.08	0.37	0.25	0.00	-0.43	0.33	0.19	-0.41	0.56	**0.88**	**0.61**	0.17	-0.18	**0.63**	**0.72**	1			
NH_4^+	-0.52	-0.13	**-0.69**	0.16	0.08	0.07	0.29	0.11	0.19	0.19	-0.24	0.49	0.48	0.06	0.07	0.13	0.12	**0.70**	**0.60**	1		
$Si(OH)_4$	-0.29	-0.37	-0.35	0.03	0.34	0.26	0.01	-0.38	0.29	0.15	-0.33	0.54	**0.89**	**0.60**	0.31	-0.10	0.56	**0.75**	**0.94**	0.55	1	
SO_4^{2-}	0.15	0.01	0.14	0.23	-0.34	0.26	-0.29	-0.25	-0.45	-0.12	-0.17	0.09	0.05	-0.08	0.25	-0.08	0.03	-0.32	-0.06	-0.41	0.11	1

$p < 0.01$, $p < 0.001$

Appendix 23. Pearson correlation matrix for pore water parameters measured in the core K7 from the Krka River estuary

	Mo	Pb	U	Al	V	Cr	Mn	Fe	Co	Ni	Cu	Zn	Ba	As	pH	Eh	DOC	DIC	PO_4^{3-}	NH_4^+	$Si(OH)_4$	SO_4^{2-}
Mo	1																					
Pb	-0.48	1																				
U	**0.90**	-0.55	1																			
Al	0.29	0.21	-0.01	1																		
V	**0.87**	-0.44	**0.91**	0.12	1																	
Cr	0.49	-0.12	0.29	**0.63**	0.53	1																
Mn	-0.19	0.44	-0.16	-0.13	-0.37	-0.52	1															
Fe	-0.34	0.43	-0.23	-0.22	-0.32	-0.58	0.41	1														
Co	0.03	0.27	0.09	-0.15	-0.11	-0.43	**0.95**	0.34	1													
Ni	0.12	0.44	0.18	-0.10	0.01	-0.38	**0.87**	0.52	**0.90**	1												
Cu	0.09	**0.68**	0.01	0.49	-0.01	-0.01	0.49	0.34	0.45	**0.66**	1											
Zn	0.22	0.17	0.02	**0.82**	0.09	0.41	-0.12	-0.02	-0.09	-0.06	0.45	1										
Ba	0.01	-0.28	-0.07	-0.19	0.00	0.33	-0.36	-0.29	-0.30	-0.40	-0.59	-0.15	1									
As	0.21	0.14	0.31	-0.11	0.24	-0.23	0.30	**0.80**	0.41	**0.61**	0.36	0.10	-0.19	1								
pH	0.18	-0.08	0.04	0.37	0.12	0.24	0.04	0.19	0.05	-0.03	0.03	0.38	-0.15	0.32	1							
Eh	0.15	-0.32	0.29	-0.18	0.07	-0.03	0.25	0.18	0.35	0.27	-0.15	-0.28	0.31	0.38	0.06	1						
DOC	**0.65**	-0.39	**0.80**	-0.12	**0.61**	0.02	0.25	-0.14	0.41	0.45	0.19	-0.10	-0.27	0.27	-0.06	0.25	1					
DIC	-0.33	0.57	-0.45	0.03	-0.43	-0.20	0.49	0.51	0.41	0.51	0.40	-0.06	0.14	0.37	-0.17	0.51	-0.27	1				
PO_4^{3-}	0.23	-0.24	-0.13	0.55	0.50	**0.80**	**-0.83**	-0.53	**-0.80**	**-0.78**	-0.05	0.48	0.49	-0.45	-0.02	-0.57	-0.35	-0.28	1			
NH_4^+	0.07	0.06	0.11	-0.10	-0.11	-0.28	**0.85**	-0.02	**0.91**	**0.69**	0.26	-0.10	-0.14	0.09	-0.03	0.37	0.45	0.27	**-0.63**	1		
$Si(OH)_4$	-0.40	**0.69**	**-0.63**	0.46	-0.45	0.27	-0.10	0.15	-0.31	-0.14	0.35	0.32	0.10	-0.14	0.06	-0.30	**-0.65**	0.44	**0.92**	-0.39	1	
SO_4^{2-}	0.21	0.13	0.28	-0.16	0.28	-0.33	0.09	0.39	0.18	0.35	0.29	0.07	-0.27	0.51	-0.11	0.00	0.21	0.18	-0.19	-0.03	-0.19	1

$p < 0.01$, $p < 0.001$

Appendix 24. Pearson correlation matrix for pore water parameters measured in the core K8 from the Krka River estuary

	Mo	Pb	U	Al	V	Cr	Mn	Fe	Co	Ni	Cu	Zn	Ba	As	pH	Eh	DOC	DIC	PO_4^{3-}	NH_4^+	$Si(OH)_4$	SO_4^{2-}
Mo	1																					
Pb	-0.35	1																				
U	**0.93**	-0.46	1																			
Al	-0.19	**0.69**	-0.16	1																		
V	0.16	0.33	0.17	0.25	1																	
Cr	-0.16	0.59	-0.15	0.40	0.20	1																
Mn	0.11	-0.68	0.28	-0.52	-0.62	-0.13	1															
Fe	-0.34	-0.04	-0.15	0.12	-0.59	0.34	**0.69**	1														
Co	-0.48	0.60	-0.42	0.35	-0.22	0.67	0.02	0.59	1													
Ni	0.04	0.23	-0.05	0.12	0.61	-0.27	**-0.78**	**-0.85**	-0.33	1												
Cu	0.12	-0.56	0.29	-0.43	-0.41	0.15	**0.93**	**0.70**	0.10	**-0.83**	1											
Zn	-0.05	0.12	-0.05	0.13	-0.27	0.03	-0.05	0.19	0.34	-0.16	-0.09	1										
Ba	-0.32	**0.93**	-0.39	**0.76**	0.17	**0.70**	-0.58	0.11	**0.69**	0.08	-0.46	0.19	1									
As	**0.69**	**-0.81**	**0.77**	-0.60	-0.26	-0.39	0.65	0.06	-0.48	-0.30	0.56	0.14	**-0.74**	1								
pH	0.38	**-0.89**	0.60	-0.58	-0.28	-0.17	**0.79**	0.66	-0.19	**-0.71**	**0.77**	0.01	**-0.86**	**0.78**	1							
Eh	0.32	**-0.97**	0.54	**-0.78**	-0.55	-0.22	**0.92**	**0.80**	0.02	**-0.77**	**0.82**	0.13	**-0.89**	**0.84**	**0.93**	1						
DOC	-0.03	0.05	0.11	0.14	-0.31	0.56	0.59	**0.84**	0.60	**-0.86**	**0.74**	0.11	0.21	0.09	0.65	0.68	1					
DIC	-0.46	**0.86**	-0.48	**0.76**	0.17	0.61	-0.56	0.16	**0.70**	0.06	-0.44	0.33	**0.94**	**-0.75**	**-0.82**	**-0.90**	0.23	1				
PO_4^{3-}	-0.31	**0.82**	-0.49	0.44	0.54	0.47	**-0.87**	-0.46	0.24	0.53	**-0.71**	-0.09	**0.73**	**-0.79**	**-0.85**	**-0.97**	-0.33	0.66	1			
NH_4^+	-0.44	**0.95**	-0.56	0.62	0.31	0.63	**-0.69**	-0.04	0.59	0.19	-0.54	0.21	**0.92**	**-0.82**	**-0.85**	**-0.94**	0.05	**0.91**	**0.85**	1		
$Si(OH)_4$	-0.08	0.64	-0.29	0.27	0.65	0.37	**-0.88**	-0.68	0.02	0.63	**-0.70**	-0.12	0.52	-0.60	**-0.80**	**-0.95**	-0.45	0.45	**0.94**	0.68	1	
SO_4^{2-}	0.07	0.01	0.03	0.06	-0.21	0.07	0.04	0.03	0.24	-0.08	0.06	0.16	0.03	-0.04	-0.16	-0.07	0.10	-0.05	-0.09	-0.12	-0.01	1

$p < 0.01$, $p < 0.001$

Appendix 25. Pearson correlation matrix for pore water parameters measured in the core K20 from the Krka River estuary

	Mo	Pb	U	Al	V	Cr	Mn	Fe	Co	Ni	Cu	Zn	Ba	As	pH	Eh	DOC	DIC	PO_4^{3-}	NH_4^+	$Si(OH)_4$	SO_4^{2-}
Mo	1																					
Pb	-0.15	1																				
U	**0.88**	-0.14	1																			
Al	-0.08	**0.63**	-0.22	1																		
V	0.03	**0.72**	-0.13	0.56	1																	
Cr	-0.33	**0.77**	-0.56	0.60	**0.77**	1																
Mn	-0.48	0.00	-0.39	0.06	-0.14	0.01	1															
Fe	-0.14	**-0.66**	0.12	-0.57	**-0.75**	**-0.65**	0.17	1														
Co	-0.06	-0.31	0.09	-0.23	-0.43	-0.44	**0.85**	0.42	1													
Ni	0.39	**0.70**	0.48	0.48	0.53	0.22	-0.33	-0.56	-0.31	1												
Cu	0.30	-0.42	0.11	-0.48	-0.40	-0.18	0.18	0.26	0.40	-0.55	1											
Zn	0.41	0.57	0.52	0.50	0.27	0.16	-0.18	-0.14	-0.09	**0.69**	-0.18	1										
Ba	-0.56	0.58	**-0.71**	**0.61**	**0.67**	**0.82**	0.42	-0.55	-0.08	0.06	-0.34	-0.11	1									
As	**0.61**	**-0.69**	**0.73**	**-0.69**	-0.50	**-0.80**	-0.29	0.59	0.20	-0.18	0.34	-0.04	**-0.83**	1								
pH	**0.62**	-0.24	0.48	-0.08	**-0.62**	**-0.64**	**0.93**	-0.01	**0.92**	-0.08	**0.71**	-0.06	0.35	0.10	1							
Eh	0.20	**-0.72**	0.58	-0.38	**-0.98**	**-0.71**	**0.73**	**0.73**	**0.82**	**-0.72**	0.26	**0.75**	0.04	0.50	0.56	1						
DOC	0.12	**0.87**	-0.02	**0.66**	**0.82**	**0.74**	-0.20	**-0.86**	-0.46	**0.75**	-0.43	0.43	0.58	-0.59	-0.26	**-0.84**	1					
DIC	0.36	-0.44	0.48	0.14	-0.44	**-0.62**	-0.16	0.44	0.14	0.03	-0.12	0.35	-0.53	0.45	0.26	0.54	-0.38	1				
PO_4^{3-}	-0.38	0.06	**-0.64**	0.44	0.08	0.44	-0.07	-0.40	-0.30	-0.22	0.16	-0.22	0.37	**-0.73**	-0.30	**-0.74**	0.19	-0.07	1			
NH_4^+	0.23	**0.63**	0.06	0.44	**0.69**	0.56	-0.59	-0.55	**-0.75**	0.51	**-0.61**	0.35	0.35	-0.25	**-0.64**	**-0.72**	**0.71**	-0.16	-0.03	1		
$Si(OH)_4$	-0.57	**0.62**	-0.52	0.28	**0.72**	**0.86**	**0.84**	-0.57	0.51	-0.09	-0.22	0.01	**0.88**	-0.54	#DIV/0!	#DIV/0!	0.56	-0.57	-0.36	**0.66**	1	
SO_4^{2-}	0.11	-0.52	0.36	-0.51	-0.57	-0.58	0.04	**0.86**	0.36	-0.29	0.32	0.08	**-0.66**	**0.71**	-0.16	**0.73**	**-0.72**	0.35	-0.50	-0.55	-0.41	1

p < 0.05, p < 0.01, p < 0.001

Appendix 26. Pearson correlation matrix for pore water parameters measured in the core K36 from the Krka River estuary

	Mo	Pb	U	Al	V	Cr	Mn	Fe	Co	Ni	Cu	Zn	Ba	As	pH	Eh	DOC	DIC	PO_4^{3-}	NH_4^+	$Si(OH)_4$	SO_4^{2-}
Mo	1																					
Pb	0.60	1																				
U	0.54	-0.11	1																			
Al	0.79	**0.86**	0.10	1																		
V	0.47	0.25	0.59	0.20	1																	
Cr	0.72	**0.97**	-0.04	**0.93**	0.24	1																
Mn	**-0.85**	-0.79	-0.18	-0.73	-0.48	**-0.85**	1															
Fe	-0.55	-0.57	-0.13	-0.57	-0.45	-0.55	0.59	1														
Co	-0.64	-0.41	-0.09	-0.33	-0.40	-0.46	**0.84**	0.51	1													
Ni	-0.09	0.56	-0.26	0.42	-0.04	0.48	-0.04	0.03	0.42	1												
Cu	0.04	0.71	-0.29	0.52	0.00	0.64	-0.25	-0.13	0.21	**0.96**	1											
Zn	-0.31	0.04	-0.16	0.17	-0.35	-0.01	0.52	0.11	**0.84**	0.64	0.48	1										
Ba	0.78	0.69	0.30	0.58	0.66	0.70	**-0.94**	-0.63	**-0.85**	0.00	0.18	-0.59	1									
As	-0.51	0.14	-0.32	-0.16	-0.12	-0.02	0.30	0.34	0.49	0.80	0.70	0.44	-0.20	1								
pH	0.08	-0.38	0.80	0.03	-0.45	-0.24	0.44	0.25	0.53	-0.23	-0.34	0.47	-0.68	-0.49	1							
Eh	-0.79	-0.73	0.70	-0.66	-0.52	-0.79	**0.99**	0.54	**0.88**	-0.03	-0.21	0.51	**-0.94**	0.30	0.42	1						
DOC	-0.20	0.55	-0.45	0.18	0.06	0.37	-0.15	-0.17	0.03	0.75	0.77	0.22	0.24	**0.81**	-0.78	-0.23	1					
DIC	0.75	0.75	0.28	0.61	0.52	0.71	**-0.88**	-0.67	-0.76	0.08	0.25	-0.43	**0.94**	-0.09	-0.69	**-0.81**	0.36	1				
PO_4^{3-}	0.62	**0.98**	-0.15	**0.86**	0.26	**0.97**	**-0.81**	-0.54	-0.45	0.48	0.63	-0.01	0.67	0.02	-0.27	**-0.80**	0.44	0.68	1			
NH_4^+	-0.11	0.61	-0.44	0.25	0.13	0.43	-0.25	-0.25	-0.08	0.72	0.75	0.15	0.34	0.74	**-0.81**	-0.34	**0.99**	0.44	0.51	1		
$Si(OH)_4$	0.52	**0.81**	-0.36	0.65	0.13	**0.82**	**-0.85**	-0.48	-0.73	0.20	0.41	-0.40	0.74	-0.08	-0.55	**-0.97**	0.39	0.68	**0.84**	0.48	1	
SO_4^{2-}	0.18	-0.32	0.19	0.16	-0.21	-0.13	0.22	0.03	0.24	-0.33	-0.38	0.28	-0.38	-0.64	**0.87**	0.15	-0.78	-0.46	-0.22	-0.77	-0.30	1

$p < 0.05$, **$p < 0.01$**, **$p < 0.001$**

10. CURRICULUM VITAE

10. CURICULUM VITAE

Nuša Cukrov was born on 2nd July 1987 in Šibenik, where she finished elementary school and grammar school "Antun Vrančić". She received her bachelor's degree in 2009 at the Department of Geology, Faculty of Science, University of Zagreb. In the same year, she enrolled in the graduate study of Environmental Geology at the Faculty of Mining, Geology and Petroleum Engineering, University of Zagreb, where in 2011 she earned a master's degree in geological engineering with a diploma thesis "Mineralogical and surface physical chemical properties of soils developed on hard limestone and dolomite: terra rossa and calcomelanosol" led by Prof. Dr. Goran Durn and Prof. Dr. Ivan Sondi. Since 2013, she has been working in the Laboratory for Physical Chemistry of Traces, Division for Marine and Environmental Research, Ruđer Bošković Institute. In 2015 she enrolled in doctoral study in Geology at Department of Geology, Faculty of Science, University of Zagreb. Her research interest is studying the distribution, behaviour and fate of metals in the aquatic environment, with emphasis on metal dynamic in the sediment and at the sediment-water interface.

Peer-review publications

Aguzzi, J., Iveša, N., Gelli, M., Costa, C., Gavrilović, A., Cukrov, Ne., Cukrov, M., **Cukrov, Nu.,** Omanović, D., Štifanić, M., Marini, S., Piria, M., Azzurro, E., Fanelli, E. and Danovaro, R. (2020): Ecological video monitoring of Marine Protected Areas by underwater cabled surveillance cameras. Marine Policy, 119, 104052.

Cukrov, Nu., Doumandji, N., Garnier, C., Tucaković, I., Dang, D.H., Omanović, D. and Cukrov, Ne. (2020): Anthropogenic mercury contamination in sediments of Krka River estuary (Croatia). Environmental science and pollution research, 27, 7628-7638.

Chen, X., Cukrov, Ne., Santos, I.R., Rodellas, V., **Cukrov, Nu.** and Du, J. (2020): Karstic submarine groundwater discharge into the Mediterranean: Radon-based nutrient fluxes in an anchialine cave and a basin-wide upscaling. Geochimica et cosmochimica acta, 268, 467-484.

Knežević, L., **Cukrov, N.** and Bura-Nakić, E. (2020): Ion-exchange chromatography as a tool for investigating vanadium speciation in sediments: preliminary studies. Journal of soils and sediments, 20, 2733-2740.

Durn, G., Škapin, S.D., Vdović, N., Rennert, T., Ottner, F., Ružičić, S., **Cukrov, N.** and Sondi, I. (2019): Impact of iron oxides and soil organic matter on the surface physicochemical properties and aggregation of Terra Rossa and Calcocambisol subsoil horizons from Istria (Croatia). Catena, 183, 104184.

Conference proceedings

Cukrov, Nu., Garnier, C., Dang, D.H., Cindrić, A.M., Omanović, D. and Cukrov, Ne. (2017): Spatial distribution and mobility of trace metals in sediments of the Krka River estuary (Adriatic Sea, Croatia). 4th Coastal & Maritime Mediterranean Conference CM2 Split, Croatia.

Cukrov, Nu., Garnier, C., Dang, D.H., Cindrić, A.M., Omanović, D. and Cukrov, Ne. (2017): Trace metal content and mobility in estuarine sediments of the Krka River (Adriatic Sea, Croatia). Goldschmidt2017 Paris, France.

Cukrov, Nu., Pađan, J., Cindrić, A.M., Marguš, M., Cukrov, Ne., Omanović, D. and Garnier, C. (2017): An impact of nautical tourism on copper concentrations in the Krka River estuary. 3rd International Scientific and Professional Conference „The Challenges of today: sustainable coastal and maritime tourism" Šibenik, Croatia.

Cukrov, Nu., Lojen, S., Cukrov, Ne. and Omanović, D. (2017): Spatial distribution of trace metals in surface sediments of Lake Brljan (NP KRKA). Scientific and Technical Conference "Managing lakes and reservoirs in Croatia – Process, protection and evaluation" Biograd na Moru, Croatia.

Romić, M., Cukrov, Ne., Meštrović, E., Romić, D., **Cukrov, Nu.** and Kralj, D. (2017): Mineralogical and geochemical assessment of marine peloids used for therapeutic purposes from Lokrunja Bay nearby the Pag salt pans (Eastern Adriatic). 2nd PTIM 2017 Proceedings Book 2nd International Caparica Conference on PollutantToxic Ions and Molecules, Portugal, 66-67.

Cukrov, Nu., Pađan, J., Cindrić, A.M., Marguš, M., Cukrov, N., Omanović, D. and Garnier, C. (2016): An impact of nautical tourism on copper concentrations in the Krka River estuary (Croatia). Rapp. Comm. int. Mer Médit., 41.

Cukrov, Nu., Pađan, J., Cindrić, A.M., Marguš, M., Cukrov, Ne., Omanović, D. and Garnier, C. (2016): An impact of nautical tourism on copper concentrations in the Krka River estuary (Croatia). Book of abstracts, 18th International Congress on Marine Corrosion and Fouling Toulon, France.

Cukrov, Ne., Cuculić, V., Mlakar, M., **Cukrov, Nu.,** Omanović, D., Kwokal, Ž., Jalžić, B. and Garnier, C. (2015): Ecotoxic metals in water columns of anchialine caves along Eastern Adriatic coast (Croatia). Book of abstracts, 31st International Conference of the Society for Environmental Geochemistry and Health, 29.

Cindrić, A.M., Garnier, C., Oursel, B., Pižeta, I., Cukrov, Ne., **Cukrov, Nu**., Marguš, M., Omanović, D. (2015): Raspodjela i specijacija metala u tragovima u uslojenom estuariju rijeke Krke. Scientific and Technical Conference "Vizija i izazovi upravljanja zaštićenim područjima prirode u Republici Hrvatskoj: aktivna zaštita i održivo upravljanje u Nacionalnom parku 'Krka'" Šibenik, Croatia.

Cukrov, Nu., Lojen, S., Barišić, D. and Cukrov, Ne. Koliko je važan reprezentativni uzorak za interpretaciju okoliša? Primjer sedimenata iz jezera Visovac. Scientific and Technical

Conference “Vizija i izazovi upravljanja zaštićenim područjima prirode u Republici Hrvatskoj: aktivna zaštita i održivo upravljanje u Nacionalnom parku 'Krka'” Šibenik, Croatia.

Cukrov, Nu., Dolenc, M., Lojen, S., Barišić, D., Cukrov, Ne. (2014): Sediments from the karstic lake Visovac (Krka River, Croatia). Book of abstracts, 5th International Students Geological Conference, 18.

Cukrov, Nu., Barišić, D., Heller, B., Lojen, S. and Cukrov, Ne. (2013): Importance of representative sediment sample for environmental interpretation: a case study in the lake Visovac, Krka river, Croatia. Natura Montenegrina, Podgorica, 2013, 12(3-4):787-792.

Cukrov, Nu., Heller, B., Lojen, S. and Cukrov, Ne. (2013): How to obtain representative sediment sample in a lacustrine environment. Book of abstracts, Man and Karst 2013, 17-18.

Cukrov, N., Durn, G., Sondi, I. and Škapin, S. (2012): Surface physico-chemical properties of terra rossa and calcomelanosol developed on hard limestone. Book of abstracts, 6th Mid-European Clay Conference (MECC'12), 111.

Cukrov, Ne., Lojen, S., Zavadlav, S., **Cukrov, Nu.,** Vázquez Navarro, J. and Omanović, D. (2011) Distribution of ecotoxic metals in sediments of tufa-precipitating karstic stream (Krka, Croatia). Book of abstracts, 28th IAS Meeting of Sedimentology, 547.